COMPARISON OF MEASURED AND PREDICTED CONSOLIDATION SETTLEMENTS IN SOFT GROUND.

A THESIS SUBMITTED TO
THE GRADUATE SCHOOL OF NATURAL AND APPLIED SCIENCES
OF
MIDDLE EAST TECHNICAL UNIVERSITY

BY

SERHAN ERGİN

IN PARTIAL FULFILLMENT OF THE REQUIREMENTS
FOR
THE DEGREE OF THE MASTER OF SCIENCE
IN
CIVIL ENGINEERING

JUNE 2014

Approval of the thesis:

COMPARISON OF MEASURED AND PREDICTED CONSOLIDATION SETTLEMENTS IN SOFT GROUND

submitted by **SERHAN ERGİN** in partial fulfillment of the requirements for the degree of **Master of Science in Civil Engineering Department, Middle East Technical University** by,

Prof. Dr. Canan Özgen _____
Dean, Graduate School of **Natural and Applied Science**

Prof. Dr. Ahmet Cevdet Yalçıner _____
Head of Department, **Civil Engineering Dept., METU**

Asst. Prof. Dr. Nejan Huvaj-Sarıhan _____
Supervisor, **Civil Engineering Dept., METU**

Examining Committee Members:

Prof. Dr. Erdal Çokça _____
Civil Engineering Dept., METU

Asst. Prof. Dr. Nejan Huvaj Sarıhan _____
Civil Engineering Dept., METU

Prof. Dr. Bahadır Sadık Bakır _____
Civil Engineering Dept., METU

Inst. Dr. Kartal Toker _____
Civil Engineering Dept., METU

Zuhal Etkesen _____
Geogis City Information Systems Mapping
And Environmental Eng. Cons. Co.

Date: _____

I hereby declare that all information in this document has been obtained and presented in accordance with academic rules and ethical conduct. I also declare that, as required by these rules and conduct, I have fully cited and referenced all material and results that are not original to this work.

Name, Last name : Serhan Ergin

Signature :

ABSTRACT

COMPARISON OF MEASURED AND PREDICTED CONSOLIDATION SETTLEMENTS IN SOFT GROUND

Ergin, Serhan

M.Sc., Department of Civil Engineering

Supervisor: Asst. Prof. Dr. Nejan Huvaj-Sarıhan

June 2014, 158 pages

Accurate prediction of consolidation settlement of soft clay and silt deposits has always been a topic of interest for geotechnical engineers. The objective of this study is to investigate the use of a few different computational tools for the realistic prediction of consolidation settlement in soft ground. During the literature review phase of this study, one well-documented case history of embankment constructed on soft ground with prefabricated vertical drains has been selected for further analyses. For the selected case history, detailed subsoil profiles, measured settlements and pore water pressures at certain depths with time were collected. Settlement of soft ground was calculated by using different mehtods such as finite element method (using PLAXIS software) and analytical method based on Terzaghi consolidation theory (using SETTLE3D software). The results were compared with the measured values of settlements with time in the field.

Keywords: Finite Element Analysis, Prefabricated Vertical Drains, Soft Soil, Consolidation

ÖZ

YUMUŞAK ZEMİNLERDE ÖLÇÜLEN VE ÖNGÖRÜLEN KONSOLİDASYON OTURMALARININ KARŞILAŞTIRILMASI

Ergin, Serhan
Yüksek Lisans, İnşaat Mühendisliği Bölümü
Tez Yöneticisi: Yrd. Doç. Dr. Nejan Huvaj-Sarıhan
Haziran 2014, 158 sayfa

Yumuşak kil ve silt zeminlerin konsolidasyon oturmalarının hatasız öngörülebilmesi, geoteknik mühendisleri için her zaman ilgi çekici bir konu olmuştur. Bu çalışmanın amacı, yumuşak zeminlerdeki konsolidasyon oturmalarının gerçeğe yakın öngörülebilmesi için birkaç farklı sayısal hesaplama aracının kullanımının incelenmesidir. Bu çalışmanın kaynak taraması kısmında; bir yumuşak zemine teşkil edilmiş ve yazılı olarak iyi desteklenmiş dolgular, sonraki analizler için seçilmiştir. Seçilen vaka geçmişi için, detaylı zemin profili (ör: boşluk oranı, aşırı konsolidasyon basıncı ve sıkışma indisinin derinliğe bağlı profili) belli derinlikler ve zamanlarda ölçülmüş oturma ve boşluk suyu basıncı değerleri edinilmiştir. Yumuşak zemindeki oturma, Terzaghi'nin konsolidasyon teorisine dayanan analitik metot (Settle3D yazılımı kullanılarak) ve sonlu elemanlar metodu (PLAXIS yazılımı kullanılarak) analiz edilmiştir. Hesaplamaların sonuçları, ölçülmüş arazi değerleri ile karşılaştırılmış ve yorumlanmıştır.

Anahtar Kelimeler: Sonlu Elemanlar Analizi, Prefabrike Düşey Drenler, Zayıf Zemin, Konsolidasyon

ACKNOWLEDGEMENTS

I would like to thank my advisor Asst. Prof. Dr. Nejan Huvaj-Sarıhan for her guidance and support throughout the preparation of this thesis.

My next appreciation goes to my colleague Cemre Harzem Yardım. I believe this thesis would not be completed without his contributions.

Finally, I must thank Mr. Sina Kiziroğlu who provided the case data for this study.

TABLE OF CONTENTS

LIST OF FIGURES

LIST OF TABLES

CHAPTER 1

INTRODUCTION

Soft soil modelling has always been a major problem for geotechnical engineering. Soft soils, due to their high compressibility and low hydraulic conductivity characteristics, experience significant consolidation settlements under vertical loads. Due to low shear strength and low hydraulic conductivity of soft soils, design of foundations on soft ground have two major concerns. Namely, the bearing capacity safety of the foundation and the amount of time required for consolidation settlements.

In order to improve the foundation soil to avoid instability, soft soils can be improved by various methods such as preloading (surcharging) with or without vertical drains, vacuum preloading, stone columns with or without geosynthetic encasing, grouting etc. Preloading is one of the most practical and economical techniques that is used frequently for improvement of soft soils. Preloading involves loading the ground to develop a greater part of the ultimate settlement that the ground will experience after the constuction loading. After the significant amount of settlements take place (i.e. void ratio decreases), the surcharge is removed and construction proceeds.

For the purpose of controlling the development of excess pore water pressures and reducing the consolidation period, as well as for the weak soil to gain strength with time under each incremental surcharge loading, surcharging is typically applied in stages, with rest periods provided between each stage. This is also necessary because an embankment of more than several meter thickness cannot be constructed safely and easily in one stage with the current construction equipments. For the excess pore

water pressures to dissipate more quickly, a vertical drain system is installed in the soft soil body to provide shorter drainage path for quicker excess pore water dissipiation.

The installation of vertical drains in soft ground before the surcharge loading has become commonplace after the invention of prefabricated band drains (Kjellman, 1948) and their further development. The advantages of prefabricated vertical drains (PVDs) are, mainly, the shortening of the drainage distance and consolidation time and improvement of the soft soil to gain strength.

1.1 Problem Statement

Surcharching with prefabricated vertical drains has been used extensively to improve soft soils. And there have been significant amount of research looking into this problem. However, based on a detailed review of the literature, it appears that, the behaviour of soft soils with PVDs (specifically the time-settlement and time-pore water pressure response of the soft ground), still, cannot be predicted accurately. Therefore, the following points seem to require further evaluation.

When constructing PVDs in soft ground, there occurs a certain disturbance around the drain which is called “smear zone”. The effect of thickness of this smear zone (smear zone diameter) and the degree of disturbance of the soft ground (soil parameters) in the smear zone, are still needed to be investigated through numerical analyses. In addition, the effect of other possible factors on the consolidation behaviour of soft soil improved by PVDs are investigated to provide further understanding.

The problem of soft soil improvement by PVDs are analyzed by either analytical or numerical methods. The accuracy of various methods in predicting the field settlement-time behaviour of soft soils needs to be studied in detail. The field performance of PVDs are investigated to compare the available methods. An

embankment with preloading with PVDs case study of Republic of Turkey General Directorate of Highways (Karayolları Genel Mudurlugu, KGM) is used in this thesis. The embankment is analyzed with both numerical finite element and analytical methods (Terzaghi consolidation theory and Asaoka methods) and results are compared with site observations. The results of computations by various methods are compared with the site observations. Afterwards a parametric study is performed on the case in order to investigate the effects of different factors on the consolidation of PVD improved soft soil.

1.2 Research Objectives

The research objectives of this study are:.

1) To investigate the accuracy of the available methods to predict the settlement versus time and excess pore water pressure versus time behaviour of soft soils improved with PVDs. The results are compared with real field performance of a soft soil improved by PVDs.

2) To determine the influence of various factors such as the disturbance of the surrounding soil, the thickness of the disturbed region, drain penetration length and drain spacing, etc. on the performance of soft soil improved by PVDs.

1.3 Scope

The main scope of this thesis is described as; the comparison of analytical and numerical computational tools to analyze the behaviour of a soft soil improved by PVDs and the investigation of factors that affect the consolidation rate. Based on the prevalence of 2D finite element modelling in practical projects and because of time constraints, 2D finite element analyes are used in this study. Study is limited to the data of the used case history.

The scope of the thesis: In chapter 2, a review of the current literature is provided. In the following chapter, the case study is presented with available information about soil properties, laboratory testing and measurements available. Chapter 3 also includes analysis with various methods to predict the real measured field performance. In chapter 4, a parametric study is carried out which investigates the effect of various factors on the behaviour of soft soils improved with PVDs. Some of the factors considered are the smear zone thickness around the drain, the disturbance and soil properties within the smear zone, the spacing of vertical drains and the length of drains as compared to the compressible layer thickness. In the final chapter, discussion of results and conclusions are provided together with suggested future study topics.

CHAPTER 2

REVIEW OF LITERATURE

2.1 Prefabricated Vertical Drains

The consolidation settlement of soft ground brings a lot of problems in geotechnical engineering. Due to the very low hydraulic conductivity of soft soils, the primary consolidation takes long time to complete. In order to shorten the time required for consolidation, vertical drains are installed together with the application of preloading.

Vertical drains are defined as artificially created drainage paths which can have a variety of physical characteristics. By this method, pore water which is drained out from the soil body due to the hydraulic gradients caused by the loading, can flow faster towards the vertical drains in the horizontal direction and then flow freely through the drain in the vertical direction. Therefore, the installation of vertical drains in a soil body reduces the drainage path lengths and thus reduces the time for completion of the consolidation process (Figure 2.1.).

2.1.1 History and Development of Vertical Drains

In order to improve soft soils, different types of systems of drainage have been used over the past few decades. The development of prefabricated vertical drains paralels the development of the vertical sand drains. A patent for a system of sand drains was granted in 1926 in USA by Daniel J. Moran, an American engineer.

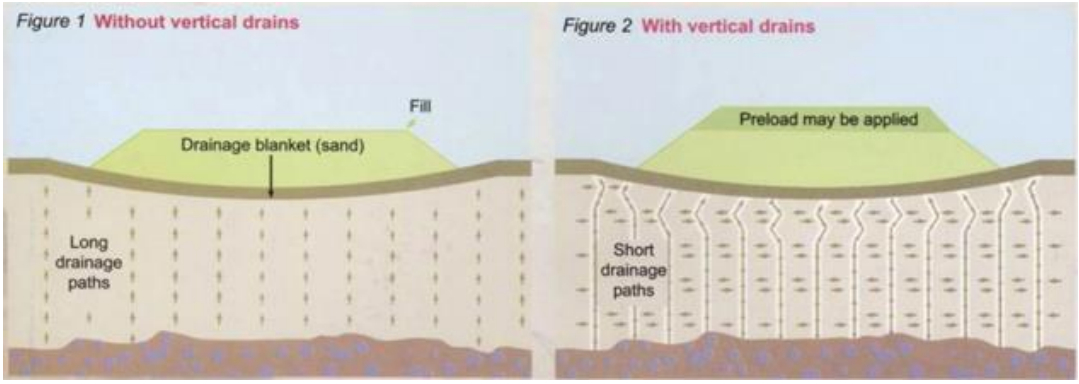

Figure 2.1 Benefit of using wick drains (HTTP://WWW.GEOSİNİNDO.CO.İD/WP-CONTENT/UPLOADS/2011/06/6-1.PNG)

Prefabricated vertical drains were first used by Walter Kjellman in 1937 (Sathananthan, 2005). Kjellman installed the prefabricated drains using tubes made from wood/fibre material in a field test. Seeing that this kind of tubes are not appropriate and also expensive, Kjellman invented and patented a band-shaped cardboard drain and a method for driving it into the soil, in 1939. This cardboard wick was produced by glueing two cardboard sheets. The wick had external dimensions 100 mm wide and 3 mm thick and had included 3 mm wide and 1 mm thick longitudinal internal channels (Figure 2.2).

The efficiency of the so called cardboard wick drains was first studied at Lilla Melosa, Sweden, in a full scale field test. After the development of the first band drain by Akzo in 1970 and the fast improvement of geotextiles and geomembranes technology, the band shaped prefabricated drains has become widespread; for instance in Sweden Geodrain, in England Alidrain, in Netherlands Mebradrain types of PVDs were developed. Actually more than 50 different types of PVDs are used worldwide (Indraratna et al., 2010).

PVDs have been used in a greater variety of projects in the last few years. While in the beginning PVDs were used mainly in transportation projects, nowadays they have been used also in other construction types such as housing projects, industrial

plants, warehouses, shopping centers, etc. Additionally, PVDs are now used in hazardous waste remediation and stabilization of very deep mine tailing ponds. It should have been noted that recent studies are mainly focused on the use of PVDs to reduce the liquefaction potential of fine grained soils.

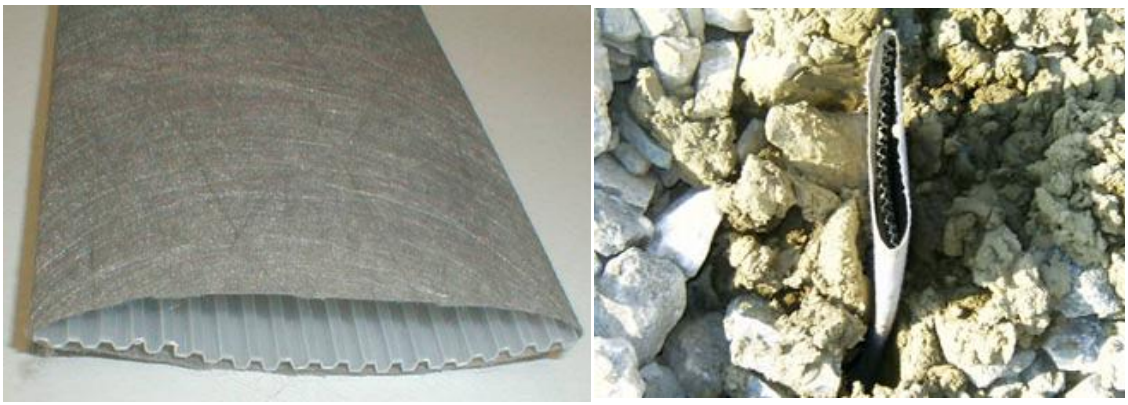

(a) (b)

Figure 2.2 (a) Inner channels and outer geotextile material of a PVD (http://www.layfieldgeosynthetics.com/Content_Files/Images/Product/wick-3.jpg), (b) Picture of a PVD Installed on Site (HTTP://ZETAS.COM.TR/İNDEX.PHP?DİL=TR&İD=211000)

2.1.2 Types of Vertical Drains

There are a variety of types of vertical drains used for soft soil improvement. The first were sand drains which were cylindrical in shape and constructed by conventional piling equipment and with a large spacing. Realizing that the performance of drains directly depend on the spacing of drains, a smaller diameter sand drain called the sandwick was used where sand is contained in a geotextile filter sock. After sandwicks, primarily the cardboard drains and finally the different types of prefabricated band drains were developed (Figure 2.3).

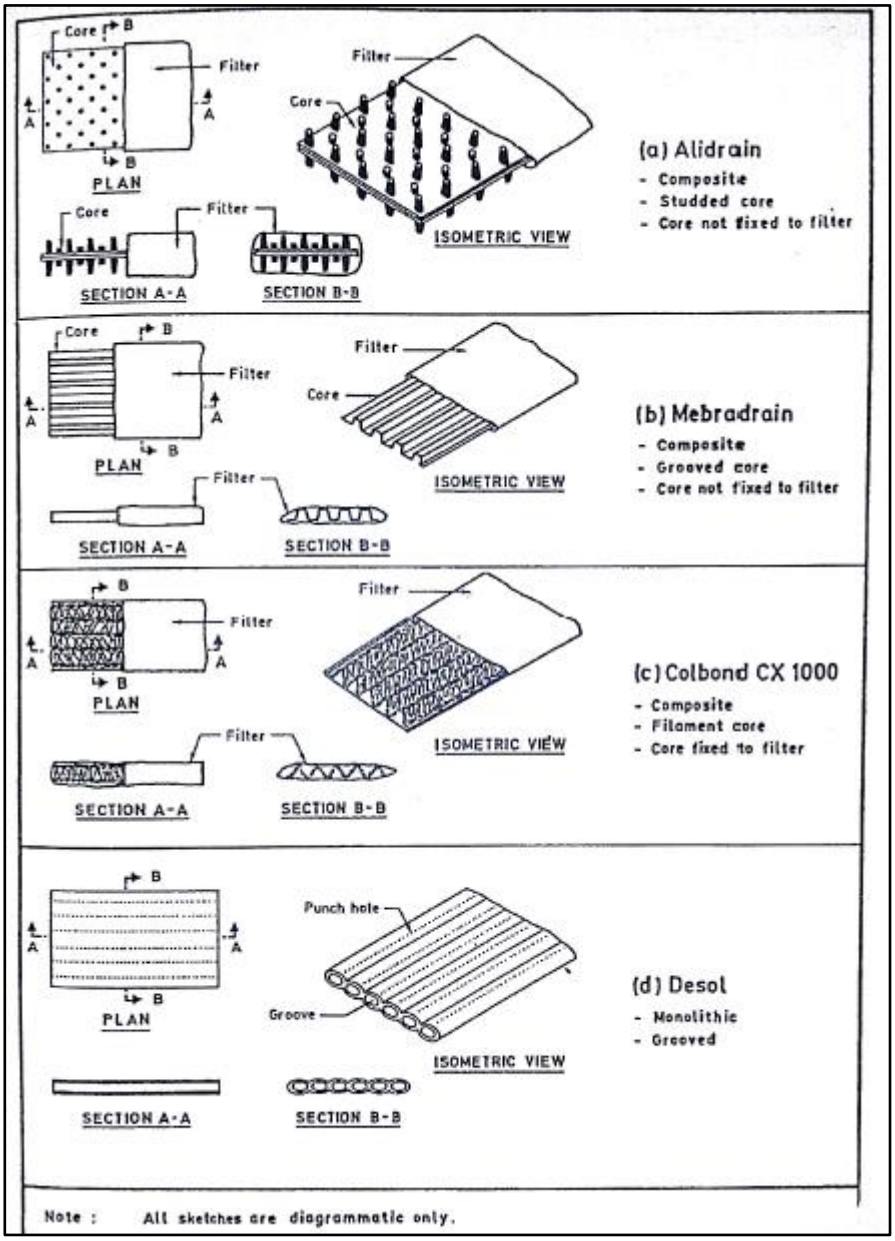

Figure 2.3 Configurations of different types of PVDs

2.1.2.1. Sand Drains

Sand drains collect the pore water from adjacent ground and by its relatively high permeability transfers water to the drained surface. The discharge capacity of a sand drain is determined by the sand's hydraulic conductivity. At first 30-70 cm diameter sand drains were used, however later sandwicks with average diameter of 50 mm had

taken place. Another type of sand drains is sand compaction piles, where the sand is compacted during its constructions in order to carry more loads.

Sand drains have certain disadvantages, some of which are listed below (Sathananthan, 2005):

i) It is mostly difficult to find an appropriate sand material near the site.
ii) Due to excessive lateral soil displacements and instabilities of the drill holes , sand drains may become discontinuous.
iii) Relatively large diameter of sand drains may result in construction problems.
iv) The effect of reinforcement of the sand drains may cause inefficiency of the preloading for the consolidation.

2.1.2.2 Prefabricated Vertical Drains

The types of commercially available PVDs has increased rapidly after the first prefabricated drain used by Kjellman. Prefabricated vertical drains are consisted of conceptually an inner channel part which is surrounded by a permeable filter jacket. After the first use of band drains by Akzo in 1970 and the recent rapid development of geotextile technology, the filter jackets of today's drains are made from synthetic geotextiles which provides higher tensile strength. Most common types of prefabricated band drains have 100 mm x 4 mm dimensions.

PVDs are more efficient than sand drains mainly because thay can be easily installed, thus saves time and money. Band drains are usually installed with the help of a steel mandrel by static pull down or vibratory techniques (Figures 2.4. and 2.5.). Since the vibratory techniques create more excess pore pressure and more disturbance in the soil, static pushing may be preferable.

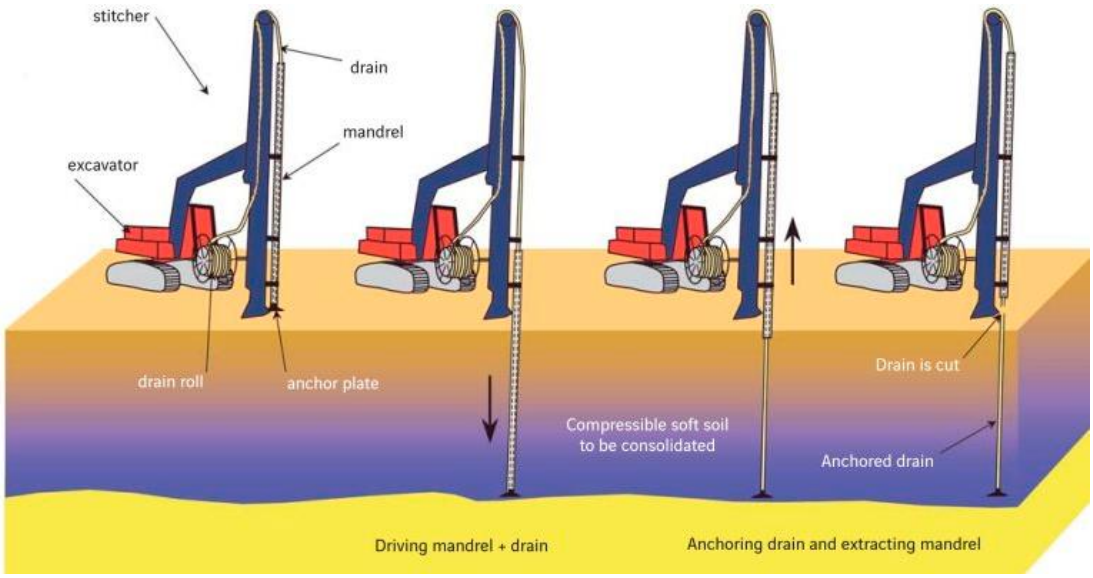

Figure 2.4 Installation of wick drains by a mandrel

(HTTP://İMG.ARCHİEXPO.COM/PDF/REPOSİTORY_AE/61481/VERTİCAL-WİCK-DRAİNS-89296_2B.JPG)

Figure 2.5. Mandrel-installed wick drains at a site

(HTTP://WW1.PRWEB.COM/PRFİLES/2010/06/15/1793074/WİCKDRAİN.JPG)

2.1.3. Properties of Vertical Drains

2.1.3.1. Equivalent Diameter of Band Shaped Vertical Drain

Most prefabricated vertical drains are rectangular in cross section. However for design and analysis, the conventional radial consolidation theory assumes a circular drain cross section. So, the rectangular cross section with dimensions a (width) and b (thickness) has to be converted into a circle with equivalent diameter, d_w.

Kjellman (1948) suggested that "the draining effect of a drain depends to a great extent upon the circumference of its cross-section, but very little upon its cross-sectional area". According to Hansbo (1979), based on the numerical analyses, circular and band shaped drains lead to approximately the same consolidation when their circumference are the same. According to the above suggestion, by equating the circumference of the two shapes, the equivalent diameter, d_w of a band shaped drain with width *a* and thickness *b* can be defined as

$$d_w = \frac{2(a+b)}{\pi} \qquad (2.1)$$

In order to take into account the throttle effects near the drain, Atkinson and Eldred (1981) suggested that a reduction factor of 1/2 should be applied to equation (2.1):

$$d_w = \frac{(a+b)}{\pi} \qquad (2.2)$$

Fellenius and Castonguay (1985) proposed to calculate the equivalent drain diameter based on the cross sectional area of the drain:

$$d_w = \left[\frac{4(ab)}{\pi}\right]^{0.5} \qquad (2.3)$$

More recently, using an electrical analoge field plotter, Long and Covo (1994) suggested to compute d_w as follows:

$$d_w = 0.5a + 0.7b \qquad (2.4)$$

Rixner et al. (1986), taking into account the shape of the band-shaped drains and the drainage area, suggested to take d_w as the average of the width and thickness of the drain:

$$d_w = \frac{(a+b)}{2} \qquad (2.5)$$

There is no research which definitely concludes that one of these approaches is superior to the others (Figure 2.6.). Different studies on this topic supports each of them seperately. As it is the most commonly used approach among the above equations, Hansbo (1979) suggestion for the equivalent drain diameter is used in this study.

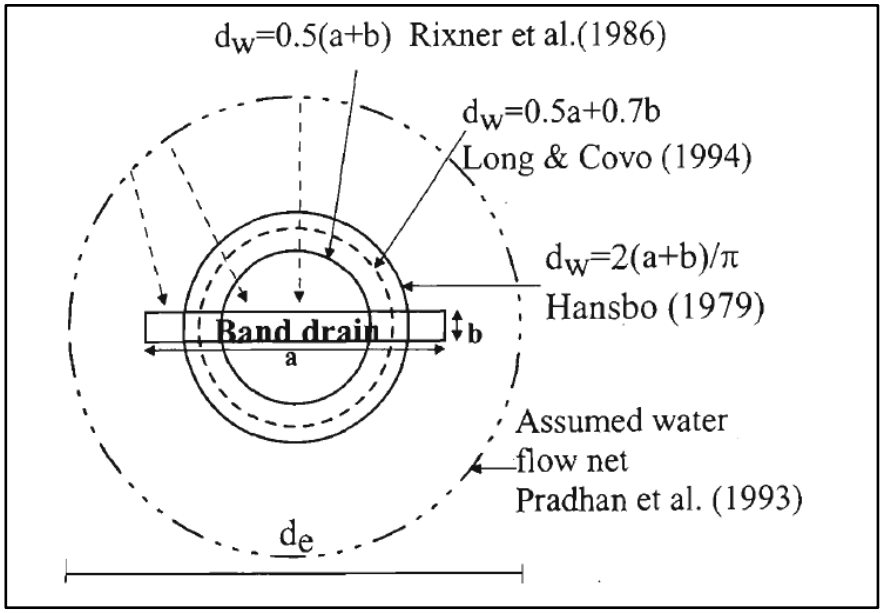

Figure 2.6 Different Proposals for the Equivalent Diameter of a Band-Shaped Drain (reproduced from Indraratna et al., 2003)

2.1.3.2. Diameter of the Influence Zone

PVDs are usually installed either in a square or triangular pattern as shown in Figure 2.7. Most of the vertical drain consolidation analysis approaches assumes a unit cell where both the drain and its influence zone are cylindrical. For the influence area, often a cylinder is defined with an equivalent cross sectional area. Hansbo (1981) suggested to determine the influence zone diameter in terms of spacing, S, as follows:

$$De = 1.13\ S \quad \text{(for square pattern)} \tag{2.6}$$

$$De = 1.05\ S \quad \text{(for triangular pattern)} \tag{2.7}$$

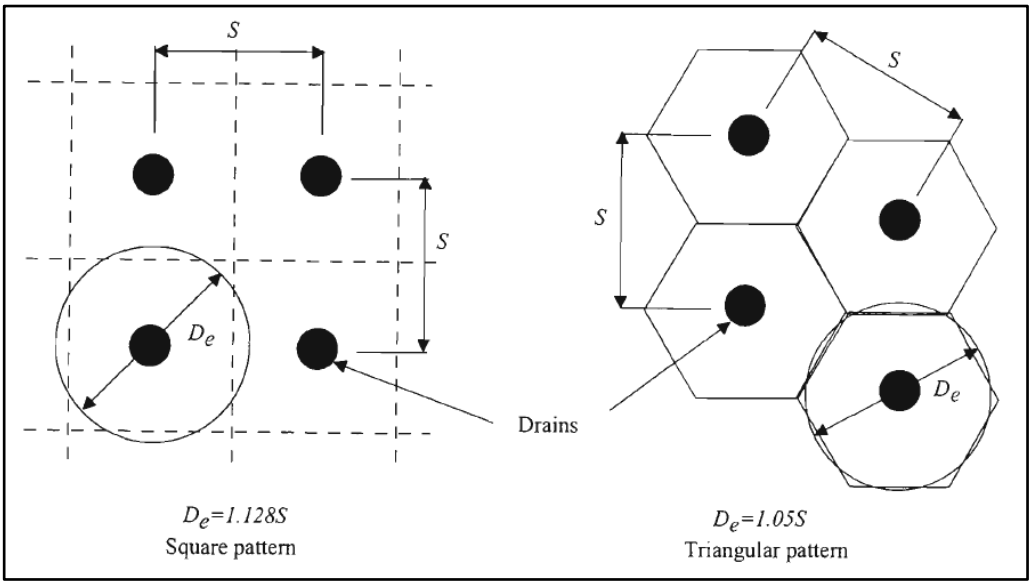

Figure 2.7 Influence zone of PVDs with different installation patterns (Sathananthan, 2005)

2.1.4. Factors Affecting the Consolidation with Vertical Drains

2.1.4.1. Smear Zone

PVDs are installed in the ground with the help of a steel mandrel which is penetrated into the soil by vibrating or static pushing methods. When mandrel is withdrawn from soil, it leaves the drain installed in the subsoil. This mentioned process results in remoulding of the soil near the mandrel which in turn causes significant changes in the permeability characteristics of the soil adjacent to the drain. The adjacent soil zone which is disturbed, remoulded and have a smaller value of lateral permeability is called the "smear zone".

In order to efficiently model the smear zone, two major properties that has to be known are the smear permeability and the diameter of the smear zone. However, there has been no standard method for measuring these properties either in the field or in the laboratory. Studies performed on the smear zone in the field and also in laboratory showed that there occurs a continuous variation of lateral permeability in the radial distance away from the center of the drain (Onoue et al. 1991; Madhav et al. 1993; Bergado et al. 1996, Sharma and Xiao 2001). The mentioned permeability variation is suggested by various researchers to be divided into 3 main regions:

i) an inner smear zone where the permeability is greatly reduced due to remoulding,
ii) an outer smear zone where the permeability is slightly reduced due to the change in the void ratio during the installation process,
iii) the undistubed zone where the soil permeability is not changed.

For the modelling purposes, the use of three different but constant lateral permeability values for the above mentioned three zones helps to obtain closed form solutions for the drain installed soil consolidation. However, because of the complex permeability changes in the horizontal direction, the solution for this approach is

difficult. For practical purposes, the transition zone across where the permeability is changed in the horizontal direction can be replaced by an equivalent smear zone.

For the estimation of the smear zone permeability, several researchers have proposed different equations. Some of the researchers suggested that the horizontal permeability within the smear zone is equal to the vertical permeability (Hansbo, 1981; Bergado et al. 1991; Indraratna & Redana, 1998). Based on the laboratory tests on the specimens taken from different distances in the horizontal direction from the drain have shown that the smear zone permeability near the soil is decreased to one fifth of the undisturbed soil permeability (Madhav et al., 1993). Indraratna and Redana (2000) stated that the ratio of undisturbed soil permeability to smear zone permeability can change from 1 to 8.

Indraratna & Redana (1998) have concluded that the horizontal permeability decreases in a non-linear manner within the smear zone towards the drain. Walker and Indraratna (2007) concluded that the difference between the consolidation degrees resulted from a linear and a non-linear variation of permeability is insignificant since the undisturbed soil permeability and the minimum smear zone permeability approach the same value.

Smear zone diameter, which is the second necessary property to model the smear zone, is also studied by various reseachers and different proposals are reported in the literature. Since the mandrels used to install the drains in the subsoil are not necessarily cylindrical in shape, estimation of equivalent smear diameter brings a further problem. Most of the researchers suggested to take smear zone diameter as 2~3 times the diameter of the well or the equivalent diameter of the mandrel (Akagi, 1977; Indraratna&Redana, 1998; Sharma&Xiao, 2000).

The degree of distubance which is expressed as the reduced lateral permeability is the most affecting factor for the consolidation (Basu et al., 2009). Within the smear zone, the inner smear zone which is defined above is found to be the dominant factor

for the consolidation process (Hawlader et al., 2002). Table 2.1 summarizes the smear zone parameter proposals by different researchers.

Table 2.1 Proposed smear zone parameters (after Xiao, 2001)

Source	Smear Zone Radius	Smear Permeability	Remarks
Barron (1948)	$r_s = 1.6r_w$	$k_h/k_s=3$	Assumed
Hansbo (1979)	$r_s = 1.5\sim3.0r_w$	*Open*	Based on available literature at that time
Hansbo (1981)	$r_s = 1.5r_w$	$k_h/k_s=3$	Assumed in case study
Bergado et al. (1991)	$r_s = 2.0r_w$	$k_h/k_v=1$	Laboratory investigation and back analysis for Bangkok soft clay
Onoue (1991)	$r_s = 1.6r_w$	$k_h/k_s=3$	From test interpretation
Almeida et al. (1993)	$r_s = 1.5\sim2.0r_w$	$k_h/k_s=3\sim6$	Based on experiences
Indraratna et al. (1998)	$r_s = 4.0\sim5.0r_w$	$k_h/k_v=1.15$	Laboratory investigation (for Sydney clay)
Chai and Miura (1999)	$r_s = 2.0\sim3.0r_w$	$k_h/k_s=C_f(k_h/k_s)$	Cf the ratio between laboratory and field values
Hird et al. (2000)	$r_s = 1.6r_w$	$k_h/k_s=3$	Recommenden dor design
Xiao (2000)	$r_s = 4.0r_w$	$k_h/k_s=1.3$	Laboratory investigation (for Kaolin clay)

r_s: radius of smear zone, k_s: smear zone permeability, r_w: radius of equivalent drain, k_h: horizontal permeability, and k_v: vertical permeability

2.1.4.2. Well Resistance

The discharge capacity of the PVD is required to analyse the drain (well) resistance issue. The function of PVD is to receive all the radial flow coming from the nearby consolidating soil, and to transfer this flow in the vertical direction. Most vertical drains have a finite discharge capacity, i.e. there is an upper limit to the drain discharge.

$$q_w = \pi \cdot r_w^2 \cdot k_w \qquad (2.8)$$

Where k_w is the permeability of the drain. The discharge capacity of PVDs depends considerably on the make of the drain. Additionally, the discharge capacity decreases

as lateral pressure on the soil increases. This can be caused by the reduction of the cross sectional area of the drain resulting from the squeezing in of the filter into the channels, or, for drains without filter sleeve, the squeezing of channels themselves together. Sengul et al. (2013) found that a 40% decrease in discharge capacity is observed when lateral stress is increased from 25 kPa to 200 kPa. Sengul et al. (2013) noted that clogging of the core zone, shapes of deformation, structure of PVD, and resistance against buckling have varying effects on the discharge capacity of PVDs depending on the soil type.

Bo (2004) found that the drain discharge capacities measured in the field are the highest during the first months after installation. For most spacings, field measured discharge capacities are two orders of magnitude lower than the maximum discharge capacity measured at initial stage.

Well resistance is defined as the resistance to flow of water through the well. With increasing drain length the well resistance increases and thus lengthens the consolidation time. It retards the dissipation of pore pressure and the settlement. Besides the drain length, deterioration of the filter which is in turn the reduction of drain cross section, intrusion of silt into the filter which causes the reduction of pore space the drain folding, are the other factors which increases well resistance.

The well resistance is controlled by the parameters q_w, the drain's discharge capacity; l_m, the maximum drainage length and k_h, the lateral permeability of the soil. Mesri and Lo (1991) studied the flow within the vertical drain. The well resistance factor, R, can be defined based on the Mesri's equations as,

$$R = \frac{q_w}{k_h . l_m^2} \tag{2.8}$$

Based on the field performance of wick drains Mesri and Lo (1991) suggested that for R greater than 5, well resistance is negligible. Using typical values for k_h and l_m

for soft clays and vertical drain installations, minimum q_w value required for negligible well resistance can be found to be 2 to 80 m^3/year (Mesri et al. 1996). These q_w values are needed only at the beginning of consolidation, because as k_h decreases during consolidation (with time), less water will enter into the drain and a smaller q_w will be sufficient. The proposals for the well resistance factor of different researchers who investigated the influence of finite drain discharge on the radial condolidation are summarized in Table 2.2.

Table 2.2 Proposals for well resistance factor (Sathananthan, 2005)

Source	Well Resistance Factor
Aboshi and Yoshikuni (1967)	$Ri = \frac{(n^2-1)}{4F(n)n^2}\ \frac{k_h}{k_w}\ \left[\frac{l_m}{r_w}\right]^2 = \frac{\pi(n^2-1)}{4F(n)n^2}\ \frac{1}{R}$
Yoshikuni and Nakanodo (1974) and Onoue (1988)	$L = \frac{8}{\pi^2}\ \frac{k_h}{k_w}\ \left[\frac{l_m}{r_w}\right]^2 = \frac{8}{\pi}\ \frac{1}{R}$
Hansbo (1981)	$W = 2\ \frac{k_h}{k_w}\ \left[\frac{l_m}{r_w}\right]^2 = 2\pi\ \frac{1}{R}$
Stamatopoulos and Kotzias (1985)	$Ri = \frac{1}{F(n)}\ \frac{k_h}{k_w}\ \left[\frac{l_m}{r_w}\right]^2 = \frac{\pi}{F(n)}\ \frac{1}{R}$
Zeng and Xie (1989)	$G = \frac{1}{4}\ \frac{k_h}{k_w}\ \left[\frac{l_m}{r_w}\right]^2 = \frac{\pi}{4}\ \frac{1}{R}$
Mesri and Lo (1989)	$R = \pi\ \frac{k_h}{k_w}\ \left[\frac{l_m}{r_w}\right]^2 = \frac{q_w}{k_h (l_m)^2}$

The rate of radial consolidation depends not only on k_h and D_e, but also on q_w/k_h ratio when well resistance is taken into account.

Well resistance may have a significant effect on the consolidation rate when very long PVDs are used with q_w/k_h values typically less than $500m^2$ (Jamiolkowski et al., 1983). When the drain lengths are not very long, most of the commercial PVDs' discharge capacities have almost no effect on the consolidation of clay (Indraratna et

al., 1994). For values of q_w greater than 150 m^3/year and if the drains are shorter than 30 m, probably there would not be any incrase in the consolidation time. Based on the studies in the literature, it can be claimed that when the drain lengths are not very long, for commercial PVDs, the well resistance effects are negligible.

2.1.4.3. Macro Fabric of Soil

The effectiveness of PVDs depend also on the macro fabric of the subsoil. This means the ratio of horizontal permeability (k_h) to vertical permeability (k_v) of the soil is an important factor for PVDs' performance, because as the k_h/k_v ratio increases the benefit that is to be taken from the vertical drains also becomes greater.

Another important property that affects the performance of PVDs is the existence of any lateral sand or silt lenses in the body of the soil. Because these lenses will provide a shorter drainage path for pore water to PVDs they may have an effect on the consolidation behaviour of the PVD improved soil. However, if the the sand or silt lenses are continuous in the horizontal direction and if the number of these lenses are high, there occurs a rapid drainage of the pore water independant of the PVDs are installed or not, that is to say, the effectiveness of PVDs decreases in this case.

2.2 Development of Consolidation Theories

2.2.1. One – Dimensional Consolidation

Terzaghi's (1923) one-dimensional consolidation theory is the first rational and quantitative approach for the deformation problem of soft soils which was also considered by many as the birth of modern soil mechanics. Since then, the prediction of a deformation problem is a major concern of geotechnical studies and many contributions are made still today.

The one-dimensional governing equation for the pore water pressure dissipation proposed by Terzaghi is as follows:

$$\frac{\partial u}{\partial t} = c_v \frac{\partial^2 u}{\partial z^2} \tag{2.9}$$

Here, u is the excess pore water pressure, t is time, z is the vertical coordinate and c_v is the coefficient of consolidation in the vertical direction, which can be expressed as,

$$c_v = \frac{k_v}{\gamma_w m_v} \tag{2.10}$$

where k_v is the coefficient of vertical permeability, γ_w is the unit weight of water and m_v is the coefficient of volume compressibility.

Several assumptions are made in deriving Equation (2.9). These assumptions are listed below:

- The soil is fully saturated and homogeneous
- Water and soil particles are incompressible
- Darcy's linear flow rule is valid
- Compression and flow are one-dimensional and vertical
- Soil skeleton follows time independent constitutive law
- External loading is applied suddenly and remains unchanged
- Soil deformations are small
- The permeability is constant throughout the soil and throughout the consolidation process
- Soil is isotropic and linearly elastic.

2.2.2. Coupled Consolidation Theory

One of the theories for two or three dimensional consolidation is derived directly from the Biot's (1941) theory of elasticity and is commonly known as the Biot's theory. This theory couples the magnitude and time dependent behaviour of displacement, i.e. it takes into account the continuous interaction between dissipating excess pore pressure and changing total stress at any point in the soil medium consolidating. In terms of excess pore pressure, Biot's equation is as follows:

$$G\nabla^2 u_i + \frac{G}{(1-2v)}\frac{\partial \varepsilon}{\partial x_i} + \frac{\partial u}{\partial x_i} = 0 \qquad (i = 1\sim3) \tag{2.11}$$

$$\frac{\partial \varepsilon}{\partial t} = -\frac{k}{\gamma_w}\ \nabla^2 u \tag{2.12}$$

Here, x_i is cartesian coordinate, k is permeability constant, u_i is the displacement in the x_i direction, G is shear modulus, ∇^2 is the Laplacian operator ($\nabla^2 = \Sigma\frac{\partial^2}{\partial x_i^2}$) and ε is the volumetric strain.

Because there occurs a certain amount of stress redistribution in two or three dimensional problems, it has to be noted that, the degree of consolidation is no longer the average degree of dissipated pore pressure.

2.3. Development of Vertical Drain Consolidation Theories

All of the analytical solutions developed for the radial consolidation of a soft soil which is improved by vertical drains uses the "unit cell" model which is illustrated in the Figure 2.8. Taking into consideration that the water flow towards a vertical drain is axisymmetric, the so called unit cell model is a reasonable and appropriate approach for the problem.Theories for radial consolidation around a vertical drain has been studied by many investigators (Rendulic, 1936; Carillo, 1942; Barron,

1948; Yoshikuni and Nakanodo, 1974; Hansbo, 1981, 1997; Onoue, 1988a, 1988b; and Zeng and Xie, 1989).

2.3.1. Rendulic and Carillo Diffusion Theory

For one-dimensional vertical deformation by radial pore water flow is formulated by Rendulic (1936) as follows:

$$\frac{\partial u}{\partial t} = c_h \left(\frac{\partial^2 u}{\partial r^2} + \frac{1}{r} \frac{\partial u}{\partial r} \right) \tag{2.13}$$

where r is radial coordinate, c_h is the horizontal coefficient of consolidation.

Based on the Equation (2.13), Carillo (1942) found that the excess pore pressure $u_{r,z}$, can be expressed as;

$$\frac{\partial u}{\partial t} = c_h \left(\frac{\partial^2 u}{\partial r^2} + \frac{1}{r} \frac{\partial u}{\partial r} \right) + c_v \frac{\partial^2 u}{\partial z^2} \tag{2.14}$$

$$u_{r,z} = \frac{u_r u_z}{u_0} \tag{2.15}$$

where, u_r and u_z are respectively the excess pore water pressure due to radial and vertical flow only and u_0 is the initial pore water pressure.

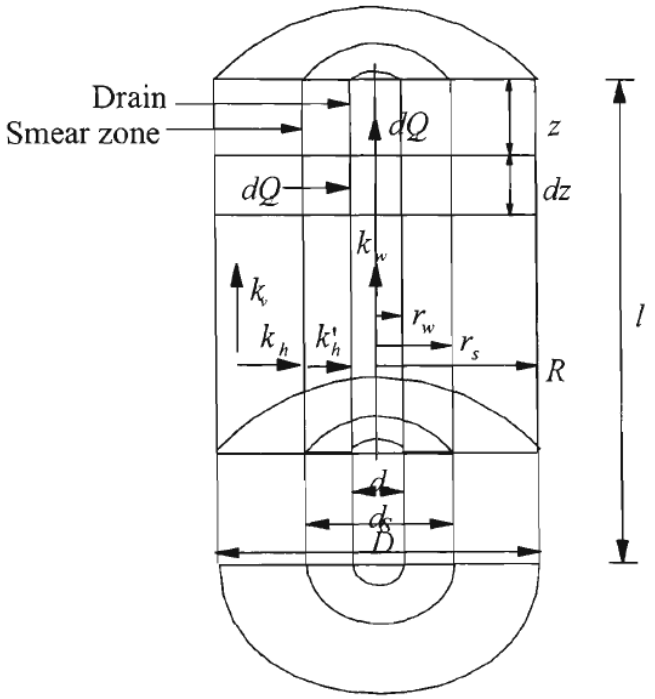

Figure 2.8 Schematic view of a unit cell model for a vertical drain
(after Hansbo, 1979)

The average degree of consolidation can be expressed by the combination of $\overline{U}_z$, the average degree of consolidation in the vertical direction obtained from Terzaghi's equation and $\overline{U}_r$, the average degree of consolidation in the radial direction obtained from Rendulic's equation, by substituting the average excess pore water pressure into Equation (2.15) which gives,

$$(1 - \overline{U}) = (1 - \overline{U}_z)(1 - \overline{U}_r) \qquad (2.16)$$

where, $\overline{U}$ is the average degree of consolidation of the soft soil at time *t* for combined vertical and radial flow.

Both Rendulic's and Carillo's proposals accounts for drains with infinite discharge capacity and no smear zone.

2.3.2. Barron's (1948) Proposal – Equal Strain Hypothesis

Barron (1948) included the smear effect in the solution for consolidation behaviour of a PVD improved soft soil. Barron found solutions to the extreme cases for a radial drainage problem, namely "free strain" and "equal strain" conditions.

"The free strain hypothesis" assumes that the load is uniform over a circular influence zone and the differential settlements do not affect the stress redistribution by arching of the fill load. On the contrary, "the equal strain hypothesis" assumes that arching occurs in the upper layer without any differential settlement in the clay layer, that means the vertical strain is uniform along a horizontal section of the soil.

It is shown that there is not any significant difference between the predicted pore pressures calculated by equal strain and free strain hypotheses and thus, the approximate solution of "equal strain hypothesis" gives satisfactory results compared to the "free strain hypothesis" solution.

Barron (1948) proposed a solution for the excess pore pressure for the case of radial flow only incorporating the smear effect and based on the Terzaghi's assumptions. Barron's solution is given as;

$$u_r = \overline{u_r}\frac{1}{v}\left[ln\left(\frac{r}{r_s}\right) - \frac{(r^2 - r_s^2)}{2R^2} + \frac{k_h}{k_h'}\left(\frac{n^2 - s^2}{n^2}\right)\ln(s)\right] \quad (2.17)$$

where,

$$\bar{u} = u_0 exp\left[-\frac{8T_h}{v}\right] \quad (2.18)$$

Here, r is the drain radius; r_s is the smear zone radius, R is the soil cylinder radius, k_h

is the horizontal permeability of the undisturbed soil, k_h' is the horizontal permeability in the smear zone. Smear factor, ν, is given by;

$$\nu = F\,(n, s, k_h, k_h') = \left[\frac{n^2}{n^2 - s^2} ln\left(\frac{n}{s}\right) - \frac{3}{4} + \frac{s^2}{4n^2} + \frac{k_h}{k_h'}\left(\frac{n^2 - s^2}{n^2}\right)\ln(s)\right] \qquad (2.19)$$

where, n is the spacing ratio and defined as $n=R/r_w$ and s is the smear zone extent factor and expressed as $s=r_s/r_w$.

In this case, the average degree of consolidation $\overline{U}_r$ is given by;

$$\overline{U}_r = 1 - \frac{u}{\bar{u}_0} = 1 - exp\left[-\frac{8T_h}{\nu}\right] \qquad (2.20)$$

Here, T_h is the time factor for radial drainage and is expressed as:

$$T_h = \frac{c_h t}{D_e^2} \qquad (2.21)$$

The radial consolidation coefficient, *ch* is given as:

$$c_h = \frac{k_h(1+e)}{a_v \gamma_w} \qquad (2.22)$$

where e is the void ratio and a_v is the coefficient of compressibility.

2.3.3. Rigorous Solution (Yoshikuni and Nakanode, 1974)

Based on the "free strain hypothesis", Yoshikuni and Nakanode (1974) developed a rigorous solution for the consolidation with vertical drain problem. In this solution, the smear effect is not taken into consideration, whereas well resistance is taken into account.

Below, the governing equation for the consolidation of a soil cylinder with vertical drain at r=r_w and at depth z is given:

$$\left(\frac{\partial^2 u}{\partial z^2}\right)_{r_w} + \frac{2}{r_w}\frac{k_h}{k_w}\left(\frac{\partial u}{\partial t}\right)_{r_w} = 0 \qquad (2.23)$$

k_w is the hydraulic conductivity of the drain.

The effect of well resistance on the analytical solution of the problem is taken into account by the following factor, L, which is expressed as;

$$L = \frac{32}{\pi^2}\frac{k_h}{k_w}\left(\frac{l_m}{d_w}\right)^2 = \frac{8}{\pi}\frac{k_h l_m^2}{q_w} \qquad (2.24)$$

2.3.4. Hansbo (1981) Solution

Hansbo's (1981) approximate solution is based on the equal strain hypothesis and it takes into account both the smear and well resistance effects on the radial consolidation of a soft soil with vertical drain. The general approach of this solution is similar as illustrated in the Figure 2.8. The average degree of consolidation at depth z, $\bar{U}_{rz}$ can be represented by the below expression as proposed by Hansbo (1981):

$$\bar{U}_{rz} = 1 - exp\left[-\frac{8T_h}{\mu}\right] \qquad (2.25)$$

Here, the factor of smear zone, μ is given as;

$$\mu = \frac{n^2}{n^2-1}\left[ln\left(\frac{n}{s}\right) + \left(\frac{k_h}{k_h'}\right)\ln(s) - 0.75\right] + \frac{s^2}{n^2-1}\left(1 - \frac{s^2}{4n^2}\right)$$

$$+\frac{k_h}{k_h'}\frac{1}{n^2-1}\left(\frac{s^2-1}{4n^2}-s^2+1\right)+\pi z(2l-z)\frac{k_h}{q_w}\left(1-\frac{1}{n^2}\right) \qquad (2.26)$$

Neglecting the minor significant terms, Equation (2.26) becomes;

$$\mu=\left[ln\left(\frac{n}{s}\right)+\left(\frac{k_h}{k_h'}\right)\ln(s)-0.75\right]+\pi z(2l-z)\frac{k_h}{q_w} \qquad (2.27)$$

2.3.5. λ - Method (Hansbo, 1975 and 1997)

The theory of radial consolidation of a soil with vertical drain (Barron, 1948) and its development assumes that Darcy's linear flow rule is valid. However, it is later shown that during the consolidation process permeability is subjected to a gradual reduction. A deviation from the Darcy's flow rule was observed at small permeability values during the laboratory researches performed by Hansbo (1960) on Ska-Edeby clay. As a result, replacing the Darcy's flow rule of $v=k.i$ by exponential flow correlation was concluded to be appropriate. Giving that n is exponential correlation factor, exponential flow correlation is represented as follows:

$$v=\kappa.i \quad when \quad i\le i_l \qquad (2.28a)$$

$$v=\kappa n\, i_l^{n-1}(i-i_0) \quad when \quad i\ge i_l \qquad (2.28b)$$

Here, $i_0 = i_l\,(n-1)/n$ is thresold gradient, below which no flow takes place.

An alternative equation for consolidation based on the exponential flow concept was suggested by Hansbo (1979,1997) based on the full-scale tests at Ska-Edeby, Sweden. Therefore, the average degree of consolidation is related with time as follows:

$$\overline{U}_r = 1 - \left[1 + \frac{\lambda t}{\alpha D^2}\left(\frac{u_0}{D\gamma_w}\right)^{n-1}\right]^{\frac{1}{n-1}} \qquad (2.29)$$

Here, λ is the coefficient of consolidation and is given as, $\lambda = \kappa_h M/\gamma_w$. $M=1/m_v$ where m_v is the oedometer modulus of volume compressibility, D is the influence zone diameter, $\alpha = n^{2n}\,\beta^n / 4(n-1)^{n+1}$ and β is given omitting the minor significance terms by;

$$\beta = \frac{1}{3n-1} - \frac{n-1}{n(3n-1)(5n-1)} - \frac{(n-1)^2}{2n^2(5n-1)(7n-1)}$$

$$+\frac{1}{2n}\left[\left(\frac{\kappa_h}{\kappa_s}-1\right)\left(\frac{D}{d_s}\right)^{1/(n-1)} - \frac{\kappa_h}{\kappa_s}\left(\frac{D}{d_w}\right)^{1/(n-1)}\right]$$

$$+\frac{\left(1-\frac{1}{n}\right)\left(\frac{d_w}{D}\right)^{1-\frac{1}{n}}\left(1-\frac{d_w^2}{D^2}\right)\kappa_h \pi z(2l-z)}{2q_w} \qquad (2.30a)$$

Substituting the last term in the above expression for,

$$\frac{\left(1-\frac{1}{n}\right)\left(\frac{d_w}{D}\right)^{1-\frac{1}{n}}\left(1-\frac{d_w^2}{D^2}\right)\kappa_h \pi l^2}{3q_w} \qquad (2.30b)$$

the average degree of consolidation, $\overline{U}_{r,avg}$, of the whole layer can be obtained.

It should be noted that, Equation (2.30) yields the same result with the Equation (2.25) assuming $\lambda=c_h$ and $\kappa_h/\kappa_s=k_h/k_s$ when the exponent $n\rightarrow 1$.

2.4. 2-D Modelling of Vertical Drains

Consolidation with vertical drains is an axisymmetrical problem by nature. However, finite element analyses are performed in 2D conditions commonly, which means the analyses are performed under "plane-strain" conditions. Therefore, in order to analyze a vertical drain consolidation problem with a 2D finite element tool, the unit cell, consisting of the central vertical drain surrounded by the soil cylinder has to be converted into plane-strain conditions. Figure 2.9 shows the conversion of a unit cell into plane-strain conditions (Hird et al. 1992).

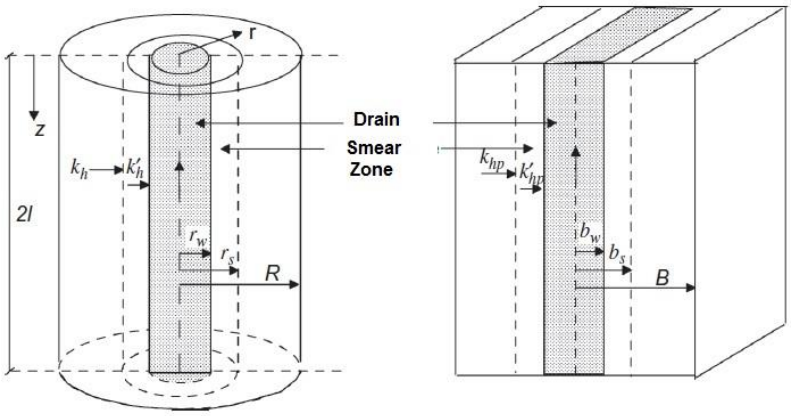

Figure 2.9 Conversion of an axisymmetric unit cell into plane-strain conditions (Hird et al. 1992)

The aforementioned conversion may be achieved in different ways. For instance;

i) *Geometric matching*, in which the drain spacing is matched accordingly in order to convert the problem into plane strain while the permeability remains the same,

ii) *Permeability matching*, in which the coefficient of permeability is matched while drain spacing remains the same, and

iii) *Combined matching*, in which for a convenient drain spacing the plane strain permeability is calculated (Indraratna and Redana, 1997).

2.4.1. Permeability Transformation (Shinsha et al. 1982)

Shinsha et al. (1982) were the first to propose an acceptable matching criterion for the conversion of an axisymmetrical unit cell into plane strain conditions. Assuming that the required time for a 50% degree of consolidation in both conditions are the same, the equivalent coefficient of horizontal permeability in plane-strain condition was computed as given below:

$$\frac{k_{pl}}{k_{ax}} = \left(\frac{B}{D_e}\right)^2 \frac{T_{h50}}{T_{r50}} \tag{2.31}$$

Here, k_{pl} is the permeability in plane-strain condition, k_{ax} is the permeability in axisymmetric condition, T_{r50} is time factor for 50% consolidation of radial flow and T_{h50} = 0.197 is a dimensionless time factor for 50% consolidation of laminar flow.

2.4.2. Hird et al. (1992) – Combined Matching

Hird et al. (1992) presented a matching procedure based on the Hansbo's (1981) theory, neglecting the well resistance effect. Matching equation is given below.

$$\frac{k_{pl}}{k_{ax}} = \frac{2B^2}{3R^2\left[ln\left(\frac{R}{r_s}\right) + \left(\frac{k_{ax}}{k_s}\right) ln\left(\frac{r_s}{r_w}\right) - \frac{3}{4}\right]} \tag{2.32}$$

In this equation, subscripts *ax* and *pl* stands for axisymmetric and plane-strain conditions respectively. In order to account for well resistance, it can be matched independently by satisfying the below conditions:

$$\frac{Q_w}{q_w} = \frac{2B}{\pi R^2} \tag{2.33}$$

It has to be noted that, only geometric matching can be done by substituting $k_{pl}=k_{ax}=k_h$ in Equation (2.32) and similarly, permeability matching can be obtained by substituting B=R in the same equation.

2.4.3 Rigorous Solution for Parallel Drain Wall – Indraratna and Redana (1997)

Indraratna and Redana (1997), while converting the axisymmetric vertical drain system into a plane-strain unit cell (i.e. equivalent parallel drain wall), assumed that the half width of unit cell, *B;* the half width of drain, *bw*; and the half width of smear zone, *bs* are equal to their axisymmetric radii, *R*, *rw* and *rs* respectively. Resultantly, the average degree of consolidation in the plane-strain condition is found as;

$$\bar{U}_{hp} = 1 - \frac{\bar{u}}{u_0} = 1 - exp\left[-\frac{8T_{hp}}{\mu_p}\right] \tag{2.34}$$

where *Thp* is the time factor for consolidation of lateral flow in the plane-strain condition. Here;

$$\mu_p = \left[\alpha + (\beta)\frac{k_{hp}}{k'_{hp}} + (\theta)(2lz - z^2)\right] \tag{2.35}$$

where, k_{hp} and k_{hp}' are equivalent lateral permeabilities for undisturbed and smear zone of the soil respectively, in the plane-strain condition.

Equivalent plane-strain permeability matching can be expressed as follows:

$$\frac{k_{hp}}{k_h} = \frac{\left[\alpha + (\beta)\frac{k_{hp}}{k'_{hp}} + (\theta)(2lz - z^2)\right]}{\left[ln\left(\frac{n}{s}\right) + \left(\frac{k_h}{k'_h}\right)ln(s) - \frac{3}{4} + \pi(2lz - z^2)\frac{k_h}{q_w}\right]} \tag{2.36}$$

In Equation (2.36), if the well resistance is ignored, that means omiting the terms containing *l* and *z*, then the effect of smear zone can be represented by the smear zone permeability to the undisturbed permeability ratio as given by;

$$\frac{k'_{hp}}{k_{hp}} = \frac{\beta}{\left[ln\left(\frac{n}{s}\right) + \left(\frac{k_h}{k'_h}\right) ln(s) - \frac{3}{4} - \alpha\right]} \tag{2.37}$$

If both smear and well resistance effects are ignored, then the ratio of plane-strain to axisymmetric permeability ratio, proposed by Hird et al. (1992) earlier can be get readily:

$$\frac{k_{hp}}{k_h} = \frac{0.67}{\left[ln(n) - \frac{3}{4}\right]} \tag{2.38}$$

α, β and θ parameters used in the above equations are defined as:

$$\alpha = \frac{2}{3} - \frac{2b_s}{B}\left(1 - \frac{b_s}{B} + \frac{b_s^2}{3B^2}\right) \tag{2.39}$$

$$\beta = \frac{1}{B^2}(b_s - b_w)^2 + \frac{b_s}{3B^3}(3b_w^2 - b_s^2) \tag{2.40}$$

$$\theta = \frac{2k_{hp}^2}{k'_{hp} q_z B}\left(1 - \frac{b_w}{B}\right) \tag{2.41}$$

Indraratna and Redana (1997) have studied the validity of this procedure by analyzing a consolidation of soft clay improved with vertical drains and subjected to a certain embankment load. They have found that, taking into account the smear effect gives more accurate results for the equivalent plane-strain analyses.

2.5. Analysis Methods

2.5.1. Finite Element Analysis

Exact solutions are available to a limited extent in geotechnical problems. On the other hand, approximate solutions may be obtained by using numerical analyses. One of the numerical modelling methods is the finite element (FE) method. FE method, divides the surface, structure or region in the model to a finite number of elements. In practice, 2D modelling in FE analyses is commonplace. 2D analyses are generally suitable for plane-strain and axisymmetric conditions. In this study, the problem of vertical drain consolidation is analyzed under 2D plane-strain conditions. In this study the finite element analysis tool, called Plaxis (version 8.2) is used for FE analyses.

While performing the analyses, the selection of element type is important. Plaxis(v.8.2) offers two element types; 6-node triangular and 15-node triangular elements (Figure 2.8). In order to maximize the accuracy of the results, 15-node triangular elements are used. So called 15-node triangular elements contains 12 stress points where the stress computations take place. It also provides 4 element interpolation functions for displacements.

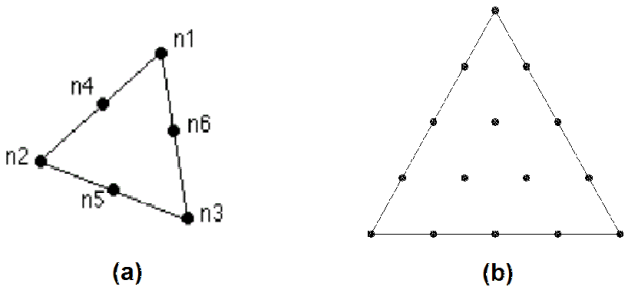

Figure 2.10 (a) 6-node triangular element, (b) 15-node triangular element (reproduced from Plaxis 2D Tutorial Manual)

For the modelling of pore pressures in Plaxis, five drainage types exist which can be summarized as follows:

i) drained type model in which the excess pore pressure generation is not taken into consideration;

ii) undrained type model, where undrained effective stress analysis is performed using effective stiffness and effective strength parameters;

iii) non-porous type model in which neither the pore pressures nor the initial stresses are taken into account.

In this study, the consolidation analyses are performed using undrained type model, in order to investigate the performance of the Soft Soil (Creep) Model and also see the generation and dissipation of excess pore pressures within the model analyzed.

For the generation of initial stresses within the analyzed model, Plaxis uses either the so-called K_0 procedure or the Gravity loading. Gravity loading is preferred for calculating initial stresses in a sloping ground. K_0 procedure is a special method of calculating the stresses in the soil body which takes into account the loading history of the subsoil. In practice, the value of K_0 for a normally consolidated soil is often taken as in the Jaky's formula, K_0=1-sinφ. For an over-consolidated soil, K_0 is expected to be larger than the value gotten from this expression. For advanced soil models (e.g. Soft Soil model, Hardening Soil model) the value is based on the parameter K_0^{nc} (K_0^{nc} is the K_0 value associated with normally consolidated states of stress which is based on the Jaky's formula) and is also affected by the overconsolidation ratio or the pre-overburden stress. Within the context of this study, K_0 procedure is used where the body stresses are calculated by the K_0 factor.

In the calculation phase, Plaxis offers different types of calculation processes. These are, i) *plastic analysis, ii) consolidation analysis, iii) phi/c reduction analysis*, and *iv) dynamic anlysis*. In order to properly model the generation and dissipation of excess pore water pressures, *consolidation analysis* is used.

One of the most crucial issues while performing a numerical analysis is the selection of the soil model to be used. In this study, for the accurate calculations of the pore water pressures and the consolidation settlements, Plaxis' advanced model called *Soft Soil* model is used in the analyses.

2.5.1.1. Soft Soil Model

In the *Soft Soil* model, a logarithmic relation between the volumetric strain, ε_v, and the mean effective stress, *p'*, is assumed (Figure 2.11). This relationship is expressed as follows:

$$\varepsilon_v - \varepsilon_v^0 = -\lambda^* \, ln\left(\frac{p'}{p^0}\right) \qquad (virgin\ compression) \qquad (2.42)$$

where, λ^* is the modified compression index, that determines the compressibility of the material in primary loading.

During isotropic unloading and reloading, a different line is followed, which is formulated below:

$$\varepsilon_v^e - \varepsilon_v^{e0} = -\kappa^* \, ln\left(\frac{p'}{p^0}\right) \qquad (unloading\ and\ reloading) \qquad (2.43)$$

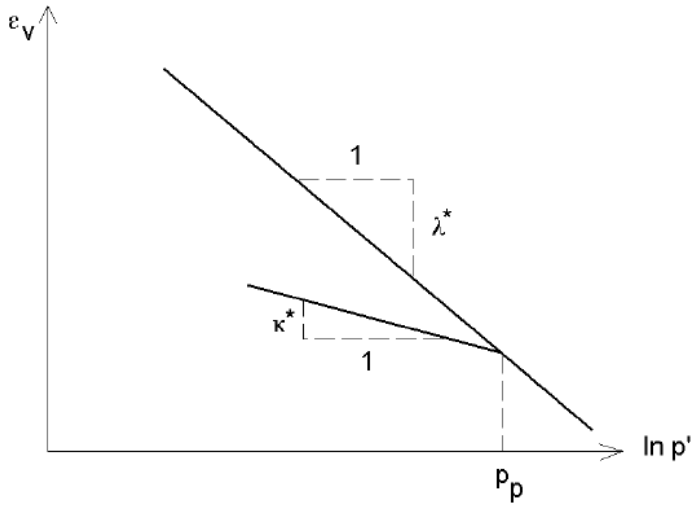

Figure 2.11 Logarithmic relationship between volumetric strain and mean stress (Plaxis v.8, Material Models Manual)

Here, the parameter κ* is the modified swelling index which determines the compressibility behaviour during the unloading and reloading conditions. The soil deformation is assumed to be elastic during unloading and reloading as denoted by superscript *e* in Equation (2.43). Equation (2.43) refers to a linear dependency on the tangent bulk modulus, that can be expressed as follows:

$$K_{ur} = \frac{E_{ur}}{3(1-2\nu_{ur})} = \frac{p'}{\kappa^*} \tag{2.44}$$

For the triaxial stress state (i.e. σ_2'= σ_3'), the yield function of the Soft Soil model is defined as;

$$f = \bar{f} - p_p \tag{2.45}$$

where, $\bar{f}$ is a function of stress state and defined as follows:

$$\bar{f} = \frac{q^2}{M^2(p' + c\ cot\varphi)} + p' \tag{2.46}$$

Here, p_p is the pre-consolidation pressure and is a function of plastic strain:

$$p_p = p_p^0 \, exp\left(\frac{-\varepsilon_v^p}{\lambda^* - \kappa^*}\right) \tag{2.47}$$

As can be seen from Figure 2.12, the yield function, *f* is an ellipse in the *p'-q* plane. The *M* parameter in Equation (2.46) determines the height of the ellipse which means that the ratio of horizontal to vertical stresses is dependent on *M*.

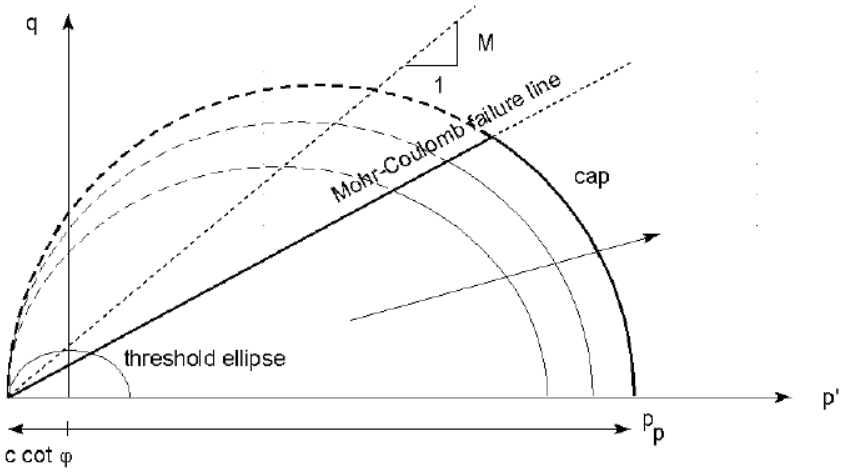

Figure 2.12 Yield surface of the Soft Soil model in p'-q-plane (Plaxis 2D Material Models Manual)

In Soft Soil model, Equation (2.45) determines the plastic volumetric strain in primary compression and builds the cap for the yield surface. In order to model the state of failure, a perfectly plastic Mohr-Coulomb type yield function is used which accounts for a straight line in *p'-q-plane* as shown of Figure 2.12. Mohr-Coulomb failure line has a slope which is smaller than the slope of the M-line.

The bold lines in Figure 2.12 which represents the total yield contour, is the elastic stress area boundary. The failure line is fixed whereas, the cap may increase in primary compression. Within this boundary, stress paths give strain increments that are elastic, on the other hand, stress paths crossing this boundary give both elastic and plastic strain increments.

The plastic behaviour of the Soft Soil model, for general stress states, is expressed by six functions; three of which are the compression yield functions and the other three are the Mohr-Coulomb yield functions. In principal stress space, the total yield envelope, is shown on Figure 2.13 (Plaxis v.8, Material Models Manual).

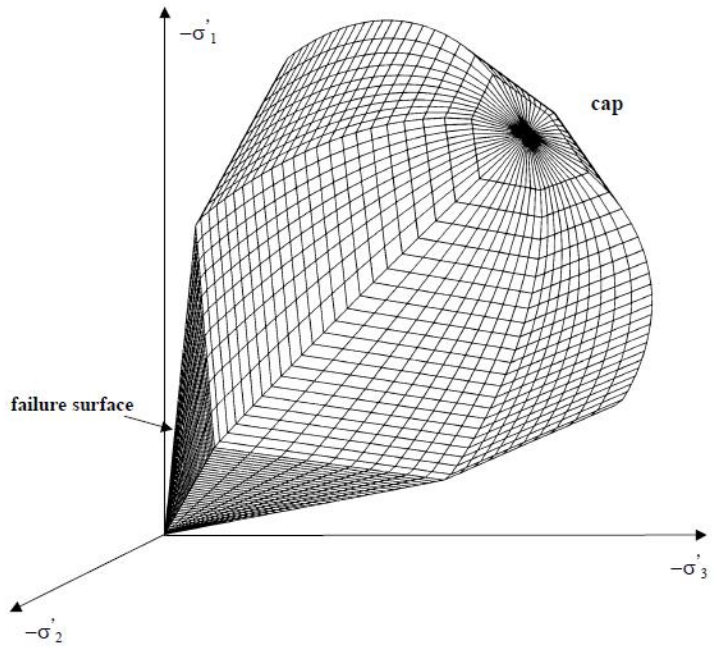

Figure 2.13 Failure envelope of Soft Soil Model in principal stress space
(Plaxis v.8, Material Models Manual)

2.5.1.2. Soft Soil Creep Model

Soft Soil Creep Model is an advanced soil model of Plaxis, which additionally takes into account secondary compression (creep) while making the other computations same as the Soft Soil Model.

Buisman (1936) proposed the following equation to describe reep behaviour under constant effective stress (Plaxis v.8, Material Models Manual):

$$\varepsilon = \varepsilon_c - C_B \log\left(\frac{t}{t_c}\right) \tag{2.42}$$

where ε_c is the strain up to the end of consolidation, t is the time measured from the beginning of loading, t_c the time to the end of primary consolidation and C_B is a material constant.

2.5.1.2. Important Aspects of Finite Element Modelling

While constructing the model of the problem studied, special care must be taken for some points. One of them is the modelling of the surcharge load. If the embankment load is modelled as a surface load, the lateral spreading force caused by the embankment fill and the embankment stiffness are not taken into account. So, to model the surcharge load more realistically, an embankment fill should be built up in the model (Chai and Bergado, 1993).

Since the subsoil hydraulic conductivity has a major effect on the consolidation, and this hydraulic conductivity changes during the loading and consolidation processes, significant changes occur on the permeability of the subsoil before and after the yield. Therefore, using constant permeability values can not model the whole problem realistically (Chai and Bergado, 1993). For a number of soft clays the relation between void ratio and permeability as measured in the laboratory can be

seen in Figure 2.14. The decrease in void ratio and therefore permeability during consolidation process can be taken into account by the term $C_k = \Delta e / \Delta \log k$ and for most soft clay deposits the empirical relation $C_k = 0.5e_o$ is applicable (Terzaghi et al. 1996).

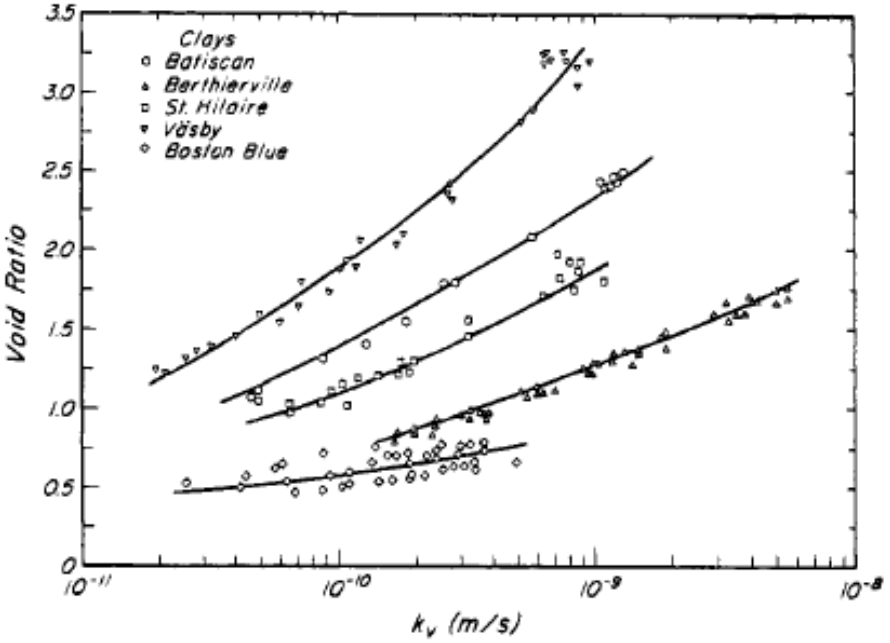

Figure 2.14 Change in permeability with change in void ratio during consolidation (Mesri et al. 1996)

Madhav et al. (1993) suggested to make additional assumptions for the nodes of the interface beacuse using two different and constant permeability values for the smear and the undisturbed zone results in problems due to the discontinuities at the interface.

Another important aspect of finite element analysis the phenomenon of updated mesh analysis. In conventional finite element analysis, the influence of the geometry change of the mesh on the equilibrium conditions is neglected. Since the deformations are relatively small in most engineering structures this approximation is usually good. However, when the deformations are large and the geometry changes

can not be neglected throughout an analysis an updated mesh analysis may be necessary (Plaxis 2D, Reference Manual). This particular feature of large displacement theory is dealt with adopting a definition of stress rate that includes rotation rate terms. In Plaxis, the co-rotational rate of Kirschoff stress is adopted. The theory of co-rotational stress rate phenomenon is far behing the scope of this study so the details of this particular theory is excluded from these explanations.

2.5.2. Analytical Method

For the purpose of comparing the numerical analyses with the analytical solutions, some of the analyzed conditions are solved by analytical methods. Within the context of this study, a software code, *Settle 3D* is used for this purpose. It performes the consolidation analysis, according to the one-dimensional consolidation equations in the literature. Depending on the model to be used, it can compute the settlement either by the linear approach, or by non linear approach.

The linear consolidation model in Settle 3D is the conventional solution for the consolidation, which is as follows:

$$\Delta\varepsilon = m_v \ \Delta\sigma' \tag{2.42}$$

where m_v is the coefficient of volume compressibility.

On the other hand, in the non-linear material model, modulus is a function of stress. The relationship between the modulus is generally shown on the void ratio vs. logarithm of effective stress (Figure 2.15).

P_c is the preconsolidation stress. Knowing that, C_c is the compression index and C_r is the recompression index, the vertical strain is calculated in terms of void ratio by;

$$\Delta\varepsilon = \frac{C_r}{1+e_0} log\left(\frac{P_c}{\sigma_i'}\right) + \frac{C_c}{1+e_0} log\left(\frac{\sigma_f'}{P_c}\right) \quad (2.42)$$

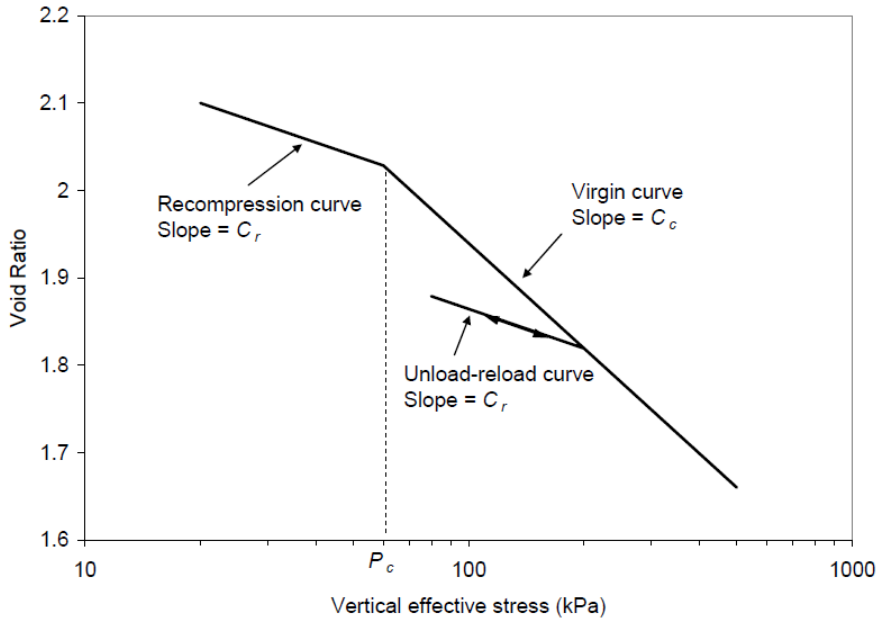

Figure 2.15 Relation of Void Ratio vs. Logarithm of Vertical Effective Stress (Settle 3D Theory Manual)

For the secondary compression calculation, Settle3D uses the analytical method which is based on the parameter C_α, secondary compression index. The change in vertical strain for a change in time frim t1 to t2 within the secondary compression period, is calculated by the following formulae:

$$\Delta\varepsilon_s = \frac{C_\alpha}{1+e_p} log\left(\frac{t_2}{t_1}\right) \quad (2.43)$$

where e_p is the void ratio at the end of primary consolidation.

For linear soil model however, since there is no void ratio associated with the material, strain based secondary compression index, $C_{\alpha\varepsilon}$ is used instead of C_α, where,

$$C_{\alpha\varepsilon} = \frac{C_\alpha}{1 + e_p} \qquad (2.44)$$

2.6. Prediction of the End of Primary Consolidation by Asaoka (1978) Method

For the prediction of the end of primary (EOP) settlement, a graphical method known as the Asaoka Graphical Procedure (Asaoka, 1978) is widely used because of its relative accuracy and simplicity. The procedure, simply, is as follows:

i. Plot the observed settlement values against time taken.
ii. Select a settlement series, S_1, S_2, S_3,…, S_j, S_{j+1} respectively at times t_1, t_2, t_3, …, t_j, t_{j+1}. Note that, $t_{j+1} - t_j$ is constant.
iii. Plot S_{j+1} against S_j which gives a straight line.
iv. Extrapolate the line to intersect a 45^0 line through origin. The point of intersetion defines EOP settlement, S_{100}, and the slope of the line is used to estimate C_v or C_h.

Asaoka graphical prediction method assumes consolidation takes place in one-dimension. Besides, a constant load for settlement is assumed and also the soil material is taken as homgeneous.

Limitations of the Method:

Asaoka graphical method for settlement prediction has some limitations. One of the limitation of the method is that the settlement data should have been recorded at regular time intervals. Because of constructional and scheduling constraints, it is very difficult to record the data with that order. Since there occurs inconsistencies is data recorded, an interpolation becomes necessary which results in decreased accuracy.

Time intervals between data points also have effect on the accuracy of the method. As the interval increases, the intersection and the angle between the 45^0-line and the

trendline becomes more distinct. Therefore, as the time interval increases estimation gets more accurate.

On the other hand, longer time intervals implies that the settlement should be observed for a longer period of time or otherwise data points would be few to make the estimation. At the early periods of settlement, as there occurs large differences between data points, it is almost impossible to apply the Asaoka method. Asaoka graphical procedure is more accurate as time passes and more data points are recorded, however sometimes it is not very helpful as settlement prediction is desired as early as possible.

One of the limitations of the Asaoka method is that in order to make a prediction, the settlement vs. time curve should start to flatten out. Before the curve begins to flatten, the trendline is almost parallel to the 45^0-line, therefore an accurate intersection could not be found.

Tan and Chew (1996) have showed that prediction made by the Asaoka procedure will be accurate in terms of EOP settlement value and the coefficient of consolidation only if the data recorded stays beyond 60% consolidation.

Additionally, when secondary compression takes place a divergence error is about to occur between the trendline and 45^0-line. This is because the rate of settlement change is prevented from approaching to zero under the effect of secondary compression which means that an intersection does not occur between the curves.

2.7. Determination of the End of Primary Consolidation - The Logarithm of Time Method (Casagrande and Fadum, 1940)

For determination of end of primary consolidation for a given settlement vs. time data, Casagrande and Fadum (1940) proposed the following method which is based on a graphical procedure.

Procedure is briefly explained below:

i) Plot the dial readings of settlement for a given load increment on a semilog paper, as shown in Figure 2.16.

ii) Project the straight line portions of primary consolidation and secondary consolidation to intersect at T. The dial reading corresponding to T, d_{100}, is the settlement for %100 primary consolidation.

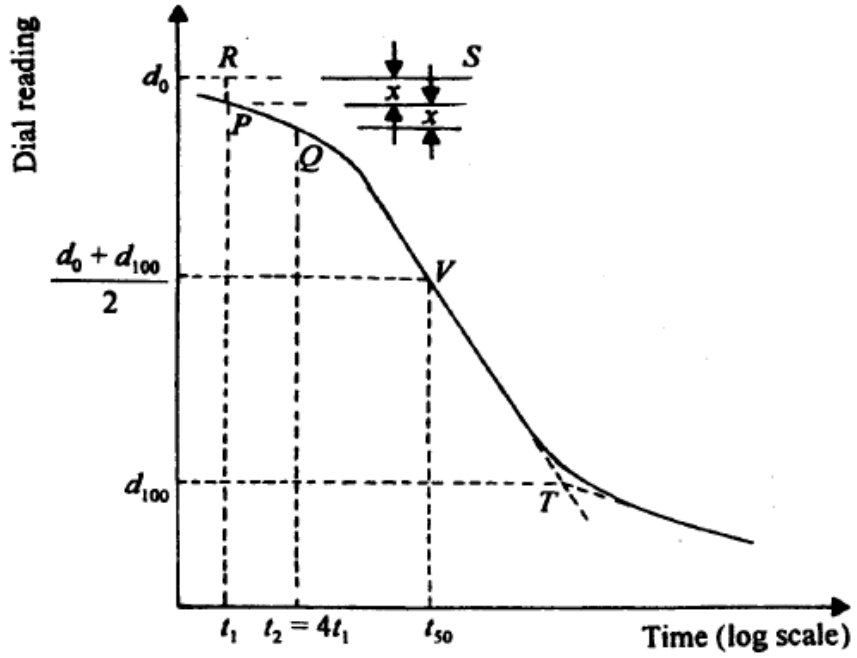

Figure 2.16 Logarithm of time method for determination of end-of-primary consolidation (Das, 1997)

2.8. Determination of the End of Primary Consolidation - The Square-Root-of-Time Method (Taylor, 1942)

The graphical procedure to determine the end of primary consolidation from a given dial reading versus time data, proposed by Taylor (1942) is as follows (Das, 1997):

i) Plot the dial reading and the corresponding square root of time as shown in Figure 2.17 below.

ii) Draw the tangent PQ to the early portion of the plot.

iii) Draw a line PR such that OR = (1.15)(OQ)

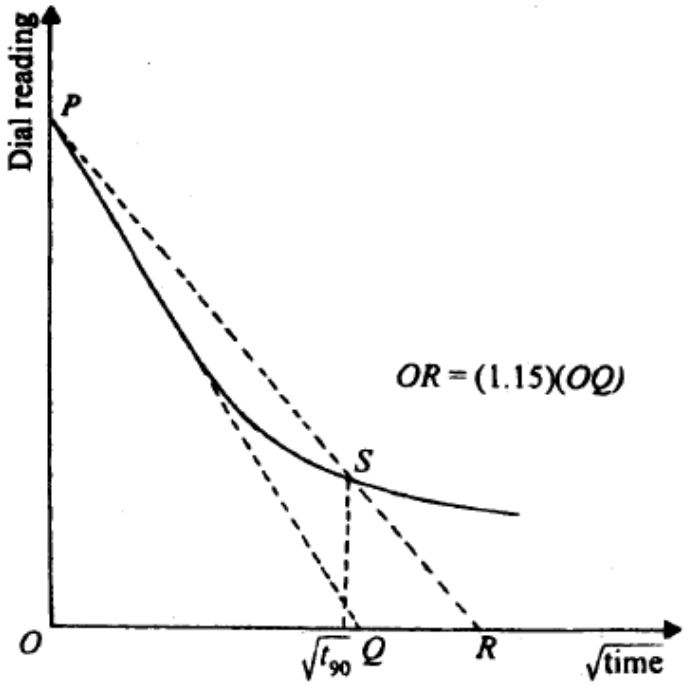

Figure 2.17 Square root of time method for determination of end-of-primary consolidation (Das, 1997)

iv) The abscissa of the point S (the intersection of line PR with consolidation curve) corresponds to the time for 90% consolidation.

2.9 Determining the Engineering Parameters of Soil Materials

Modelling the soil materials for numerical analyses requires certain parameters that the soil body contains. Besides the parameters determined with the help of the

laboratory test data, some of the parameters were determned using the literature correlations.

For the permeability of the soft soil, Equation (2.10) can be used which is given in the previous sections. On the other hand, for the horizontal permeability Das (1997) gives two recommendations;

i) $k_h/k_v = 1.5$ for soft clay, and
ii) $k_h/k_v = 1.2$~1.7 for inorganic silt and peats.

Terzaghi, Peck and Mesri (1996) suggests the k_h to k_v ratio to be often less than 3 for varved clay deposits.

Another important parameter to be used in the analyses is the effective angle of shearing resistance. For cohesive soils Terzaghi, Peck and Mesri (1996) presented the blow graph which gives a relationship between the effective angle of shearing resistance, φ' and the plasticity index, I_p (Figure 2.18).

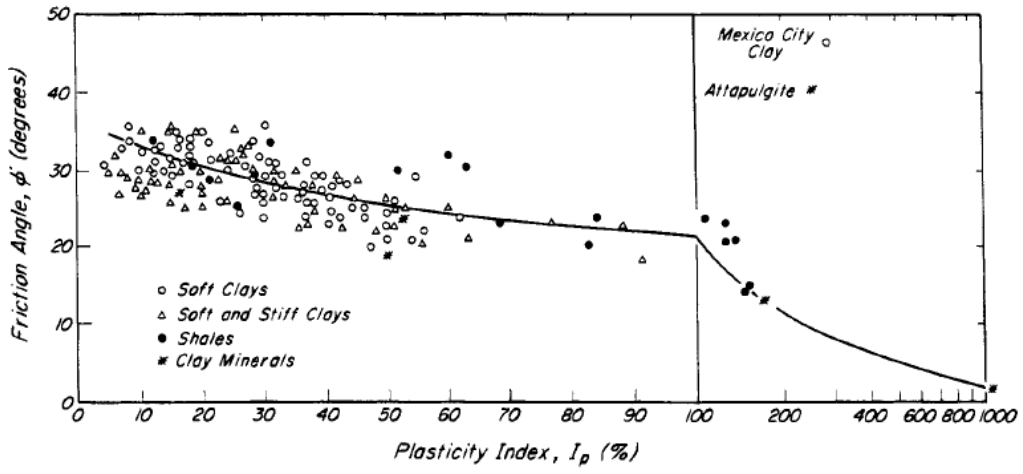

Figure 2.18 Relationship between the effective friction angle for clays vs. plasticity index (after Terzaghi, Peck and Mesri, 1996)

For the friction angle of cohesionless soils, Peck et al., (1953) offered the below graph (Figure 2.19) which relates the φ' values to standart penetration blow counts.

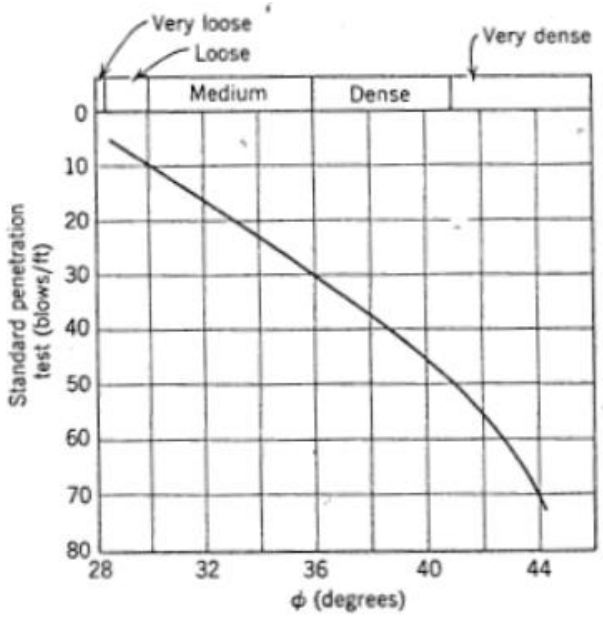

Figure 2.19 Relationship between friction angle of cohesionless soils and the SPT-N values (after Peck et al., 1953)

Another parameter to be determined using the literature recommendations is the Young's modulus of cohesionless soils. Table 2.3 shows the values recommended by Bowles (1996) for different types of sands and Table 2.4 shows the Das's (1997) recommendations for the Young's modulus values of sands.

Table 2.3 Proposals for E_s values for sands and gravels (after Bowles, 1996)

Soil	Es (Mpa)
Sand	
Silty	7-21
Loose	10-24
Dense	48-81
Sand and Gravel	
Loose	48-144
Dense	96-192

Table 2.4 Proposals for Es values of sands (after Das, 1997)

Soil	Es (Mpa)
Loose sand	10.35 - 24.15
Silty sand	10.35 - 17.25
Medium dense sand	17.25 - 27.60
Dense sand	34.50 - 55.20
Sand and gravel	69.00 - 172.5

CHAPTER 3

CASE STUDY: SAKARYA-2 VIADUCT APPROACH EMBANKMENT

Within the context of "Bozüyük-Mekece State Highway Improvement Project, Section-2" which is located in the Marmara Region of Turkey, a viaduct called "Sakarya-2" was planned to be built which includes approach embankments between 82+300 to 82-525 km's that reaches approximately to 12 meters height. Under the approach embankment of Sakarya-2 Viaduct, soft clay exists which causes large amounts of consolidation settlements. Figure 3.1. and 3.2 shows the plan and cross sections of the embankment together with borehole locations and soil profile. Four boreholes are drilled (Table 3.1 and Figure 3.2). In order to improve this soft soil, application of prefabricated vertical drains was decided among other improvement techniques. Following the installation of PVDs, the embankment was decided to be built in two stages; first one with 8 m height and the second stage with 4 m height. For the observation of settlements 2 fixing plates were installed and the settlements are recorded for 620 days.

In this study, the above mentioned embankment is analyzed with both numerical and analytical methods and results are compared with site observations. Afterwards a parametric study is performed on the case in order to investigate the effects of different factors on the consolidation of PVD improved soft soil.

Table. 3.1. The coordinates of 4 boreholes together with the 2 additional boreholes and ground water level depth

Borehole No	Coordinates			Depth (m)	Ground water level depth from ground surface (m)
	N (X)	E (Y)	Elevation (m)		
D82420-1i	4 477 911.22	504 416.29	88.664	27.45	14.2
D82420-2i	4 477 926.42	504 465.80	89.435	24.00	11.2
D82470-1i	4 477 957.12	504 400.28	89.127	42.00	8.1
D82470-2i	4 477 975.87	504 449.99	89.837	27.00	8.7
YSK - 36	4 477 903.93	504 441.38	88.000	18.45	7.3
EK-SK - 8	4 478 021.16	504 399.09	86.100	40.00	6.3

3.1 Idealized Geometry and Soil Profile

In the idealized soil profile, soft soil is 18.60 m thick and lies on a 2.20 m thick silty-clayey sand and gravel layer below which lies a gravelly, sandy clay and silt layer with 2.00 m thickness. There is a drained sand and gravel layer beneath this profile with 10.00 m thickness which is underlined by a 0.90 m thick Clay layer and at the bottom exists the bedrock classified as conglomerate (Figure 3.3). The soft soil existing in the first 18.60 m can be described as medium stiff to stiff, sandy silty clay to clayey silt (CL, CH, ML, MH), with fines content between 51 to 99%, liquid limits ranging from 29 to 77%, and plasticity index between 36 to 55%, undrained shear strength range from 20 to 114 kPa.

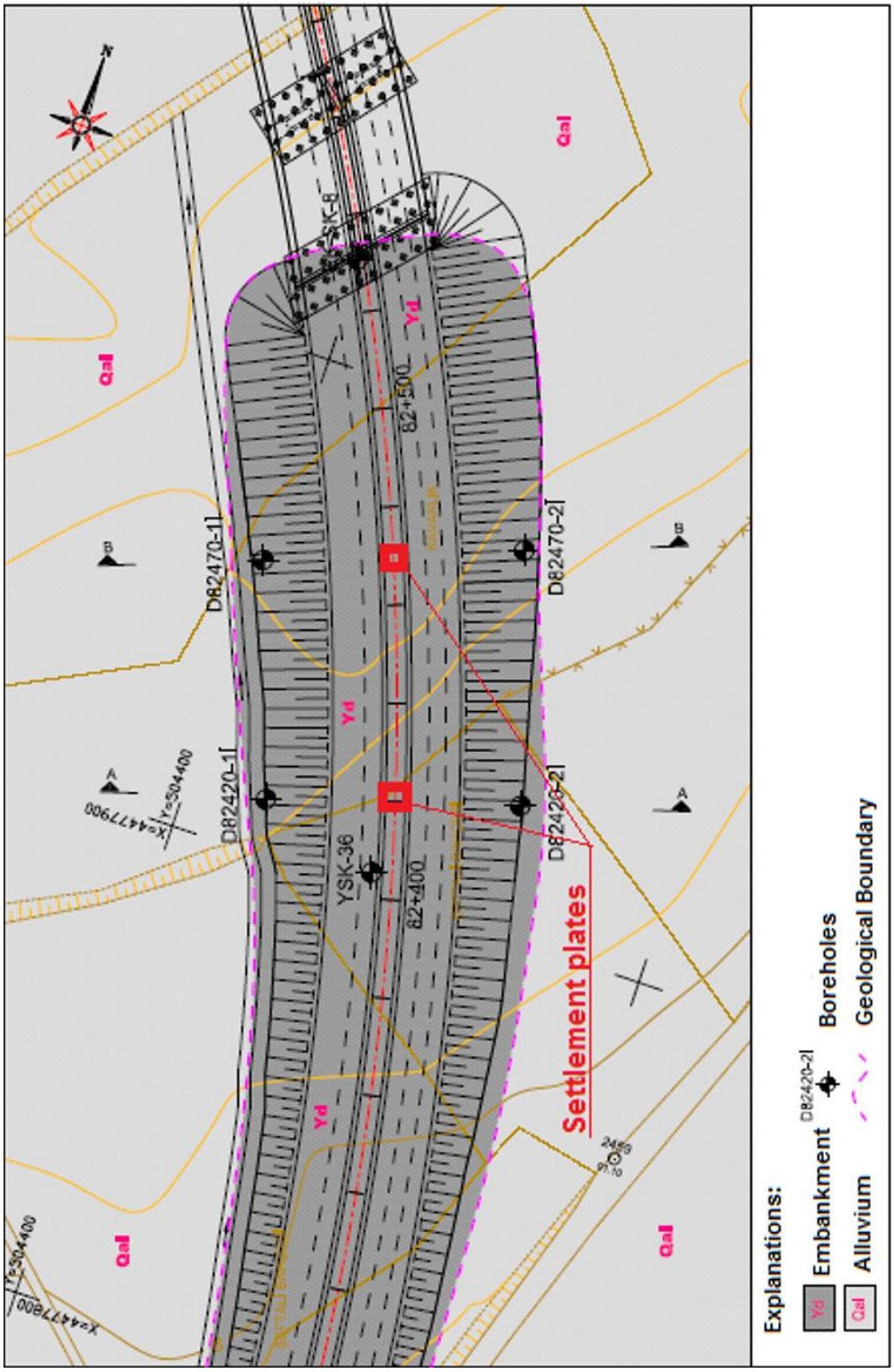

Figure 3.1. Embankment plan view showing the location of boreholes

(Yuksel Project, 2010)

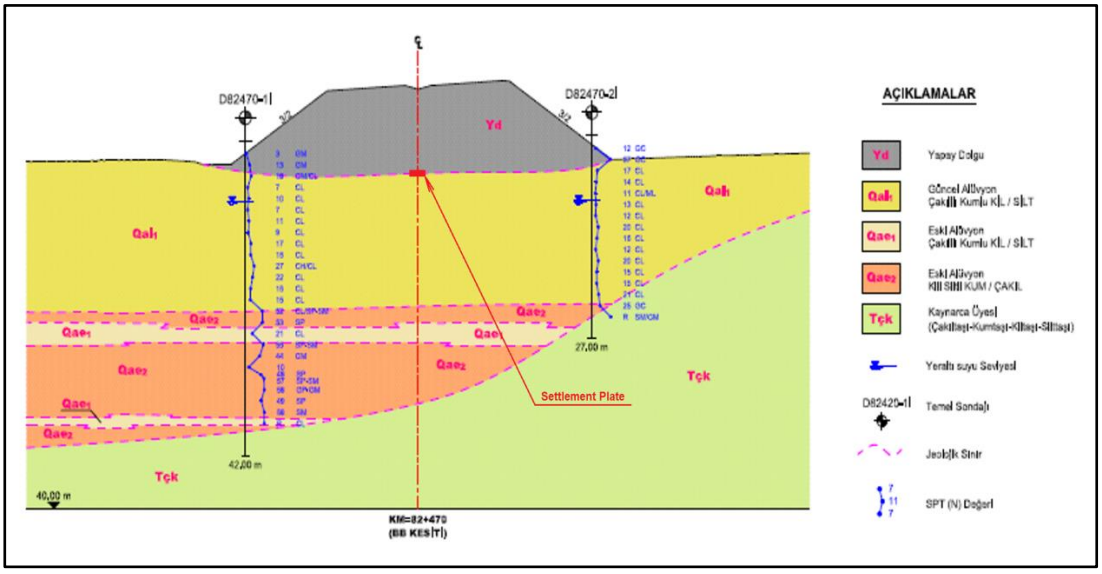

Figure 3.2. Embankment cross section and soil profile (Yuksel Project, 2010)

The embankment has 12.00 meters of height. Side slopes of the embankment are 3H:2V. Embankment material is yellow-grayish brown, clayey silty sandy gravel (GM, GC, GP) with fines content ranging from 8 to 35%. The groundwater level is at 8.00 m depth.

Prefabricated vertical drains were placed throughout the above 18.80 m – thick soft soil. PVDs are 100 mm x 4 mm in cross-section and installed in the gorund in a square pattern with 1.40 m spacing. Figure 3.3 shows the idealized geometry of the problem with settlement observation points. Note that in the idealized geometry half of the embankment is shown assuming that the other half of the embankment is symmetrical. However, the other half of the embankment is not symmetrical because the thickness of soil layers are not the same. Therefore the results of our analyses will be influenced by this. However the settlements measured in the field at the centerline of the embankment will be mostly governed by the thickest soft ground, since the inclined ground is under the right toe of the embankment, not near the centerline, and it may not be affecting the settlements too much. In this study the data of settlement plate at the section 82+470 is used.

It can be seen in Figure 3.3. that the geometry of the idealized geometry considers 90 m to the side, away from the toe of the embankment. This much distance is not needed, however in order for the stress and deformation values not to be influenced by the side boundaries, the lateral boundary is considered far away. The vertical distance underneath the embankment is 34 m below the ground surface at one of the cross sections (Figure 3.2.). It should be noted that the borehole depths should have been extended to deeper depths considering the influence zone of an embankment. For an embankment with a width of B, the stress influence zone is about 3B below the embankment, therefore if we consider B=24 m, the stresses will be transferred to about 72 m below the embankment and boreholes should make sure that there is no other soft ground within this zone. The sandstone and siltstone bedrock is detected in the boreholes.

3.2 Material Parameters

In order to determine the engineering parameters of the soil layers within the profile, 4 boreholes were drilled (Figures 3.1. and 3.2) and standard penetration and pressuremeter tests are performed during the site investigation studies. In addition to the site investigation, a series of laboratory tests are performed on the samples taken from the site, such as; sieve analysis, consolidation, triaxial compression and Atterberg limits tests.

Laboratory test results of the soil profile are tabulated in Table 3.2. m_v and c_v values measured by the laboratory one-dimensional consolidation tests that were performed on 2 undisturbed samples of the soft soil layer are given in Table 3.3.

In addition to the m_v and c_v parameters, the compression index, c_c and the recompression index, c_r values are determined from the void ratio, *e* vs logarithm of pressure, *p* graph obtained from the consolidation tests. For the upper soft soil layer, c_c=0.1600 and c_r=0.0199 and for the lower soft soil layer c_c=0.1300 and c_r=0.0199.

Here some of the parameters are determined by using the empirical correlations available in the literature. The hydraulic conductivity in the vertical direction, k_v can be determined by the Equation (2.10). For m_v = 0.016 cm^2/kg = 0.000016 m^2/kN and c_v can be taken as 0.002 cm^2/s = 0.0000002 m^2/s; k_v equals 3.14E-10 m/s = 2.71E-5 m/day.

Table 3.2 Laboratory test results of D82470-1i borehole (Yuksel Project, 2010) (other borehole data can be seen in the Appendix)

Depth	w (%)	e	γ_{dry} (kN/m_3)	γ_{sat} (kN/m_3)	Atterberg Limits			Sieve Analsis		USCS	Unconfined Compression	Triaxial Compression	
					LL	PL	PI	+ 4	- 200		qu	c	φ
					%	%		%	%		(kPa)	kPa	degrees
1.50 - 1.95	9,4				-	NP	-	56,2	25,7	GM			
3.00 - 3.45	9,9				-	NP	-	43,9	27,5	GM			
4.50 - 4.95	9,6				-	NP	-	53,1	21,7	GM			
4.50 - 4.95	21,7				44,1	22,3	21,8	-	92,2	CL			
6.00 - 6.45	25,3				37,9	22	15,9	-	87,4	CL			
7.50 - 7.95	36,6				44,4	23,3	21,1	-	97,9	CL			
7.95 - 8.45	23,9	0,6	19,9	25,8	44,4	21,8	22,6	-	89,5	CL	44		
9.00 - 9.45	24,9				36,3	20,2	16,1	-	87,2	CL			
10.50 - 10.95	27,8				44,4	22,4	22	-	95,5	CL			
12.00 - 12.45	32,3				47,7	23,2	24,5	-	98,9	CL			
13.50 - 13.95	29,4				47,4	23,7	23,7	-	98,9	CL			
13.95 - 14.45	30,4	0,79	19,2	26,4	37,9	19,6	18,3	-	98,1	CL	92		
15.00 - 15.45	27,4				38,4	21,7	16,7	-	97,1	CL			
16.50 - 16.95	32,2				52,6	25,9	26,7	-	99,6	CH			
16.50 - 16.95	29,5				Not enough sample			-	91,8	CL			
18.00 - 18.45	23,9				36,3	18,7	17,6	-	91,1	CL			
19.00 - 19.50	26,6		20,7		43,9	21,3	22,6	-	95,8	CL	59	31	2
19.50 - 19.95	27,3				40,7	21,4	19,3	-	96,6	CL			
21.00 - 21.45	29,5				40,2	20,3	19,9	-	98,2	CL			
22.50 - 22.95	27,8				29,5	21,7	7,8	-	76,1	CL			
22.50 - 22.95	8,7				-	NP	-	42,3	7,4	SP-SM			
24.00 - 24.45	10,5				-	NP	-	19,9	4,9	SP			
25.50 - 25.95	28,5				31,3	21,4	9,9	-	75,3	CL			
27.00 - 27.45	13,6				-	NP	-	26,6	10,3	SP-SM			
28.50 - 28.95	13,3				-	NP	-	44,9	29	GM			
31.00 - 31.45	8,8				-	NP	-	36,6	4,9	SP			
31.50 - 31.95	6,9				-	NP	-	39,6	8,4	SP-SM			
33.00 - 33.45	10,0				-	NP	-	48,4	7,4	GP-GM			
34.50 - 34.95	10,6				-	NP	-	26,4	4,9	SP			
36.00 - 36.45	7,7				-	NP	-	12,9	32,3	SM			
37.50 - 37.90	40,9				36,7	23,3	13,4	-	84,1	CL			

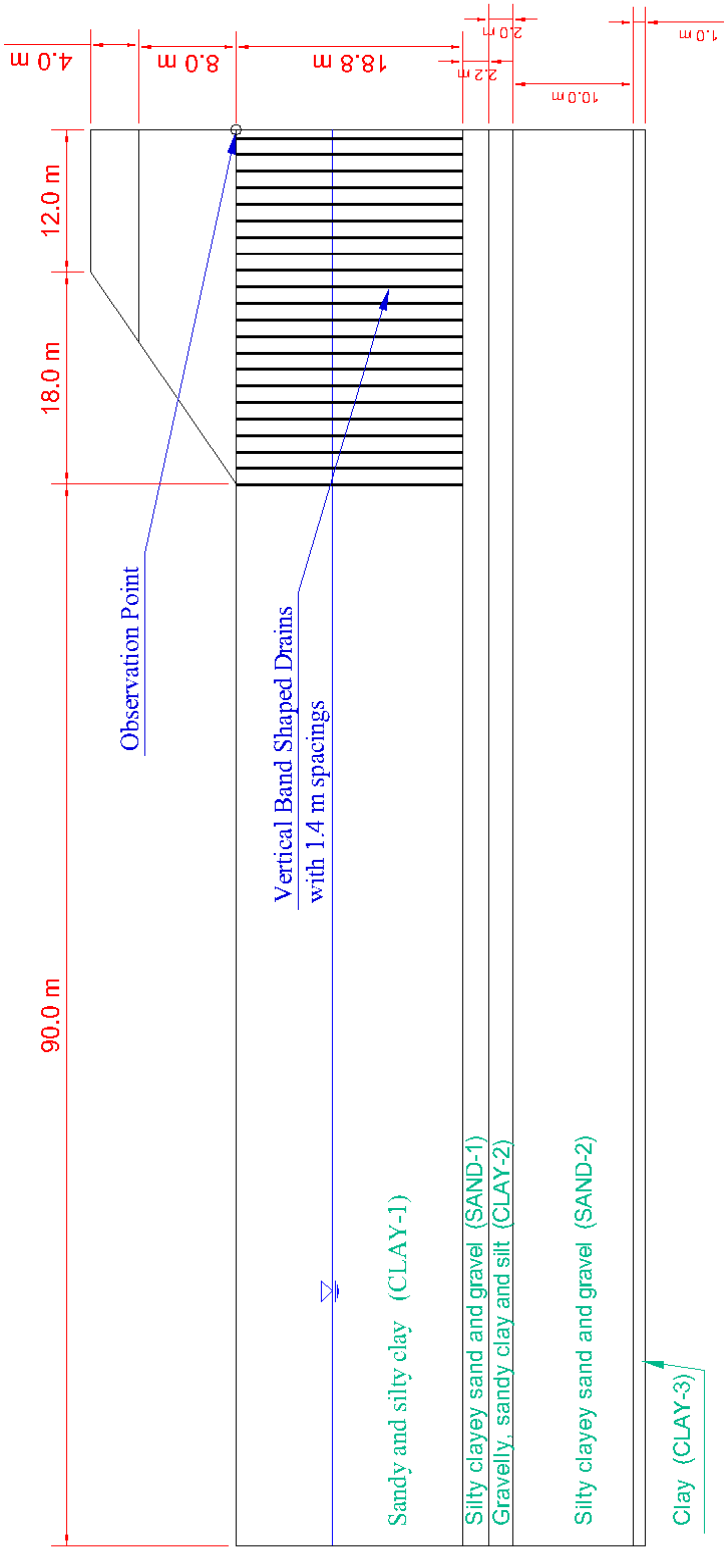

Figure 3.3 Idealized geometry of the Problem and soil profile (all units are in meters) to be used in finite element modelling

Table 3.3 Consolidation Test Results of The Soft Soil Layer

P kPa	UD-1		UD-2		UD-3		UD-4	
	Borehole:	D82470-1i	Borehole:	D82470-1i	Borehole:	D82470-2i	Borehole:	D82470-2i
	Depth:	7.95-8.45 m	Depth:	13.95 - 14.45 m	Depth:	7.00 - 7.50 m	Depth:	10.00 - 10.50 m
	m_v cm^2/kg	c_v cm^2/s	m_v cm^2/kg	c_v cm^2/s	m_v cm^2/kg	c_v cm^2/s	m_v cm^2/kg	c_v cm^2/s
0	0.0000	0.0000	0.0000	0.0000	0.0000	0.0000	0.0620	0.0040
25	0.0380	0.0020	0.0670	0.0040	0.0000	0.0000	0.0420	0.0030
50	0.0380	0.0010	0.0690	0.0040	0.0280	0.0004	0.0420	0.0020
100	0.0190	0.0009	0.0300	0.0030	0.0230	0.0004	0.0270	0.0010
200	0.0170	0.0010	0.0150	0.0040	0.0150	0.0003	0.0160	0.0010
400	0.0090	0.0010	0.0070	0.0030	0.0090	0.0003	0.0132	0.0010
800								

The shear strength parameters will not be of major concern, since the settlement of soft ground is the main study subject in this case. However, reasonable estimates of friction angle values are used as input. Effective internal friction angle of the clay layer is determined by the graph proposed by Terzaghi et al. (1996) (Figure 2.18) which gives the relationship between the plasticity index and the effective internal friction angle of soft soils. For average PI value of 20%, drained internal friction angle of soft soil layers is determined to be $\varphi'=30^0$. Drained cohesion is assumed to be 5 kPa. Initial void ratio of the upper soft soil layer is taken as the average of 4 consolidation test data which gives $e_0=0.78$. For other two soft soil layers (CLAY-2 and CLAY-3) e_0 is taken as 0.75. Material parameters used in the finite element analyses for the 3 soft soil layers are tabulated in Table 3.4.

Table 3.4 Material parameters of soft soil layers

Parameter	Unit	CLAY-1	CLAY-2	CLAY-3
γ_{dry}	kN/m^3	18	18	18
γ_{sat}	kN/m^3	20	20	20
e_0		0.78	0.75	0.75
k_h	m/d	5.42E-05	5.42E-05	5.42E-05
k_v	m/d	2.71E-05	2.71E-05	2.71E-05
C_c		0.1600	0.1300	0.1300
C_s		0.0199	0.0199	0.0199
c	kPa	5	5	5
φ	degrees	30	30	30

Parameters used for the drained silty-clayey sand and gravel layers which lie between the two soft soil layers are given in Table 3.5. In numerical analysis, there occurs large errors in results due to complex flow matrix caused by large differences between the permeability values of adjacent soil layers; so the permeability value of the sand and gravel layer is taken as 1,00E-3 m/day.

Internal friction of sand and gravel layers are determined by the graph proposed by Peck et al. (1953) (Figure 2.19) which gives the relationship between the SPT-N value and φ'. For SPT-N values between 45~50, internal friction angle of the layer is taken as 39^0. E_{ref}, the deformation modulus of the layers was determined by using tables 2.3 and 2.4. Considering the high silt and clay content and the high relative densities of the sand and gravel layers, E_{ref} was taken as 20 MPa. Poisson's ratio, ν, is assumed to be 0,25.

Table 3.5 Material parameters of granular soil layers

Parameter	Unit	SAND-1	SAND-2
γ_{dry}	kN/m^3	18	18
γ_{sat}	kN/m^3	19	19
k_h	m/d	1.00E-03	1.00E-03
k_v	m/d	1.00E-03	1.00E-03
c	kPa	1	1
φ	degrees	39	39
E	kPa	20,000	20,000
ν		0.25	0.25

3.3 Loading History

Embankment is constructed in two stages in real life, in order to avoid bearing capacity failure in the soft clay layer. In the numerical analyses as well, the embankment fill was considered to be constructed in two stages. When the measured settlement vs. time graph is investigated, it can be seen that, the first 8.0 m – high embankment is constructed approximately in 30 days. Then the partial consolidation of soft soil is waited for another 30 days and the second stage of the embankment with 4.0 m height is constructed approximately in 20 days. Settlement is observed with the help of the settlement plates for a total of 620 days. Because the observation of settlement is started after the drain installation, installation of the drains did not have any duration in the analyses performed in this study. Below, Table 3.6 explains the loading history of the problem.

Table 3.6 Phase Description of the Problem

Phase Description		Duration (days)
Initial Conditions (K_0 - procedure)		0
Installation of drains		0
1st stage of embankment with 8.0m height	(Phase 1)	30
Consolidation	(Phase 2)	30
2nd stage of embankment with 4.0m height	(Phase 3)	20
Consolidation	(Phase 4)	540

3.4 Determining the End of Primary Consolidation

For a better evaluation of the analyses results firstly the end of primary consolidation is determined from the field observation data, based on the graphical procedures that were explained in Chapter 2, namely, the log-time and square-root-of-time methods.

3.4.1. The Log-Time Method

As explained in Chapter 2 that, the field measurement data is plotted on a semilog scale with settlement readings are on the vertical axis and the log-t is on the horizontal. Then, two tangent lines, one of which is tangent to the main consolidation curve and the other is tangent to the latter part of the curve are intersected and the point of istersection is determined to the 100% primary consolidation point. The method can be shown in Figure 3.4.

It can be seen in Figure 3.4 that the end of primary consolidation and the start of secondary consolidation is not readily noticeable, since the settlement time graph does not show a generally expected S-shaped curve. However, it can be said that the secondary consolidation is a major part of the settlement. As can be seen from the figure that, the best interpretation of an intersection of two tangent lines corresponds to about ~140 days which implies a primary consolidation settlement value of about ~65 cm.

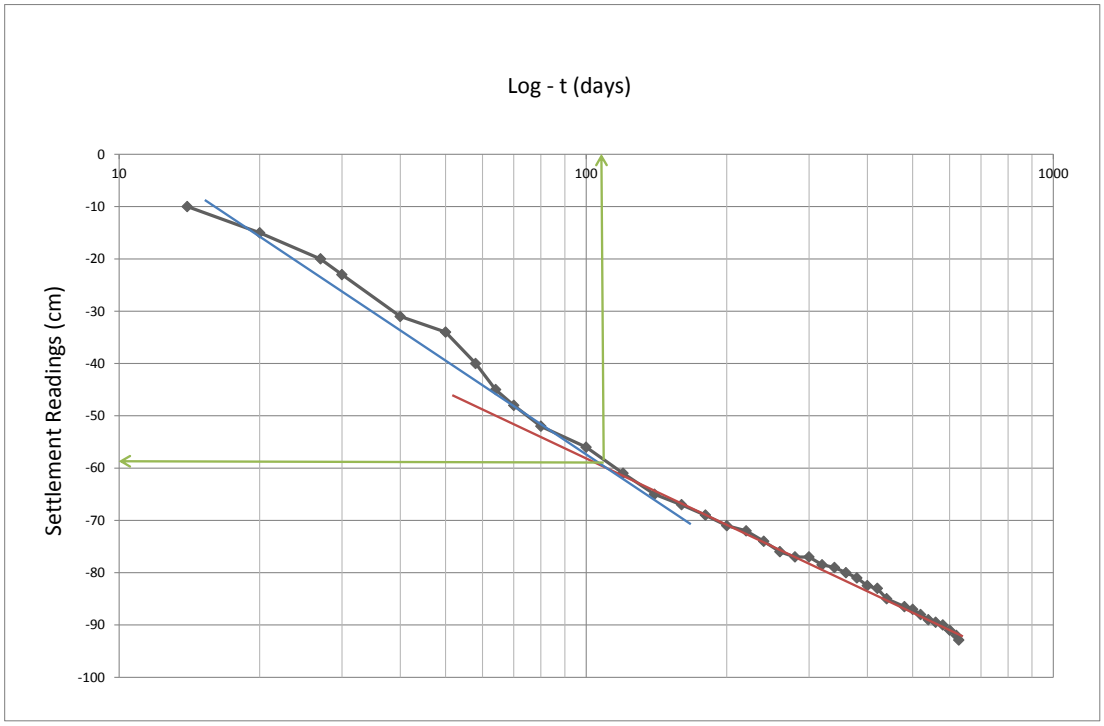

Figure 3.4 Determination of end-of-primary consolidation using the Log-Time Method using the field measured settlement values

Besides determination of end of primary consolidation, the secondary compression index, C_α has also been determined with the help of Figure 3.3. It is known that, C_α is the slope of the latter portion of a strain vs. log-t curve. Thus, C_α can be calculated from the above figure by the following formulae:

$$C_\alpha = \frac{\Delta H/H}{\log(\frac{t}{t_0})}$$

where ΔH is the settlement value in the secondary compression portion, t is time corresponding to ΔH amount of settlement after primary compression and t_0 is the time of end of primary consolidation. Therefore C_α has been found as follows:

$$C_\alpha = \frac{(90-59)/1880}{\log(\frac{625}{110})} = 0.0218$$

3.4.2. The Square-Root-of-Time Method

Square-root-of-time method (Taylor, 1942) was explained in Chapter 2. The procedure is done in Figure 3.5 which gave a 90% consolidation at 156 days with a settlement value of 67 cm.

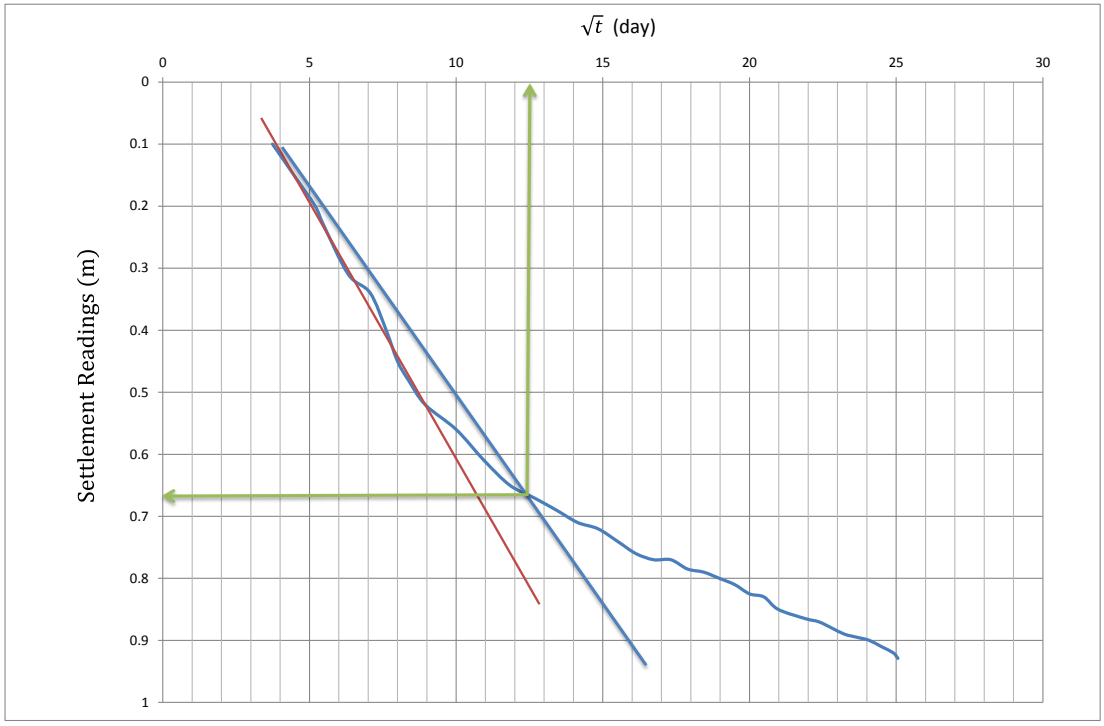

Figure 3.5 Determination of 90% primary consolidation by Square-Root-of-Time Method

To conclude, two different end-of-primary consolidation estimation methods are used with the given field observation data. From these methods, it can be said that, the primary consolidation has finished for the case at approximately 110~170 days with a primary consolidation settlement value of 59~70 cm. Both methods reveal that, there occurs a large secondary compression in the case studied.

3.5 Finite Element Analyses

Finite element analyses of the case are performed with the software Plaxis v.8.2 as explained in Chapter 2. In the first part of this study, three different analyses are performed, one of which assumes no smear zone around the drains and the other with a certain smear zone whereas third one takes into account both smear and secondary compression.

For the analyses, first the geometry of the model is constructed compatible with the explanations in Section 3.1. Boundary conditions of the model are defined as standard fixities which allows only vertical deformations at the sides, no displacement at the bottom and free boundary at the top.

Mesh dimension is set to fine coarseness and refined at least once around the drains to get more accurate results.

Water condition of the model is defined with phreatic level of groundwater which is at 8.0 m depth measured from the ground surface. Two sides of the model are set to closed flow boundary which implies that water pressure dissipation is only in the vertical direction.

In order to model a band shaped vertical drain in plane strain condition, firstly the band shaped drain has to be converted to an axisymmetric problem. Among the recommendations in Chapter 2, Hansbo (1979) equation is used for this conversion. The dimensions of the band shaped drains are 100 mm x 4 mm in cross section. With Equation (2.1), the equivalent diameter of the drains, d_w, is calculated as 0.066 m.

For the modelling of a vertical drain consolidation problem which by its nature is in axisymmetrical condition, a matching procedure has to be done in order to convert the problem into plane strain condition. This matching is done with the procedure explained in Chapter 2. For square pattern installation of PVDs, influence zone

diameter D_e is 1.13 x 1.4 m = 1.582 m. Then, the half width of the unit cell, *B,* is computed as, $B = D_e/2 = 0.791$ m.

Horizontal permeability in the plane strain condition, k_{hp}, can be calculated with Equation (2.38), with B = 0.791 m and b_w = 0.033 m, which gives k_{hp} = 1.496E-5 m/day.

For the analysis which takes into account the smear zone, the smear zone horizontal permeability in plane strain condition, k_{hp}', is calculated with Equation (2.37). The ratio of undisturbed to smear permeability, $\frac{k_h}{k_h'}$ is assumed to be 2. The smear zone diameter is also assumed to be 2.5 times the equivalent diameter of the drain ($d_s = 2.5\ d_w$). With the values;

d_e = 1.582 m
d_w = 0.066 m
d_s = 0.165 m

the smear zone horizontal permeability in plane strain condition is calculated to be k_{hp}=5.909E-7 m/day. The vertical permeability within the smear zone is taken as equal to the horizontal permeability in the smear zone as explained in Section 2.1.4.1.

Initial conditions of the numerical model are defined by giving the condition just before the embankment construction which consists of the vertical drains, the phreatic water condition and the natural ground surface as shown in Figure 3.6.

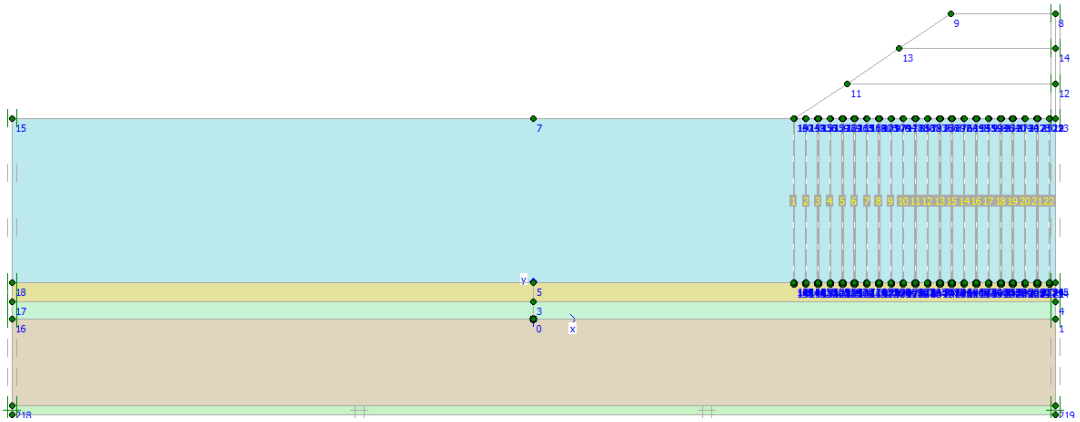

Figure 3.6 Initial Conditions of the Finite Element Analyses

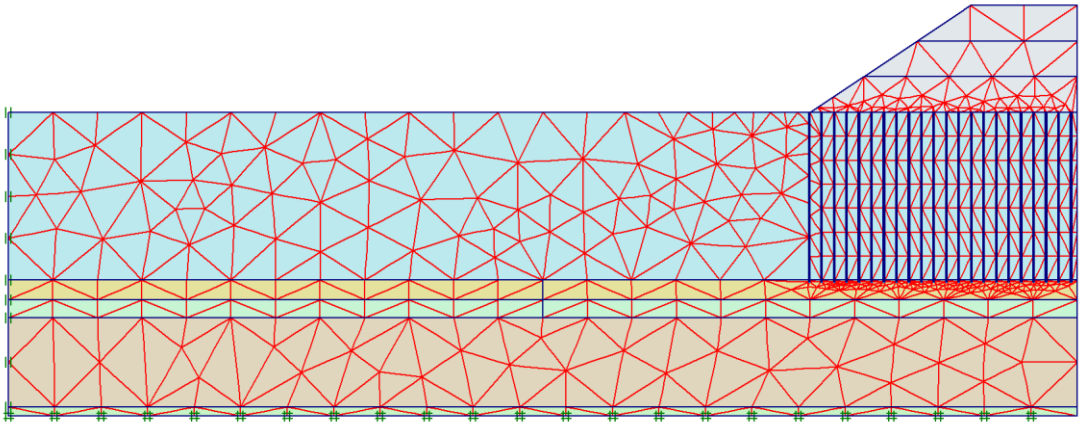

Figure 3.7 Mesh for Finite Element Analysis

3.5.1 Finite Element Analysis Results

Settlement vs. time curves for the analysis excluding the smear effect, analysis including the smear effect, analysis with both smear and creep effects and the site observation are presented in Figure 3.8 below. From the result, it can be concluded that when the smear effects are taken into account, finite element analysis using the Soft Soil model gave close agreement with in-situ measurements in terms of the time dependent settlement behaviour of the soft soil. On the other hand, analysis which

neglects the smear zone have not given a satisfactory settlement behaviour. As expected, when the smear zone is neglected, consolidation has proceeded quickly compared to the in-situ behaviour. Smear effect included analysis, have given a good agreement with the site observations especially in the early periods of consolidation, however after a certain degree there occurs a difference between the two curves. This can be resulted from the environmental effects such as drain clogging, squeezing of the PVDs, etc. which in real condition retards the settlement.

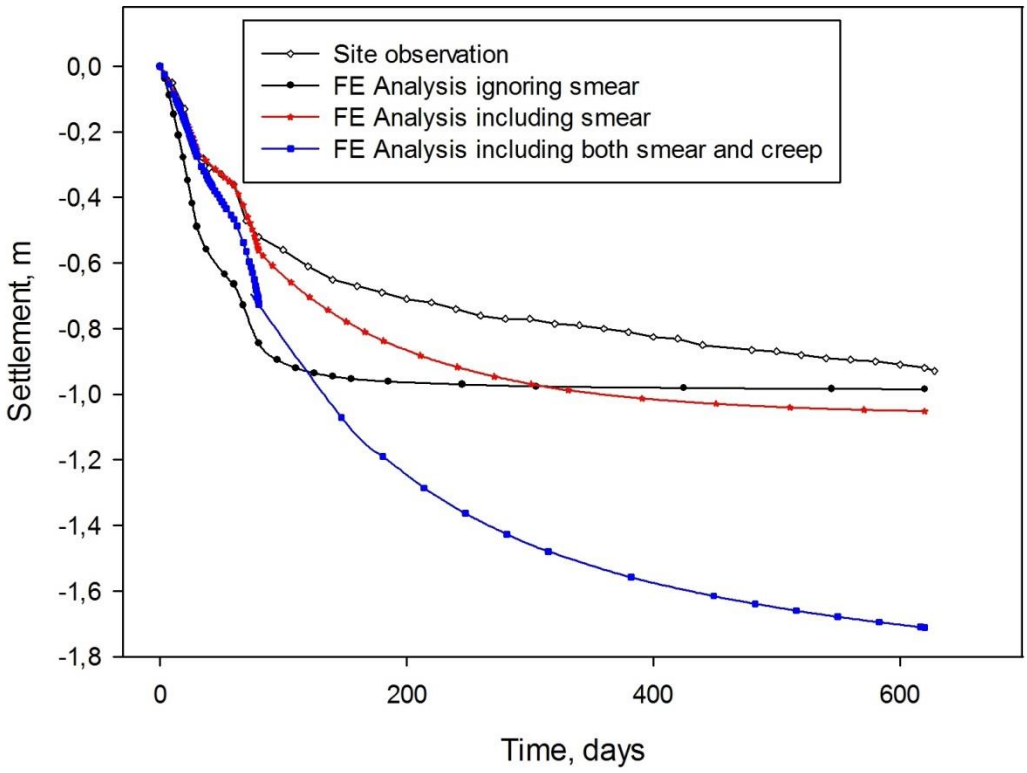

Figure 3.8 Ground surface settlement at the centerline of the embankment vs. Time Graphs for Finite Element Analyses and In-situ Measurements

The third analysis performed on the case with finite element method is the one which takes into account the creep effect. However, as can be seen from Figure 3.8 that, the analysis with creep effect taken gave a settlement curve which diverges a lot from the general trend of the in-situ measurement curve. In the early period of settlement it showed a relatively close behaviour to the other curves but after completion of most

of the primary consolidation it gave settlement values reaching to approximately 1.7 m at about 600 days.

The phenomenon of "reduction of mean effective stress" during undrained loading has a negative influence on the strength and stability of the soil structure. Because of this phenomenon, there occurs a tendency towards failure mechanism when large displacements occur within the model. The above behaviour may be explained by this issue.

As can be seen in the total displacement figure given below (Figure 3.9), the magnitude of settlement observed at 620 days is highest at the top of the embankment and it is on the order of some 90-100 cm's as measured in the field. Therefore the finite element solutions seem to give reasonable results. The total settlements at the 620 days are highest at the top of the embankment and decreases as you go toward the toe of the embankment as expected.

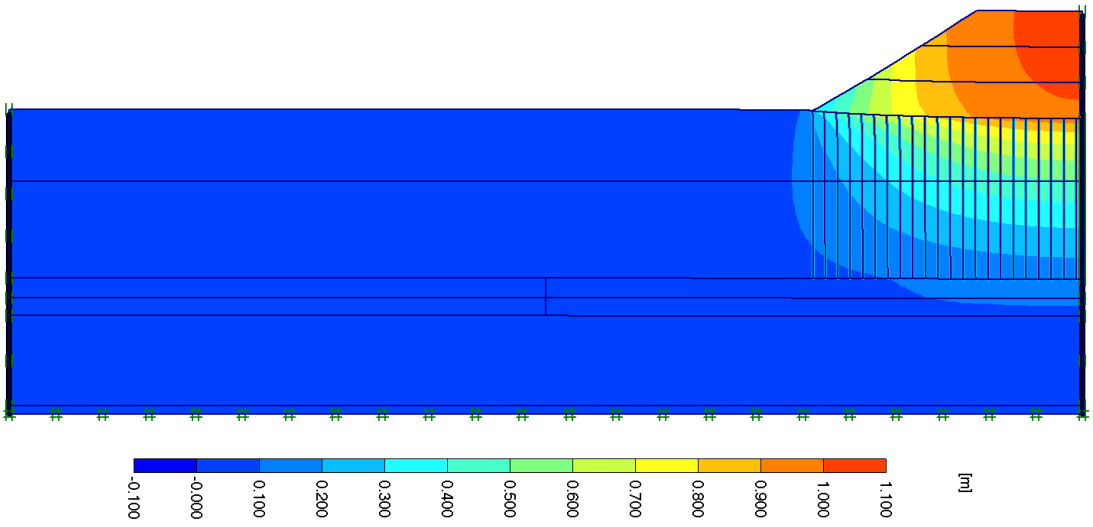

Figure 3.9 Total displacement contours for the analysis neglecting the smear zone (after 620 days)

When smear zone is included in the analysis, the rate of consolidation is slower due to the disturbance (and less permeability) in the smear zone. Therefore at 620 days,

the analysis gives more total deformations because the ground was consolidated to a lesser degree of consolidation as compared to the case without smear, and therefore slope stability/bearing capacity type of deformations are also observed as the soil did not gain enough strength yet (Figure 3.10). The vertical displacement results can be seen in Appendix C.

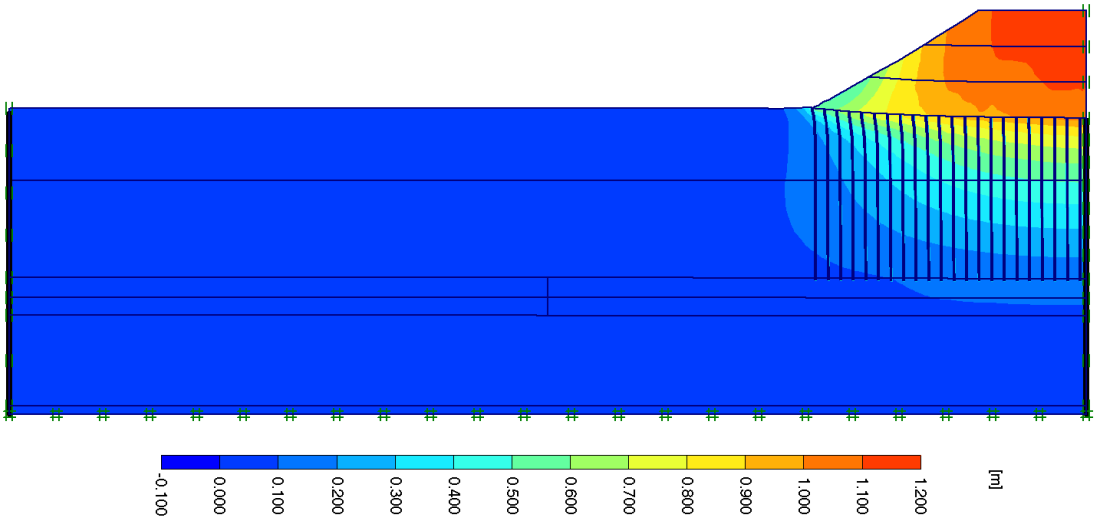

Figure 3.10 Total displacement contours for the analysis including the smear zone (after 620 days)

Figure 3.11 shows the total displacement contours of the analysis including both smear and creep. Different from the previous analyses' figures, it is observed from Figure 3.11 that large deformations caused a visible change in the geometry and deformations are effective not only in the vertical direction but also in the lateral direction. When the creep deformation is included the soil continously deforms with time in all directions, and the figure implies that a bearing capacity failure or a slope failure takes place. This kind of a failure and related lateral deformations could also explain the large ground surface settlements presented in Figure 3.8 which does not match with measured values in the field.

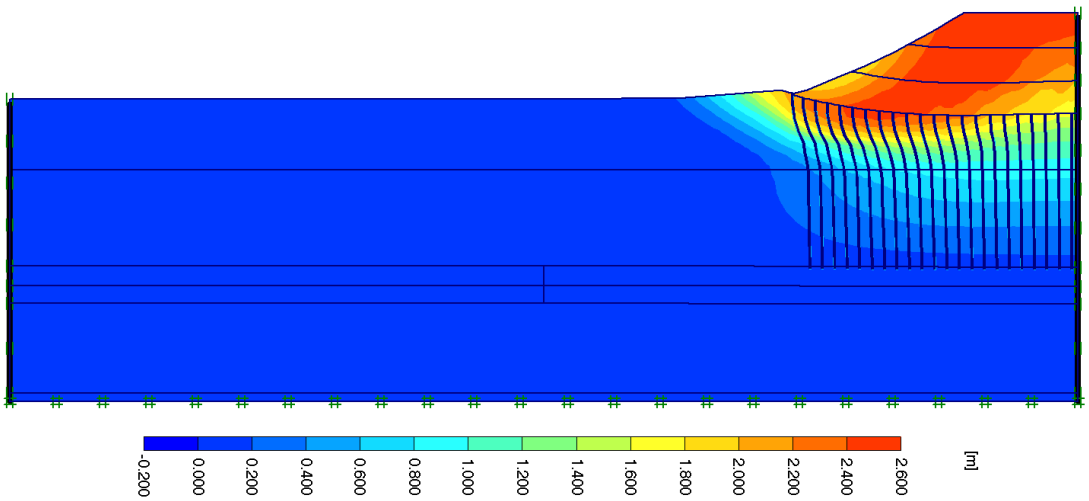

Figure 3.11 Total displacement contours for the analysis including both smear and creep effects (after 620 days)

Comparison of settlements are tabulated in two parts in Table 3.7, one of which includes the period between the beginning of the consolidation and the beginning of the major deviation of the curve of analysis including smear zone in Figure 3.8 from the curve of site observation, namely first 80 days, and the other part considers the final settlement values.

Table 3.7 Comparison of results of finite element analyses

	At the end of 80th Day				At the end of 620th Day			
	Analysis Neglecting Smear Zone	Analysis İncluding Smear Zone	Analysis İncluding Smear and Creep	Site Observation	Analysis Neglecting Smear Zone	Analysis İncluding Smear Zone	Analysis İncluding Smear and Creep	Site Observation
Settlement (cm)	84.4	56.1	72.7	54.0	98.5	105.2	171.2	92.0
Relative error w.r.t. Observed value (%)	56.3	3.9	34.6		7.1	14.3	86.1	
Number of mesh elements	1142	1695	1417		1142	1695	1417	

Below the graph of settlement vs. distance from the toe of embankment are given (Figures 3.12). Curves gives reasonable aggrement with expected behaviour of the embankment foundation. There is a very significant difference between the curve of

the analysis which includes creep behaviour and the other two curves. In the analysis of creep behaviour the large vertical and lateral displacements resulted in the change of the geometry of the model which implies that some of the elements moved up and down with respect to each other whereas in the other two analysis elements' moves are rather regular.

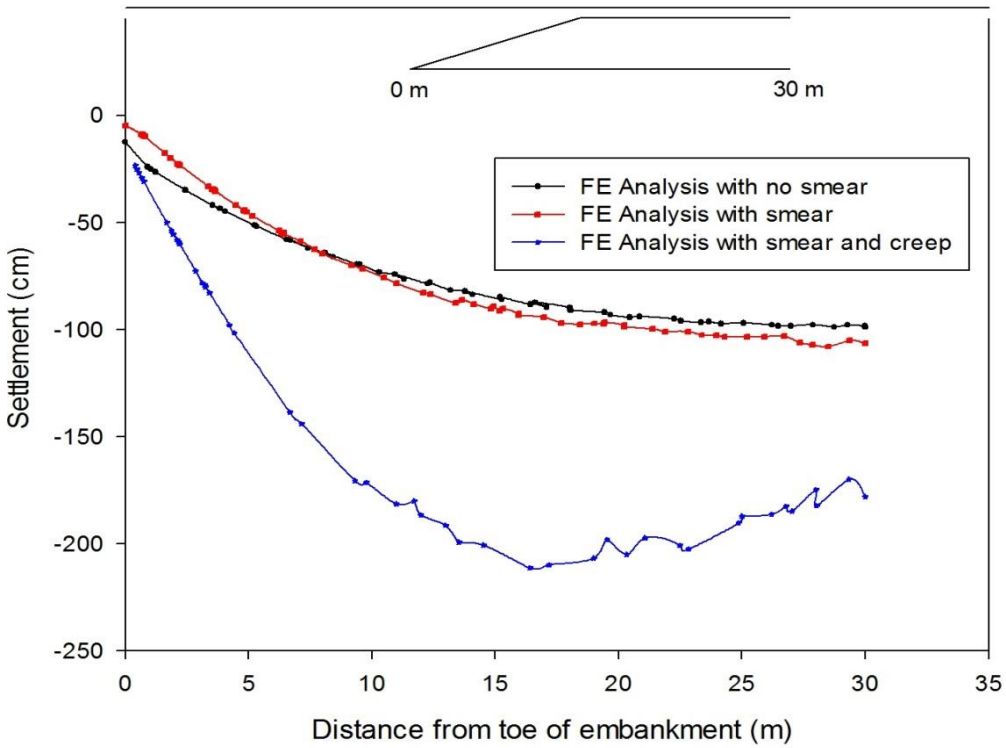

Figure 3.12 Ground surface settlement under the embankment vs. distance from toe of embankment for FE analyses

Excess pore pressure generation due to embankment loading can be seen in the figures below, for cases without and with smear zone considered (Figure 3.13 and 3.14) and the case with both smear and creep considered (Figure 3.15). The results shown below are for t=30 days, that is when the 8-m-high embankment is placed (immediately after placement). In the case without smear zone, we see that the highest initial excess pore pressure values generated in the clay are at the centerline

of the embankment, and it is on the order of 140 kPa, which is reasonably correct considering that 8x18=144 kPa additional surcharge load is placed on the clay at the centerline. As we move towards the toe of the embankment less load is applied to the clay (due to embankment side slopes) and less excess pore pressure values are observed. The pore pressures can be clearly seen to be dissipating at the drains. Whereas in the case with smear, the excess pore pressures are observed throughout the soft clay layer, and even right near the drains still very high excess pore pressures are seen, which could be because of the less permeability in the smear zone, therefore blockage of the water and hence excess pore pressures.

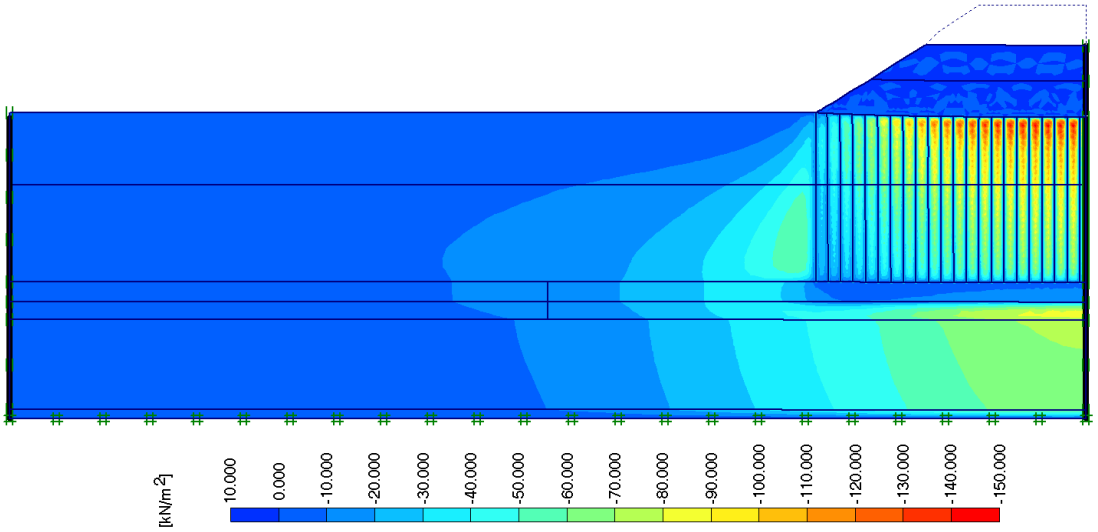

Figure 3.13 Phase-1 (when 8-m-high embankment is placed, at t=30 days) pore pressure generation for analysis, ignoring the smear effect

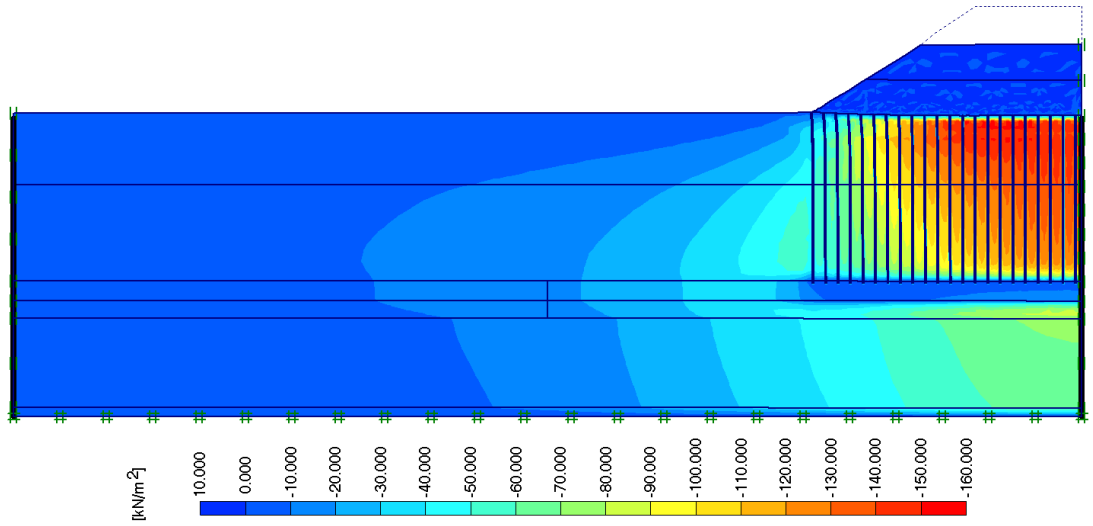

Figure 3.14 Phase-1 (when 8-m-high embankment is placed, at t=30 days) pore pressure generation for analysis including the smear effect

In Figure 3.15, pore pressures are far more different from the previous figures. It is seen that, excess pore pressures generate not only under the embankment loading but also throughout the whole soft soil cluster. It is thought from this figure that, due to large strains and the boundaries of the model, large lateral stresses occur within the soil body that causes excess pore pressures throughout the whole model. It should be noted that, the highest excess pore pressure values under the embankment are on the order of 200 kPa which is a value not exerted to the soft soil by the embankment.

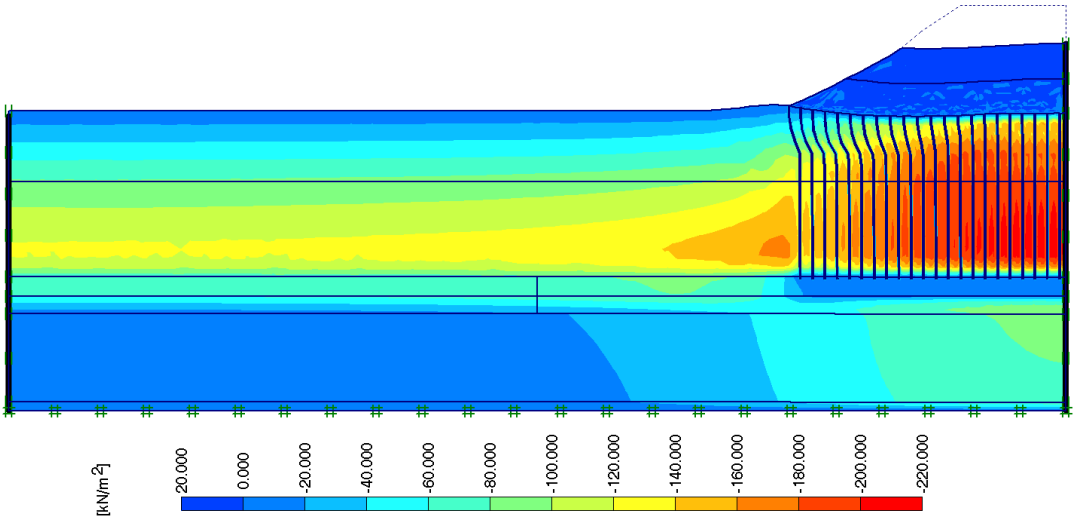

Figure 3.15 Phase-1 (when 8-m-high embankment is placed, at t=30 days) pore pressure generation for analysis including both the smear and creep effects

In order to see whether the used degree of mesh fineness is enough or not, a sensitivity study is carried out on the model in which the smear zone is taken into account. The results shown above are for a model with number of elements is equal to 1695. The whole model mesh have been refined once and a number of elements of 2320 was gotten. The comparison of these two analyses is shown below in Figure 3.16 and Table 3.8. It can be seen from Table 3.8 that the difference between two analyses results using different mesh finenesses does not exceed %0.5, therefore used mesh fineness is thought to be enough for the given case.

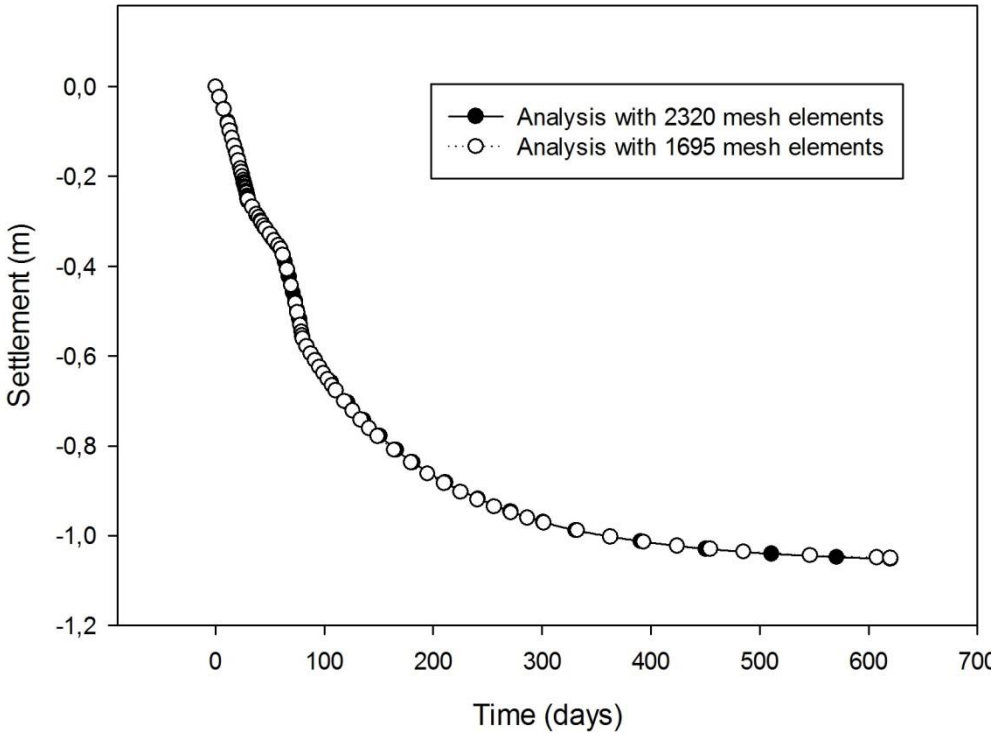

Figure 3.16 Ground surface settlement vs. time curves for sensitivity study analyses

Table 3.8 Mesh sensitivity and comparison of results of analyses performed with different numbers of mesh elements

	At the end of 90th day		At the end of 620th day	
	Analysis Including Smear Zone	Analysis Including Smear Zone	Analysis Including Smear Zone	Analysis Including Smear Zone
Settlement (cm)	60.71	60.99	105.10	105.00
Relative error w.r.t. Observed value (%)	12.4	12.9	14.2	14.1
Number of elements	1695.0	2320.0	1695.0	2320.0

3.5.2 Benefit of Using PVD

In order to investigate the effect of vertical drains on the consolidation time of soft soil, an additional analysis was performed using no drains at all. The ground surface settlement versus time curve for this analysis is presented in Figure 3.17 below.

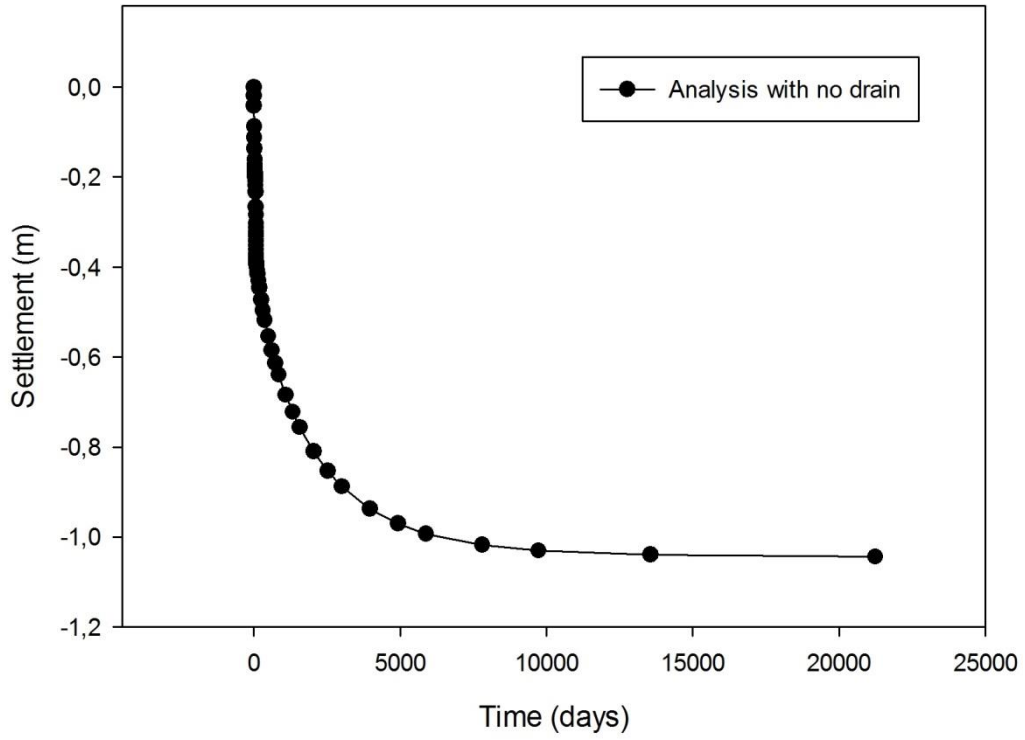

Figure 3.17 Ground surface settlement vs. time curve for finite element analysis with no drains

As can be seen from the figure that, when drains are not applied, primary consolidation finishes approximately after 4000 days whereas it finishes at approximately 120 days when PVDs are installed in the ground.

3.6 Analytical Methods

Analytical methods of the case are performed with the computational tool called Settle3D, which uses Terzaghi consolidation theory. As in the case of finite element analyses, three different analyses are performed, one of which neglects the smear zone, one including the smear and the last one including both smear and secondary compression. In Settle3D, the consolidation model is not plane-strain, therefore there is no need for a matching procedure as in the case of Plaxis.

The geometry of the problem is defined in the software as given in Figure 3.3. Ground water table is set to 8.0 m depth and staged construction is defined as explained in the phase description of the case.

PVD cross section is defined as rectangular with 100 mm x 4 mm dimensions. In the analyses which takes into account the smear effect, the smear zone diameter is taken as 2.5 times the equivalent diameter of the drain the ratio of undisturbed soil permeability to smear zone permeability is taken as 2. Well resistance has been ignored for all the analyses.

In Settle3D, there are some options for modeling a settlement case. One of them is the stress computation method. The stresses generated throughout the soil body can be calculated by 4 different methods, namely, Boussinesq, 2:1, Westergaard and Multiple Layer methods. In this study, Boussinesq method is used for stress computation.

For the clay layers no immediate settlement has been taken whereas for cohesionless layers only the immediate settlement option has been chosen.

For the modeling of the secondary compression behaviour, there are two options in SETTLE3D. One of the options allow the user to start the secondary compression when 95% of the primary consolidation finishes. In the other option secondary

settlement starts immediately after the loading is placed. The first option is used in the analyses.

As mentioned earlier in Chapter 2 that, Settle3D allows the user to analyze a soft soil consolidation with two different soil models. One of them is the linear soil model whereas the other is the non-linear model. Below, the analyses performed by using both the linear and the non-linear models are presented.

3.6.1 Analytical Method Using the Linear Soil Model

For the analyses performed with the linear soil model, coefficient of volume compressibility, m_v is taken as 0.00016 m^2/kN and the other parameters were used as given in Table 3.4. Figure 3.18 shows the model for the Settle3D analyses.

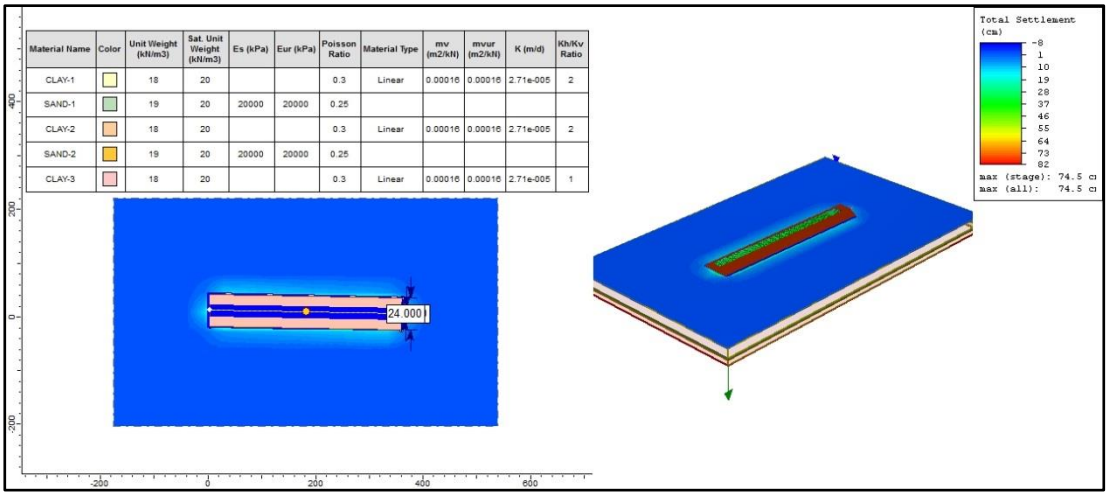

Figure 3.18 Model for analytical method using linear soil model

Figure 3.19 below shows the curves of ground surface settlement vs. time results get from the analytical method which consist of analysis ignoring smear effect, including smear effect and analysis in which the secondary compression has been taken into consideration.

From the curves, it can be concluded that in terms of final settlement values, linear soil model gave reasonable and satisfactory results when the secondary compression has taken place. On the other hand, during the primary consolidation period, it has been seen that, analyzed model have consolidated much quicker than the observed case on site. When compared to the finite element analyses, analytical solutions with linear model gave smaller final settlement values. Additionally, it has been seen that the primary consolidation have finished in a relatively short period.

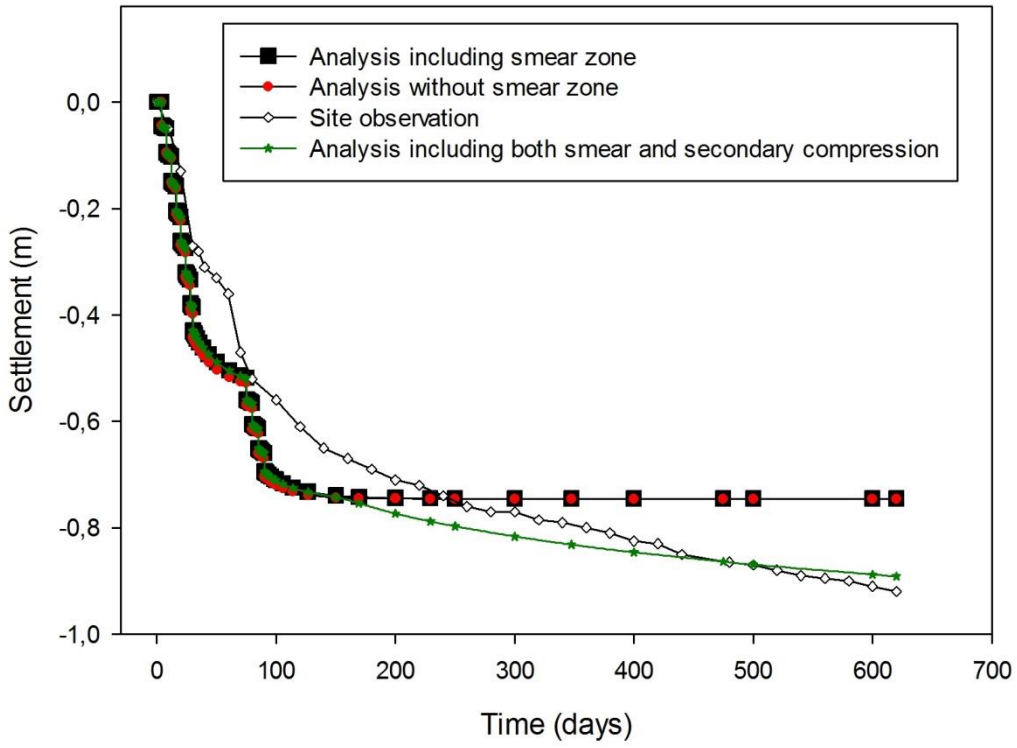

Figure 3.19 Ground surface settlement vs. time graphs for the analyses of analytical method using the linear soil model

3.6.2 Analytical Method Using the Non-Linear Soil Model

For the analyses performed with the non-linear soil model, parameters were used as given in Table 3.4 and 3.5. Figure 3.20 shows the model for the analyses.

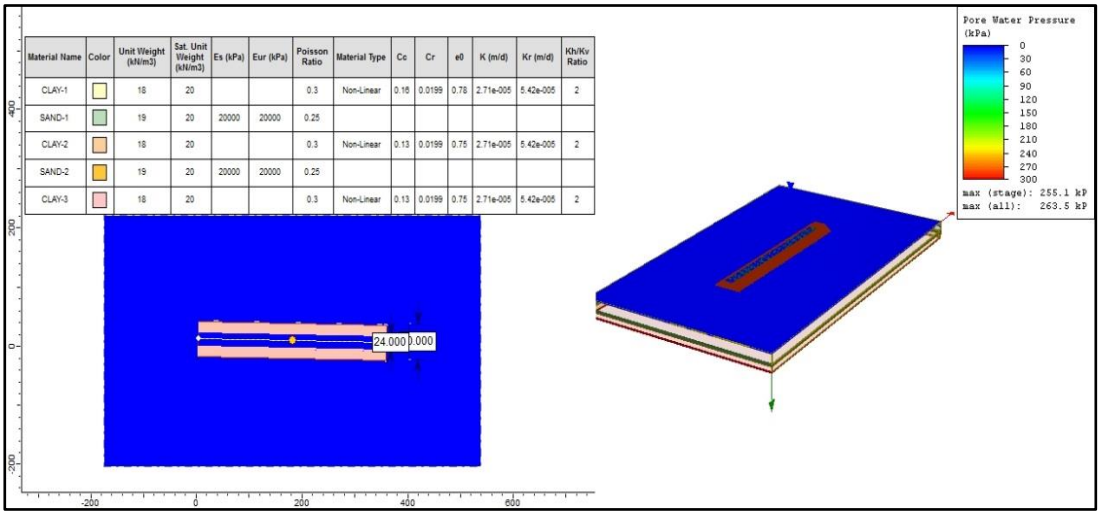

Figure 3.20 Model for analytical method using non-linear soil model

Curves of settlement vs. time results get from the analytical method using the non-linear soil model which consist of analysis ignoring smear effect, including smear effect and analysis in which the secondary compression has been taken into consideration has been presented in Figure 3.21 below.

From the curves, it can be concluded that in terms of final settlement values, non-linear soil model gave closer values to the in-situ measurement than both the linear soil model of analytical method and FE analyses. It can be clearly seen from Figure 3.21 that, primary consolidation has taken more time with less settlement amounts on the site compared to the estimated behaviour. It has to be mentioned that, non-linear soil model gave results on the safe side in contrast to the linear soil model.

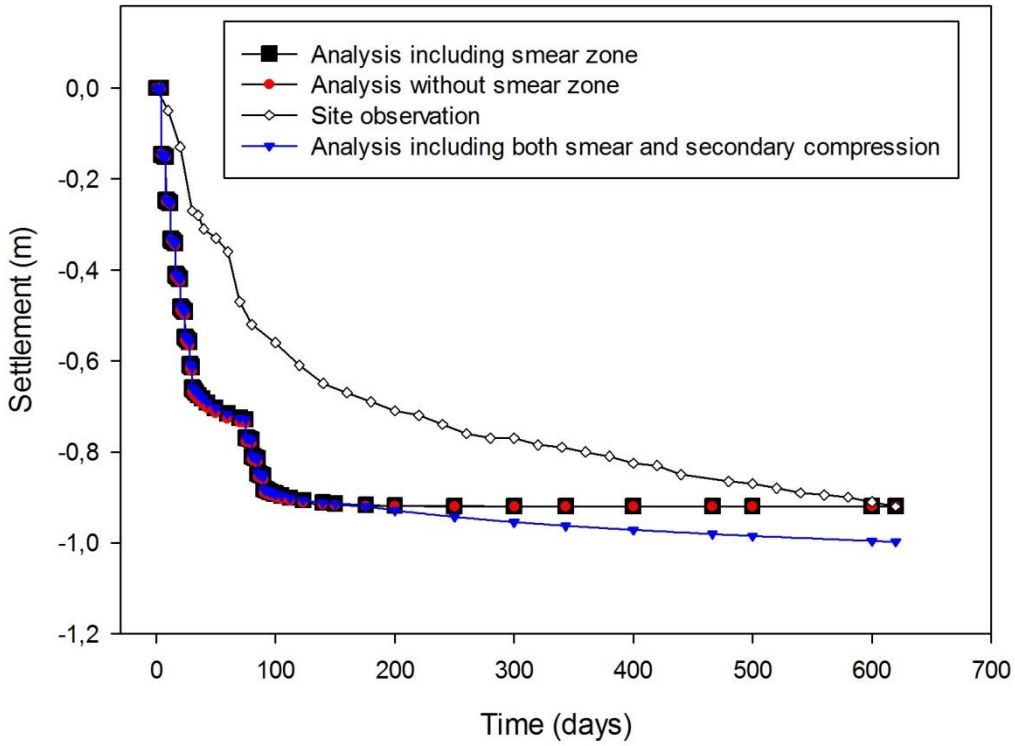

Figure 3.21 Ground surface settlement vs. time curves for the analyses of analytical method using the non-linear soil model

It has been observed that, analytical method gave closer values of settlement amounts to in-situ measurements when compared to the FE analyses. On the other hand, analytical method with non-linear soil model and the FE analyses have overestimated the consolidation settlements, whereas analytical method with linear soil model have underestimated slightly. Both the analytical and finite element methods gave good agreements with site observations for the time for the end-of primary consolidation. All of the curves reveal an obvius slope change at approximately 100~120 days. Another important result that took attention is that, in FE analyses when the smear effect is taken into consideration, the primary consolidation portion of the curve showed very close behaviour to the in-situ measurement curve.

Figure 3.22 below shows the ground settlement values with respect to distance from toe of embankment at 620 days.

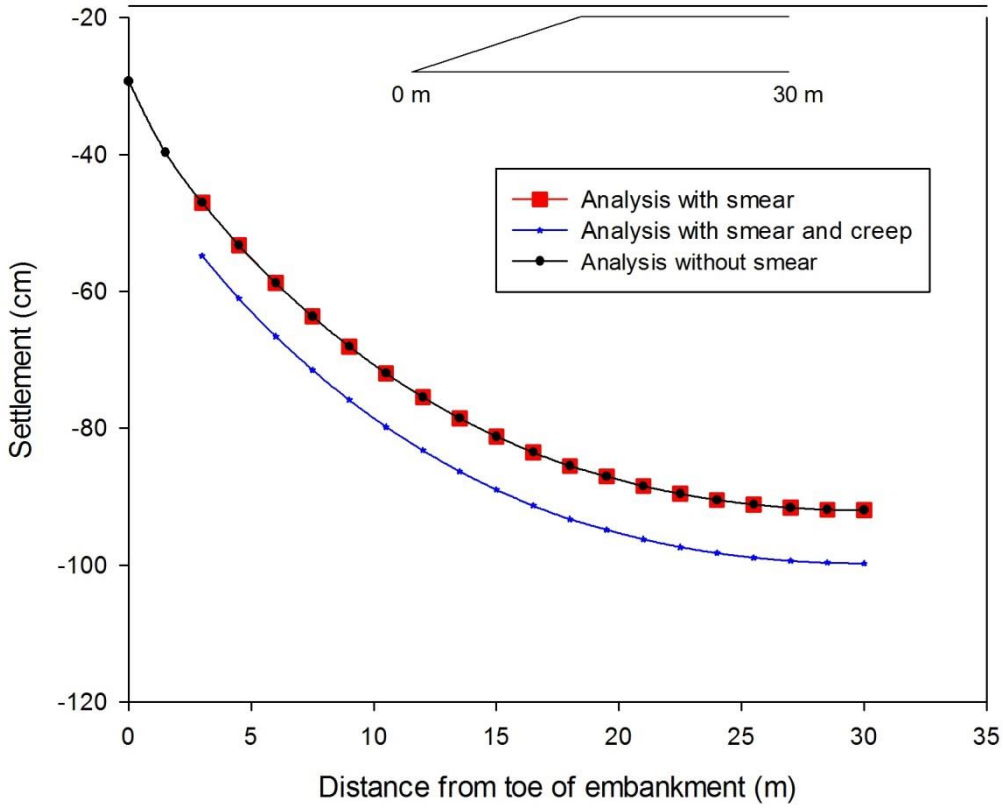

Figure 3.22 Settlement vs. distance from toe of embankment for analyses of analytical method using non linear soil model (after 620 days)

It can be concluded that all the 3 curves gave the expected behaviour as increasing the settlement values when going towards the centerline of the embankment.

3.7 Prediction of End of Primary Settlement – Asaoka Graphical Method

As explained in Chapter 2, Asaoka graphical method is used to predict the end of primary consolidation. For the application of the method, the measured values of settlement used are tabulated below.

Table 3.9 Settlement vs. time values used for Asaoka graphical method

Time (days)	Settlement (m)
20	0.13
40	0.31
60	0.36
80	0.52
100	0.56
120	0.61

Using the values of Table 3.9 the graphical method is applied and the intersection of the trendline with the 45^0-line is determined by extrapolating the best line of the trend of S_{j+1} vs S_j data.

As can be seen from Figure 3.23 that, the trendline intersects the 45^0-line approximately at settlement equals 75 cm. This implies a period of approximately 200 days. Asaoka graphical method gave a larger value for primary consolidation settlement and also a longer duration for the completion of it than the case occured on site. This can be explained with the staged constuction of the case. First part of the embankment is constructed in 30 days, however the second part of embankment finishes at 80th day. And primary consolidation finishes approximately at 120 days. Therefore, data used for graphical procedure involves the loading stages of soft soil and the difference between estimated time and settlement from the graphical procedure and the in-situ measurements arises from this.

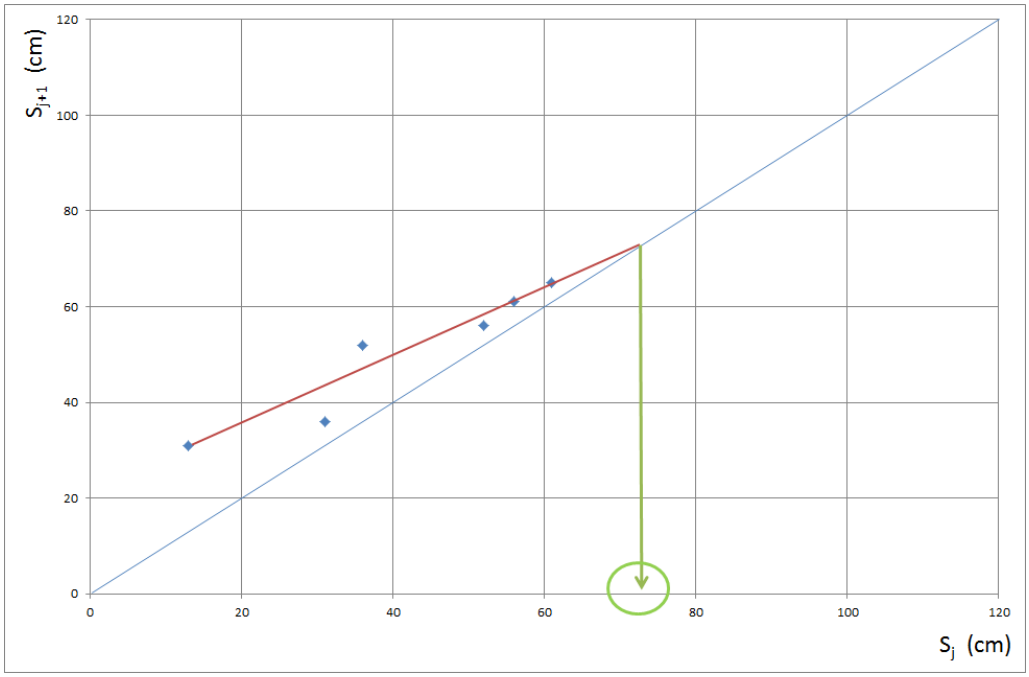

Figure 3.23 Application of Asaoka graphical method to the case study

CHAPTER 4

PARAMETRIC STUDY

For the purpose of investigating the effects of different factors on consolidation behaviour of a soft soil which is improved by vertical drains, a series of parametric studies were performed by finite element method in the context of this study. Such factors are namely, the diameter of smear zone, d_s; the ratio of smear zone horizontal permeability to undisturbed soil horizontal permeability, $\frac{k_h}{k_h'}$ and spacing of vertical drains, *s*; penetration length of vertical drains, *Lw*. Each factor is discussed individually in the following sections. The finite element results of each case including the total deformations, vertical deformations and excess pore pressures etc can be seen in Appendices A through C.

Parametric study analyses have been performed by using only the finite element method. Additionally, the model of the problem was simplified by ignoring the two layers at the bottom one of which is 1 m-thick clay layer and the other one is 10 m-thick sand and gravel because it has been thought that those two layers do not contribute much to the consolidation settlement of the ground and for a less complex and less time consuming study the two soil layers were omitted from the model.

All of the parametric study analyses were performed with the same parameters and boundary conditions explained in Chapter 3.

4.1 Effect of Smear Zone Diameter on Consolidation

As explained in Chapter 2, different researchers who studied the vertical drain consolidation problem, have proposed different values of smear zone diameter.

Proposals vary from 1.5 to 5.0 times the equivalent drain diameter as shown in Table 2.1. In order to see the effect of smear zone diameter on consolidation, numerical finite element analyses were performed with different diameters of smear zone, for the highway embankment case study presented in Chapter 3. Settlement vs. time graphs of the results of analyses mentioned are illustrated in Figure 4.1.

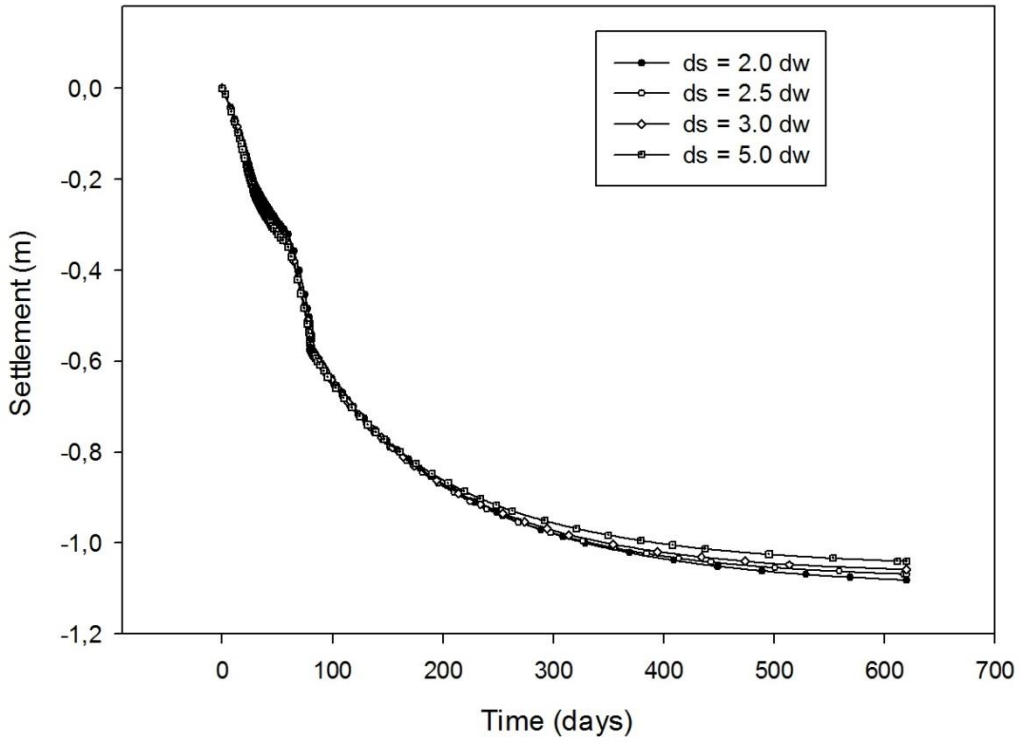

Figure 4.1 Settlement vs. time graph for different smear zone diameters

From Figure 4.1 it can be concluded that the extent of the smear zone around a vertical drain does not have significant effect on the consolidation behaviour. Therefore typical values recommended in the literature (such as ratio of 2.5 or 3) could be used. Compared to the drainage distance (i.e. half of spacing = 0.7 m), even the largest value of proposed smear zone diameters, which is actually $d_s = 5.0\ d_w = 0.33$ m is so small to make a difference in the consolidation behaviour.

4.2 Effect of Degree of Disturbance within the Smear Zone on Consolidation

As explained in Chapter 2, installation of vertical drains create a disturbed smear zone within the soil around the drain. Disturbance degree, which is expressed by the ratio of horizontal permeability within the undisturbed soil to the horizontal permeability of the disturbed soil, $\frac{k_h}{k_h'}$, is investigated to see the effect of disturbance around the drains on the consolidation behaviour. For this purpose, a series of numerical analyses were performed with different values of $\frac{k_h}{k_h'}$, namely; 1.5, 2.0, 3.0 and 4.0. The results of these analyses are presented in Figure 4.2 in terms of settlement vs. time graphs.

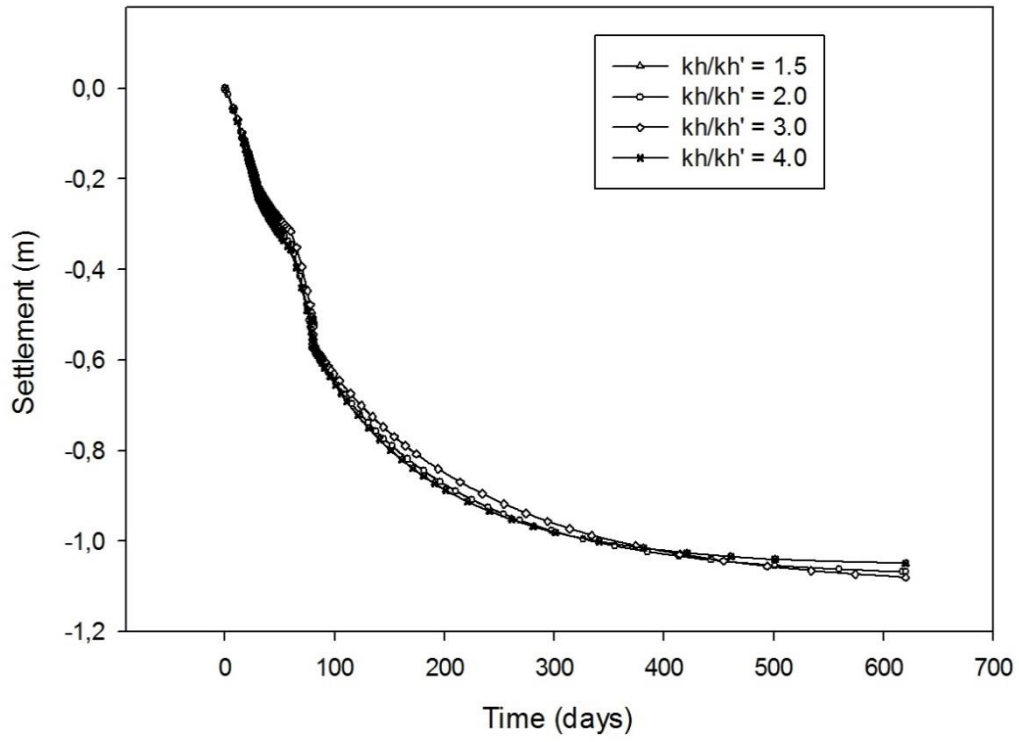

Figure 4.2 Settlement vs. time graph for different degrees of disturbance within the smear zone

From the graphs, it can be seen that the degrees of disturbance within the smear zone which are proposed in the literature do not cause significant differences in the results of analyses. Within the range of 1.5 to 4.0 value of $\frac{k_h}{k_h'}$, there occurs no significant change in the results of the analyses. Once there occurs a disturbed zone in any degree, the flow of water experiencs a retardation and the general dissipation behaviour takes shape depending on this issue and in the range mentioned, this behaviour do not change notably.

4.3 Effect of Drain Spacing on Consolidation

In order to investigate the effect of drain spacing on consolidation behaviour of a soft soil improved by PVDs, a series of numerical analyses were conducted and the settlement vs. time curves are presented in Figure 4.3 for each analysis result.

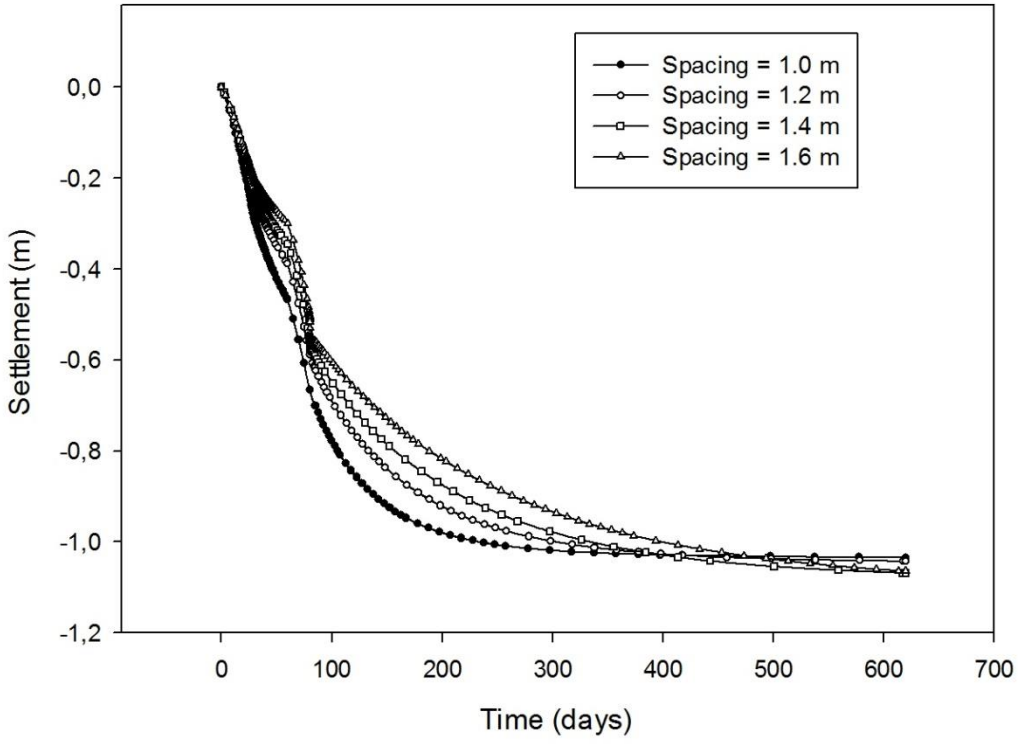

Figure 4.3 Settlement vs. time graph for different drain spacings

Figure 4.3 shows that spacing of drains have a vital effect on the consolidation beaviour of a soft soil. Even small changes in spacings, cause large differences on the time required for a certain degree of consolidation. There occurs no significant change on the final settlement value however, the time dependent behaviour of the settlement (especially the rate of settlement within the primary consolidation) is noticably affected by the spacings between two adjacent drains, as expected.

Comparison of the excess pore pressures generated and dissipated after the 8-m-high embankment is placed (phase 2, at t=60 days) is presented in figures below for spacing 1.0 and 1.6 meters (Figure 4.4 and 4.5). When drain spacing is 1 m, the excess pore pressures under the center of the embankment is 140 kPa at some shallower locations underneath the embankment but significant portion of the compressible layer's excess pore water has dissipated toward the drains. When the spacing of drains is 1.6 m, as expected, a more significant portion of the compressible layer has on the order of 140 kPa excess pore pressures still 30 days after the load is applied, that means it takes longer distance and longer time for the exces pore water do move towards the drains.

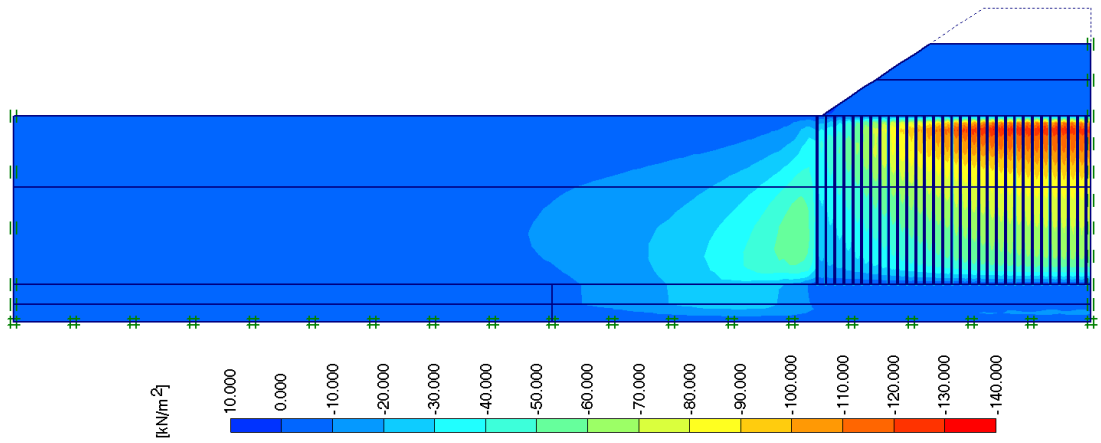

Figure 4.4 Phase-2 pore pressure generation for parametric study analysis with drain spacing, s = 1.0 m

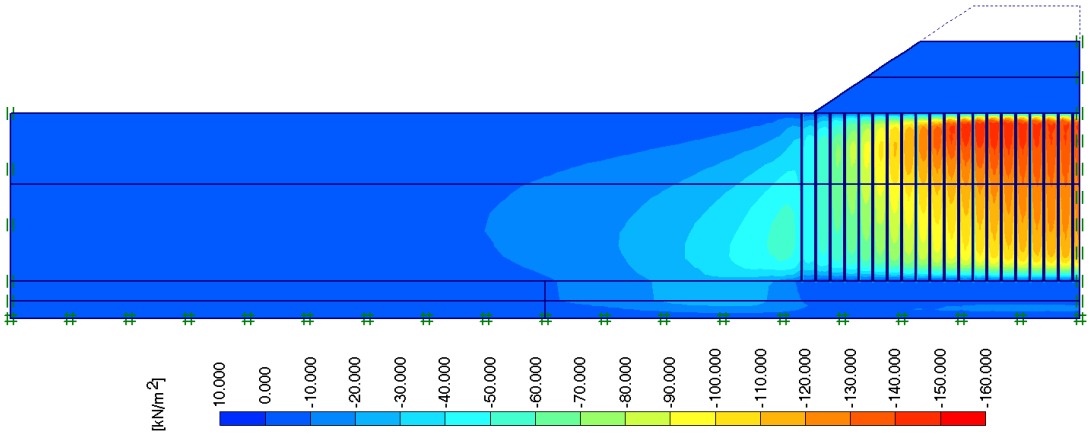

Figure 4.5 Phase-2 pore pressure generation for parametric study analysis with drain spacing, s = 1.6 m

4.4 Effect of Drain Penetration on Consolidation

For the case of Sakarya-2 Viaduct approach embankment, the foundation contains an approximately 18.0 m thick soft soil above a drained layer. By conducting a series of numerical analyses with different drain lengths on the same model, the effect of penetration length of vertical drains is investigated. Setlement vs. time curves are illustrated in Figure 4.6. Penetration lengths are given in a normalized order, where H denotes the compressible layer thickness, 18.0 m and L_p denotes the length of drains penetrated.

It can be concluded from Figure 4.6 that, penetration length of drains have a vital effect on both the final settlement time and the time dependent settlement behaviour of the soft soil. As the drain lengths increase, consolidation time decreases significantly. Resultantly, drain lengths to use on a project have to be studied in detail depending on the desired time for a certain degree of consolidation to complete, especially for very thick clay layers where the full-depth drain penetration may not be economical/practical.

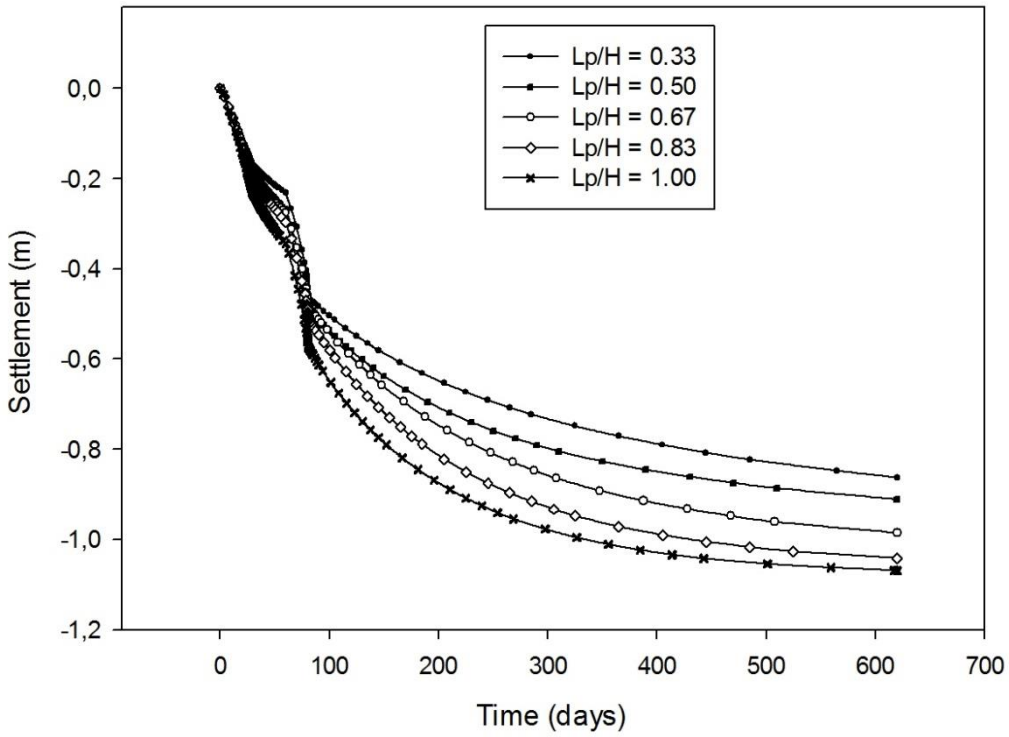

Figure 4.6 Settlement vs. time graph for different drain penetration length ratios

The figures below show the excess pore pressures at phase-4 (t=620 days) for drain penetration ratio of L_p/H=0.33 and 0.83 (6 m and 15 m penetration of drains into 18-m-thick compressible layer, respectively). It is clearly seen that the portion of the layer where drains did not penetrate have significant excess pore pressures, on the contrary the zone where drains are penetrated have dissipated almost all of the excess pore pressures. When the drain penetration ratio is 0.83, most of the excess pore pressure in the whole soft clay layer have dissipated, as compared to the penetration ratio of 0.33 where still almost all excess pore pressures exist within the zone where drains did not penetrate.

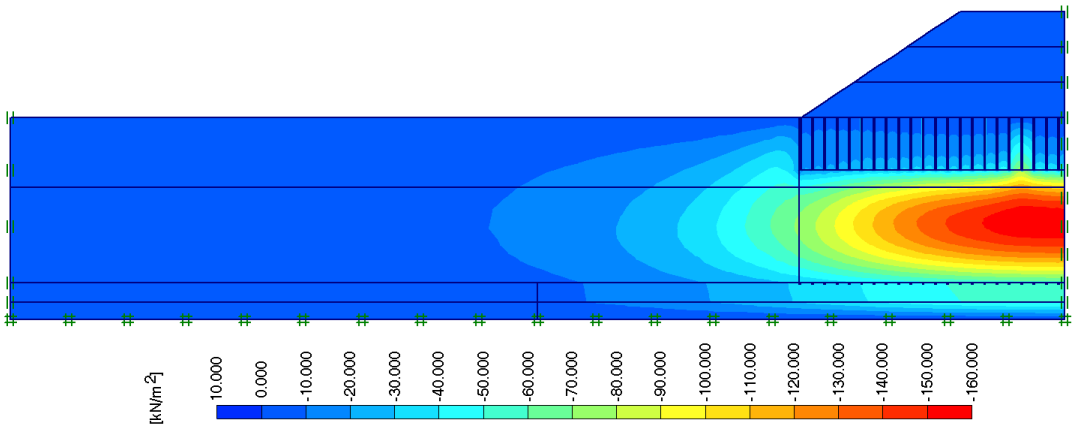

Figure 4.7 Phase-4 pore pressure generation for parametric study analysis with drain penetration length, L_p = 6.0 m

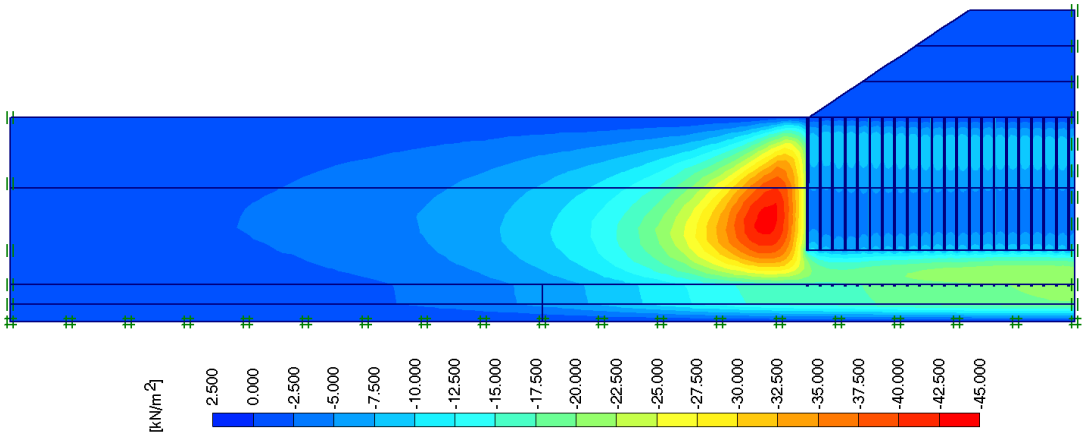

Figure 4.8 Phase-4 pore pressure generation for parametric study analysis with drain penetration length, L_p = 15.0 m

CHAPTER 5

SUMMARY AND CONCLUSIONS

5.1 Summary

This study firstly presented a review of literature about consolidation of soft soils which are improved by prefabricated vertical drains. In the next stage, an embankment loading on a soft ground case-history is studied and analyzed by both finite element and analytical methods and the two methods were compared considering the measured time-settlement behaviour of the improved soft soil.

Finally, a series of parametric studies were performed in order to investigate the effects of certain factors among various factors on the settlement behaviour of a PVD improved soft soil. Parametric study is performed by using solely the finite element method with Soft Soil model. The case history chosen to be analyzed for this study is introduced by giving information about site investigation, geometrical and material properties and loading history.

5.2 Conclusions

In the comparison studies, analytical analyses did reveal close agreement with in-situ measurements especially when the secondary compression is involved in the analysis. Results of analytical method using the linear soil model were on the unsafe side slightly, whereas the results of non-linear soil model analyses were on the safe side. Analytical method based on Terzaghi consolidation theory was very close to in-situ measurements especially in terms of the final settlement values.

On the other hand finite element analyses revealed good agreement with site observations especially for the first 90 days of consolidation. After this point there occured some deviation from the in situ measurement curve but still an error of 13% is seen in terms of the magnitude of final settlement. Finite element analysis which takes into account the secondary compression gave very overestimated results.

Within this conclusion, it has to be noted that, in such an alluvial deposit area, a certain degree of anisotropy is supposed to occur. However in this study materials are assumed to be isotropic therefore it may have affected the results. Other effects that are not taken into account during the analyses are the buckling, clogging and squeezing of the drains. On site these factors may retard the consolidation therefore the time difference between the analyses results and the site observations may arise from this issue.

For the parametric study, conclusions can be summarized as follows;

- Changes in the extent of the smear zone did not affect the results noticably within the values of $d_s=2.0\sim5.0d_w$ which are recommended by various researchers.
- Degree of disturbance within the smear zone which is expressed as k_h/k_h' ratio, did not have a considerable influence on settlement behaviour within the values $k_h/k_h' =1.5\sim4.0$ as recommended in the literature.
- PVD spacing plays a vital role in the consolidation behaviour of a soft soil improved by vertical drains. Even small changes of 0.2 m are studied, there occured significant differences among time vs. settlement curves of the analyses. As the drain spacing decreased from 1.6 m to 1 m rate of settlement increased. The final settlement amount is not inluenced much, only the rate of settlement is influenced within the primary settlement process, as expected. For each project optimum drain spacing can be determined based on such sensitivity analyses for spacing.

- As in the case of PVD spacing, PVD penetration length also had a considerable effect on the settlement values for certain time periods. As the penetration length increased from 0.33H penetration ratio (6-m-long drains in an 18-m-thick soft clay layer), to 1H (full penetration of drain into the layer), the rate of settlement increased as expected. Therefore within a given time, drains that are penetrating more will be draining more water and causing more of the consolidation settlement to take place.

To sum up, for analysis or design of a soft soil foundation improved by PVDs, drain spacing and drain length have to be accurately determined in order to get desired outcomes. On the contrary smear zone extent and the degree of disturbance within the smear zone do not need to be studied as accurately as the above mentioned properties of drains, and suggested values in the literature could be sufficient But still, it should be kept in mind that project-specific sensitivity analyses are recommended to be done for individual cases.

5.3 Future Study

The 2D analyses in this study can be conducted with 3D finite element method and compared with 2D solutions and real measurements.

A similar study may be performed using different soil constitutive models to investigate the accuracy of the used model.

Additional parametric studies on different case histories can strengthen the findings of this study.

In order to validate the findings of the parametric study, a laboratory study may be conducted to investigate the effect of different factors on the consolidation behaviour of a PVD improved soft soil.

REFERENCES

Aboshi, H., & Yoshikuni, H. (1967). A study on the consolidation process affected by well resistance in the vertical drain method. *Soils and Foundations, 7*(4), 38-58.

Almeida, M. S., & Ferreira, C. A. (1993). Field in-situ and laboratory consolidation parameters of a very soft clay. *Predictive Soil Mechanics. Proceedings of the Wroth Memorial Symposium* (s. 73-93). London: Thomas Telford.

Asaoka, A. (1978). Observational procedure of settlement prediction. *Soils and Foundations, 18*(4), 87-101.

Atkinson, M. S., & Eldred, P. J. (1981). Consolidation of soil using vertical drains. *Geotechnique, 31*(1), 33-43.

Basu, D., Prezzi, M., & Madhav, M. R. (2009). Effect of soil disturbance on consolidation by prefabricated vertical drains installed in a rectangular pattern. *Geotech Geol Eng, 28*, 61-77.

Bergado, D. T., Asakami, H., Alfaro, M. C., & Balasubramaniam, A. S. (1991). Smear effects of vertical drains on soft Bangkok clay. *Journal of Geotechnical Engineering, 117*(10), 1509-1530.

Bergado, D. T., Manivannan, R., & Balasubramaniam, A. S. (1996). Proposed criteria for discharge capacity of prefabricated vertical drains. *Journal of Geotextiles and Geomembranes, 14*, 481-505.

Biot, M. (1941). General theory of three dimensional consolidation. *Journal of Applied Physics, 12*, 155-164.

Bo, M. (2004). Discharge capacity of prefabricated vertical drain and their measurements. *Geotextiles and Geomembranes, 22*, 37-48.

Bowles, J. (1996). *Foundation Analysis and Design.* Mc-Graw Hill.

Carillo, N. (1942). Simple two and three dimensional cases in the theory of consolidation of soils. *Journal of Mathematics and Physics, 21*(1), 1-5.

Chai, J. C., & Bergado, D. T. (1993). Some techniques for finite element analysis of embankments on soft ground. *Canadian Geotechnical Journal, 30*, 710-719.

Chai, J., & Miura, N. (1999). Investigation of factors affecting vertical drain behaviour. *Journal of Geotechnical Engineering, 125*(3), 216-226.

Das, B. (1997). *Advanced Soil Mechanics.* Taylor and Francis.

Fellenius, B. H., & Castonguay, N. G. (1985). The efficiency of band-shaped drains: a full scale laboratory study. *Report to National Research Council and the Industrial Research Asistance Programme*.

Hansbo, S. (1960). Consolidation of clay with special reference to influence of vertical sand drains. *Swedish Geotechnical Institute, Proceedings, 18.*

Hansbo, S. (1979). Consolidation of clay by band shaped prefabricated drains. *Ground Engineering, 12*(5), 16-25.

Hansbo, S. (1981). Consolidation of fine grained soils by prefabricated vertical drains. *Proceedings of the 10th International Conference on Soil Mechanics and Foundation Engineering, 3,* s. 677-682. Stocholm.

Hansbo, S. (1997). Aspects of vertical drain design: Darcian or non-Darcian flow. *Geotechnique, 47*(5), 983-992.

Hawlader, B. C., Imai, G., & Muhunthan, B. (2002). Numerical study of the factors affecting the cosolidation of clay with vertical drains. *Geotextiles and Geomembranes, 20,* 213-239.

Hird, C. C., Pyrah, I. C., & Russell, D. (1992). Finite element modelling pf vertical drains beneath embankments on soft ground. *Geotechnique, 42*(3), 499-511.

Hird, C., & Moseley, V. (2000). Model study of seepage in smear zones around vertical drains in layered soil. *Géotechnique, 50*(1), 89-97.

Indraratna, B., & Redana, I. W. (1997). Plane strain modelling of smear effects associated with vertical drains. *Journal of Geotechnical Engineering, 123*(5), 474-478.

Indraratna, B., & Redana, I. W. (1998). Laboratory determination of smear zone due to vertical drain installation. *Journal of Geotechnical Engineering, 124*(2), 180-184.

Indraratna, B., & Redana, I. W. (2000). Numerical modelling of vertical drains with smear and well resistance installed in soft clay. *Canadian Geotechnical Journal, 37,* 132-145.

Indraratna, B., & Rujikiatkamjorn, C. (2010). Review of methods of analysis for the use of vacuum preloading and vertical drains for soft clay improvement. *Geomechanics and Geoengineering: An International Journal, 5*(4), 223-236.

Indraratna, B., Balasubramaniam, A. S., & Ratnayake, P. (1994). Performance of embankment stabilized wşth vertical drains on soft clay. *Journal of Geotechnical Engineering, 120*(2), 257-273.

Indraratna, B., Bamunawita, C., Redana, I., & McIntosh, G. (2003). Modelling of geosynthetic vertical drains in soft clays. *Journal of Ground Improvement, 7*(3), 127-138.

Indraratna, B., Rujikiatkamjorn, C., Geng, X., Kelly, R., McIntosh, G., & Buys, H. (2010). Performance monitoring of vacuum preloading for stabilising soft foundations for transportation and port infrastructure. *Indian Geotechnical Conference, 2010, GEOtrendz, IGS Mumbai Chapter & IIG*, (s. 27-37). Bombay.

Jamiolkowski, M., Lancelotta, R., & Wolski, W. (1983). Precompression and speeding up conslidation. *Proceedings of the 8th European Conference on Soil Mechanics and Foundation Engineering, 3*, s. 1201-1226. Helsinki.

Kjellman, W. (1948). Accelerating consolidation of fine grained soils by means of cardboard wicks. *Proceedings of the 2nd International Conference on Soil Mechanics and Foundation Engineering, ICSMFE, 2*, s. 302-305. Rotterdam.

Long, R. P., & Covo, A. (1994). Equivalent diameter of vertical drains with an oblong cross-section. *Journal of Geotechnical Engineering Division, ASCE, 120*(9), 1625-1630.

Madhav, M., Park, Y. M., & Miura, N. (1993). Modelling and study of smear zone around band shaped drains. *Soils and Foundations, 33*(4), 135-147.

Mesri, G., & Huvaj-Sarihan, N. (2009). The Asaoka method revisited. *Proceedings of the 17th International Conference on Soil Mechanics and Geotechnical Engineering*, (s. 131-134).

Mesri, G., & Lo, D. (1991). Field performance of prefabricated vertical drains. *Proceedings of the Geotechnical Conference on Geotechnical Engineering*

for Coastal Development - Theory to Practice, 1, s. 231-236. Yokohama, Japan.

Onoue, A. (1988). Consolidation with vertical drains taking well resistance and smear into consideration. *Soils and Foundations, 28*(4), 165-174.

Onoue, A., Ting, N. H., Germaine, J. T., & Whitman, R. V. (1991). Permeability of disturbed zone around vertical drains. *Proceedings of the ASCE Geotechnical Engineering Congress* (s. 879-890). Colorado: ASCE.

Peck, R., Hansen, W., & Thornburn, T. (1953). *Foundation Engineering.* New York: John Wiley and Sons.

Rendulic, L. (1936). Relation between void ratio and effective principal stress for a remoulded silty clay. *Proceedings of the 1st International Conference on Soil Mechanics and Foundation Engineering, 3*, s. 48-51. Cambridge.

Rixner, J., Kramer, S., & Smith, A. (1986). *Prefabricated vertical drains, Vol.s I, II and III: Summary of Research Report: Final Report.* Federal Highway Administration, Washington D.C.

Rujikiatkamjorn, C., & Indraratna, B. (2010). Radial consolidation modeling incorporating effect of a smear zone for a multi layer soil with downdrag caused by mandrel action. *Canadian Geotechnical Journal, 47*, 1024-1035.

Sathananthan, I. (2005). Modeling of vertical srains with smear installed in soft clay. *M.Sc. Thesis, University of Wollongong*. Wollongong, New South Wales, Australia.

Sengul, T., Edil, T., & Özaydın, K. (2013). Determination of the factors affecting the discharge capacity of prefabricated vertical drains. *İMO Teknik Dergi*, s. 6529-6557.

Sharma, J., & Xiao, D. (2000). Characterization of a smear zone around vertical drains by large scale laboratory tests. *Canadian Geotechnical Journal, 37*(6), 1265-1271.

Sharma, J., & Xiao, D. (2001). Determination of Smear Zone around Vertical Drains. *Proceedings of the Soft Ground Technology Conference, editors Hanson, J.L. and Termaat, R.J., Netherlands.*

Shinsha, H., Hara, H., Abe, T., & Tanaka, A. (1982). Consolidation settlement and lateral displacement of soft ground improved by sand drains. *Tsushi-to-Kiso, Japan Society of Soil Mechanics and Foundation Engineering, 7*(12), 7-12.

Tan, S., & Chew, S. (1996). Comparison of the hyperbolic and the Asaoka observational method of monitoring consolidation with vertical drains. *Soils and Foundations, 36*(3), 31-42.

Terzaghi, K. (1943). *Theoretical Soil Mechanics.* John Wiley and Sons.

Terzaghi, K., Peck, R., & Mesri, G. (1996). *Soil Mechanics in Engineering Practice* (3rd b.). New York: John Wiley and Sons.

Walker, R., & Indraratna, B. (2007). Vertical drain consolidation with overlapping smear zones. *Geotechnique, 57*(5), 463-467.

Whiteley, C. (2009). Determining the end of primary settlement using a simple analytical model progressively calibrated to field settlement data. *M.Sc. Thesis, Bringham Young University*. Utah, USA.

Yoshikuni, H., & Nakanodo, H. (1974). Consolidation of fine grained soils by drain wells with finite permeability. *Soils and Foundations, 14*(2), 35-46.

Yuksel Project. (2010). *Bozüyük-Mekece Devlet Yolu II. Kısım İnşaatı İşi, Km:82+300-82+525 Dolgusu Stabilite Sorunları Geoteknik Proje Raporu.*

APPENDIX - A

Test Results

(Yuksel Project, 2010)

Table A.1 Laboratory test results of the samples taken from borehole D82470-1i

Depth	w (%)	e	γ_{dry} (kN/m$_3$)	γ_{sat} (kN/m$_3$)	Atterberg Limits			Sieve Analsis		USCS	Unconfined Compression	Triaxial Compression	
					LL %	PL %	PI	+4 %	- 200 %		qu (kPa)	c kPa	φ degrees
1.50 - 1.95	9,4				-	NP	-	56,2	25,7	GM			
3.00 - 3.45	9,9				-	NP	-	43,9	27,5	GM			
4.50 - 4.95	9,6				-	NP	-	53,1	21,7	GM			
4.50 - 4.95	21,7				44,1	22,3	21,8	-	92,2	CL			
6.00 - 6.45	25,3				37,9	22	15,9	-	87,4	CL			
7.50 - 7.95	36,6				44,4	23,3	21,1	-	97,9	CL			
7.95 - 8.45	23,9	0,6	19,9	25,8	44,4	21,8	22,6	-	89,5	CL	44		
9.00 - 9.45	24,9				36,3	20,2	16,1	-	87,2	CL			
10.50 - 10.95	27,8				44,4	22,4	22	-	95,5	CL			
12.00 - 12.45	32,3				47,7	23,2	24,5	-	98,9	CL			
13.50 - 13.95	29,4				47,4	23,7	23,7	-	98,9	CL			
13.95 - 14.45	30,4	0,79	19,2	26,4	37,9	19,6	18,3	-	98,1	CL	92		
15.00 - 15.45	27,4				38,4	21,7	16,7	-	97,1	CL			
16.50 - 16.95	32,2				52,6	25,9	26,7	-	99,6	CH			
16.50 - 16.95	29,5				Not enough sample			-	91,8	CL			
18.00 - 18.45	23,9				36,3	18,7	17,6	-	91,1	CL			
19.00 - 19.50	26,6		20,7		43,9	21,3	22,6	-	95,8	CL	59	31	2
19.50 - 19.95	27,3				40,7	21,4	19,3	-	96,6	CL			
21.00 - 21.45	29,5				40,2	20,3	19,9	-	98,2	CL			
22.50 - 22.95	27,8				29,5	21,7	7,8	-	76,1	CL			
22.50 - 22.95	8,7				-	NP	-	42,3	7,4	SP-SM			
24.00 - 24.45	10,5				-	NP	-	19,9	4,9	SP			
25.50 - 25.95	28,5				31,3	21,4	9,9	-	75,3	CL			
27.00 - 27.45	13,6				-	NP	-	26,6	10,3	SP-SM			
28.50 - 28.95	13,3				-	NP	-	44,9	29	GM			
31.00 - 31.45	8,8				-	NP	-	36,6	4,9	SP			
31.50 - 31.95	6,9				-	NP	-	39,6	8,4	SP-SM			
33.00 - 33.45	10,0				-	NP	-	48,4	7,4	GP-GM			
34.50 - 34.95	10,6				-	NP	-	26,4	4,9	SP			
36.00 - 36.45	7,7				-	NP	-	12,9	32,3	SM			
37.50 - 37.90	40,9				36,7	23,3	13,4	-	84,1	CL			

Table A.2 Laboratory test results of the samples taken from borehole D82470-2i

Depth	w (%)	e	γ_{dry} (kN/m$_3$)	γ_{sat} (kN/m$_3$)	Atterberg Limits			Sieve Analsis		USCS	Unconfined Compression	Triaxial Compression	
					LL %	PL %	PI	+ 4 %	- 200 %		qu (kPa)	c kPa	φ degrees
1.50 - 1.95	9.5				40.1	20.2	19.9	68.7	21.3	GC			
3.00 - 3.45	9.5				31.8	17.5	14.3	39.7	35.1	GC			
4.50 - 4.95	18.8				39.9	19.3	20.6	3.3	86	CL			
6.00 - 6.45	26.7				37	19.7	17.3	0.2	95.2	CL			
7.00 - 7.45	27.9	0.8	19.4	27.3	52.2	26.9	25.3	-	98.8	CH	102	56	0
7.50 - 7.95	32.6				41.2	25.9	15.3	-	98.6	CL/ML			
9.00 - 9.45	23.3				34.4	19.4	15	-	88.6	CL			
10.00 - 10.50	38.9	0.94	17.8	24.8	38.4	20.8	17.6	-	89.5	CL	41		
10.50 - 10.95	29.8				49.9	24.6	25.3	0.6	91	CL			
12.00 - 12.45	26.1				33.6	18.6	15	-	85.5	CL			
13.50 - 13.95	28.0				45.9	20.4	25.5	-	95.5	CL			
14.50 - 15.00	26.2				45.7	22.1	23.6	-	96.4	CL		66	1
15.00 - 15.45	35.2				35.6	20.1	15.5	-	89.8	CL			
16.50 - 16.95	29.8				33.9	19.5	14.4	0.8	81.3	CL			
18.00 - 18.45	21.8				38.2	20	18.2	0.9	64.6	CL			
18.00 - 18.45	20.2				29.5	17.2	12.3	3.4	54.3	CL			
19.50 - 19.95	16.8				38.7	19.9	18.8	2.8	60.1	CL			
21.00 - 21.45	11.7				30.5	17.4	13.1	37.7	50.7	CL			
21.00 - 21.45	30.9				Not enough sample			-	88.1	CL			
22.50 - 22.95	11.8				24.9	15.1	9.8	47.2	24.6	GC			
24.00 - 24.45	23.6				-	NP	-	13.9	45.9	SM			
24.00 - 24.45	7.4				-	NP	-	50.3	13.5	GM			

Table A.3 Laboratory test results of the samples taken from borehole D82420-1i

Depth	w (%)	e	γ_{dry} (kN/m$_3$)	γ_{sat} (kN/m$_3$)	Atterberg Limits			Sieve Analsis		USCS	Unconfined Compression	Triaxial Compression	
					LL %	PL %	PI	+ 4 %	- 200 %		qu (kPa)	c kPa	φ degrees
1.50 - 1.95	11.3				-	NP	-	41.8	33.4	GM			
3.00 - 3.45	24.9				28.7	17.7	11	-	82.2	CL			
4.50 - 4.95	29.1				40.3	22.3	18	-	95.3	CL			
5.50 - 6.00	28.9	0.81	19	26.7	47.9	25.2	22.7	-	98.8	CL	126		
6.00 - 6.45	30.7				56.2	27.6	28.6	-	96.4	CH			
7.80 - 8.25	26.7				35.7	20.3	15.4	-	88.6	CL			
9.00 - 9.45	35.2				47.9	25.8	22.1	-	98.8	CL			
10.30 - 10.80	24.9	0.68	19.9	26.7	43.2	20.8	22.4	0.4	89.9	CL	89		
10.80 - 11.25	20.4				30.2	17	13.2	-	79.2	CL			
12.00 - 12.45	27.7				40.4	20.5	19.9	-	93.4	CL			
13.50 - 13.95	25.9				32.3	18.9	13.4	-	97.8	CL			
14.50 - 15.00	27.3		21.3		42	20.8	21.2	-	99	CL	82		
15.00 - 15.45	34.3				42.8	22.2	20.6	-	99.4	CL			
16.50 - 16.95	28.1				41.6	20.7	20.9	-	94.5	CL			
18.00 - 18.45	23.4				37.2	19.1	18.1	-	80.2	CL			
19.50 - 19.95	26.2				43.1	20.1	23	-	98.4	CL			
21.00 - 21.45	32.5				56.6	26.7	29.9	-	99.2	CH			
22.50 - 22.95	32.9				53.3	24.2	29.1	-	97.3	CH			
24.00 - 24.45	20.5				30.3	17.2	13.1	5.9	51.1	CL			
25.50 - 25.95	8.7				-	NP	-	45.6	12.4	GM			
27.00 - 27.45	35.5				32.3	24.7	7.6	-	93.5	ML			

Table A.4 Laboratory test results of the samples taken from borehole D82420-2i

Depth	w (%)	e	γ_{dry} (kN/m$_3$)	γ_{sat} (kN/m$_3$)	Atterberg Limits			Sieve Analsis		USCS	Unconfined Compression	Triaxial Compression	
					LL %	PL %	PI	+ 4 %	- 200 %		qu (kPa)	c kPa	φ degrees
1.50 - 1.95	3.1				-	NP	-	79.3	7.6	GP			
1.50 - 1.95	18.9				Not enough sample			-	88.0	CH			
3.00 - 3.45	30.0				51.5	27.9	23.6	-	99.3	CH			
4.50 - 4.95	24.5				50.0	24.2	25.8	-	97.0	CH/CL			
5.50 - 6.00	23.4	0.7	20.0	26.8	48.4	24.5	23.9	-	99.0	CL	228	65	7
6.00 - 6.45	25.0				58.7	26.4	32.3	2.8	93.6	CH			
7.50 - 7.95	23.1				32.1	18.4	13.7	-	86.6	CL			
9.00 - 9.45	26.8				76.7	21.4	55.3	-	85.7	CH			
9.00 - 9.45	27.8				Not enough sample			25.6	59.4	CH			
10.25 - 10.75	21.8	0.7	18.8	26.6	39.5	20.6	18.9	31.8	51.6	CL	85		
10.75 - 11.20	24.0				44.4	22.1	22.3	3.2	82.4	CL			
12.00 - 12.45	22.0				51.7	25.9	25.8	39.9	50.6	CH			
13.50 - 13.95	15.2				-	NP	-	24.6	13.7	SM			
15.00 - 15.45	5.2				-	NP	-	59.7	6.9	GP-GM			
16.76 - 17.21	4.9				-	NP	-	59.2	9.9	GP-GM			
18.00 - 18.20	11.1				-	NP	-	30.2	22.5	SM			
19.50 - 19.93	11.8				-	NP	-	25.2	26.7	SM			
21.00 - 21.14	16.5				35.1	20.8	14.3	5.7	70.9	CL			
22.50 - 22.60	22.5				Not enough sample			-	82.0	CL			

Table A.5 SPT test results of the 4 boreholes

D82420-1İ		D82420-2İ		D82470-1İ		D82470-2İ	
Depth (m)	SPT Blow Count	Depth (m)	SPT Blow Count	Depth (m)	SPT Blow Count	Depth (m)	SPT Blow Count
1.5	12	1.5	10	1.5	3	1.5	12
3.0	5	3.0	10	3.0	13	3.0	57
4.5	6	4.5	17	4.5	18	4.5	17
6.0	13	6.0	10	6.0	7	6.0	14
7.8	9	7.5	12	7.5	10	7.5	11
9.0	8	9.0	15	9.0	7	9.0	13
10.8	16	10.8	17	10.5	11	10.5	12
12.0	12	12.0	11	12.0	9	12.0	20
13.5	12	13.5	22	13.5	17	13.5	16
15.0	12	15.0	49	15.0	16	15.0	12
16.5	16	16.5	R	16.5	27	16.5	20
18.0	17	16.8	86	18.0	22	18.0	15
19.5	19	18.0	R	19.5	16	19.5	15
21.0	14	19.5	R	21.0	15	21.0	21
22.5	15	21.0	R	22.5	52	22.5	25
24.0	14	22.5	R	24.0	53	24.0	R
25.5	48			25.5	21		
27.0	21			27.0	55		
				28.5	44		
				30.0	10		
				31.0	48		
				31.5	57		
				33.0	58		
				34.5	49		
				36.0	68		
				37.5	R		

APPENDIX B

TOTAL DISPLACEMENT CONTOURS OF ANALYSES

Appendix B presents the total displacement contours for analysis ignoring the smear zone, analysis including the smear zone, analysis including both smear and creep and 13 parametric study analyses.

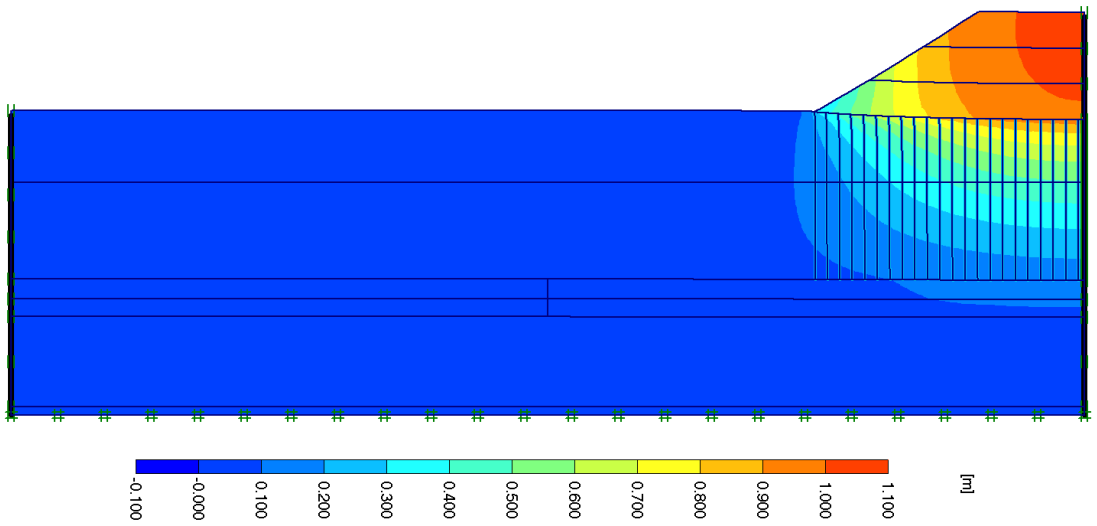

Figure B.1 Total Displacement Contours for Analysis Ignoring The Smear Effect

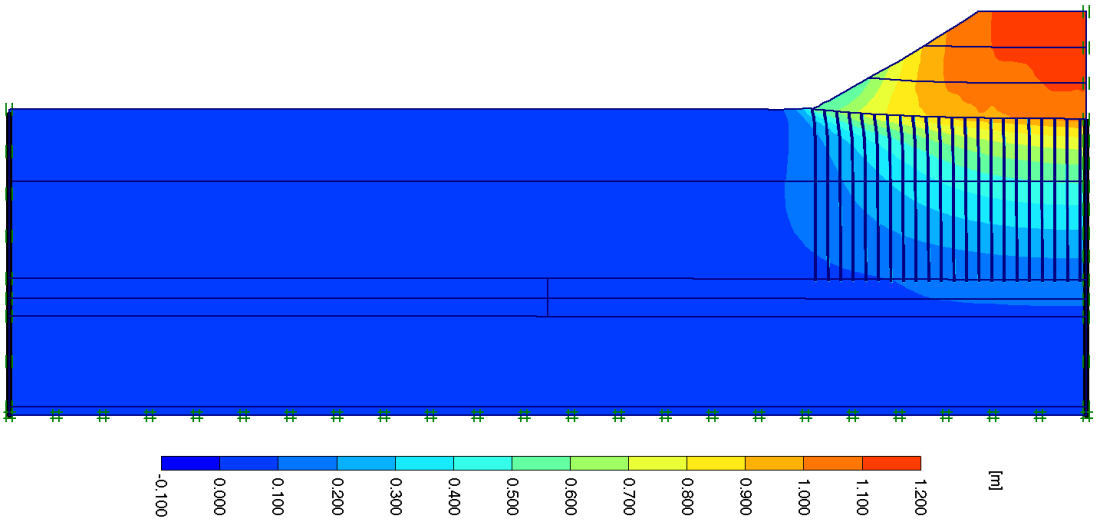

Figure B.2 Total Displacement Contours for Analysis Including The Smear Effect

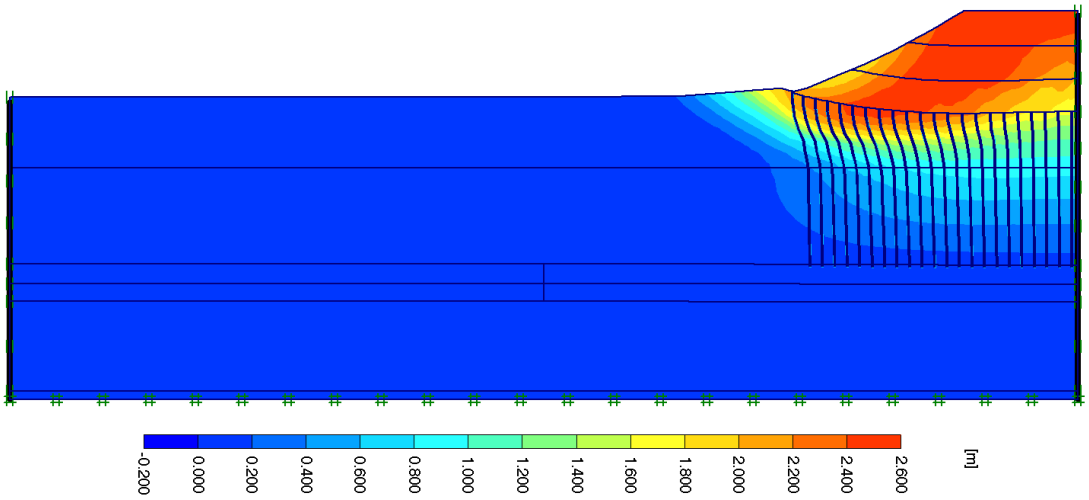

Figure B.3 Total Displacement Contours for Analysis Including Both Smear and Creep Effects

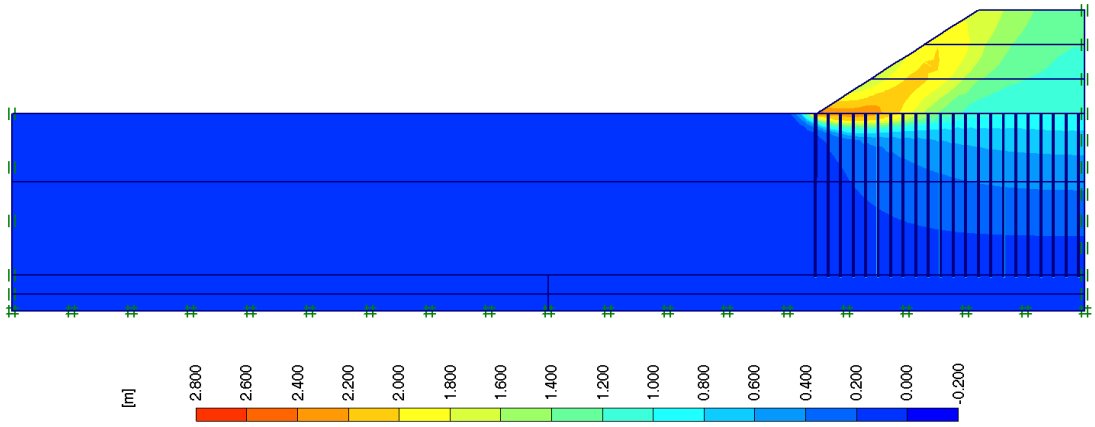

Figure B.4 Total Displacement Contours for Parametric Study Analysis for Degree of Disturbance k_h/k_h' = 1.5

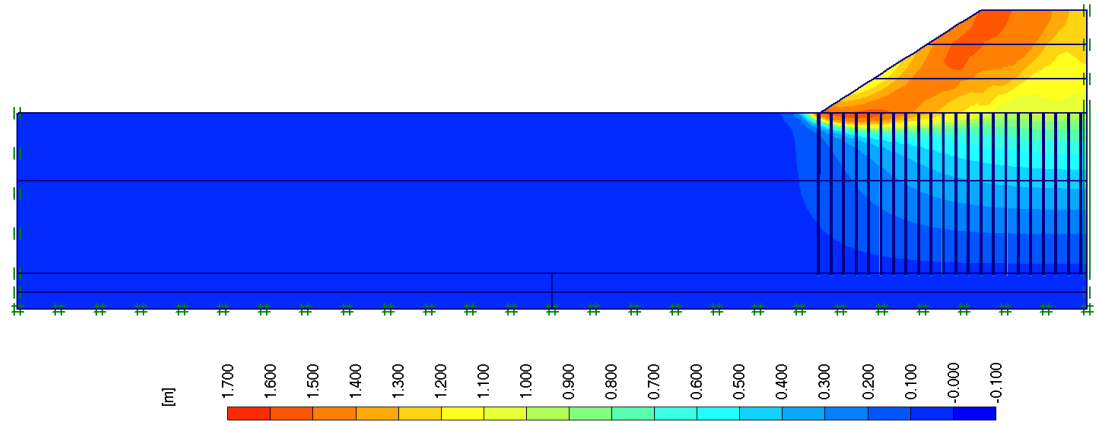

Figure B.5 Total Displacement Contours for Parametric Study Analysis for Degree of Disturbance k_h/k_h' = 2.0

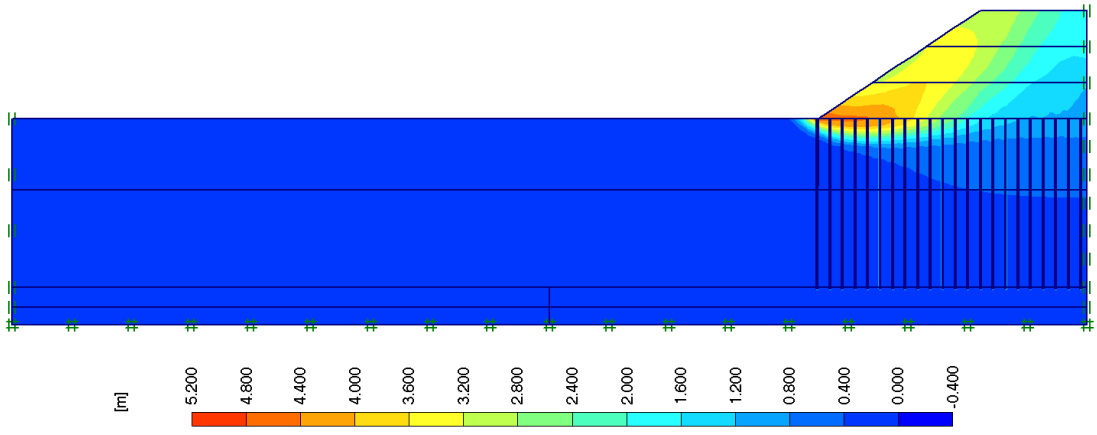

Figure B.6 Total Displacement Contours for Parametric Study Analysis for Degree of Disturbance k_h/k_h' = 3.0

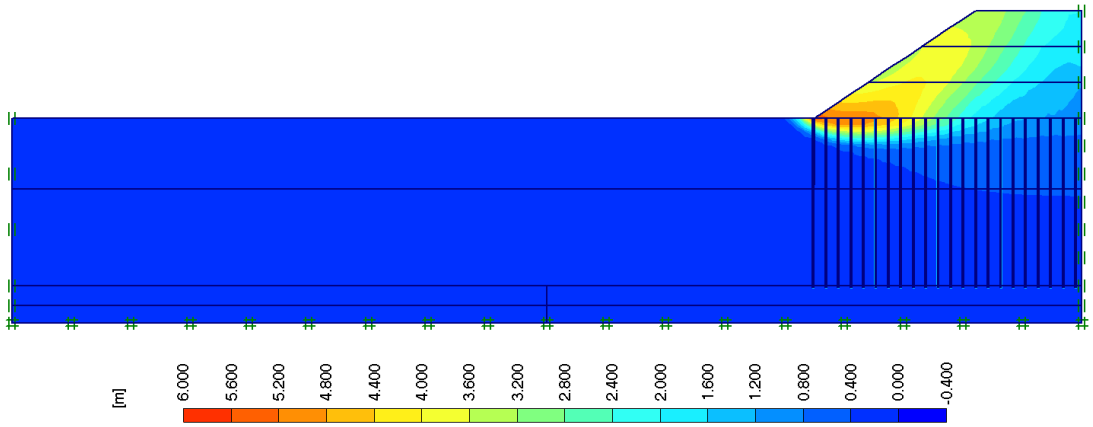

Figure B.7 Total Displacement Contours for Parametric Study Analysis for Degree of Disturbance $k_h/k_h' = 4.0$

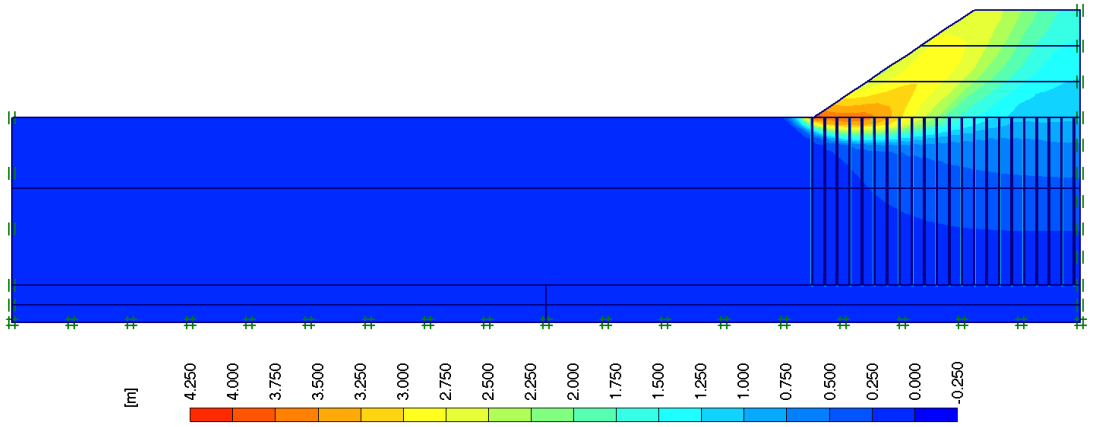

Figure B.8 Total Displacement Contours for Parametric Study Analysis for Smear Zone Diameter $d_s = 2.0d_w$

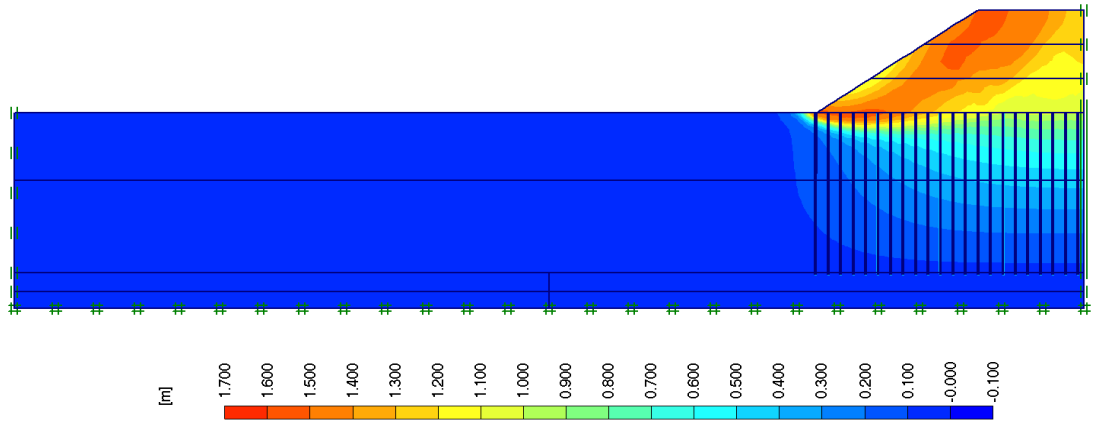

Figure B.9 Total Displacement Contours for Parametric Study Analysis for Smear Zone Diameter $d_s = 2.5d_w$

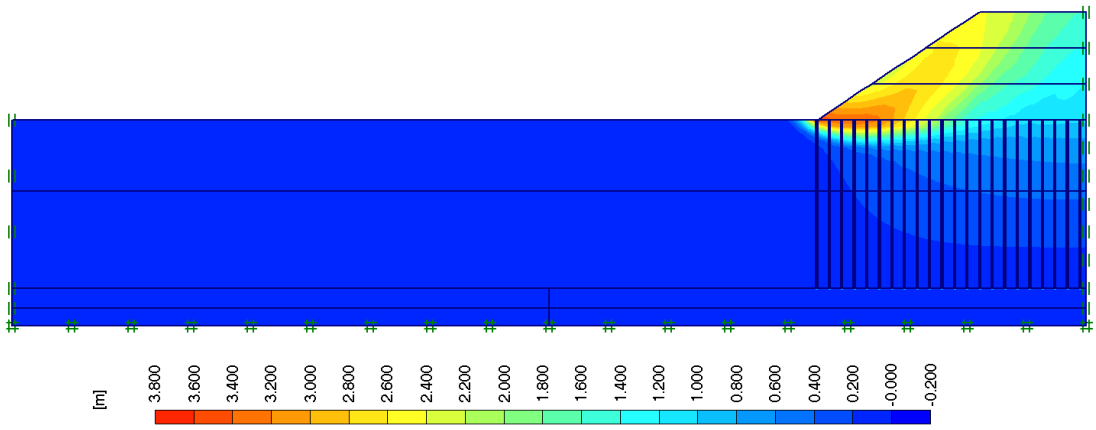

Figure B.10 Total Displacement Contours for Parametric Study Analysis for Smear Zone Diameter $d_s = 3.0d_w$

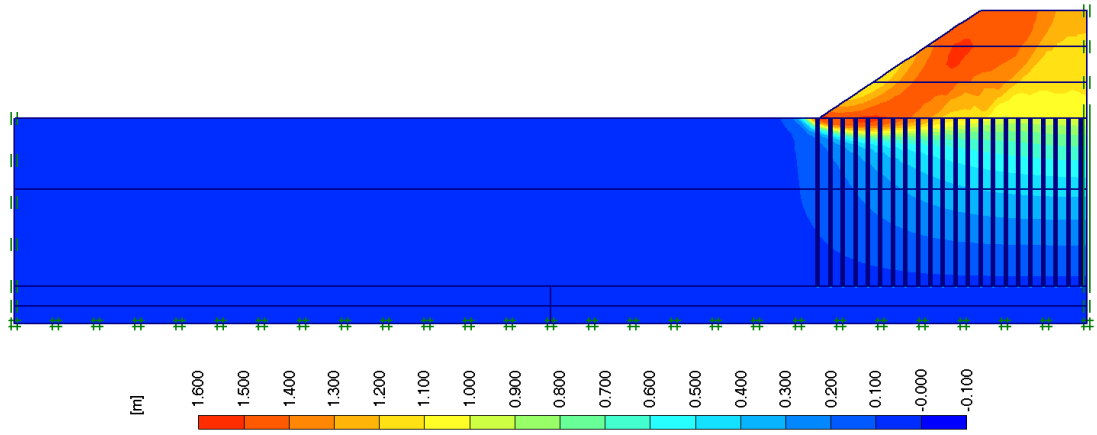

Figure B.11 Total Displacement Contours for Parametric Study Analysis for Smear Zone Diameter $d_s = 5.0d_w$

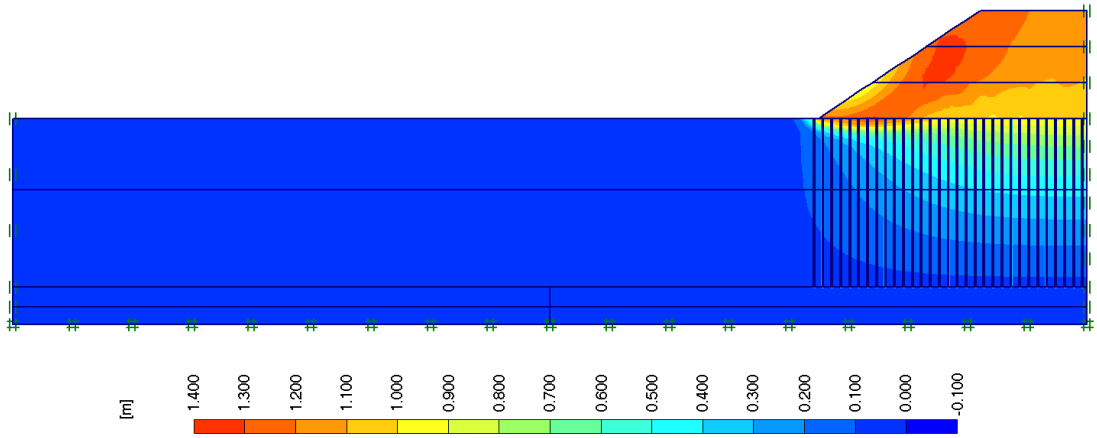

Figure B.12 Total Displacement Contours for Parametric Study Analysis for Drain Spacing S = 1.0 m

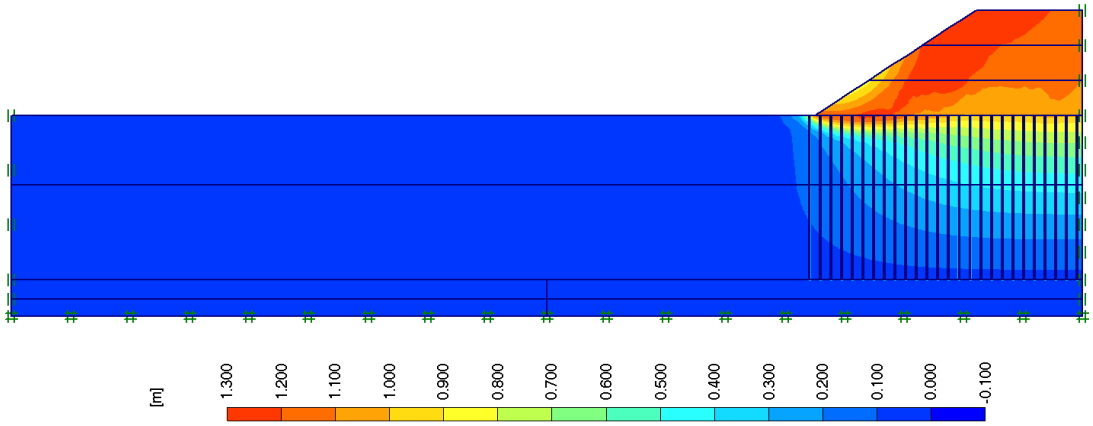

Figure B.13 Total Displacement Contours for Parametric Study Analysis for Drain Spacing S = 1.2 m

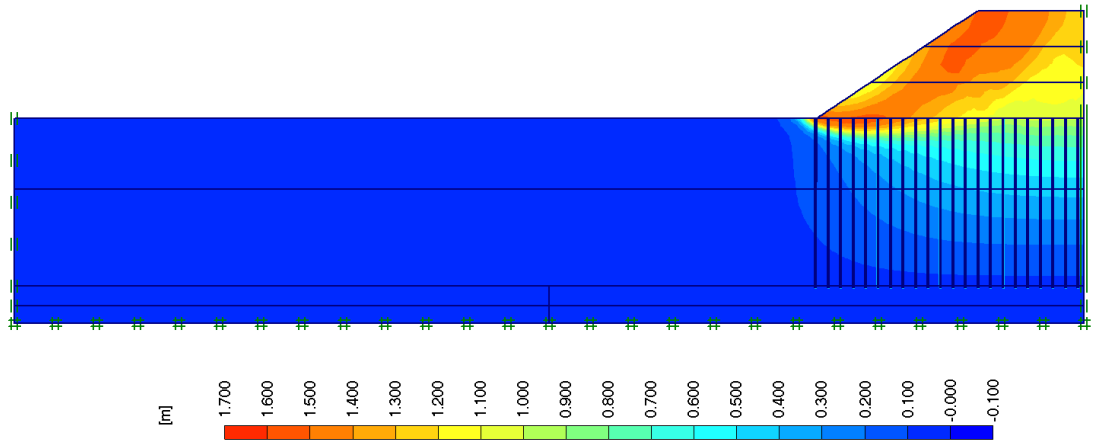

Figure B.14 Total Displacement Contours for Parametric Study Analysis for Drain Spacing S = 1.4 m

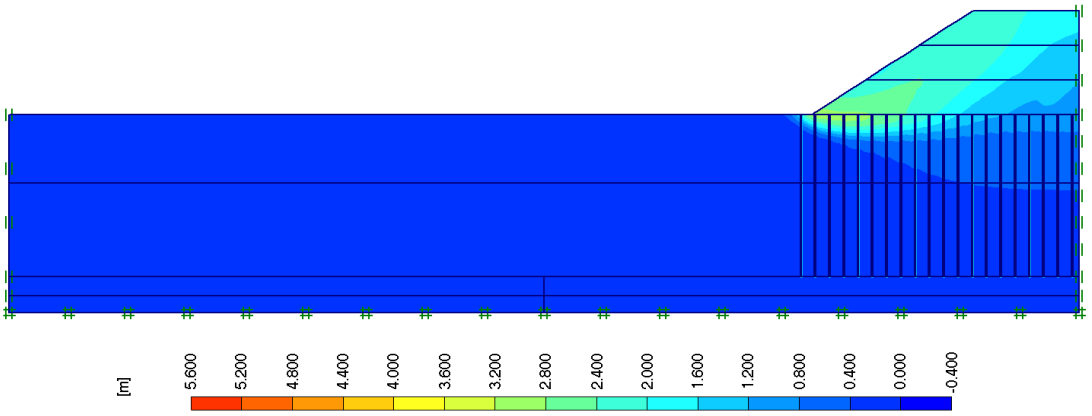

Figure B.15 Total Displacement Contours for Parametric Study Analysis for Drain Spacing S = 1.6 m

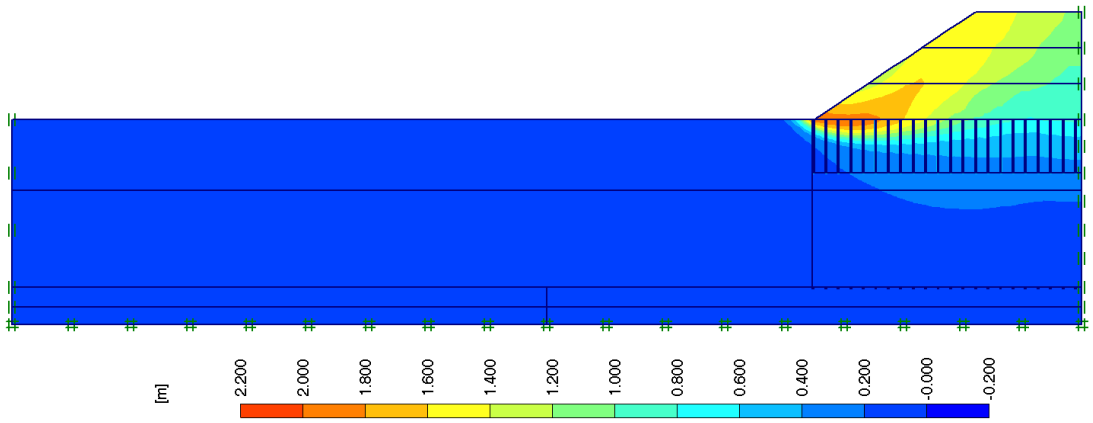

Figure B.16 Total Displacement Contours for Parametric Study Analysis for Drain Penetration Length L_p = 6.0 m

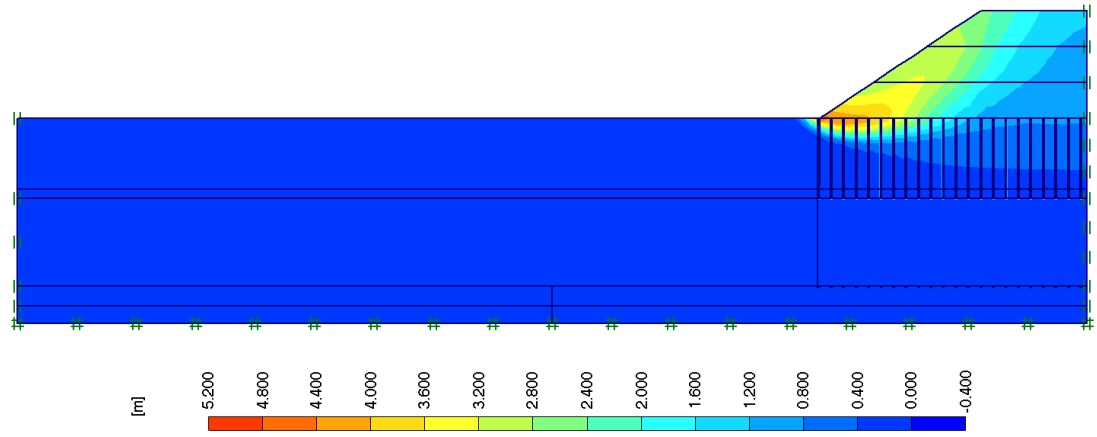

Figure B.17 Total Displacement Contours for Parametric Study Analysis for Drain Penetration Length L_p = 9.0 m

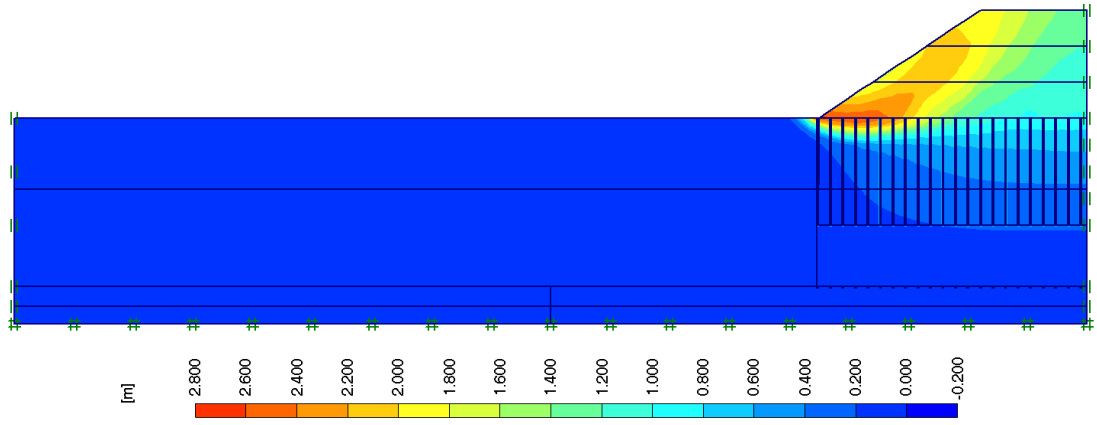

Figure B.18 Total Displacement Contours for Parametric Study Analysis for Drain Penetration Length L_p = 12.0 m

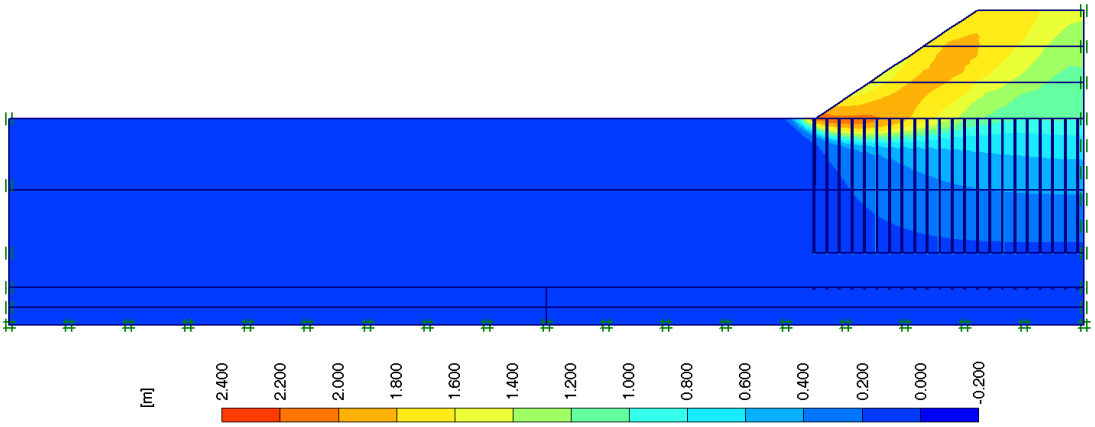

Figure B.19 Total Displacement Contours for Parametric Study Analysis for Drain Penetration Length L_p = 15.0 m

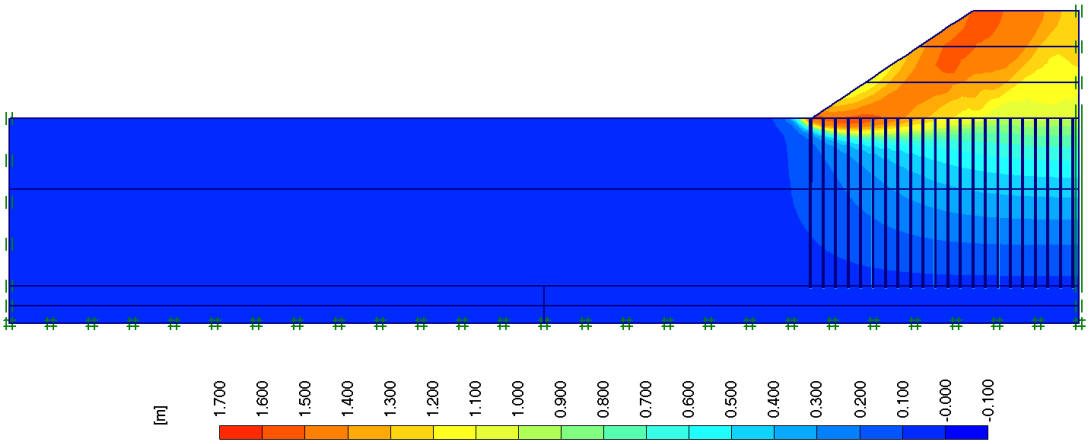

Figure B.20 Total Displacement Contours for Parametric Study Analysis for Drain Penetration Length L_p = 18.0 m

APPENDIX C

VERTICAL DISPLACEMENT CONTOURS FOR ANALYSES

Appendix C presents the vertical displacement contours for analysis ignoring the smear zone, analysis including the smear zone, analysis including both smear and creep and 13 parametric study analyses.

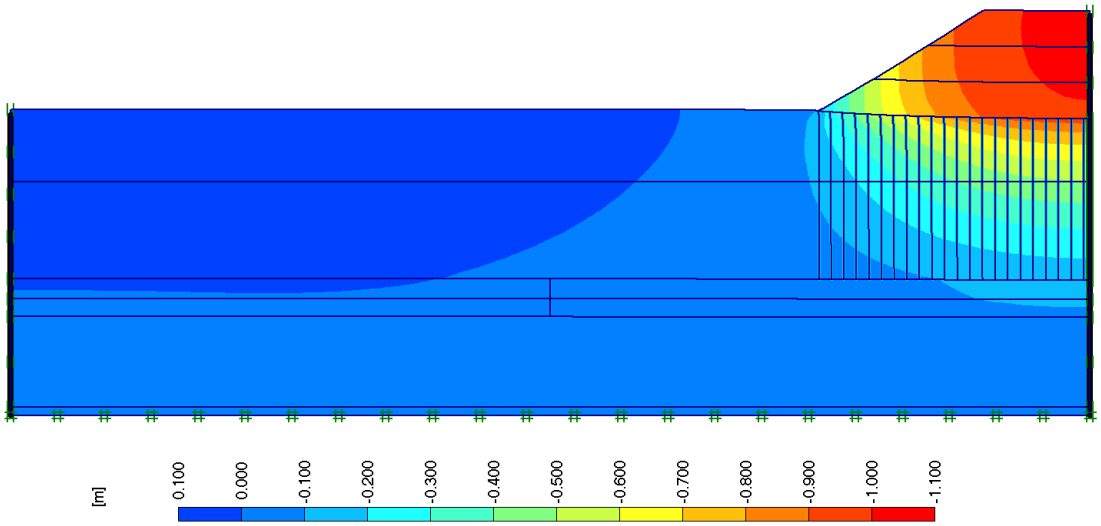

Figure C.1 Vertical Displacement Contours for Analysis Ignoring The Smear Effect

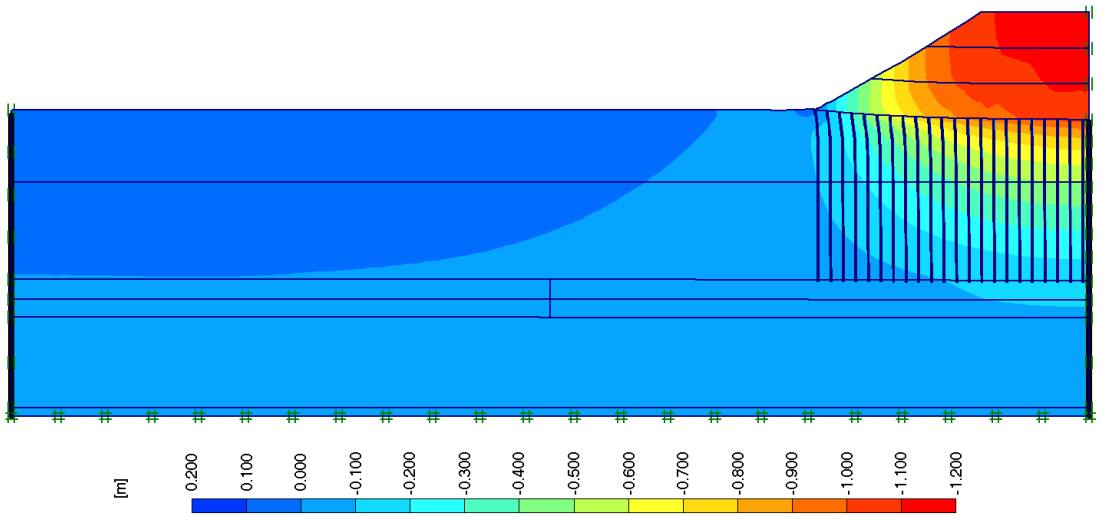

Figure C.2 Vertical Displacement Contours for Analysis Including The Smear Effect

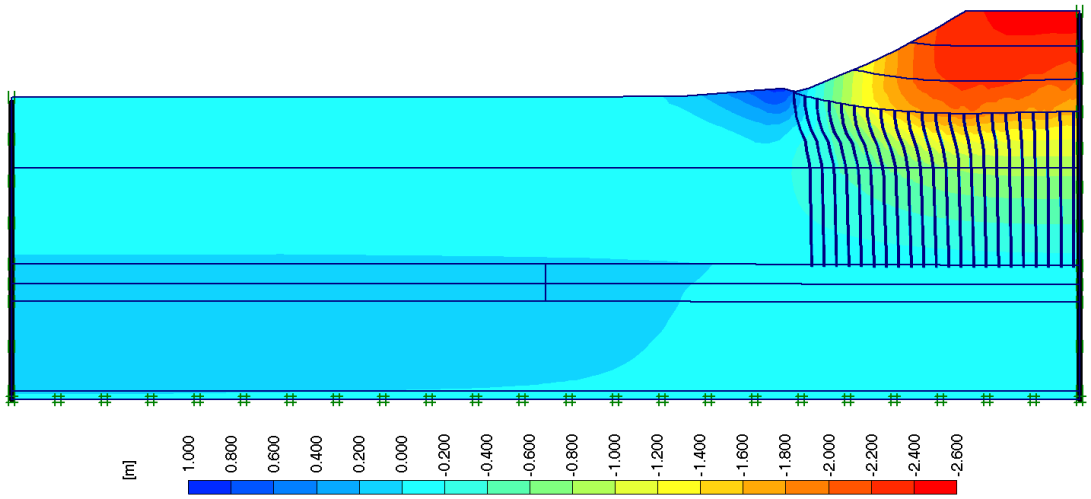

Figure C.3 Vertical Displacement Contours for Analysis Including Both Smear and Creep Effects

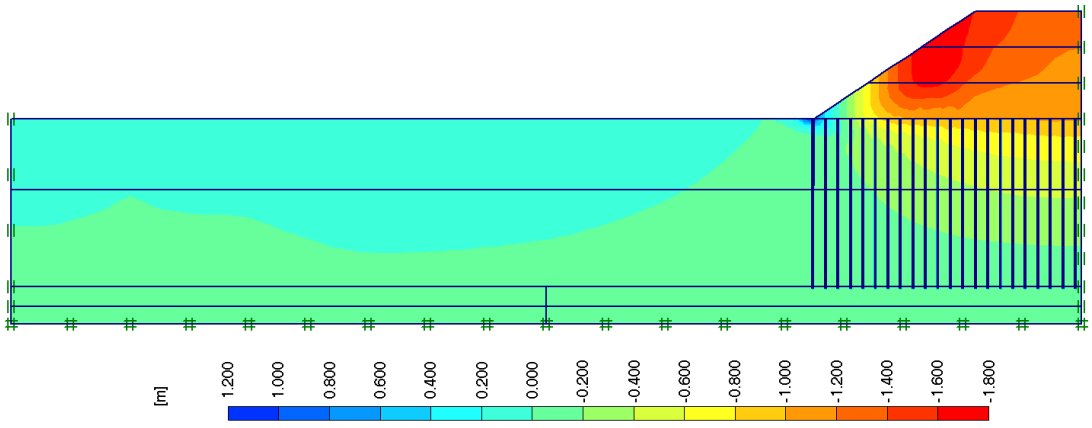

Figure C.4 Vertical Displacement Contours for Parametric Study Analysis for Degree of Disturbance $k_h/k_h' = 1.5$

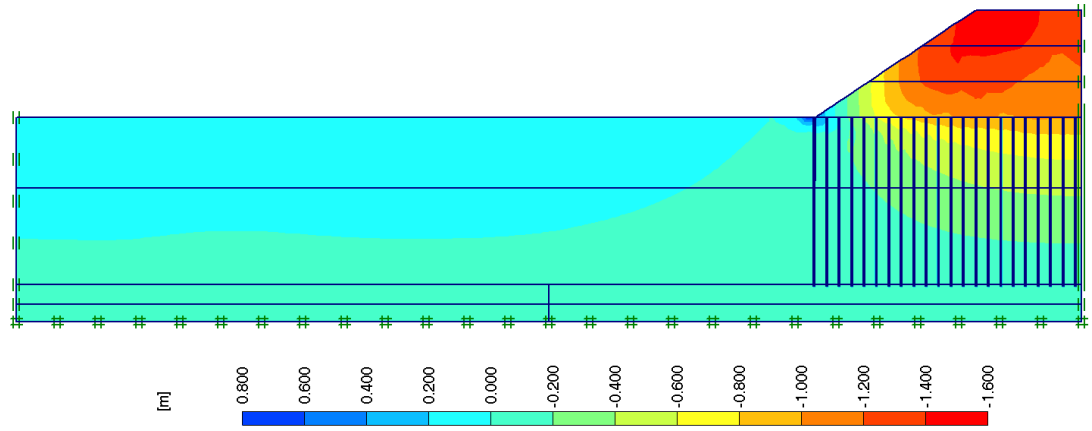

Figure C.5 Vertical Displacement Contours for Parametric Study Analysis for Degree of Disturbance $k_h/k_h' = 2.0$

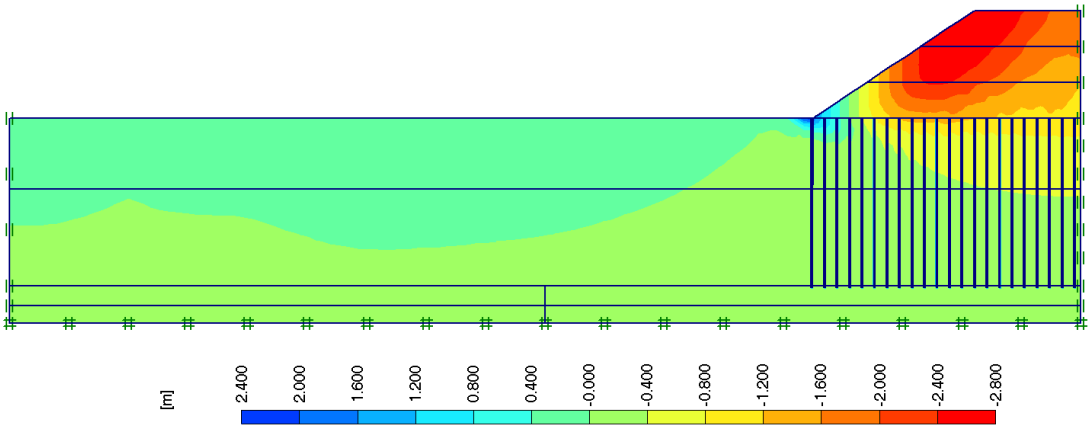

Figure C.6 Vertical Displacement Contours for Parametric Study Analysis for Degree of Disturbance $k_h/k_h' = 3.0$

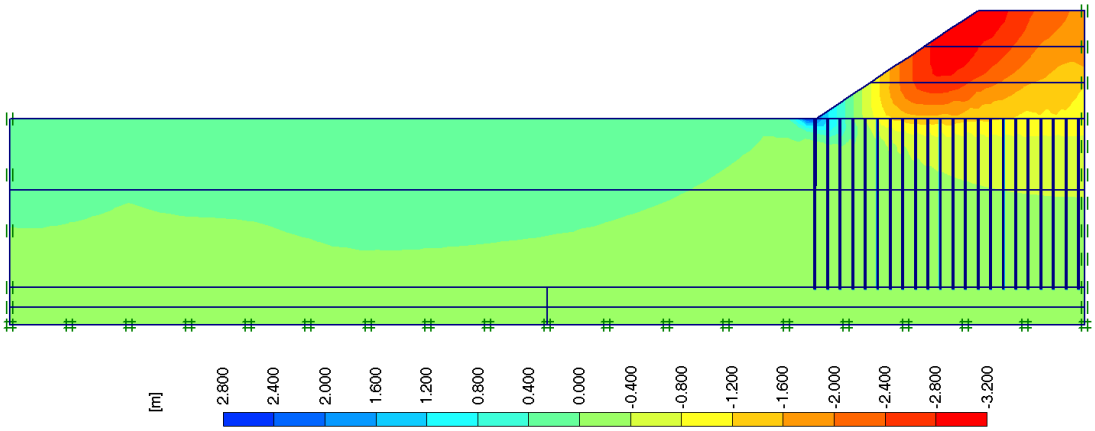

Figure C.7 Vertical Displacement Contours for Parametric Study Analysis for Degree of Disturbance $k_h/k_h' = 4.0$

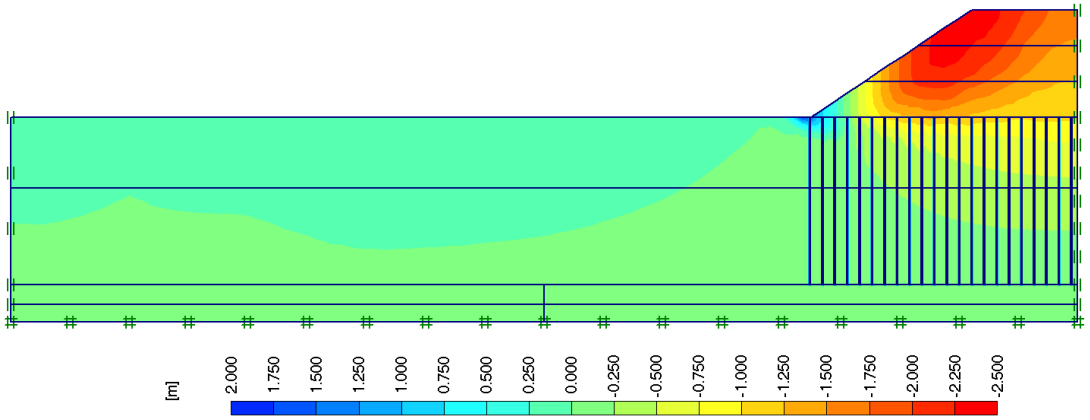

Figure C.8 Vertical Displacement Contours for Parametric Study Analysis for Smear Zone Diameter $d_s = 2.0d_w$

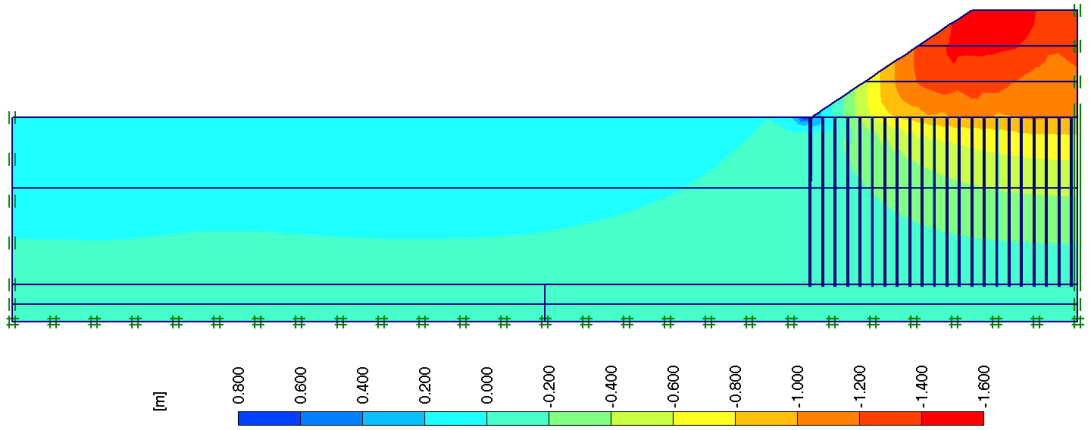

Figure C.9 Vertical Displacement Contours for Parametric Study Analysis for Smear Zone Diameter $d_s = 2.5d_w$

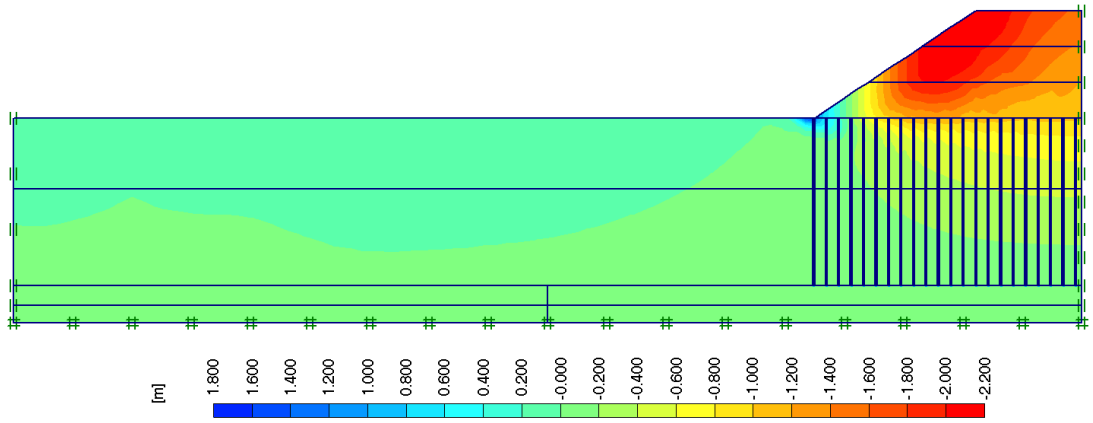

Figure C.10 Vertical Displacement Contours for Parametric Study Analysis for Smear Zone Diameter $d_s = 3.0d_w$

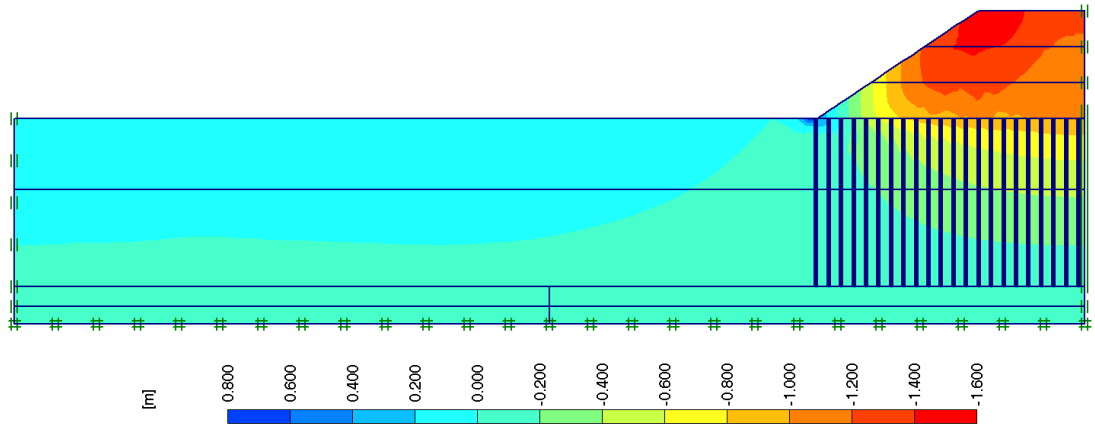

Figure C.11 Vertical Displacement Contours for Parametric Study Analysis for Smear Zone Diameter $d_s = 5.0d_w$

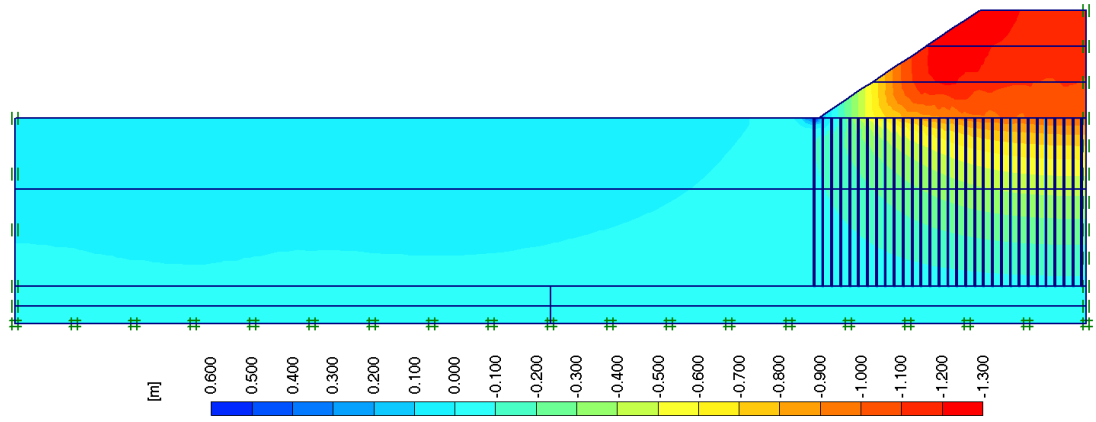

Figure C.12 Vertical Displacement Contours for Parametric Study Analysis for Drain Spacing S = 1.0 m

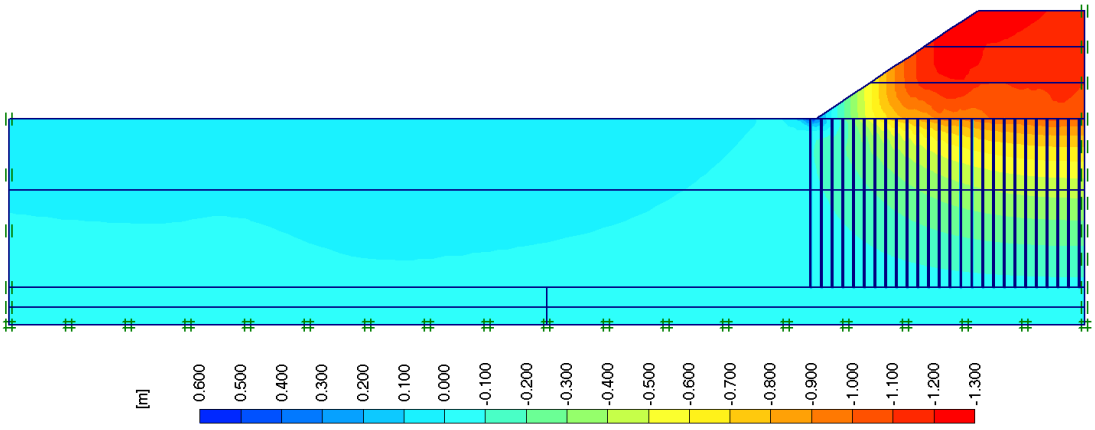

Figure C.13 Vertical Displacement Contours for Parametric Study Analysis for Drain Spacing S = 1.2 m

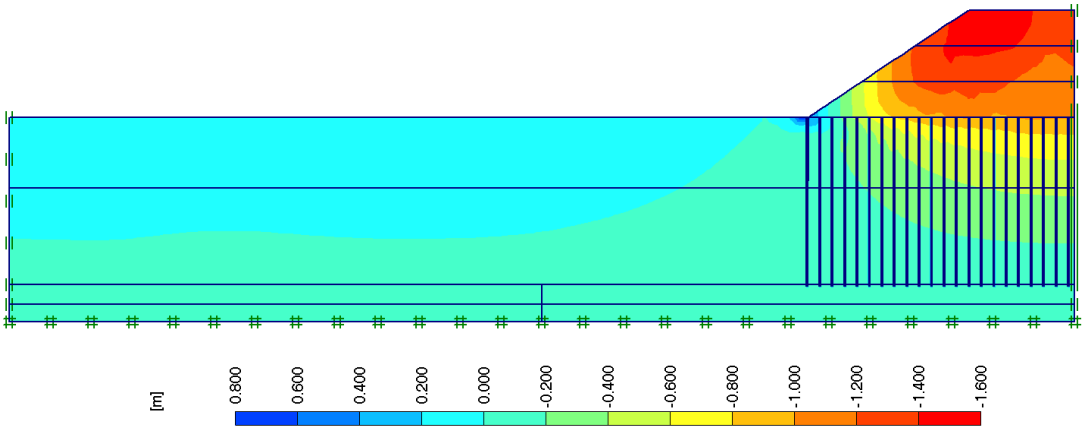

Figure C.14 Vertical Displacement Contours for Parametric Study Analysis for Drain Spacing S = 1.4 m

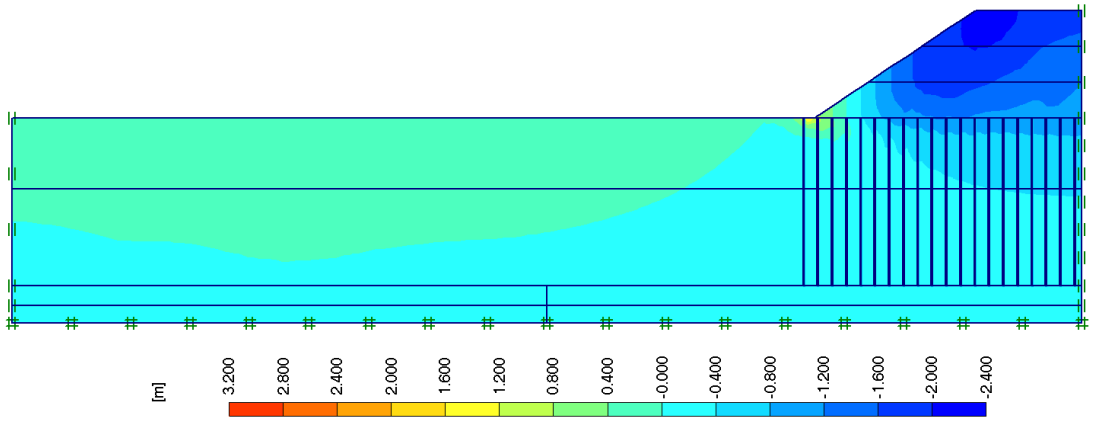

Figure C.15 Vertical Displacement Contours for Parametric Study Analysis for Drain Spacing S = 1.6 m

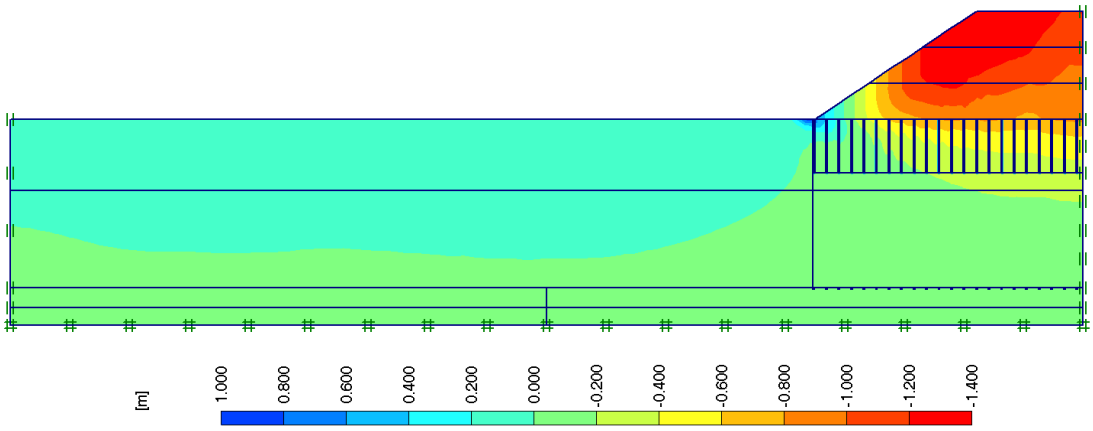

Figure C.16 Vertical Displacement Contours for Parametric Study Analysis for Drain Penetration Length L = 6.0 m

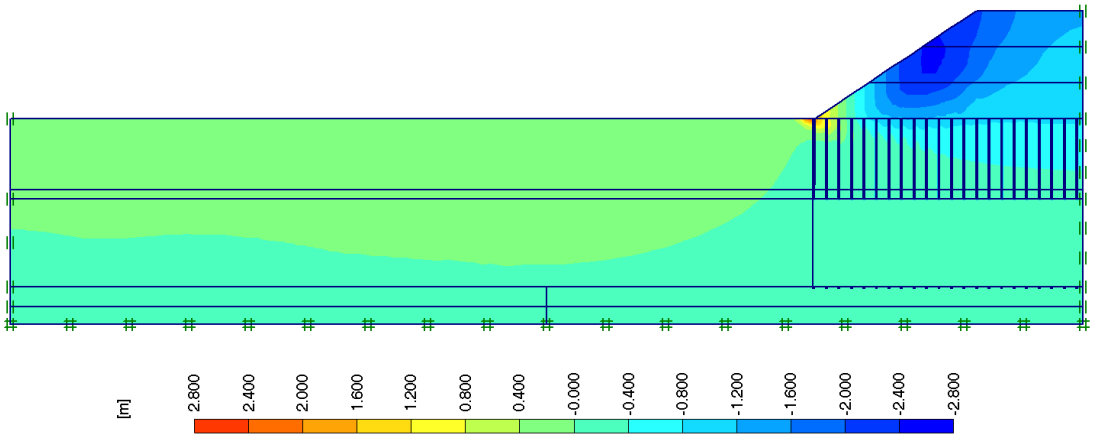

Figure C.17 Vertical Displacement Contours for Parametric Study Analysis for Drain Penetration Length L = 9.0 m

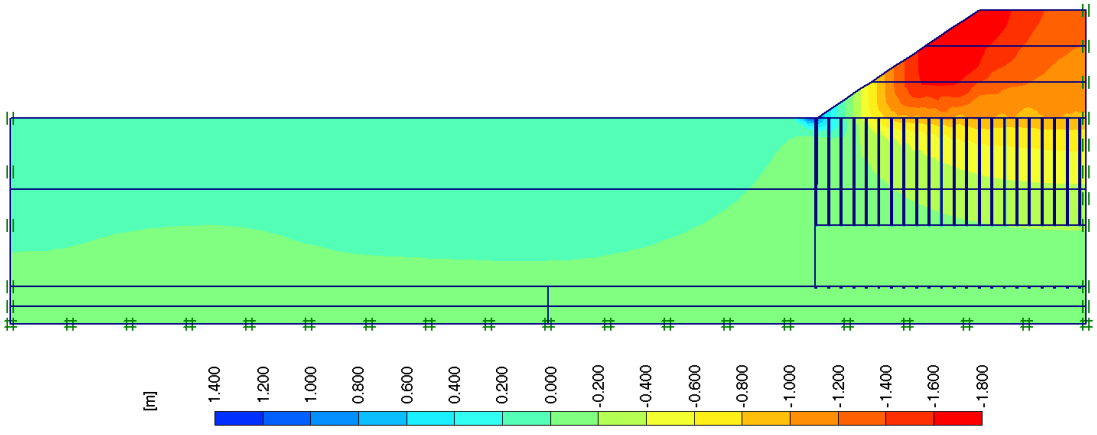

Figure C.18 Vertical Displacement Contours for Parametric Study Analysis for Drain Penetration Length L = 12.0 m

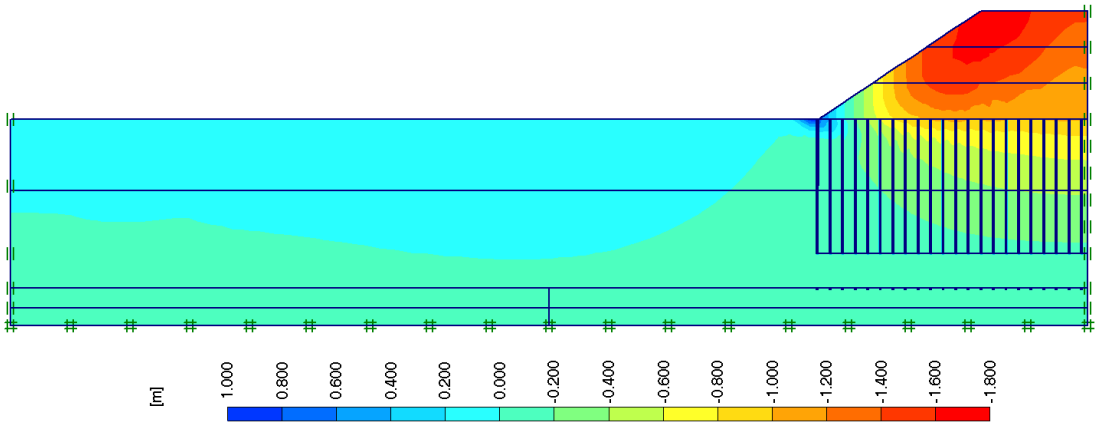

Figure C.19 Vertical Displacement Contours for Parametric Study Analysis for Drain Penetration Length L = 15.0 m

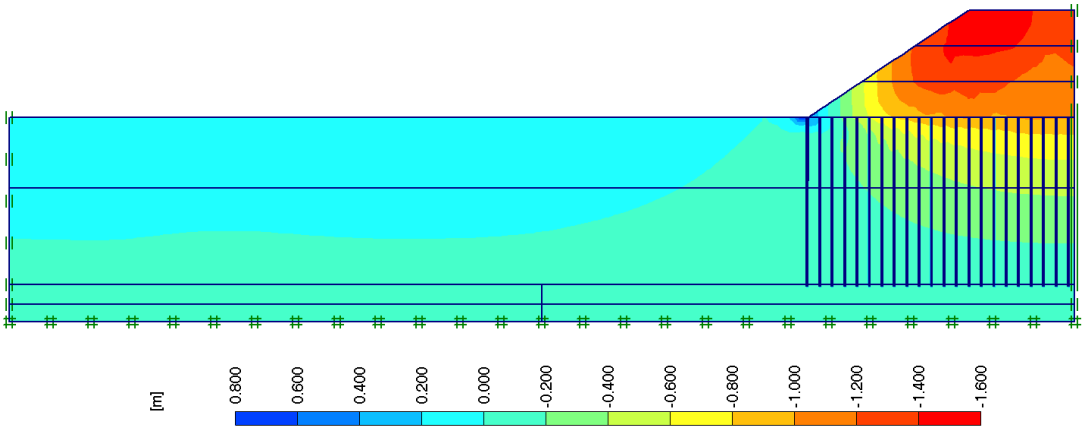

Figure C.20 Vertical Displacement Contours for Parametric Study Analysis for Drain Penetration Length L = 18.0 m

APPENDIX D

PORE PRESSURE GENERATION CONTOURS

Appendix D presents the output results of excess pore water pressures generated in 4 phases of total 16 finite element analyses.

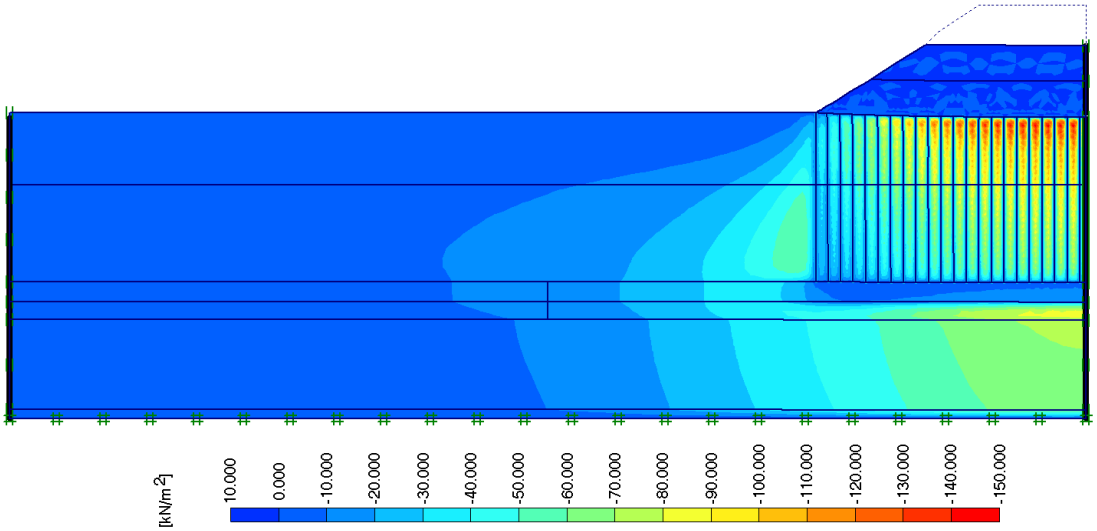

Figure D.1 Phase-1 Pore Pressure Generation for Analysis Ignoring the Smear Effect

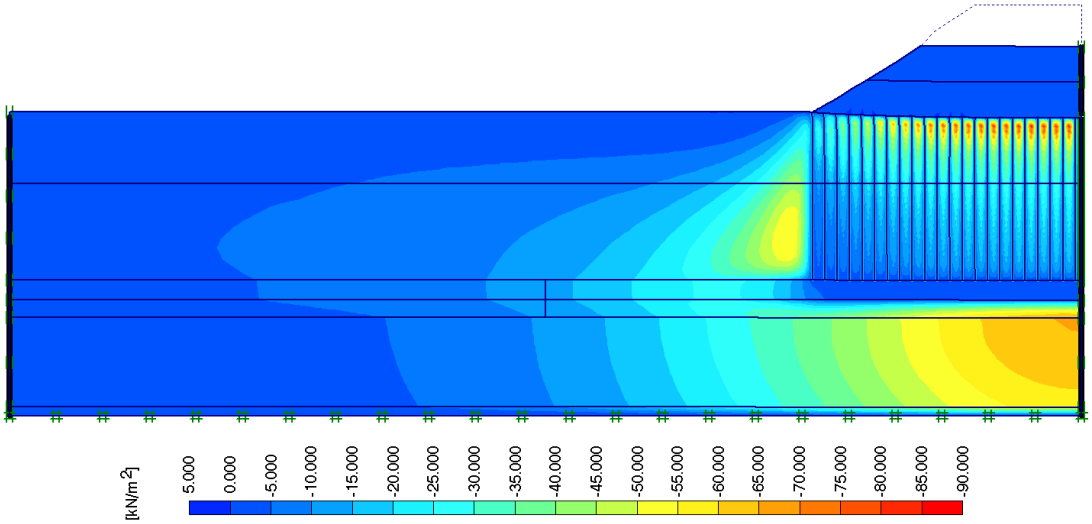

Figure D.2 Phase-2 Pore Pressure Generation for Analysis Ignoring the Smear Effect

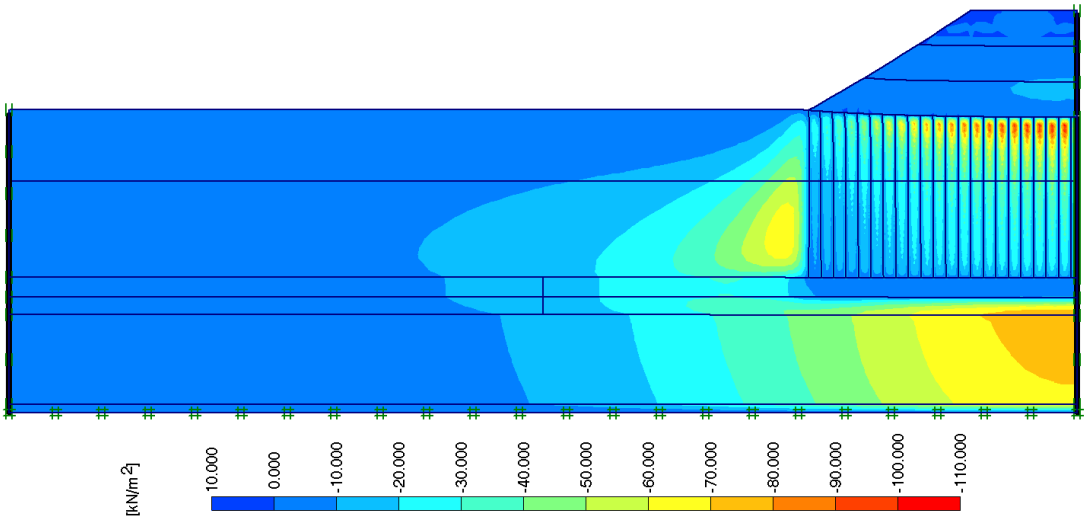

Figure D.3 Phase-3 Pore Pressure Generation for Analysis Ignoring the Smear Effect

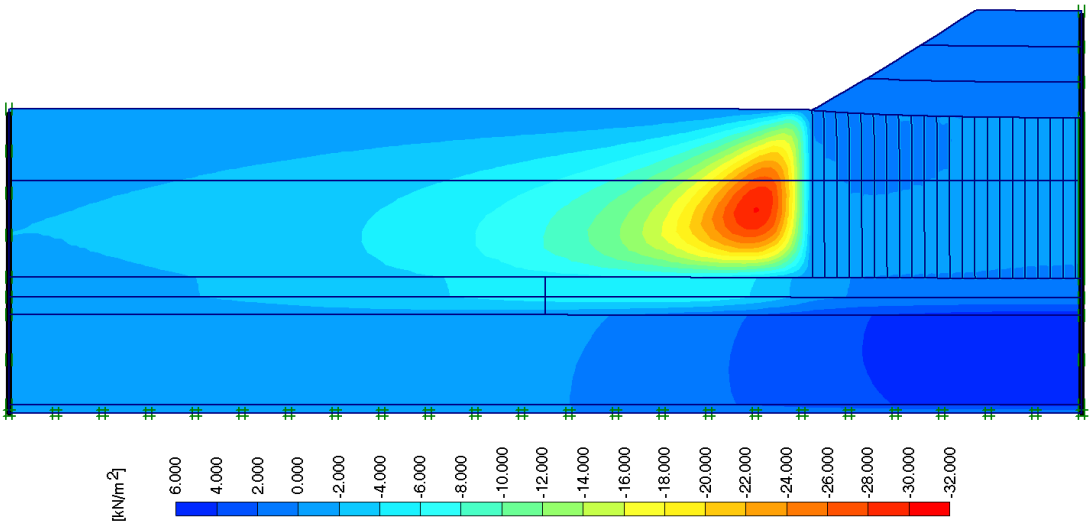

Figure D.4 Phase-4 Pore Pressure Generation for Analysis Ignoring the Smear Effect

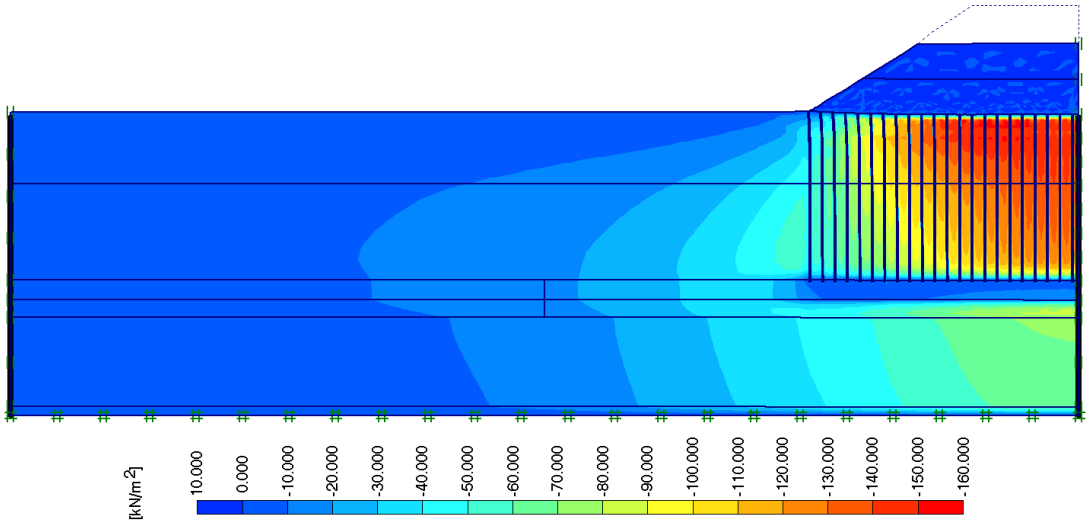

Figure D.5 Phase-1 Pore Pressure Generation for Analysis Including the Smear Effect

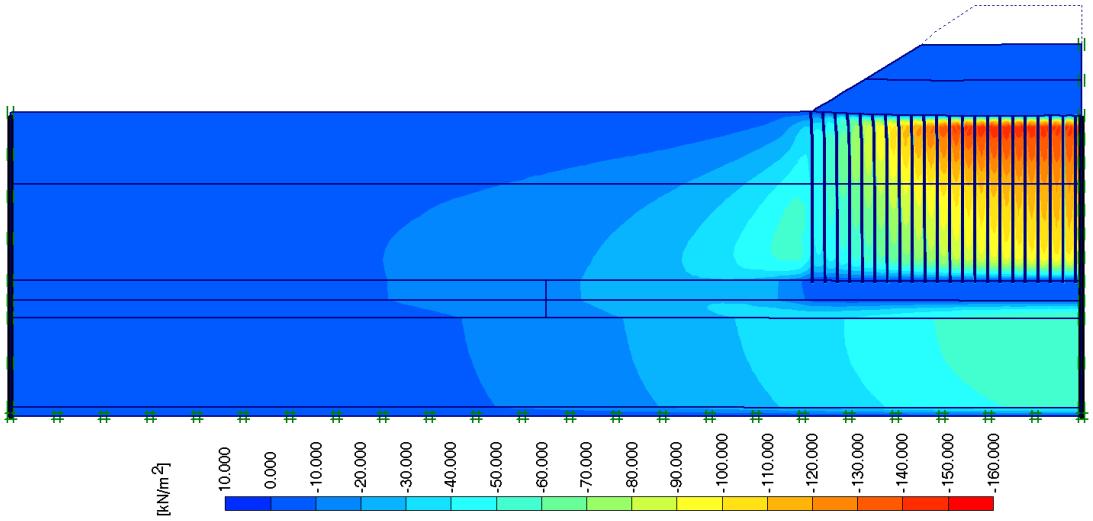

Figure D.6 Phase-2 Pore Pressure Generation for Analysis Including the Smear Effect

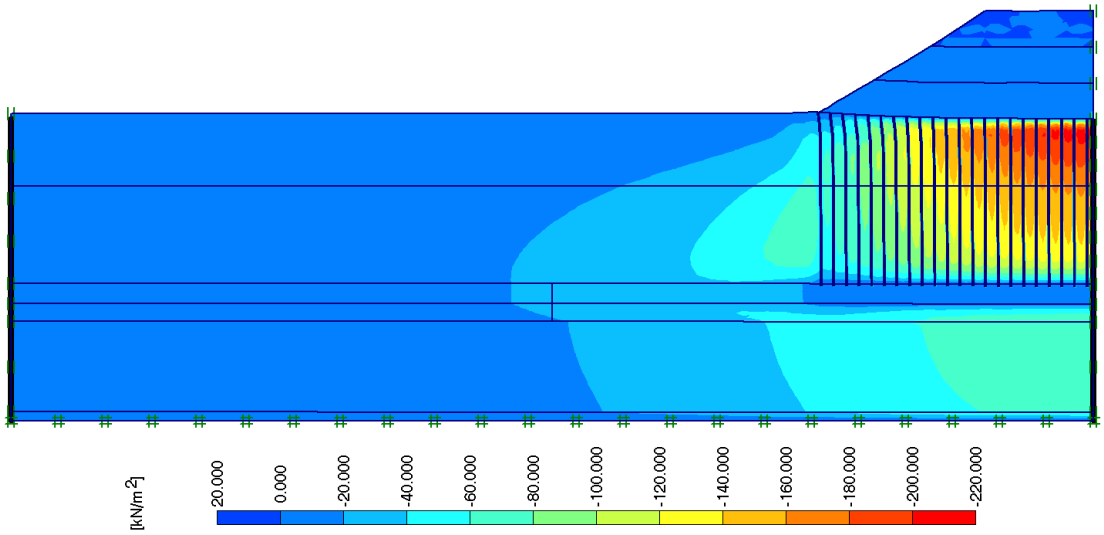

Figure D.7 Phase-3 Pore Pressure Generation for Analysis Including the Smear Effect

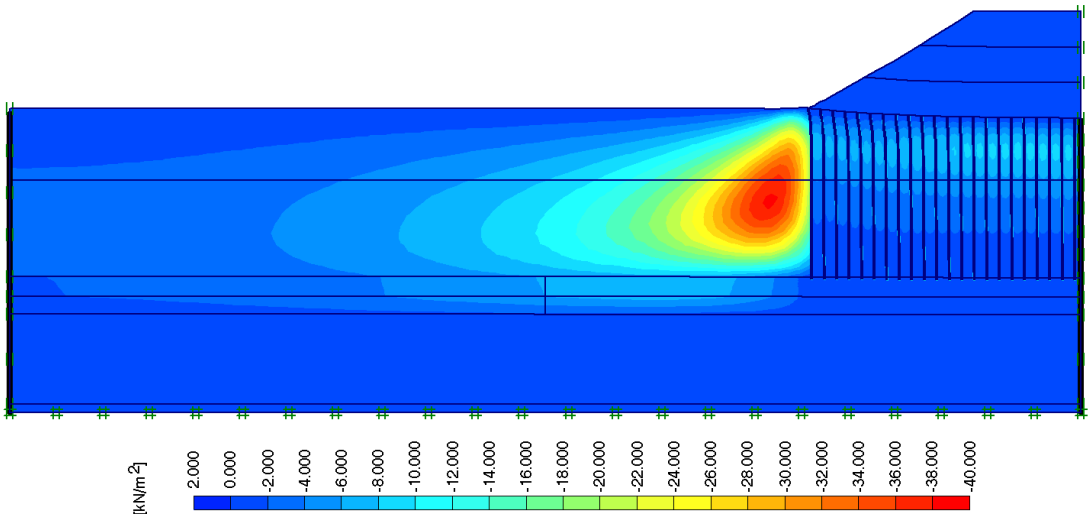

Figure D.8 Phase-4 Pore Pressure Generation for Analysis Including the Smear Effect

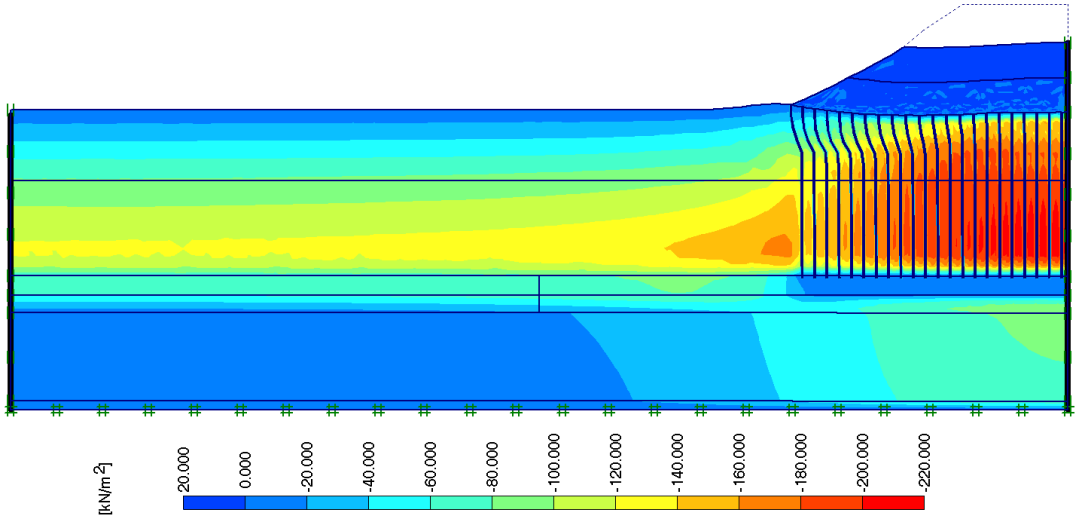

Figure D.9 Phase-1 Pore Pressure Generation for Analysis Including Both Smear and Creep Effects

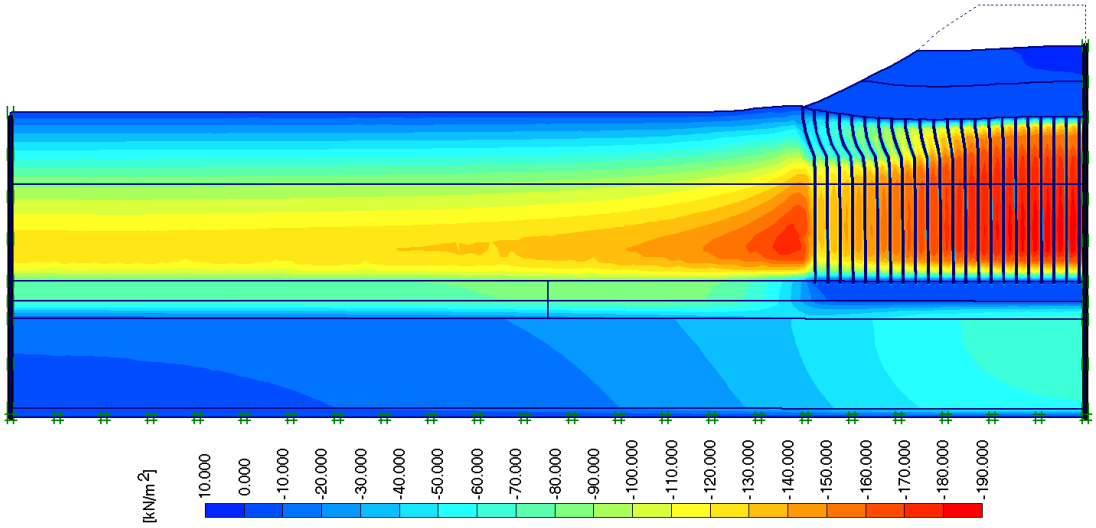

Figure D.10 Phase-2 Pore Pressure Generation for Analysis Including Both Smear and Creep Effects

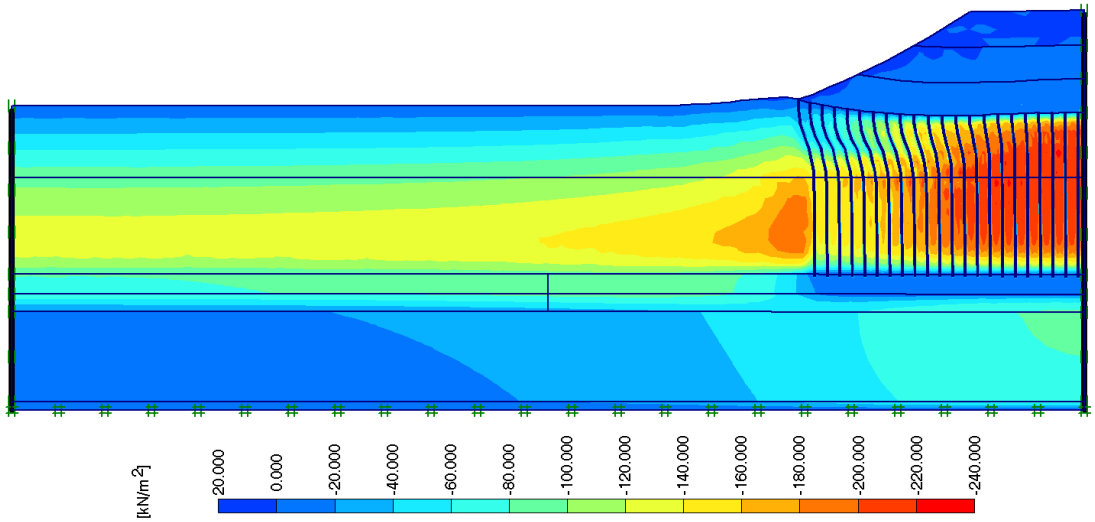

Figure D.11 Phase-3 Pore Pressure Generation for Analysis Including Both Smear and Creep Effects

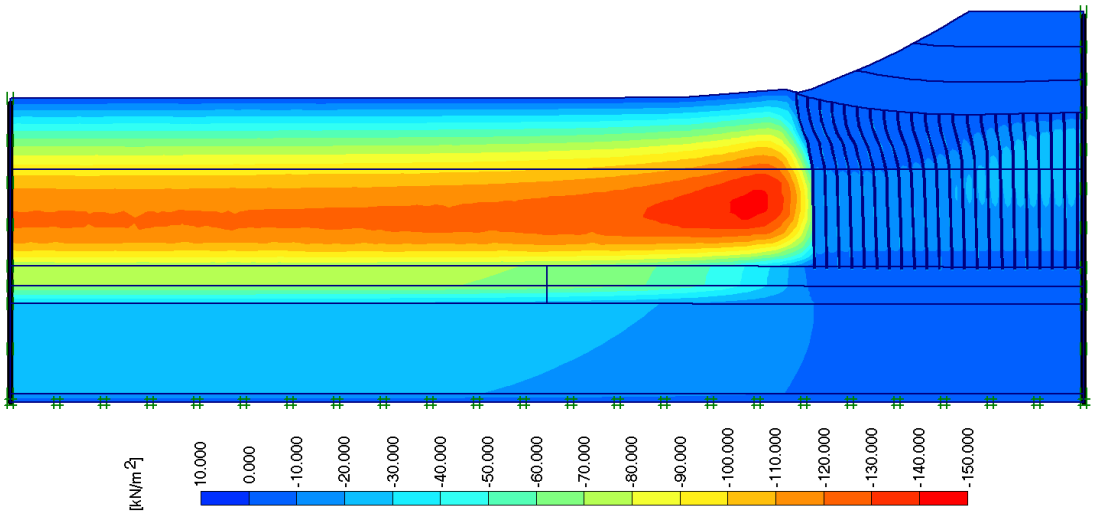

Figure D.12 Phase-4 Pore Pressure Generation for Analysis Including Both Smear and Creep Effects

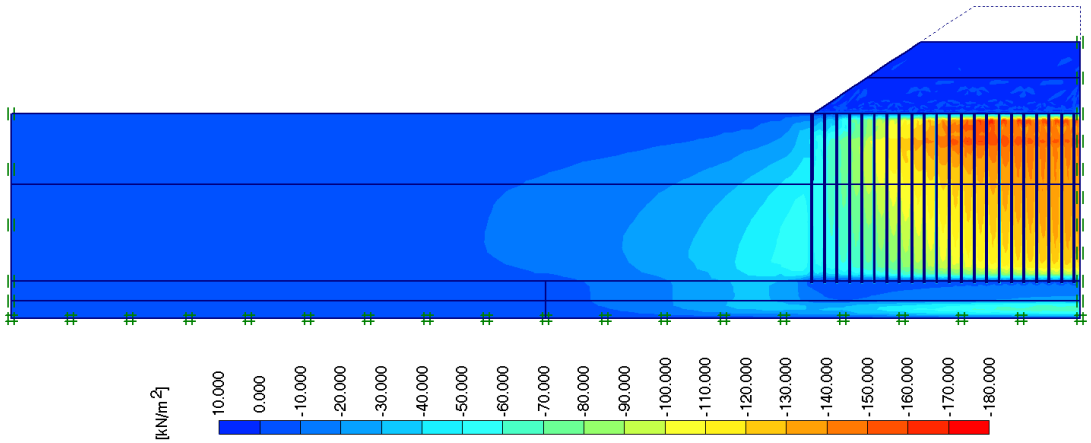

Figure D.13 Phase-1 Pore Pressure Generation for Parametric Study Analysis with Degree of Disturbance within the Smear Zone, $k_h/k_h' = 1.5$

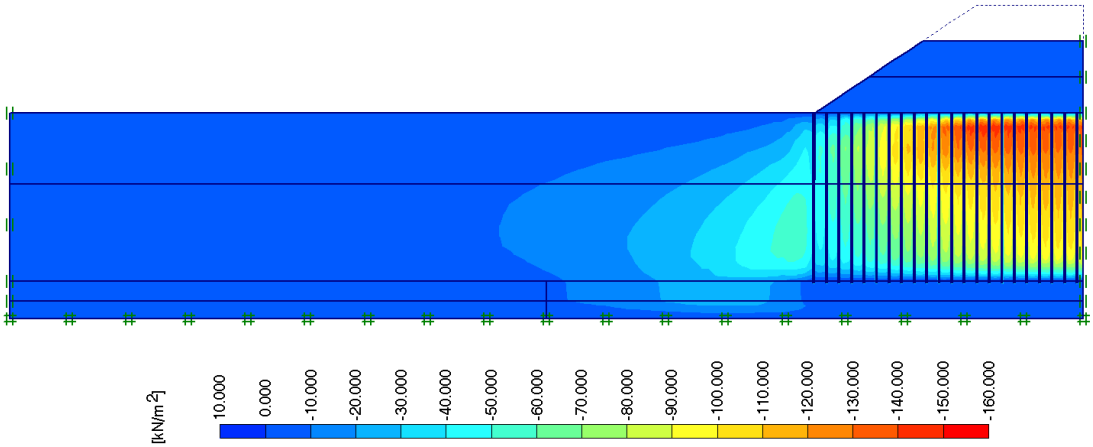

Figure D.14 Phase-2 Pore Pressure Generation for Parametric Study Analysis with Degree of Disturbance within the Smear Zone, $k_h/k_h' = 1.5$

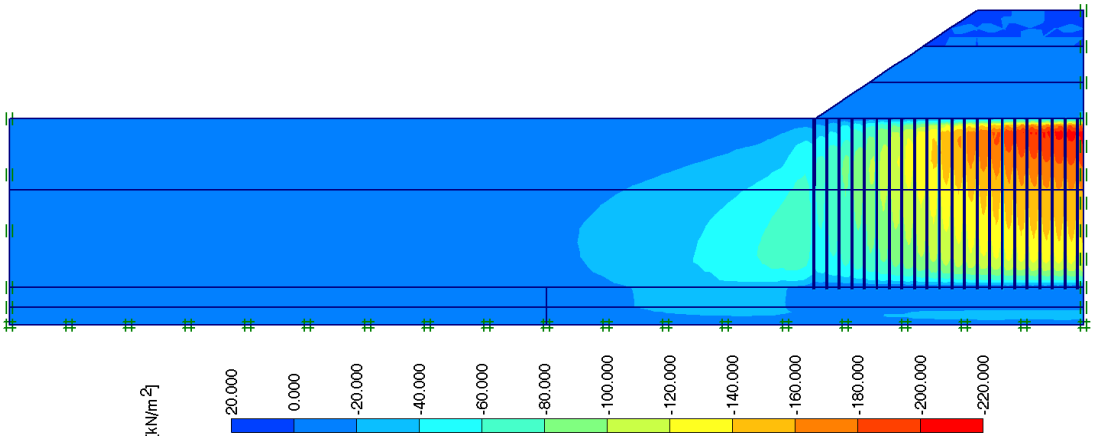

Figure D.15 Phase-3 Pore Pressure Generation for Parametric Study Analysis with Degree of Disturbance within the Smear Zone, $k_h/k_h' = 1.5$

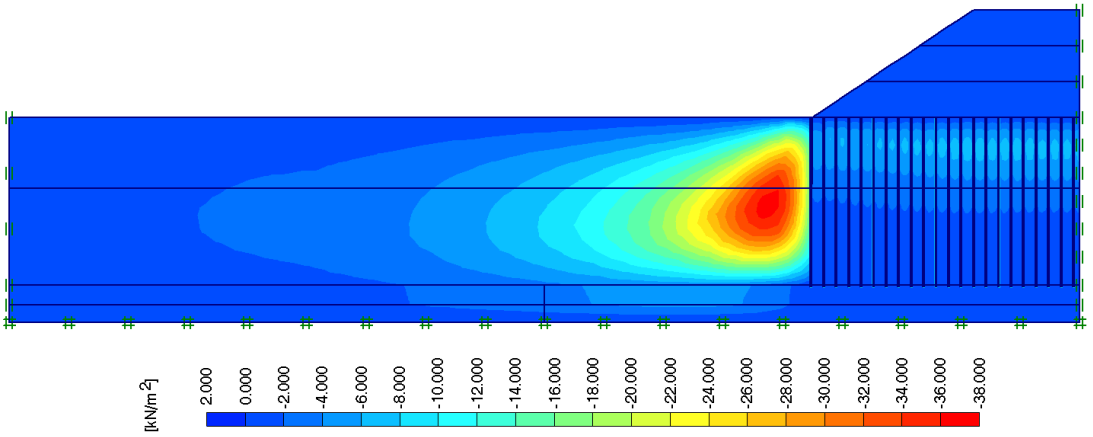

Figure D.16 Phase-4 Pore Pressure Generation for Parametric Study Analysis with Degree of Disturbance within the Smear Zone, $k_h/k_h' = 1.5$

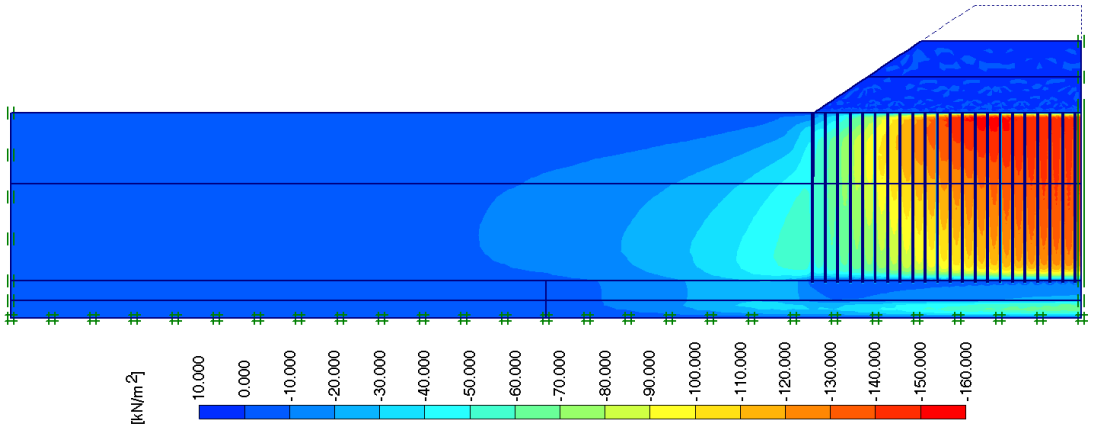

Figure D.17 Phase-1 Pore Pressure Generation for Parametric Study Analysis with Degree of Disturbance within the Smear Zone, $k_h/k_h' = 2.0$

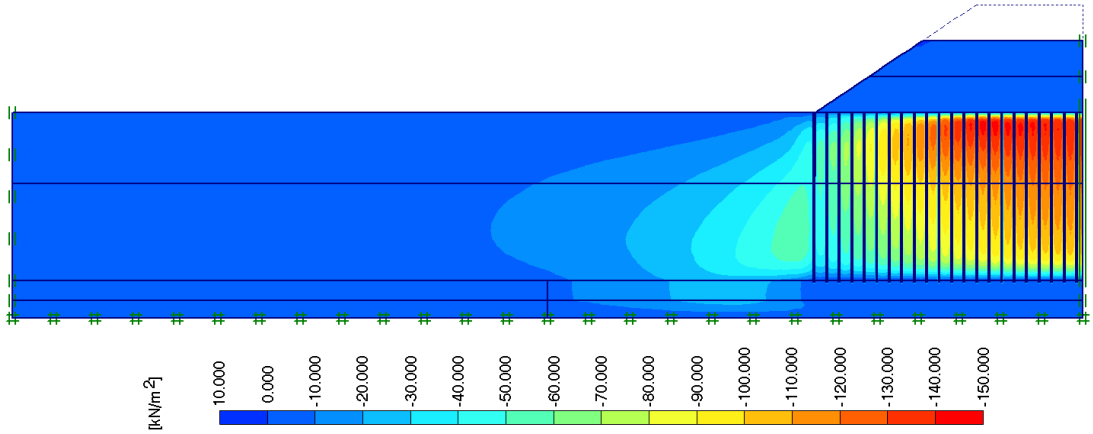

Figure D.18 Phase-2 Pore Pressure Generation for Parametric Study Analysis with Degree of Disturbance within the Smear Zone, $k_h/k_h' = 2.0$

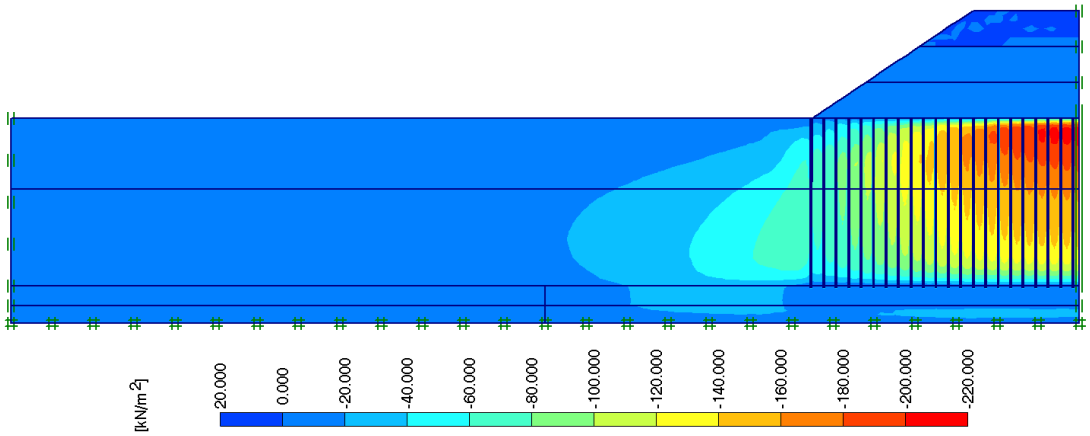

Figure D.19 Phase-3 Pore Pressure Generation for Parametric Study Analysis with Degree of Disturbance within the Smear Zone, $k_h/k_h' = 2.0$

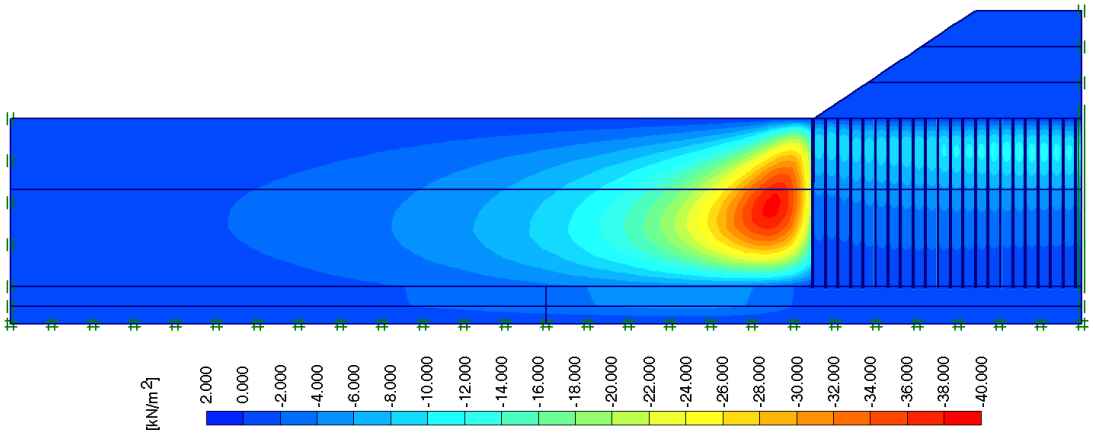

Figure D.20 Phase-4 Pore Pressure Generation for Parametric Study Analysis with Degree of Disturbance within the Smear Zone, $k_h/k_h' = 2.0$

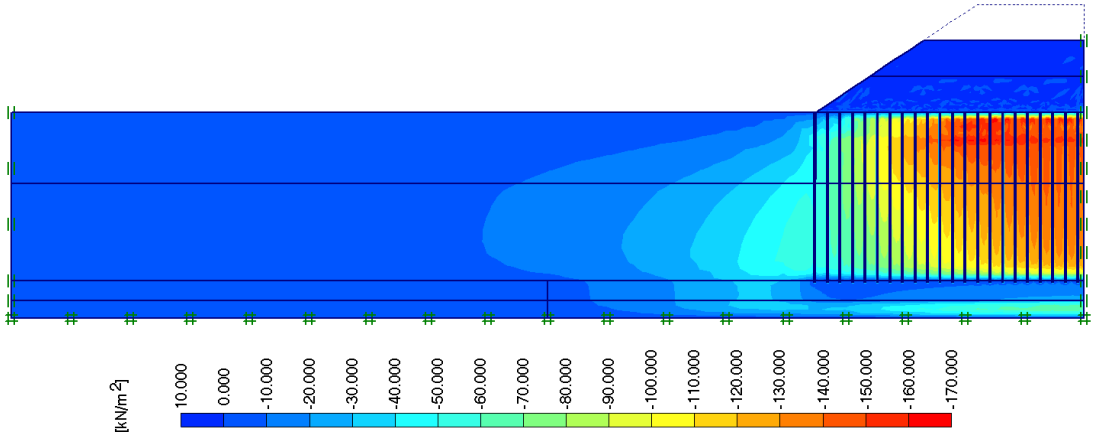

Figure D.21 Phase-1 Pore Pressure Generation for Parametric Study Analysis with Degree of Disturbance within the Smear Zone, $k_h/k_h' = 3.0$

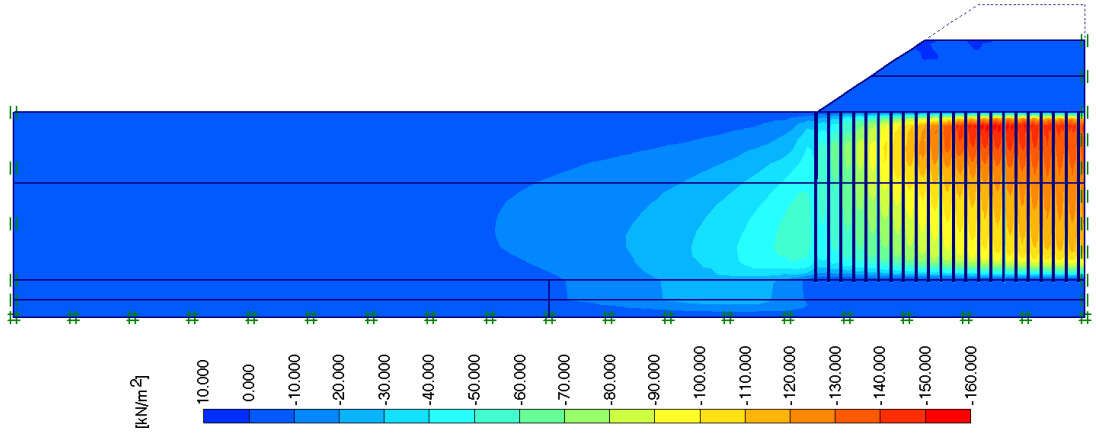

Figure D.22 Phase-2 Pore Pressure Generation for Parametric Study Analysis with Degree of Disturbance within the Smear Zone, $k_h/k_h' = 3.0$

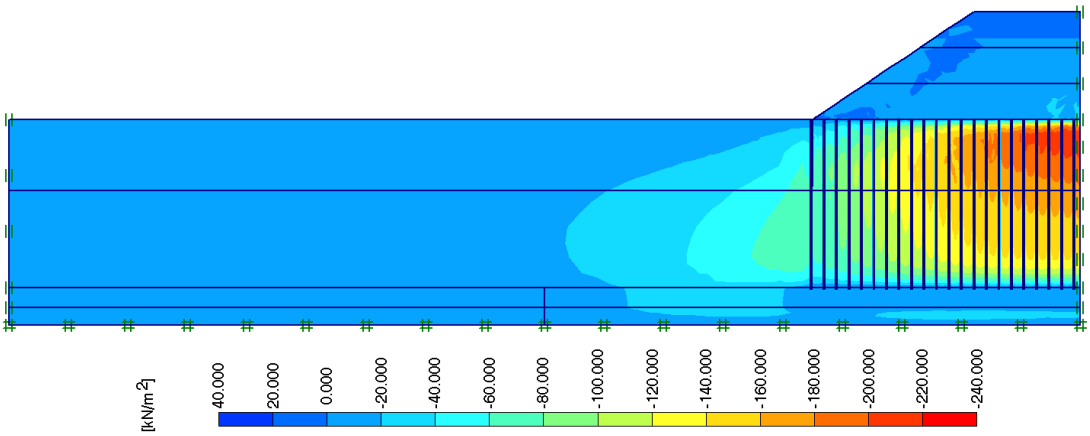

Figure D.23 Phase-3 Pore Pressure Generation for Parametric Study Analysis with Degree of Disturbance within the Smear Zone, $k_h/k_h' = 3.0$

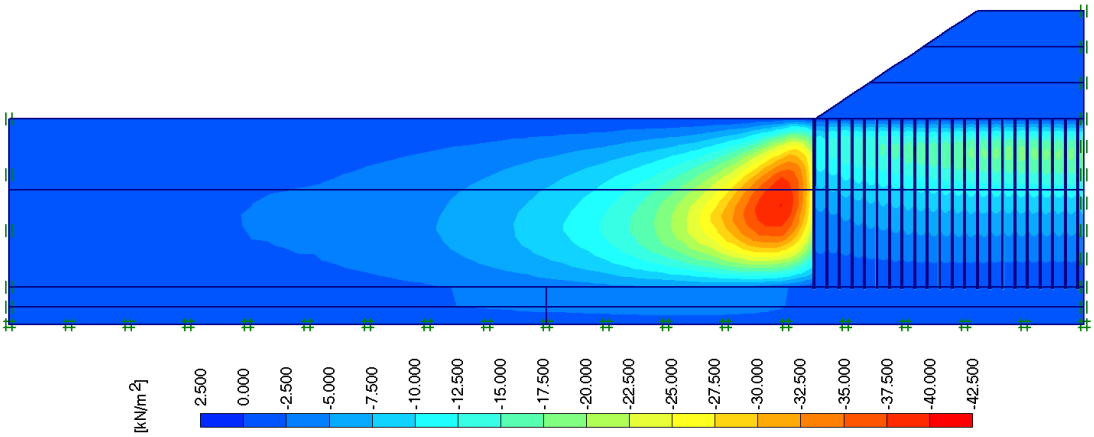

Figure D.24 Phase-4 Pore Pressure Generation for Parametric Study Analysis with Degree of Disturbance within the Smear Zone, $k_h/k_h' = 3.0$

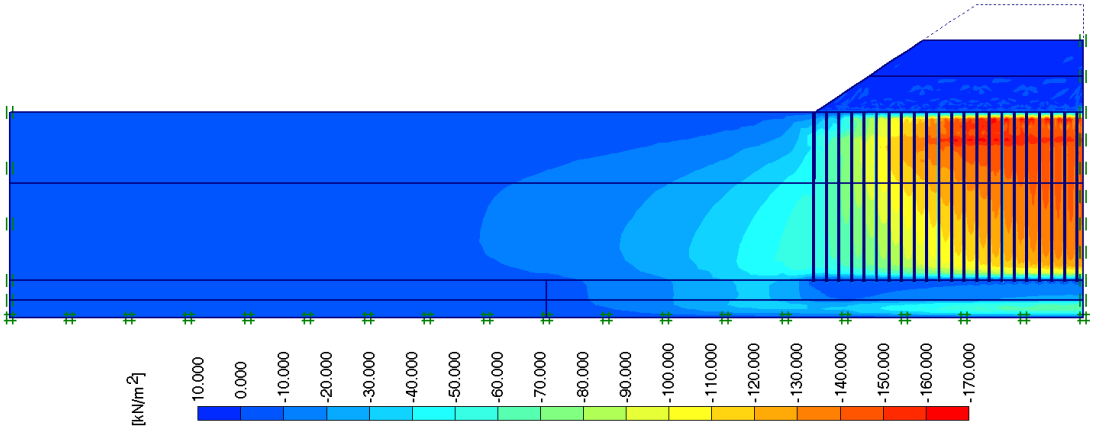

Figure D.25 Phase-1 Pore Pressure Generation for Parametric Study Analysis with Degree of Disturbance within the Smear Zone, $k_h/k_h' = 4.0$

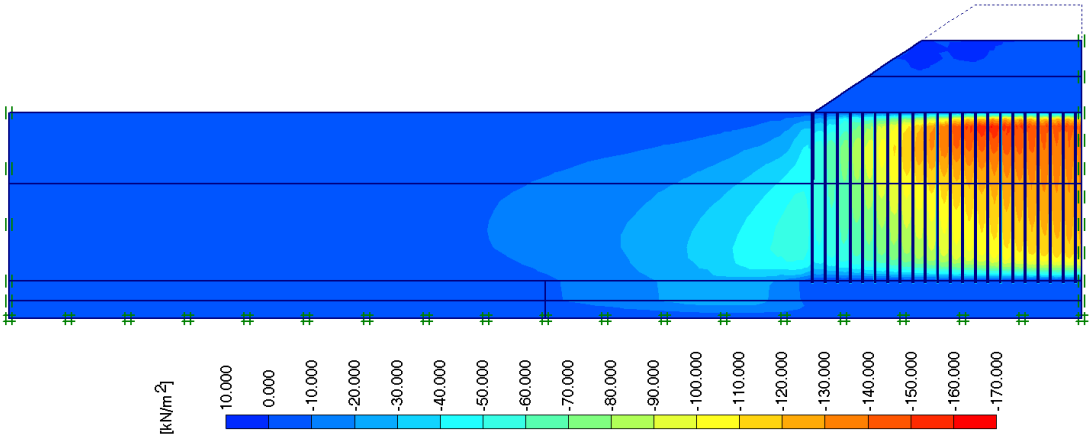

Figure D.26 Phase-2 Pore Pressure Generation for Parametric Study Analysis with Degree of Disturbance within the Smear Zone, $k_h/k_h' = 4.0$

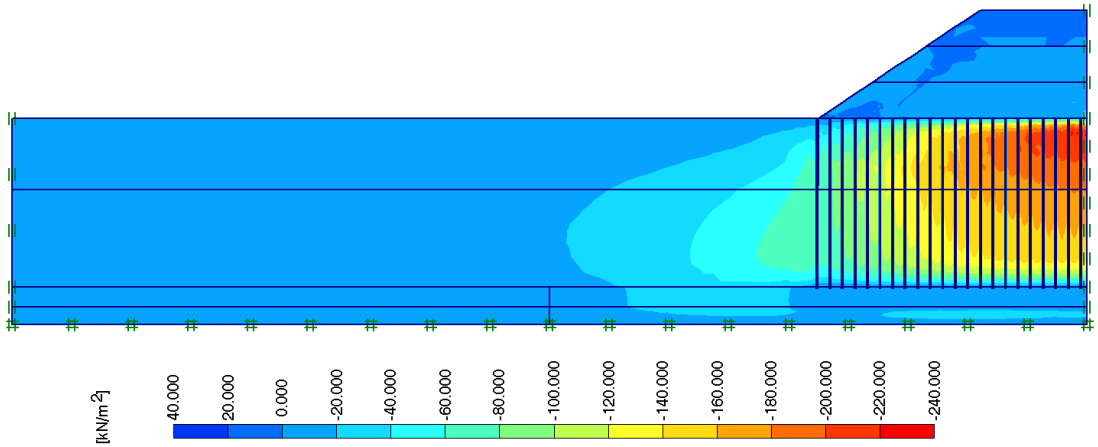

Figure D.27 Phase-3 Pore Pressure Generation for Parametric Study Analysis with Degree of Disturbance within the Smear Zone, $k_h/k_h' = 4.0$

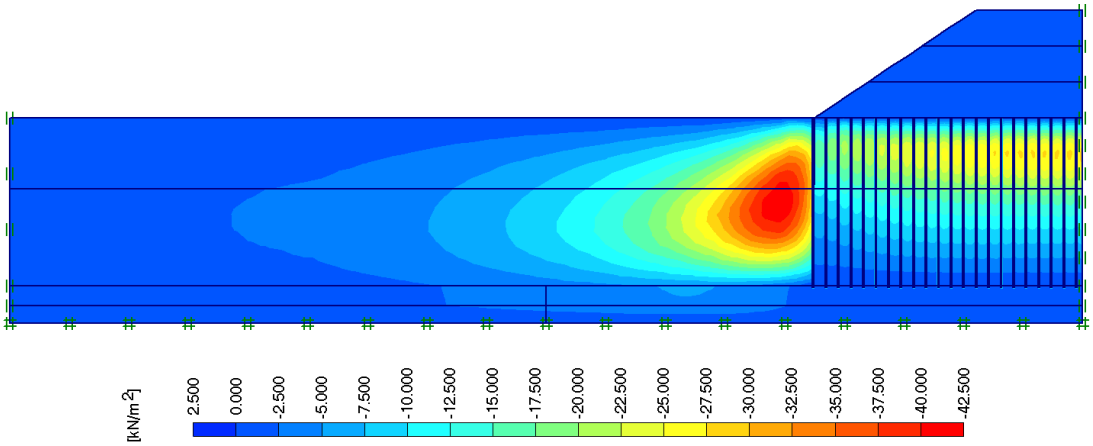

Figure D.28 Phase-4 Pore Pressure Generation for Parametric Study Analysis with Degree of Disturbance within the Smear Zone, $k_h/k_h' = 4.0$

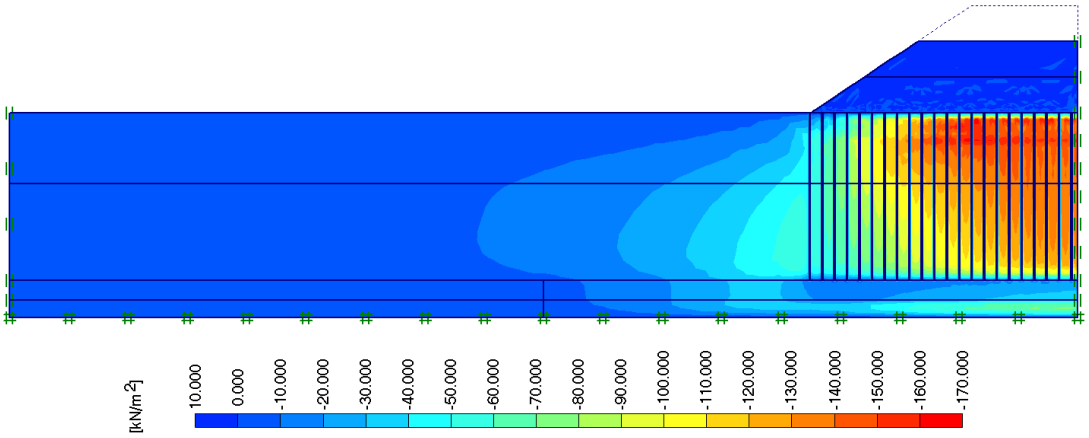

Figure D.29 Phase-1 Pore Pressure Generation for Parametric Study Analysis with Smear Zone Diameter, $d_s = 2.0\ d_w$

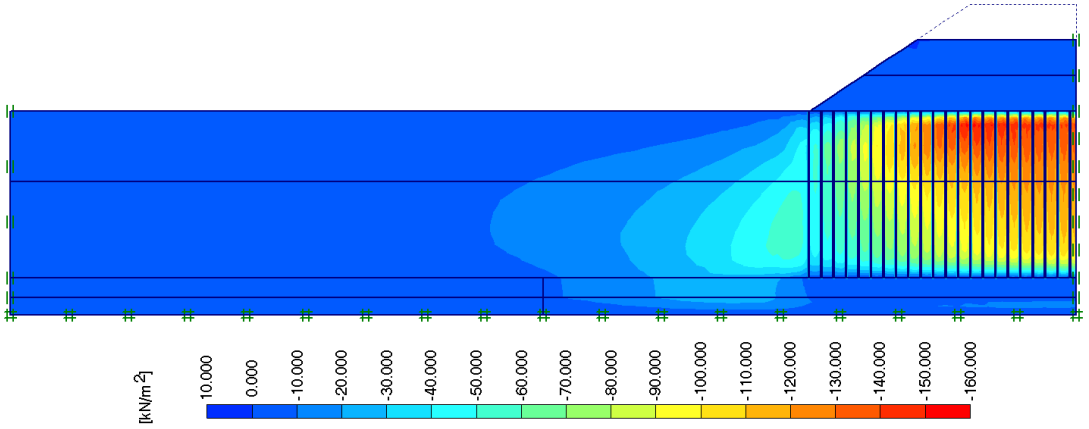

Figure D.30 Phase-2 Pore Pressure Generation for Parametric Study Analysis with Smear Zone Diameter, $d_s = 2.0\ d_w$

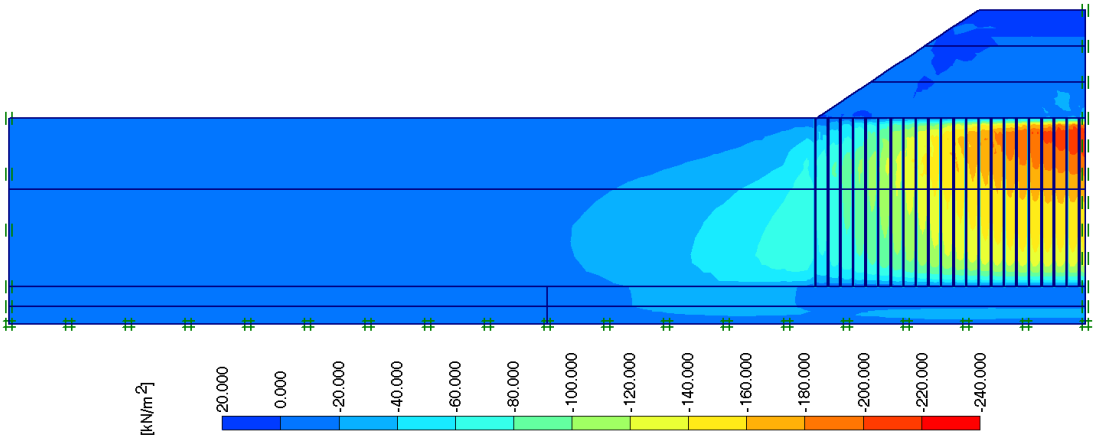

Figure D.31 Phase-3 Pore Pressure Generation for Parametric Study Analysis with Smear Zone Diameter, $d_s = 2.0\ d_w$

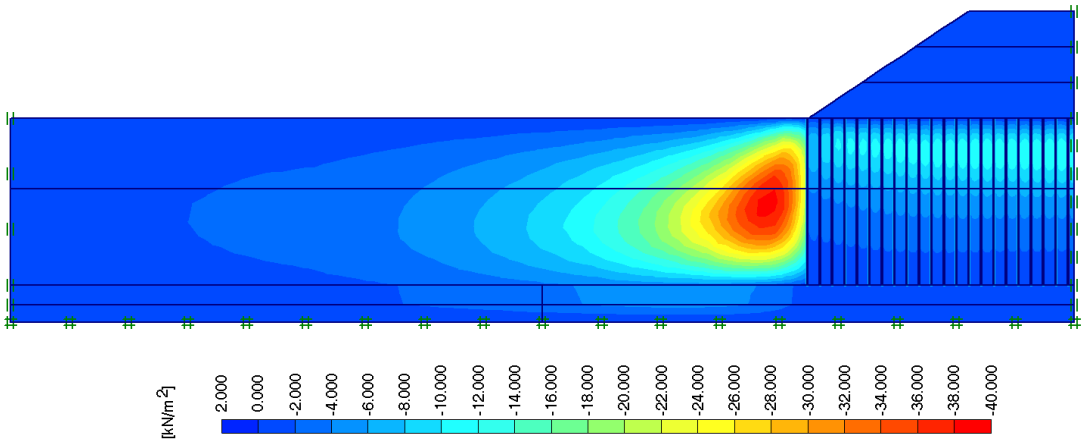

Figure D.32 Phase-4 Pore Pressure Generation for Parametric Study Analysis with Smear Zone Diameter, $d_s = 2.0\ d_w$

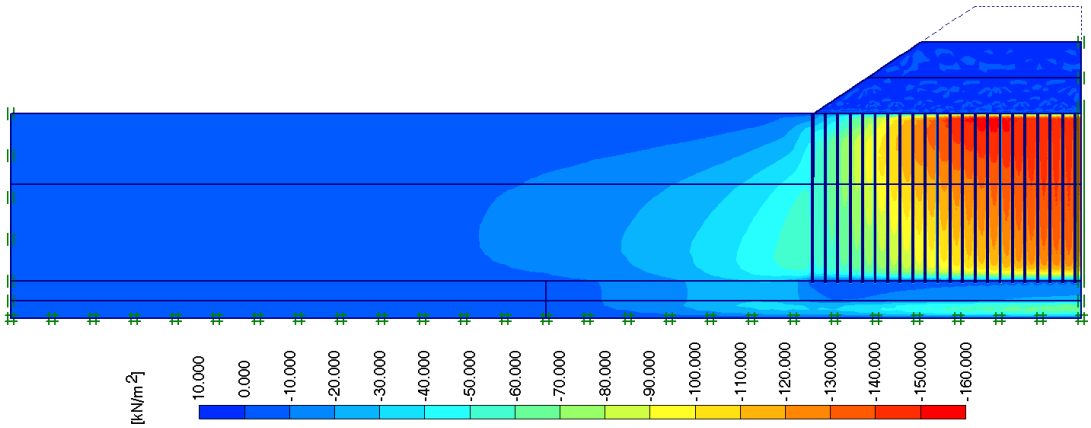

Figure D.33 Phase-1 Pore Pressure Generation for Parametric Study Analysis with Smear Zone Diameter, $d_s = 2.5\ d_w$

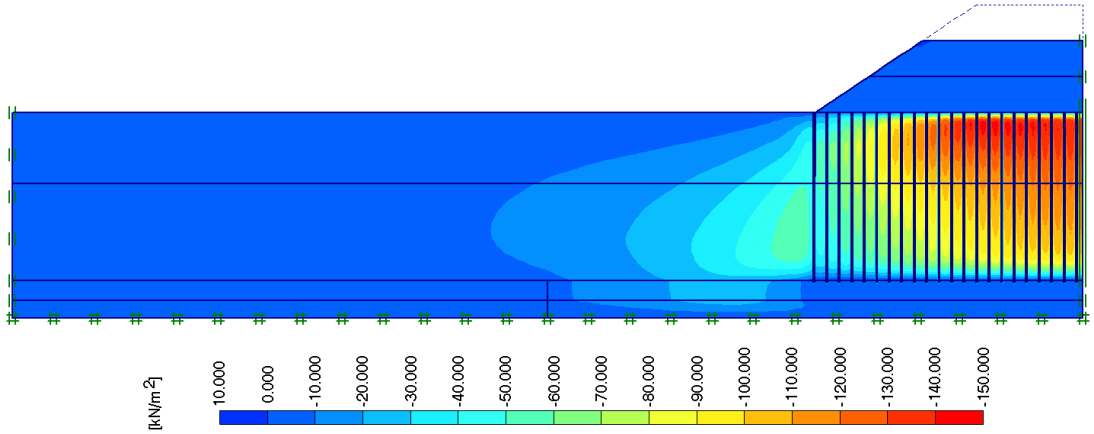

Figure D.34 Phase-2 Pore Pressure Generation for Parametric Study Analysis with Smear Zone Diameter, $d_s = 2.5\ d_w$

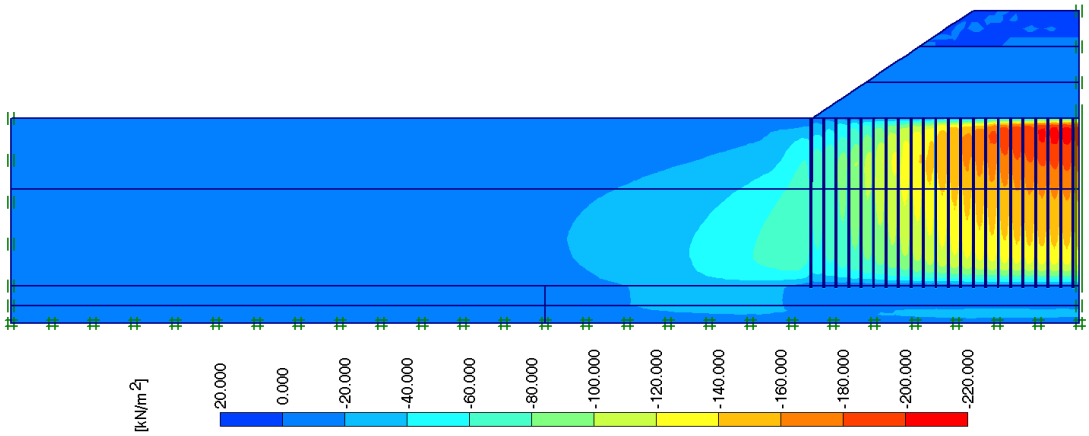

Figure D.35 Phase-3 Pore Pressure Generation for Parametric Study Analysis with Smear Zone Diameter, $d_s = 2.5\ d_w$

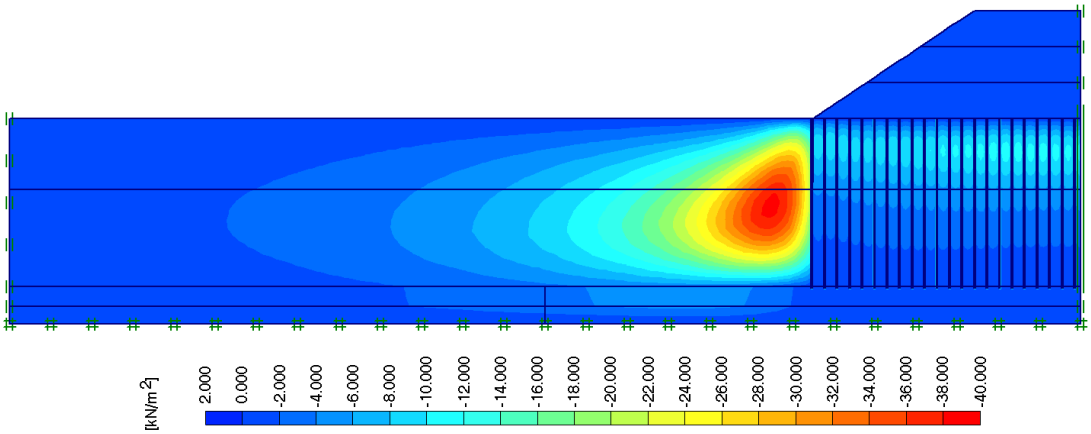

Figure D.36 Phase-4 Pore Pressure Generation for Parametric Study Analysis with Smear Zone Diameter, $d_s = 2.5\ d_w$

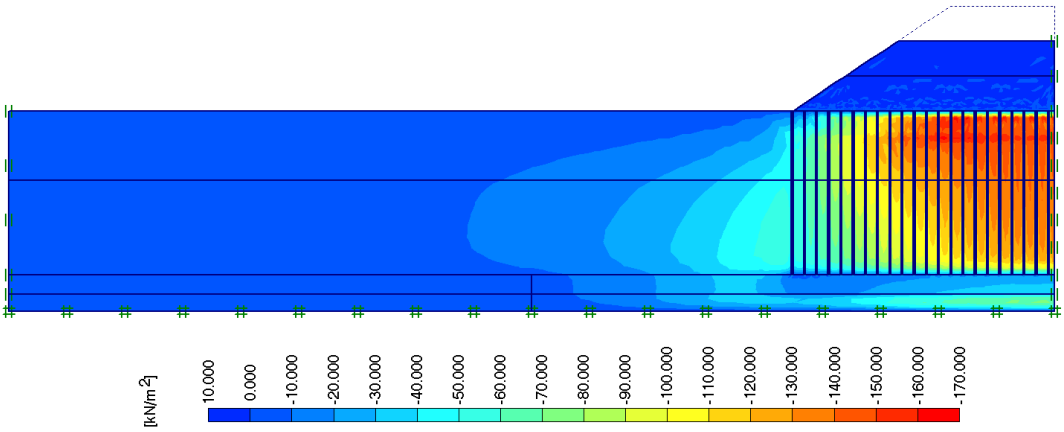

Figure D.37 Phase-1 Pore Pressure Generation for Parametric Study Analysis with Smear Zone Diameter, $d_s = 3.0\ d_w$

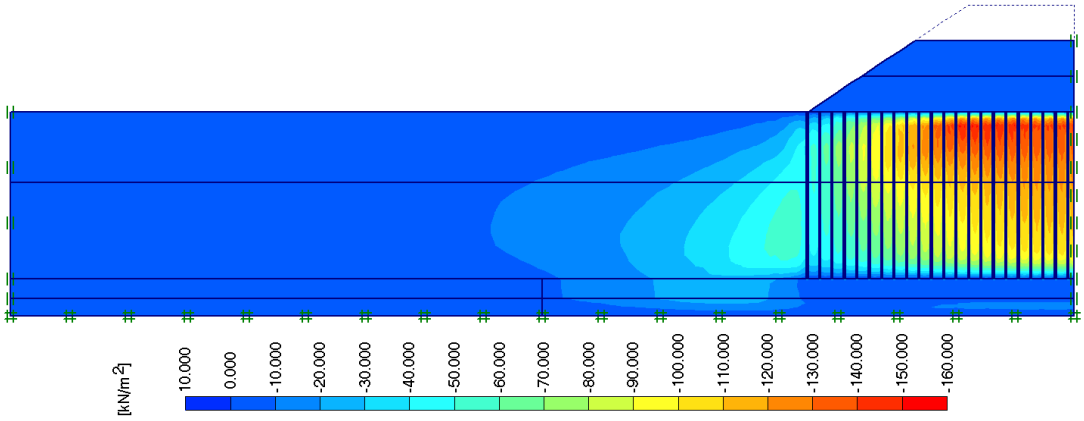

Figure D.38 Phase-2 Pore Pressure Generation for Parametric Study Analysis with Smear Zone Diameter, $d_s = 3.0\ d_w$

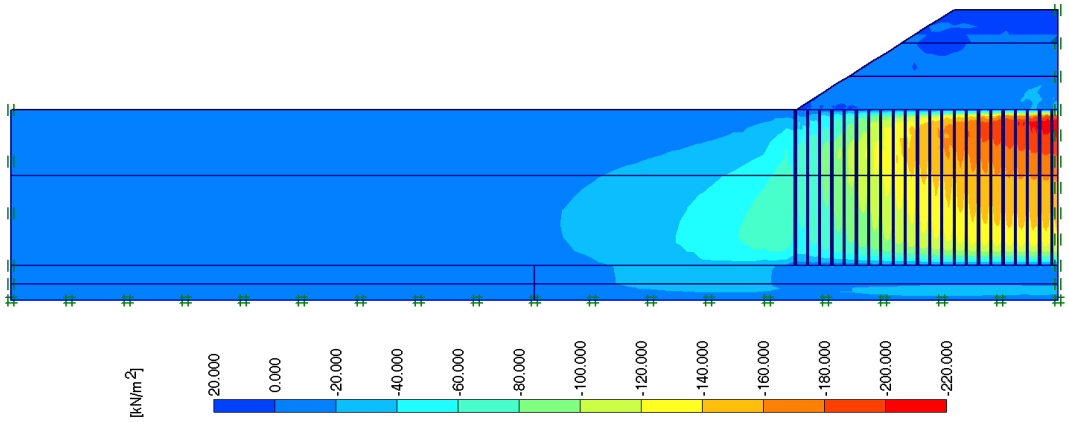

Figure D.39 Phase-3 Pore Pressure Generation for Parametric Study Analysis with Smear Zone Diameter, $d_s = 3.0\ d_w$

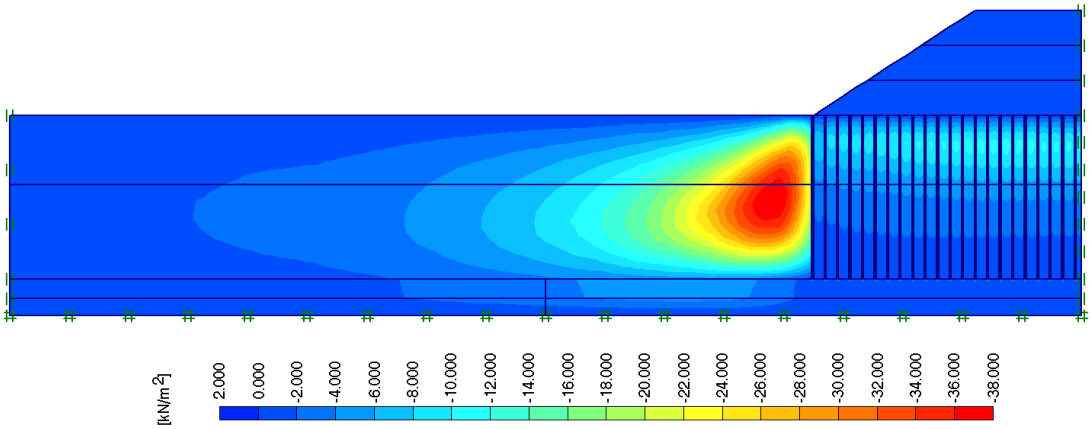

Figure D.40 Phase-4 Pore Pressure Generation for Parametric Study Analysis with Smear Zone Diameter, $d_s = 3.0\ d_w$

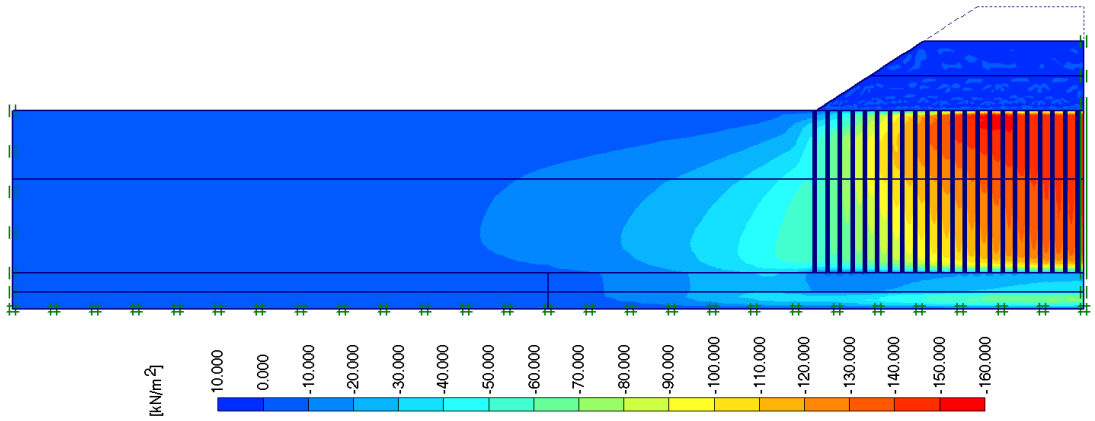

Figure D.41 Phase-1 Pore Pressure Generation for Parametric Study Analysis with Smear Zone Diameter, $d_s = 5.0\ d_w$

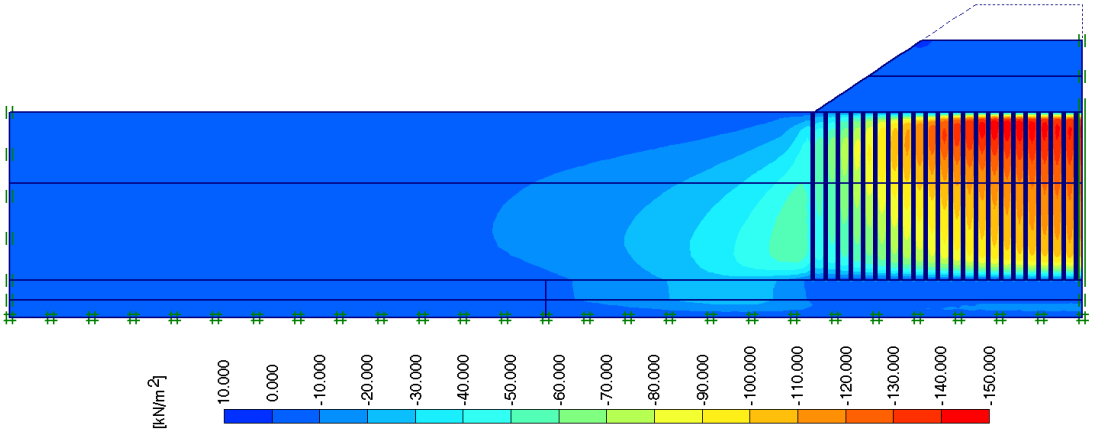

Figure D.42 Phase-2 Pore Pressure Generation for Parametric Study Analysis with Smear Zone Diameter, $d_s = 5.0\ d_w$

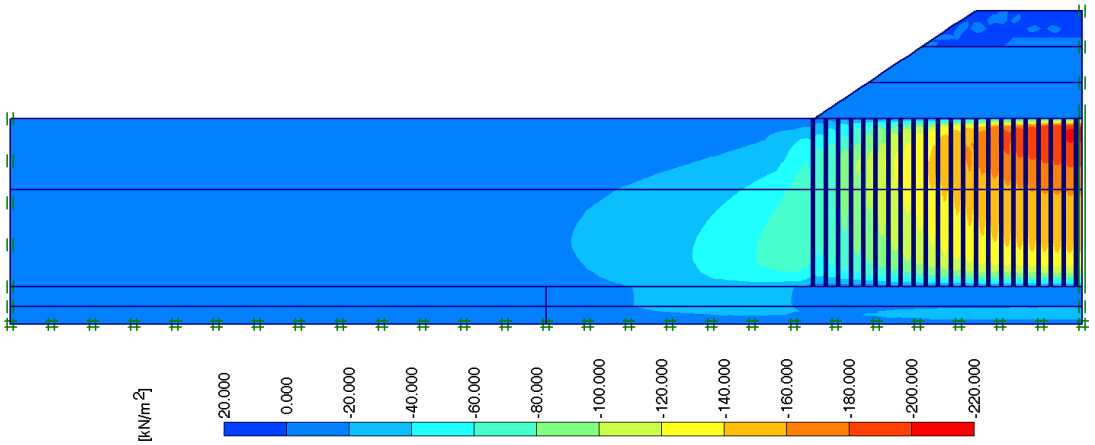

Figure D.43 Phase-3 Pore Pressure Generation for Parametric Study Analysis with Smear Zone Diameter, $d_s = 5.0\ d_w$

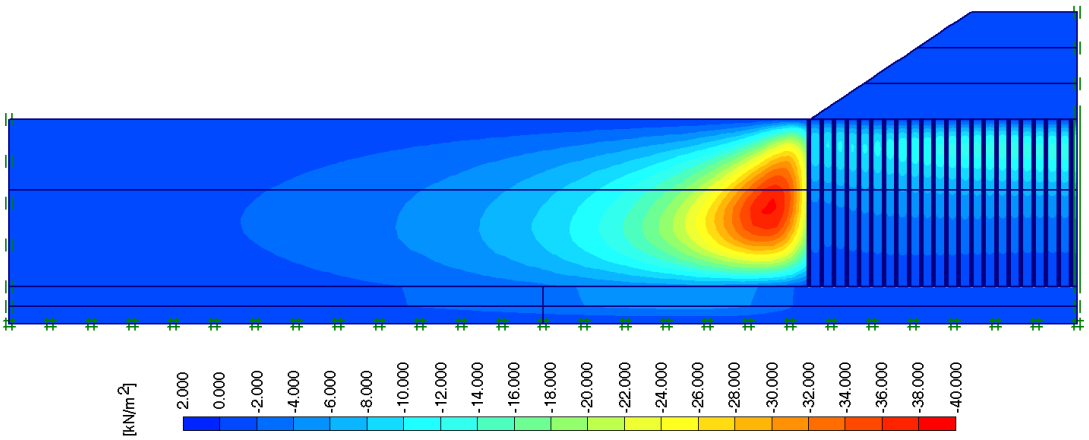

Figure D.44 Phase-4 Pore Pressure Generation for Parametric Study Analysis with Smear Zone Diameter, $d_s = 5.0\ d_w$

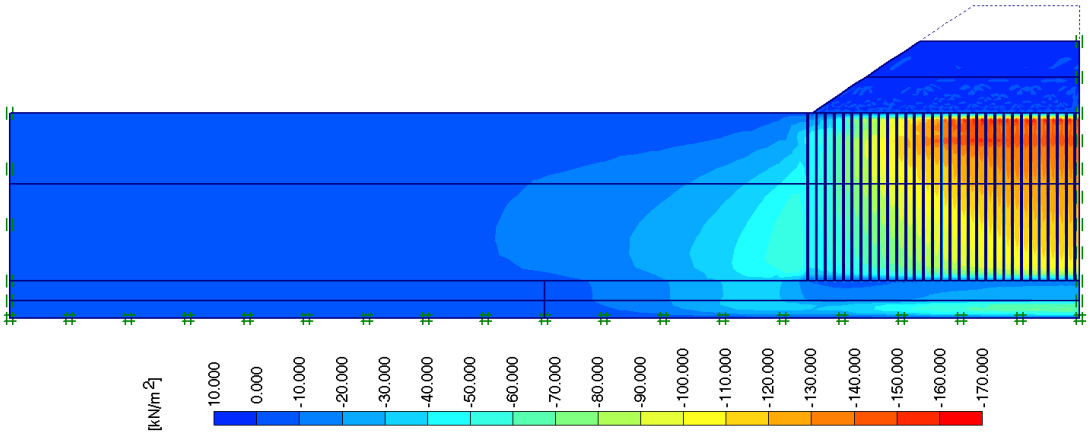

Figure D.45 Phase-1 Pore Pressure Generation for Parametric Study Analysis with Drain Spacing, S = 1.0 m

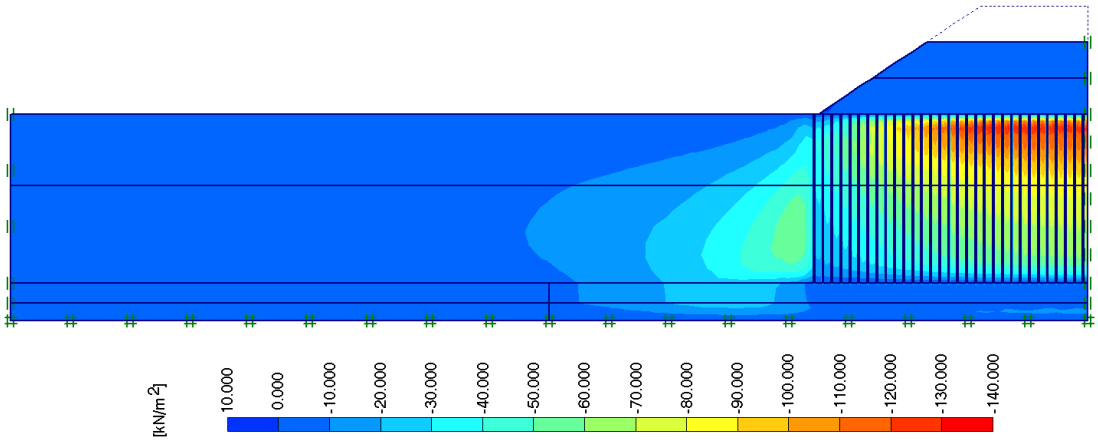

Figure D.46 Phase-2 Pore Pressure Generation for Parametric Study Analysis with Drain Spacing, S = 1.0 m

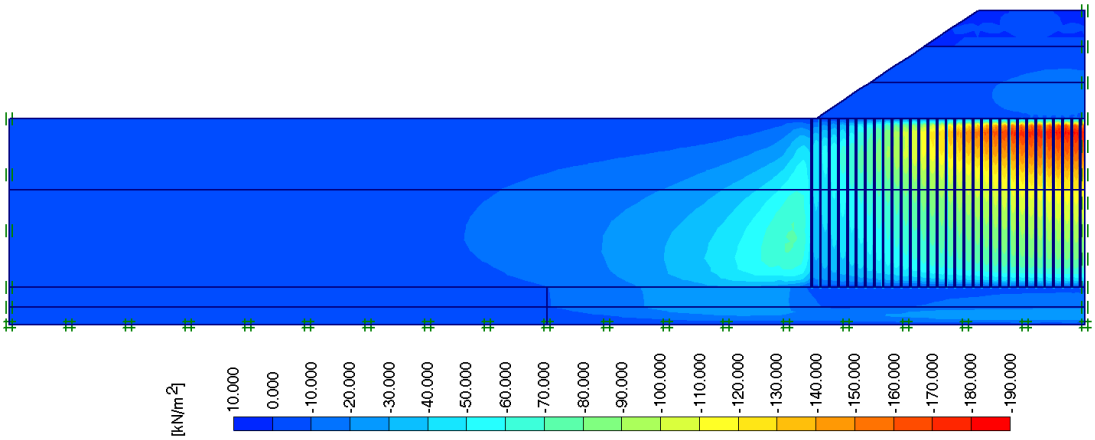

Figure D.47 Phase-3 Pore Pressure Generation for Parametric Study Analysis with Drain Spacing, S = 1.0 m

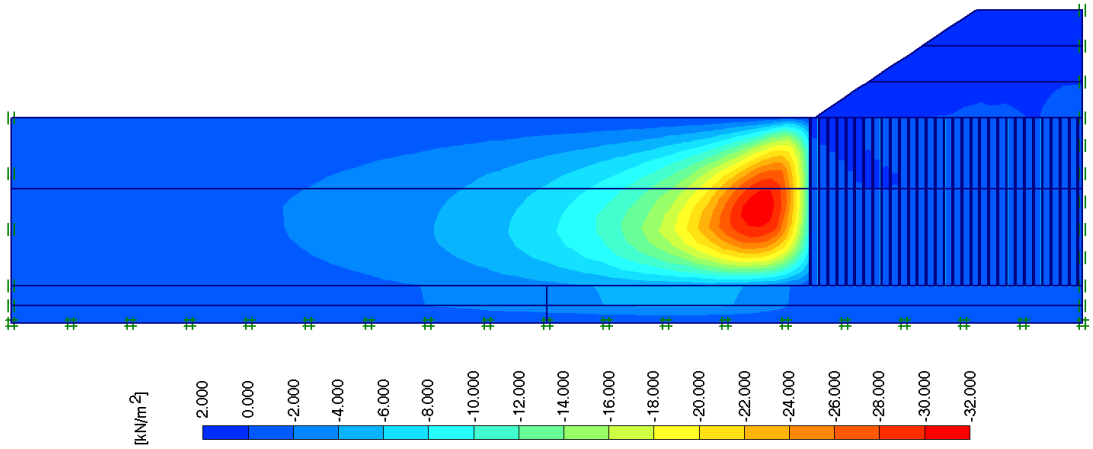

Figure D.48 Phase-4 Pore Pressure Generation for Parametric Study Analysis with Drain Spacing, S = 1.0 m

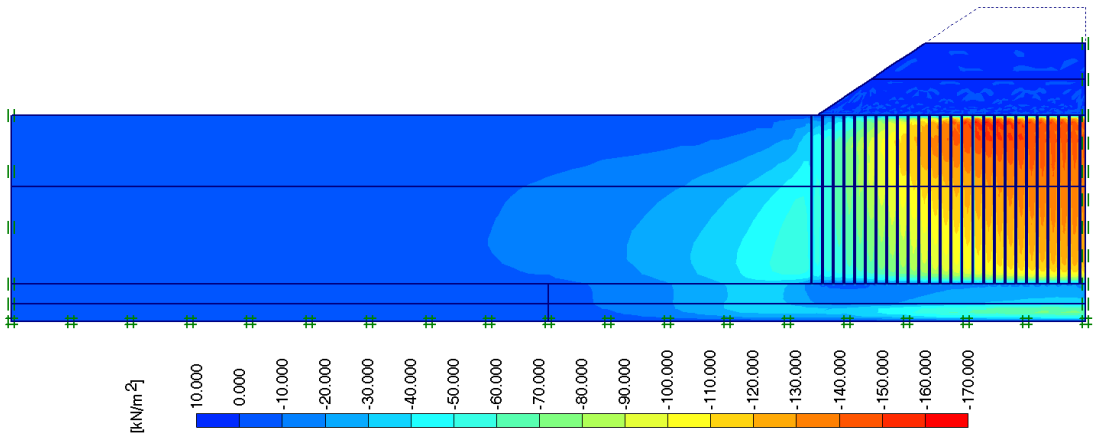

Figure D.49 Phase-1 Pore Pressure Generation for Parametric Study Analysis with Drain Spacing, S = 1.2 m

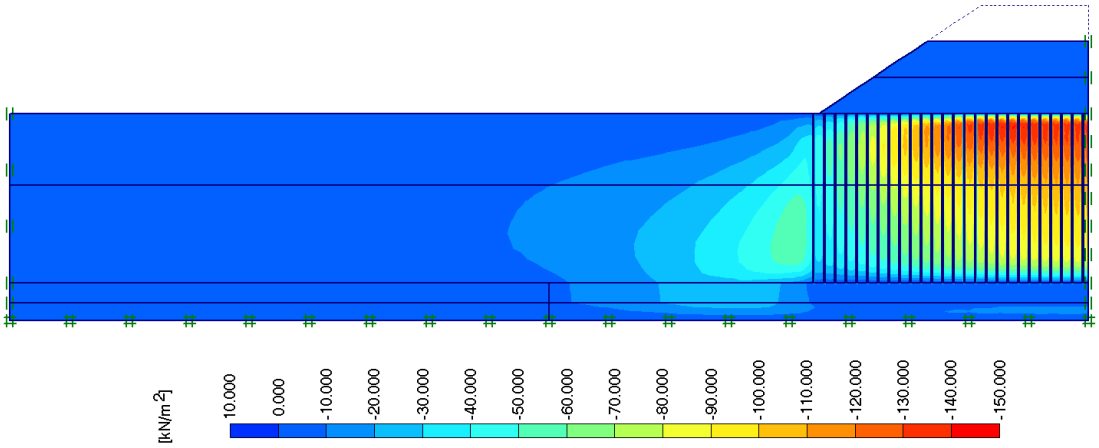

Figure D.50 Phase-2 Pore Pressure Generation for Parametric Study Analysis with Drain Spacing, S = 1.2 m

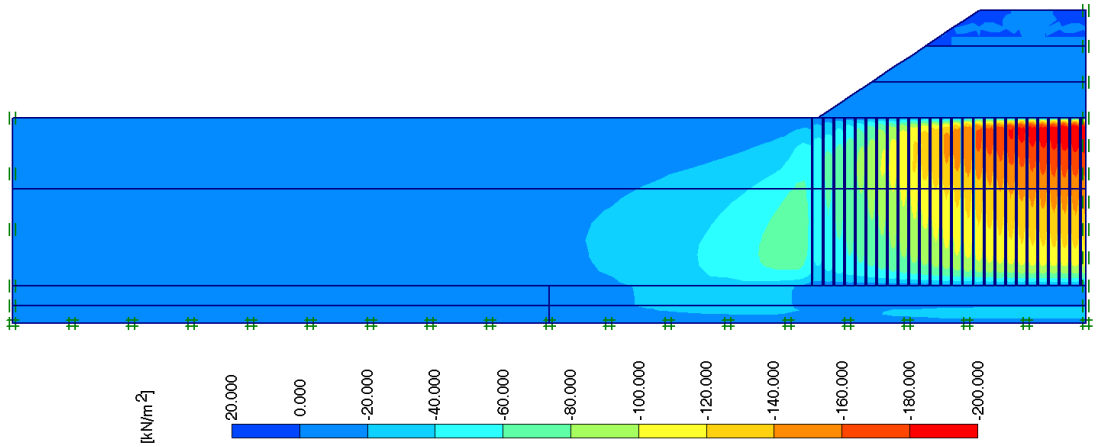

Figure D.51 Phase-3 Pore Pressure Generation for Parametric Study Analysis with Drain Spacing, S = 1.2 m

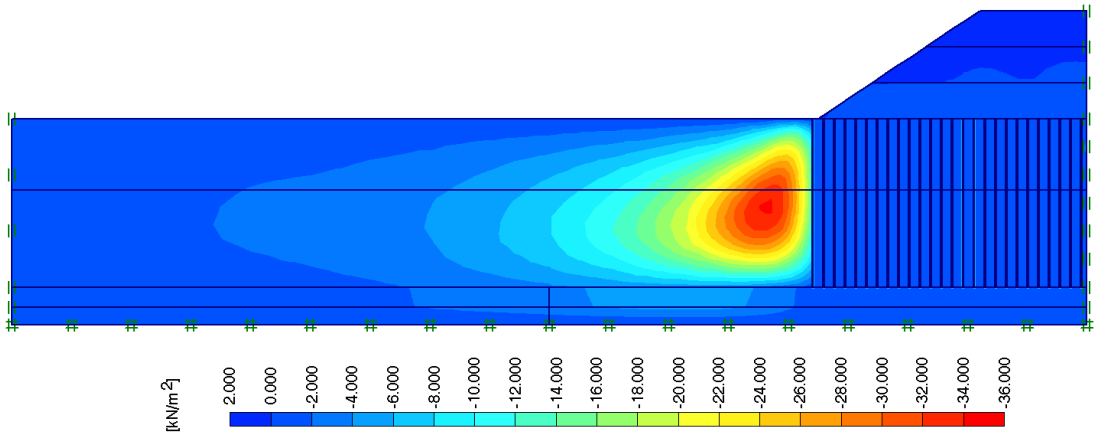

Figure D.52 Phase-4 Pore Pressure Generation for Parametric Study Analysis with Drain Spacing, S = 1.2 m

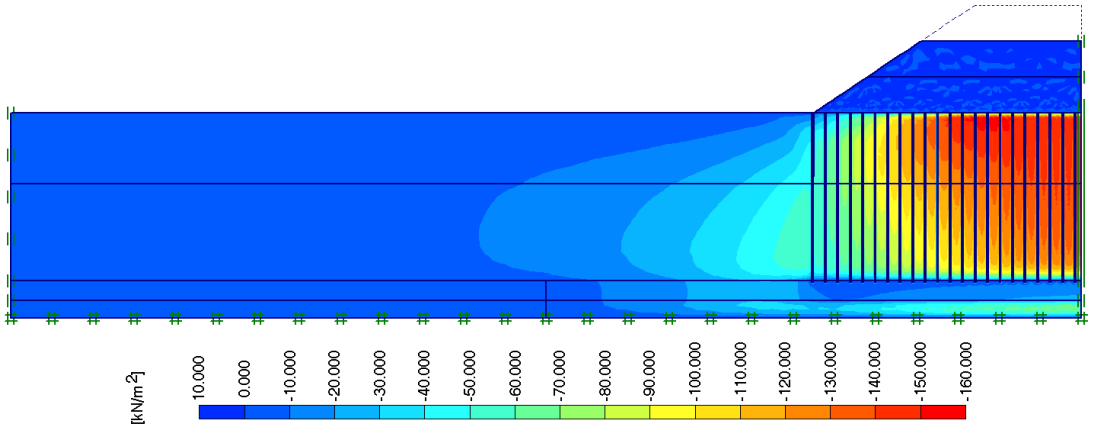

Figure D.53 Phase-1 Pore Pressure Generation for Parametric Study Analysis with Drain Spacing, S = 1.4 m

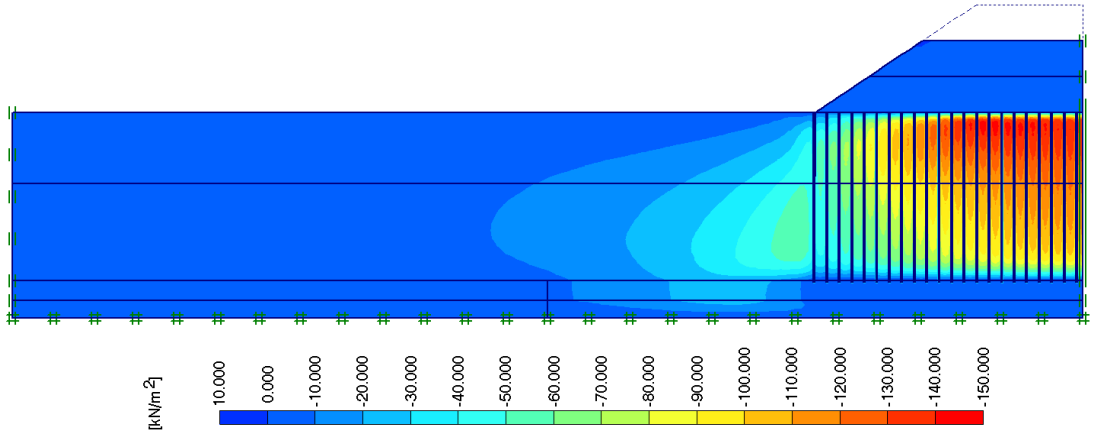

Figure D.54 Phase-2 Pore Pressure Generation for Parametric Study Analysis with Drain Spacing, S = 1.4 m

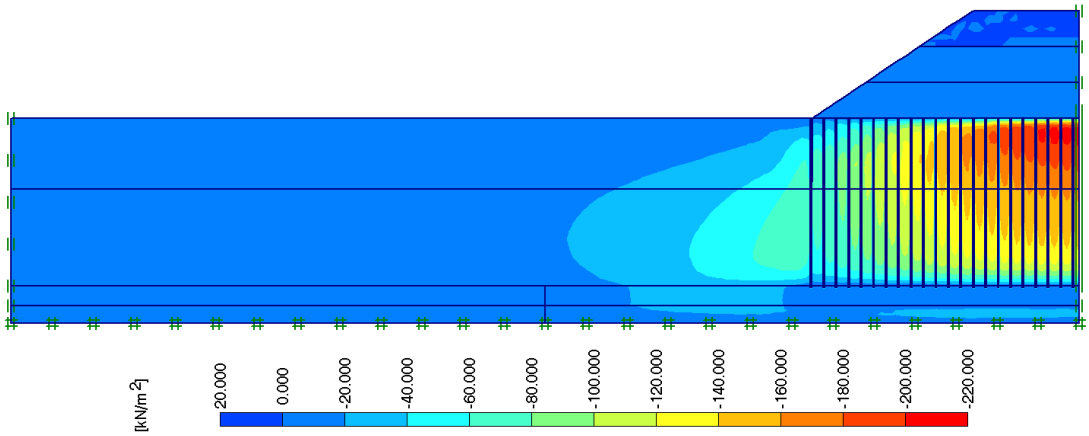

Figure D.55 Phase-3 Pore Pressure Generation for Parametric Study Analysis with Drain Spacing, S = 1.4 m

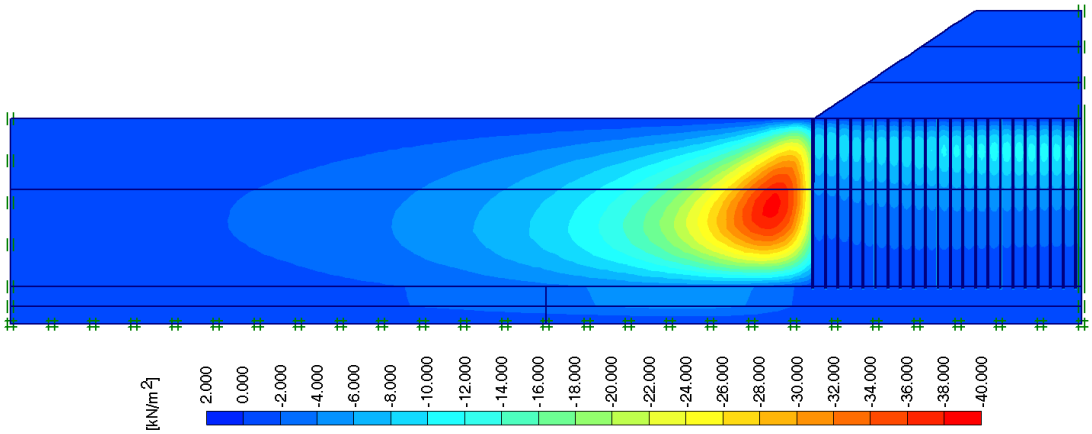

Figure D.56 Phase-4 Pore Pressure Generation for Parametric Study Analysis with Drain Spacing, S = 1.4 m

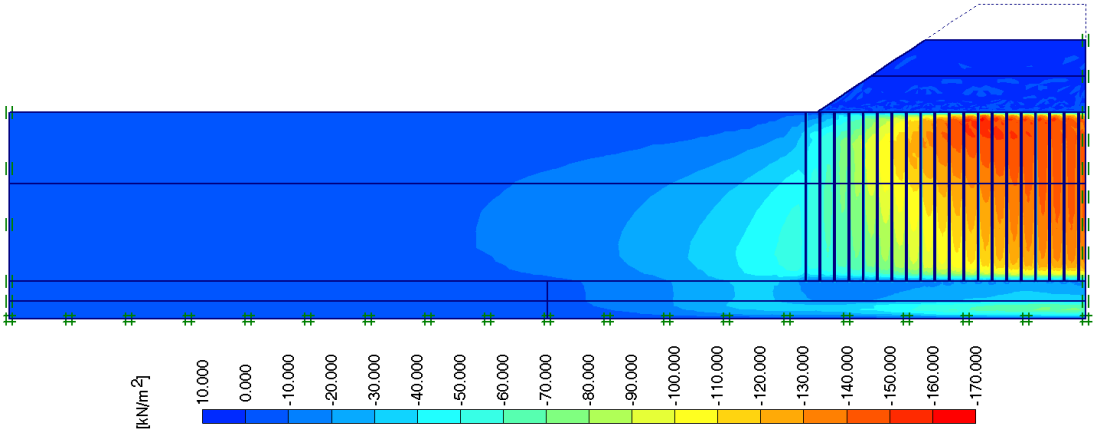

Figure D.57 Phase-1 Pore Pressure Generation for Parametric Study Analysis with Drain Spacing, S = 1.6 m

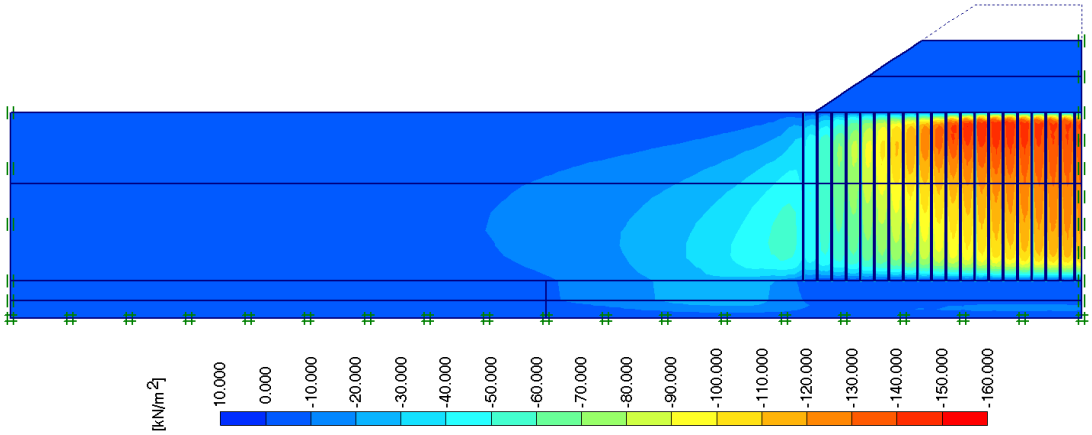

Figure D.58 Phase-2 Pore Pressure Generation for Parametric Study Analysis with Drain Spacing, S = 1.6 m

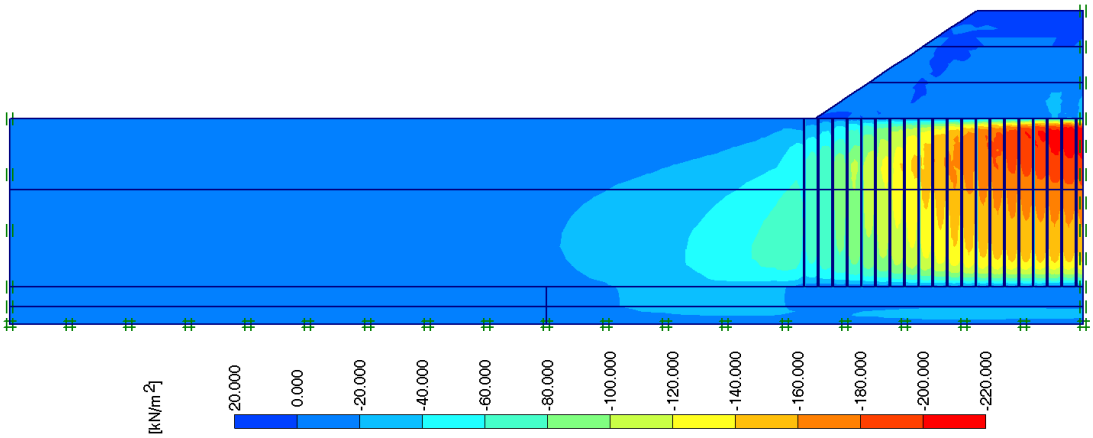

Figure D.59 Phase-3 Pore Pressure Generation for Parametric Study Analysis with Drain Spacing, S = 1.6 m

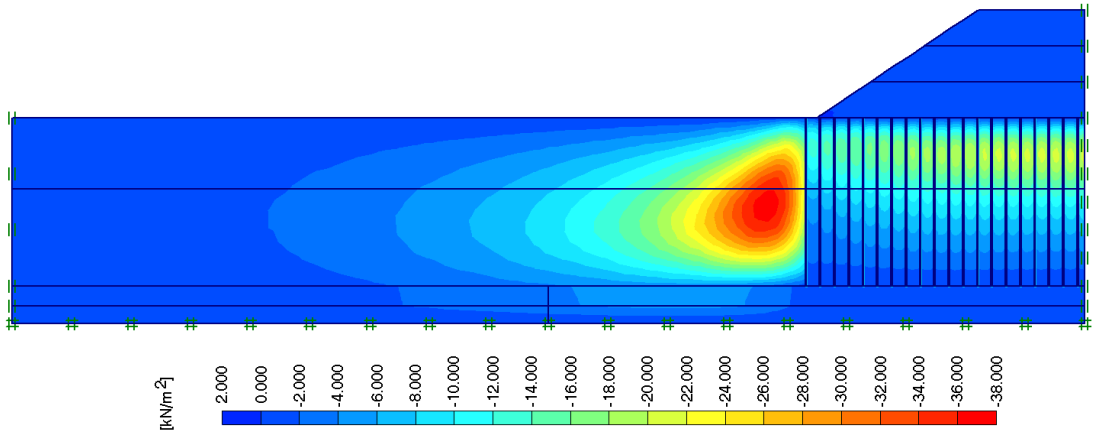

Figure D.60 Phase-4 Pore Pressure Generation for Parametric Study Analysis with Drain Spacing, S = 1.6 m

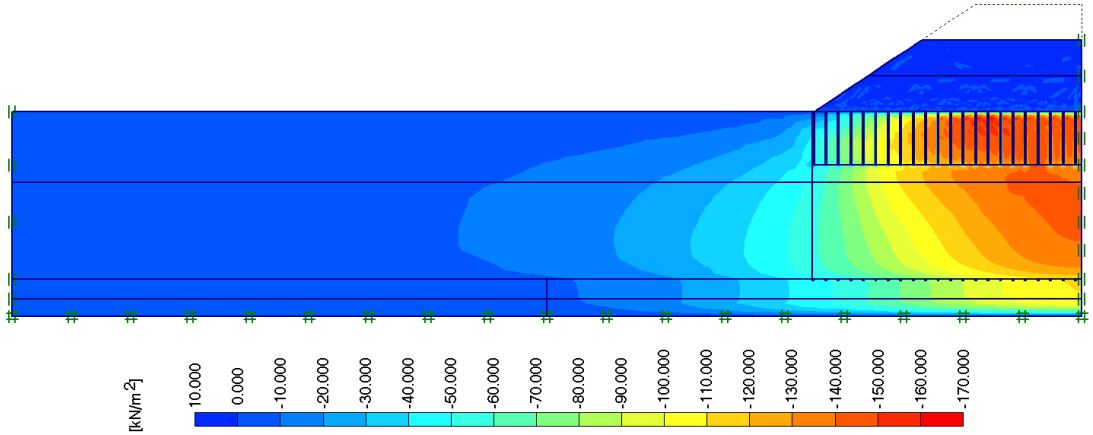

Figure D.61 Phase-1 Pore Pressure Generation for Parametric Study Analysis with Drain Penetration Length, L = 6.0 m

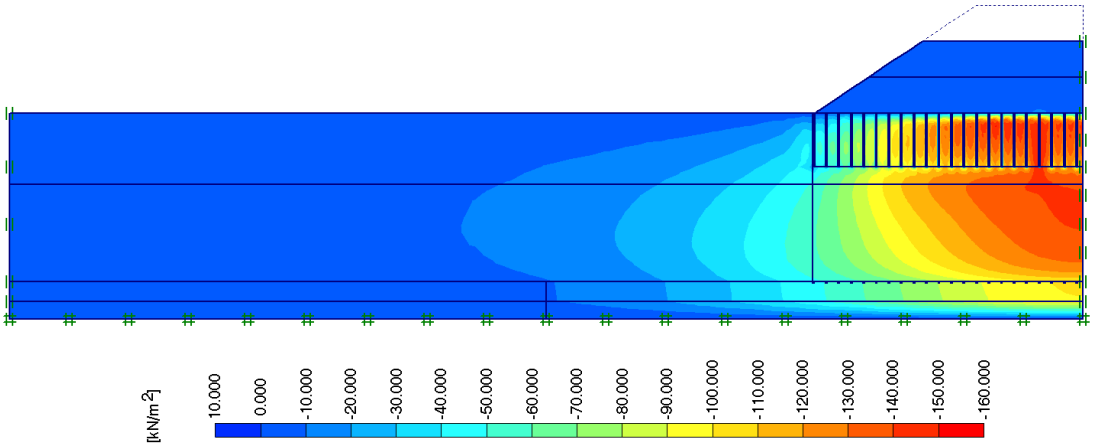

Figure D.62 Phase-2 Pore Pressure Generation for Parametric Study Analysis with Drain Penetration Length, L = 6.0 m

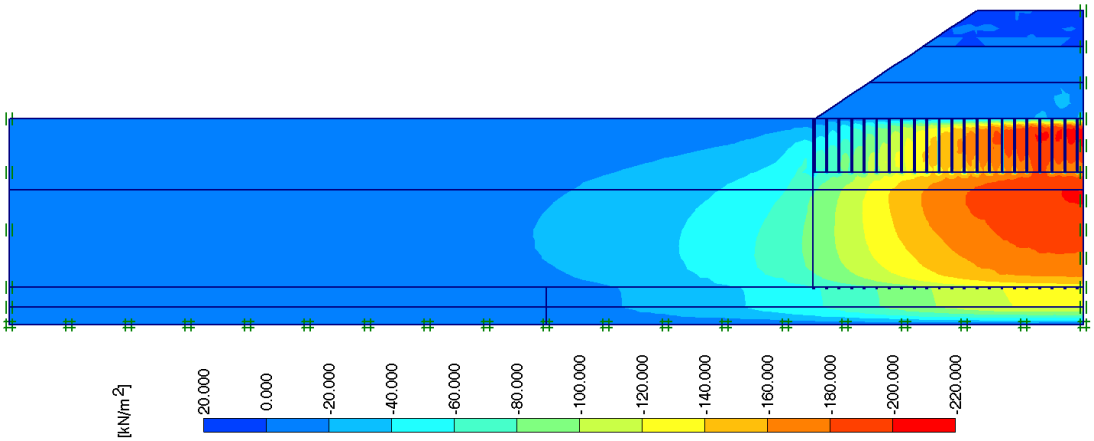

Figure D.63 Phase-3 Pore Pressure Generation for Parametric Study Analysis with Drain Penetration Length, L = 6.0 m

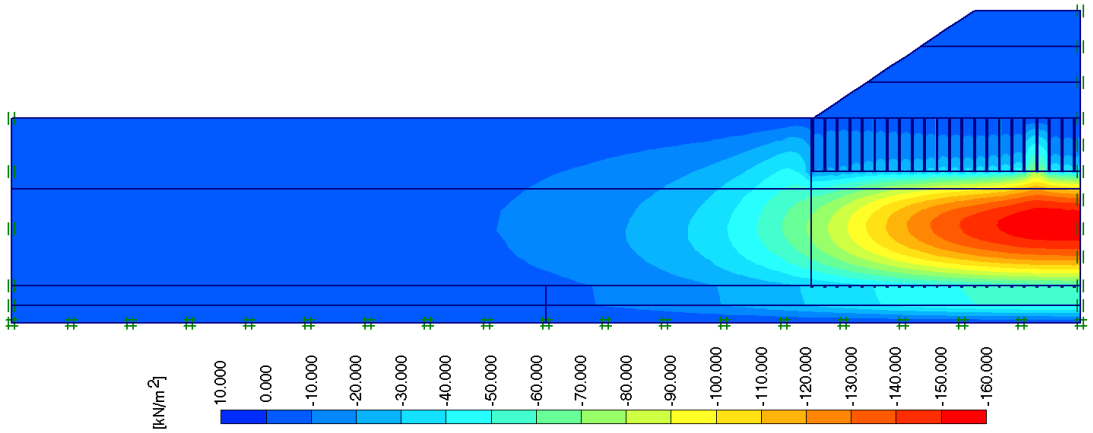

Figure D.64 Phase-4 Pore Pressure Generation for Parametric Study Analysis with Drain Penetration Length, L = 6.0 m

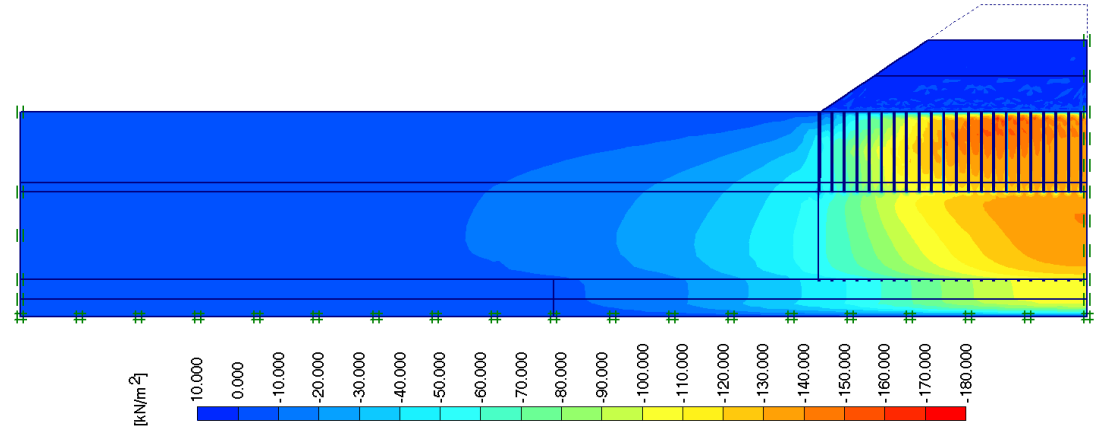

Figure D.65 Phase-1 Pore Pressure Generation for Parametric Study Analysis with Drain Penetration Length, L = 9.0 m

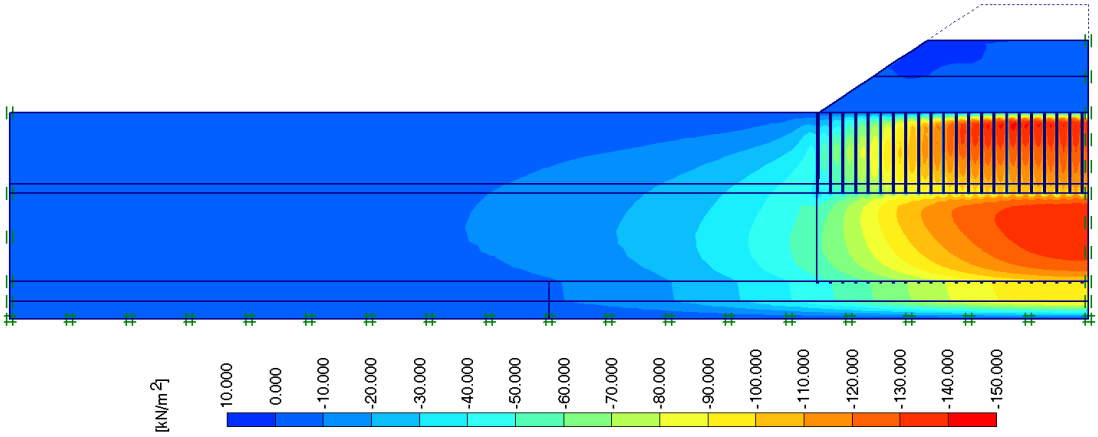

Figure D.66 Phase-2 Pore Pressure Generation for Parametric Study Analysis with Drain Penetration Length, L = 9.0 m

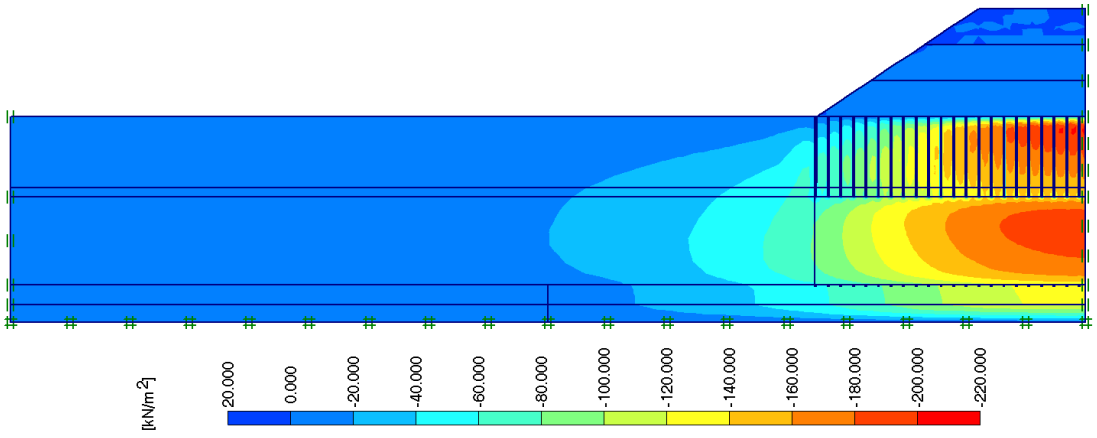

Figure D.67 Phase-3 Pore Pressure Generation for Parametric Study Analysis with Drain Penetration Length, L = 9.0 m

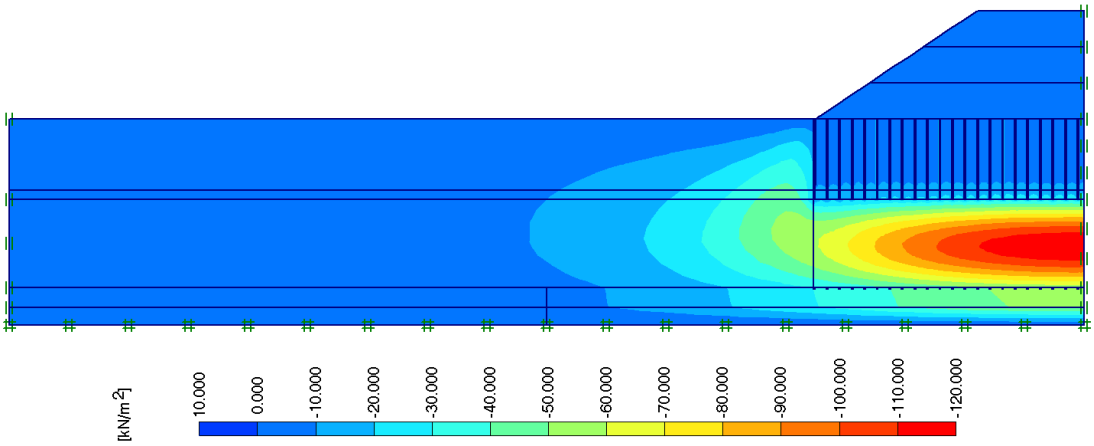

Figure D.68 Phase-4 Pore Pressure Generation for Parametric Study Analysis with Drain Penetration Length, L = 9.0 m

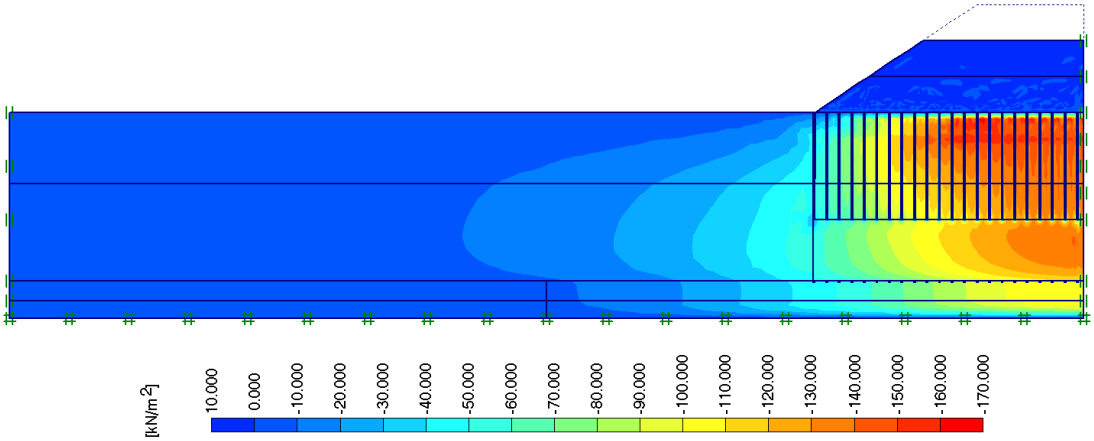

Figure D.69 Phase-1 Pore Pressure Generation for Parametric Study Analysis with Drain Penetration Length, L = 12.0 m

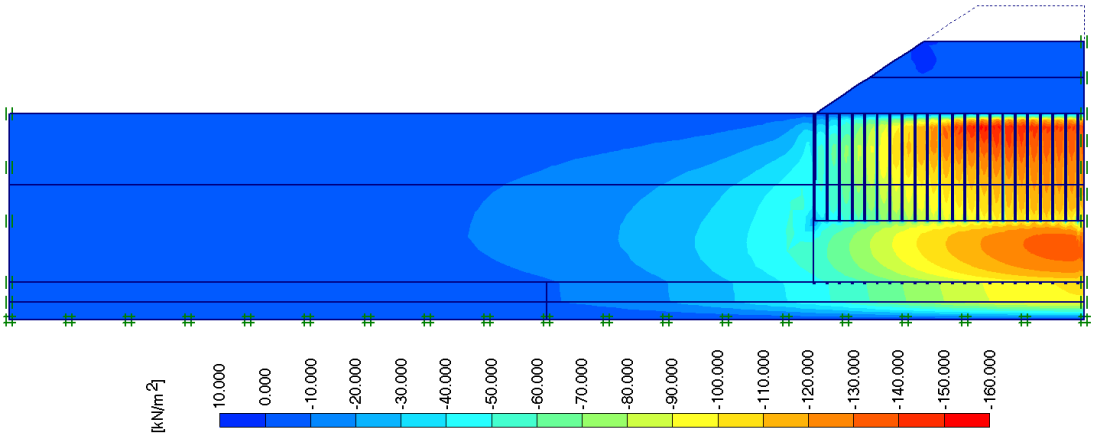

Figure D.70 Phase-2 Pore Pressure Generation for Parametric Study Analysis with Drain Penetration Length, L = 12.0 m

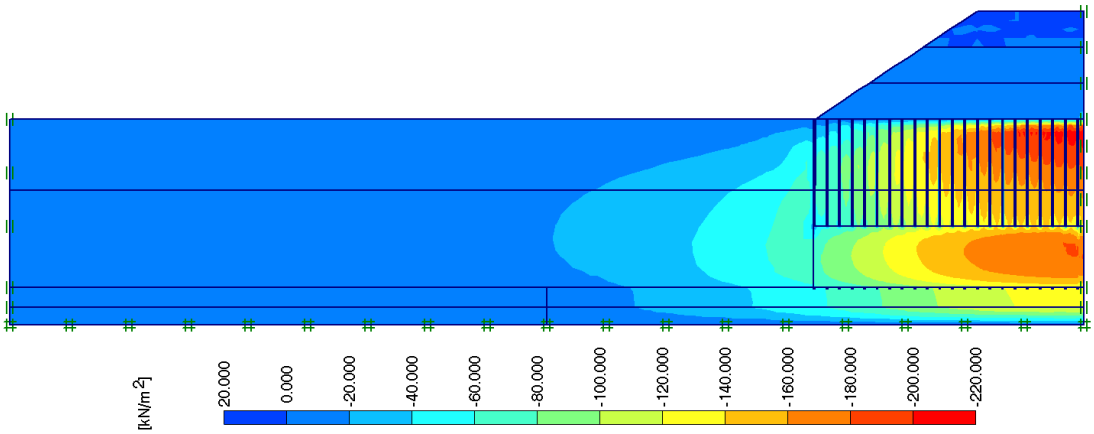

Figure D.71 Phase-3 Pore Pressure Generation for Parametric Study Analysis with Drain Penetration Length, L = 12.0 m

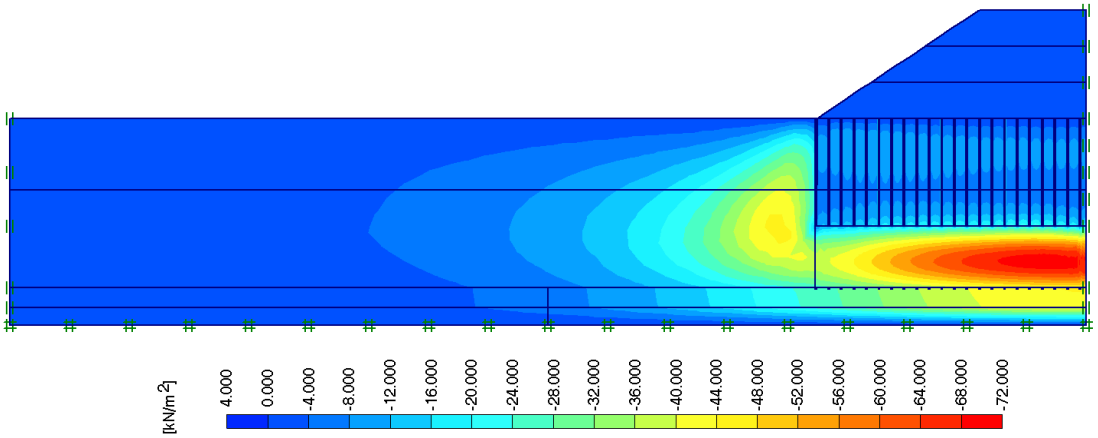

Figure D.72 Phase-4 Pore Pressure Generation for Parametric Study Analysis with Drain Penetration Length, L = 12.0 m

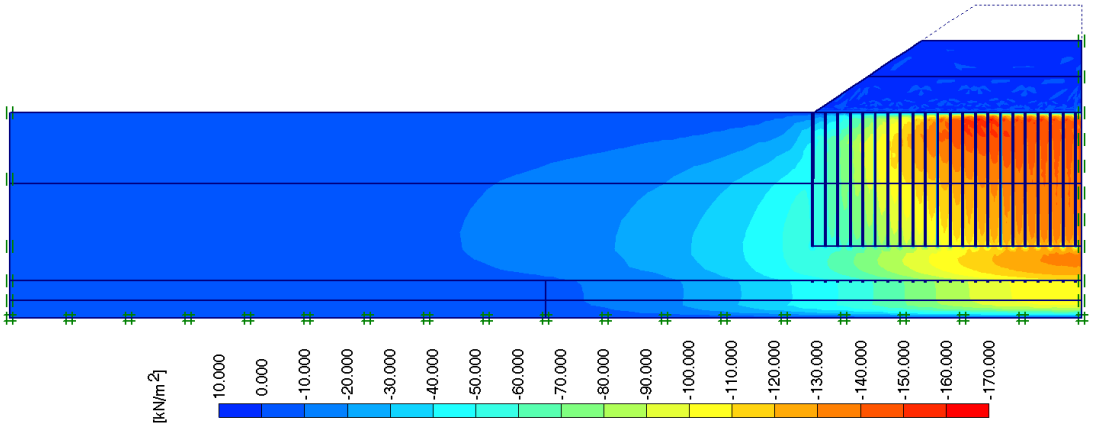

Figure D.73 Phase-1 Pore Pressure Generation for Parametric Study Analysis with Drain Penetration Length, L = 15.0 m

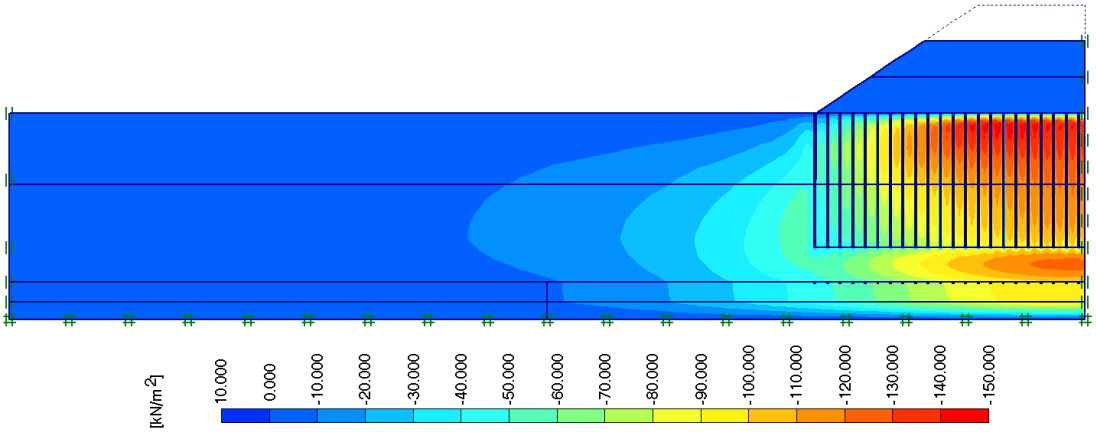

Figure D.74 Phase-2 Pore Pressure Generation for Parametric Study Analysis with Drain Penetration Length, L = 15.0 m

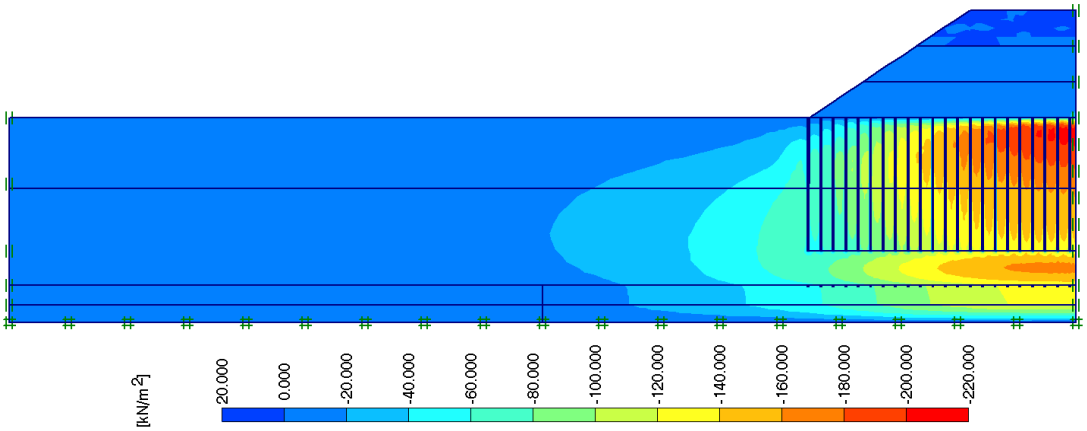

Figure D.75 Phase-3 Pore Pressure Generation for Parametric Study Analysis with Drain Penetration Length, L = 15.0 m

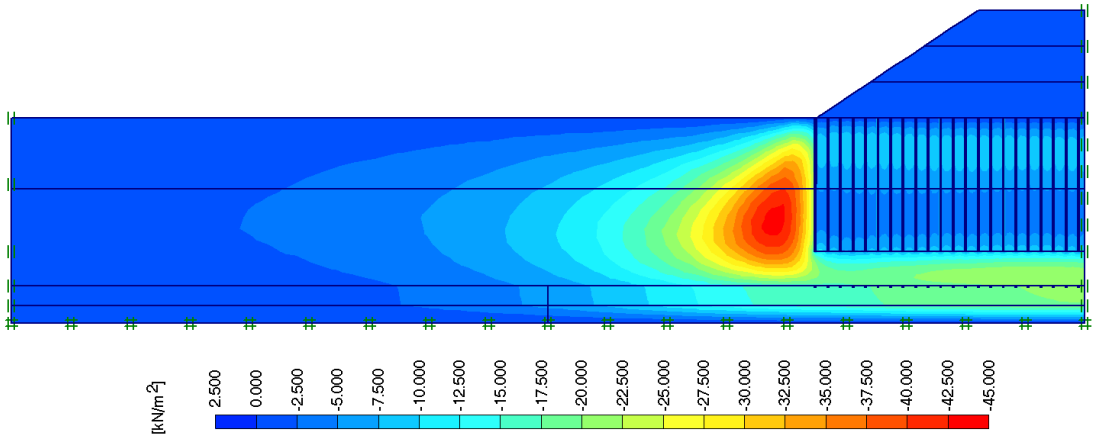

Figure D.76 Phase-4 Pore Pressure Generation for Parametric Study Analysis with Drain Penetration Length, L = 15.0 m

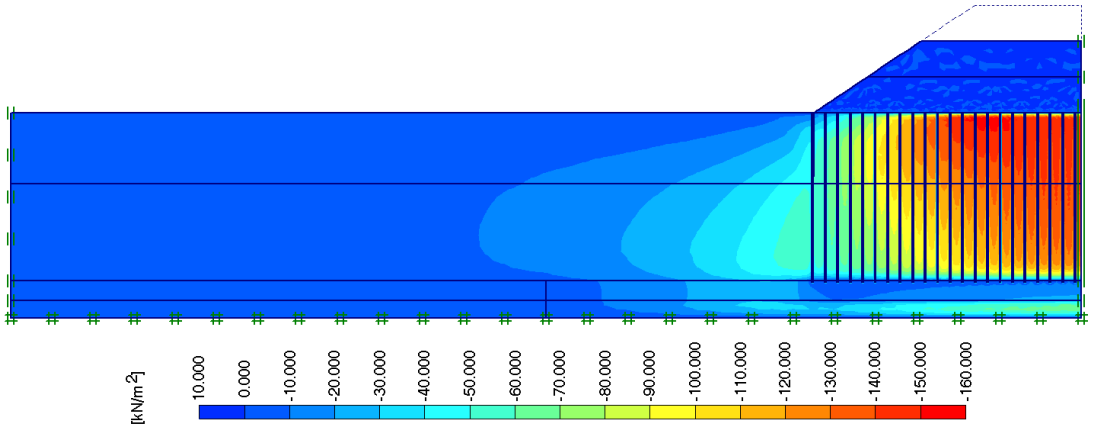

Figure D.77 Phase-1 Pore Pressure Generation for Parametric Study Analysis with Drain Penetration Length, L = 18.0 m

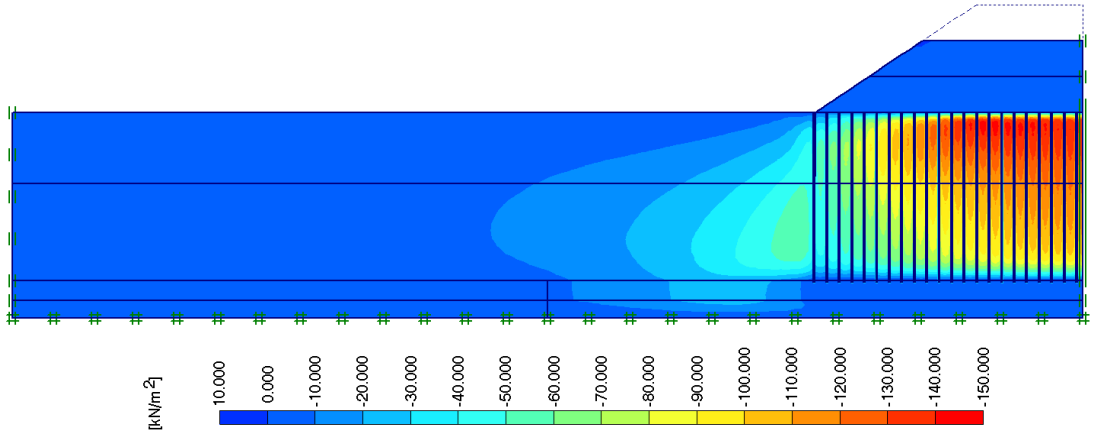

Figure D.78 Phase-2 Pore Pressure Generation for Parametric Study Analysis with Drain Penetration Length, L = 18.0 m

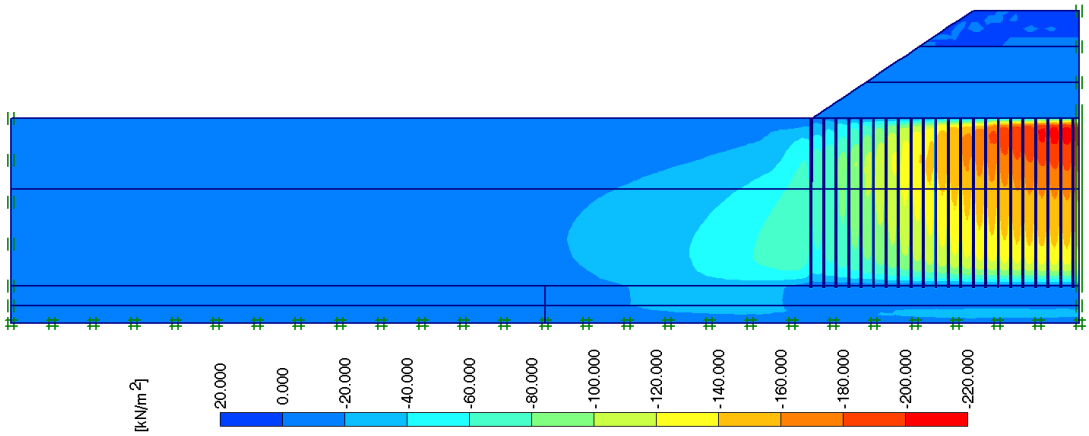

Figure D.79 Phase-3 Pore Pressure Generation for Parametric Study Analysis with Drain Penetration Length, L = 18.0 m

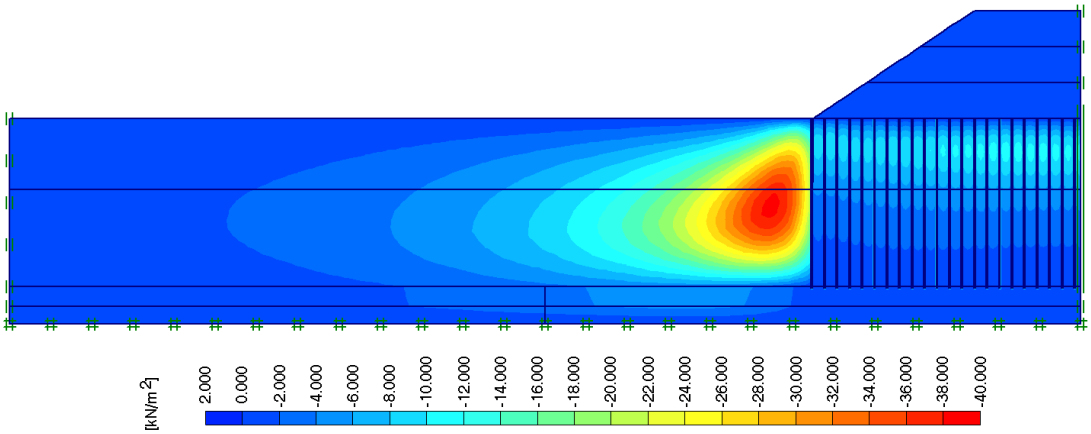

Figure D.80 Phase-4 Pore Pressure Generation for Parametric Study Analysis with Drain Penetration Length, L = 18.0 m

APPENDIX E

VOLUMETRIC STRAIN CONTOURS FOR ANALYSES

Appendix E presents the volumetric strain contours for analysis ignoring the smear zone, analysis including the smear zone, analysis including both smear and creep and 13 parametric study analyses.

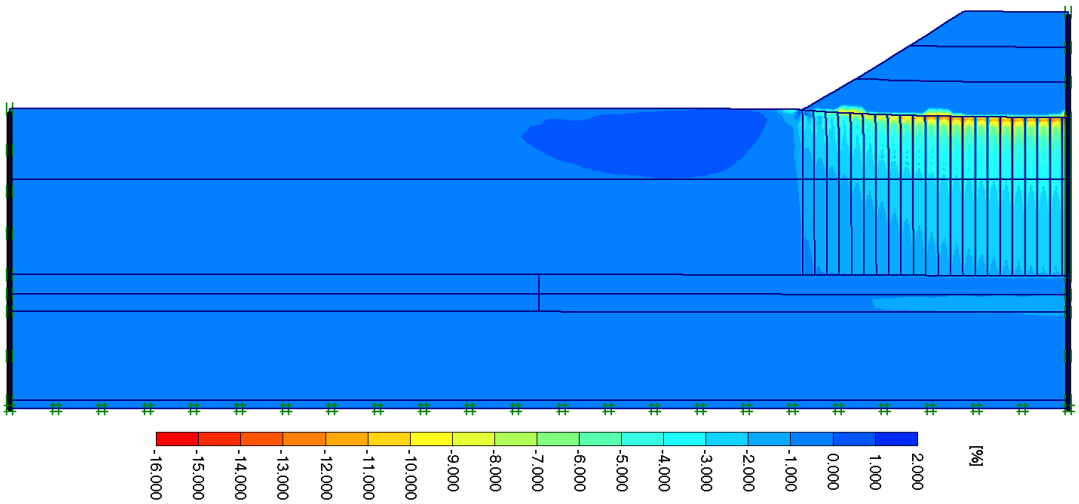

Figure E.1 Volumetric Strain Contours for Analysis Ignoring The Smear Effect

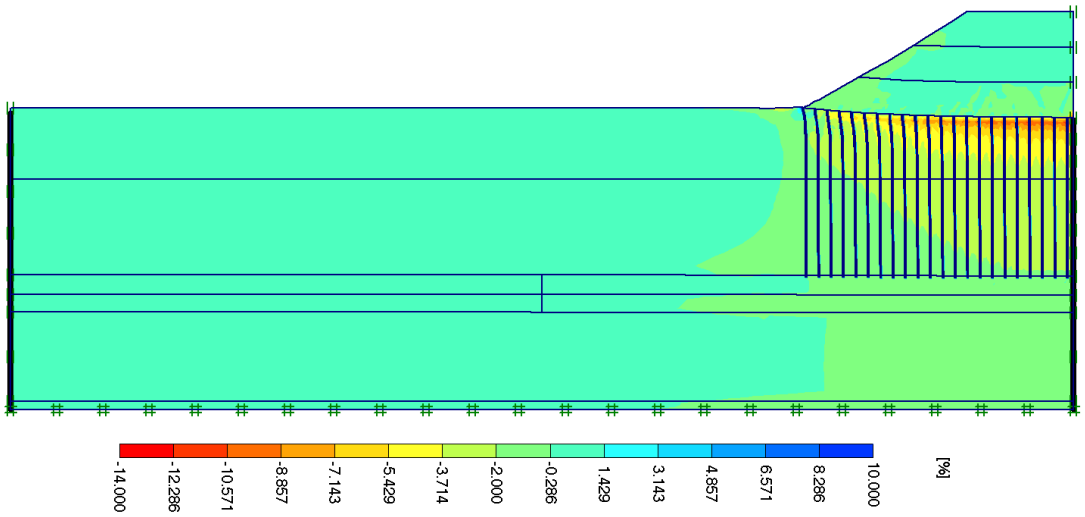

Figure E.2 Volumetric Strain Contours for Analysis Including The Smear Effect

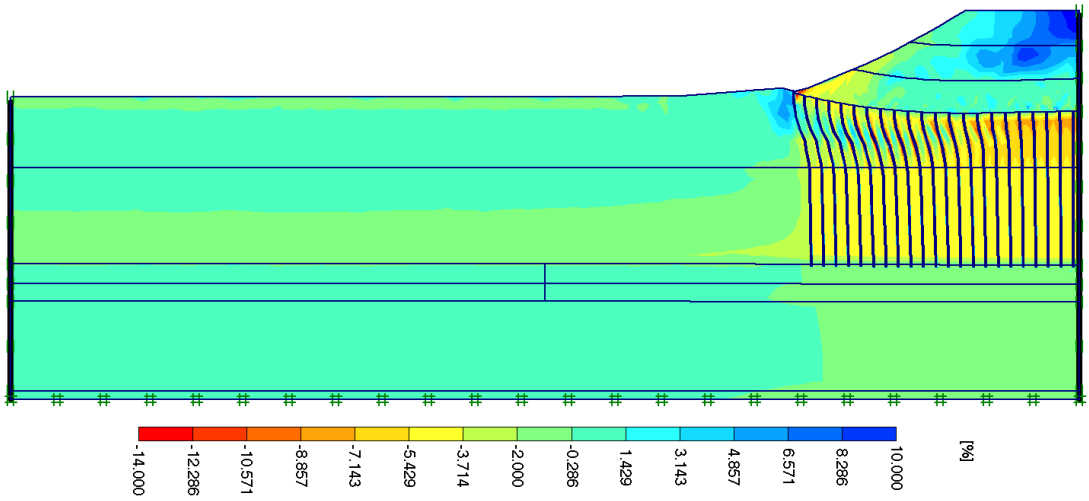

Figure E.3 Volumetric Strain Contours for Analysis Including Both Smear and Creep Effects

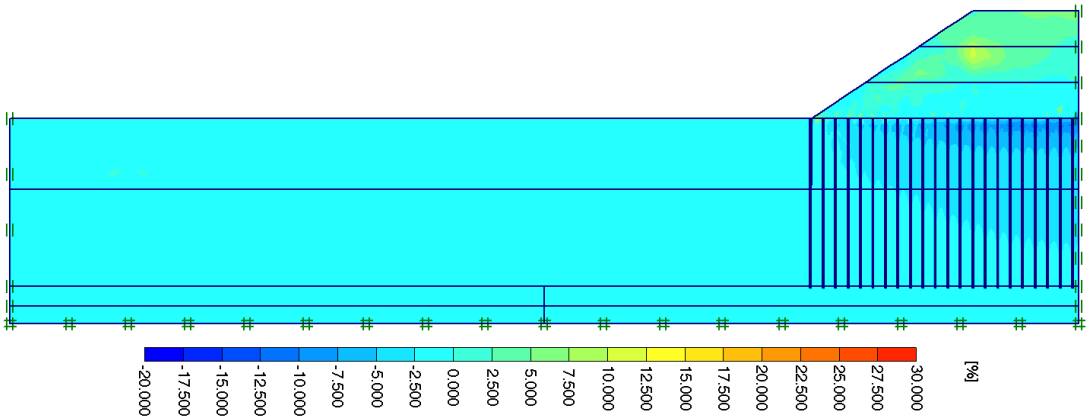

Figure E.4 Volumetric Strain Contours for Parametric Study Analysis for Degree of Disturbance $k_h/k_h' = 1.5$

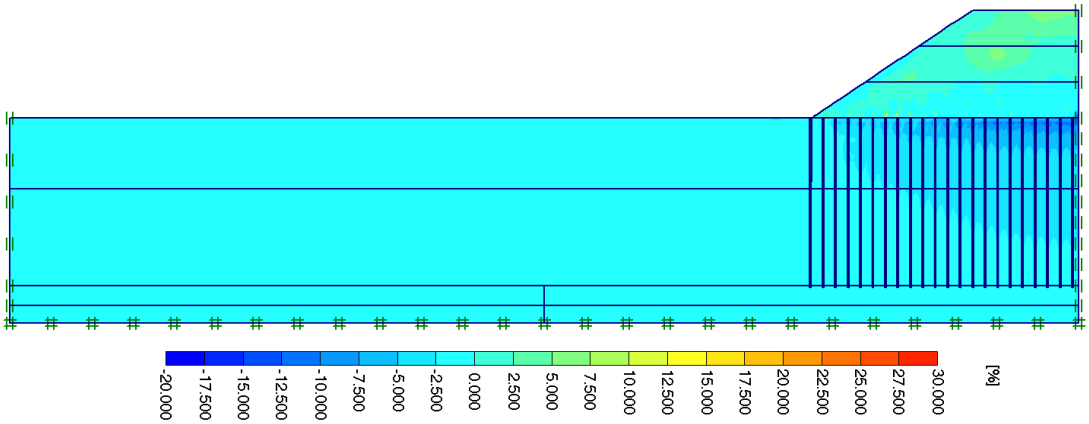

Figure E.5 Volumetric Strain Contours for Parametric Study Analysis for Degree of Disturbance $k_h/k_h' = 2.0$

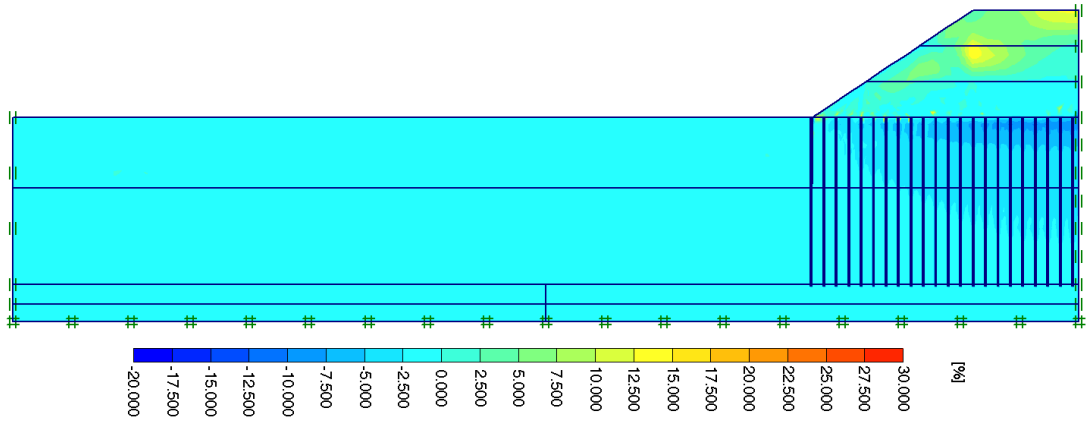

Figure E.6 Volumetric Strain Contours for Parametric Study Analysis for Degree of Disturbance $k_h/k_h' = 3.0$

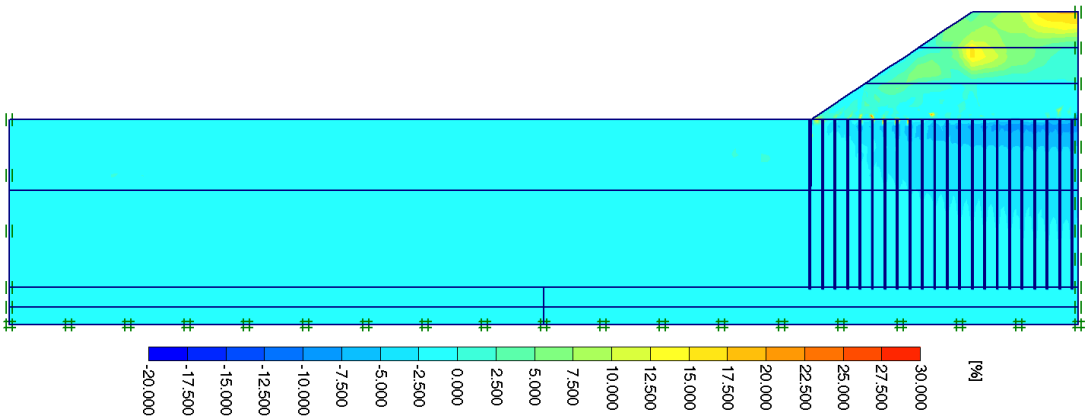

Figure E.7 Volumetric Strain Contours for Parametric Study Analysis for Degree of Disturbance $k_h/k_h' = 4.0$

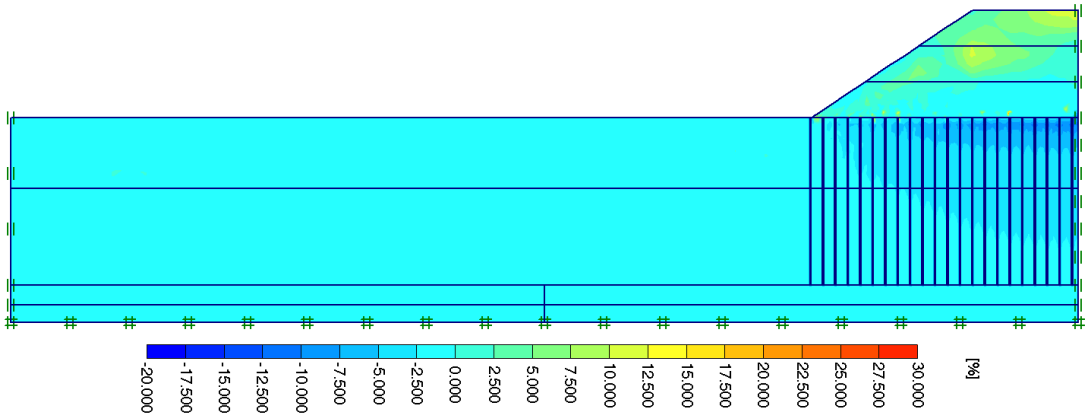

Figure E.8 Volumetric Strain Contours for Parametric Study Analysis for Smear Zone Diameter $d_s = 2.0d_w$

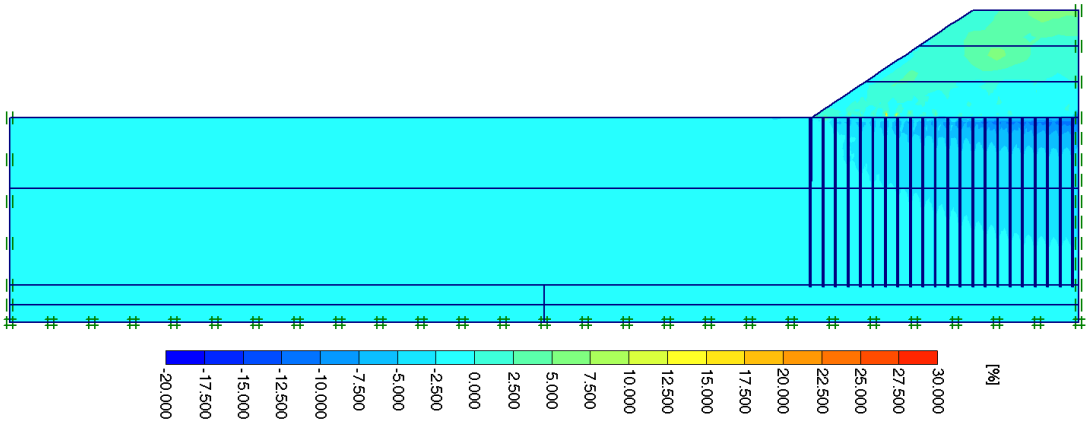

Figure E.9 Volumetric Strain Contours for Parametric Study Analysis for Smear Zone Diameter $d_s = 2.5d_w$

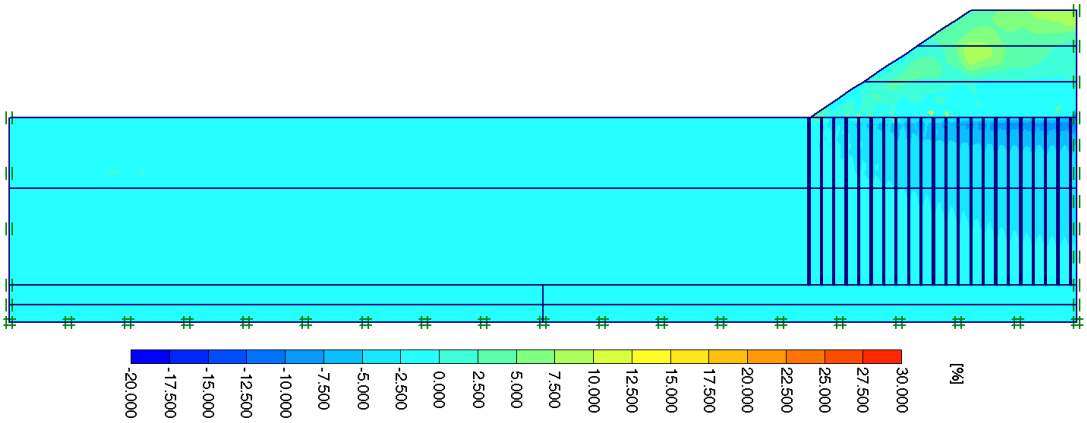

Figure E.10 Volumetric Strain Contours for Parametric Study Analysis for Smear Zone Diameter $d_s = 3.0d_w$

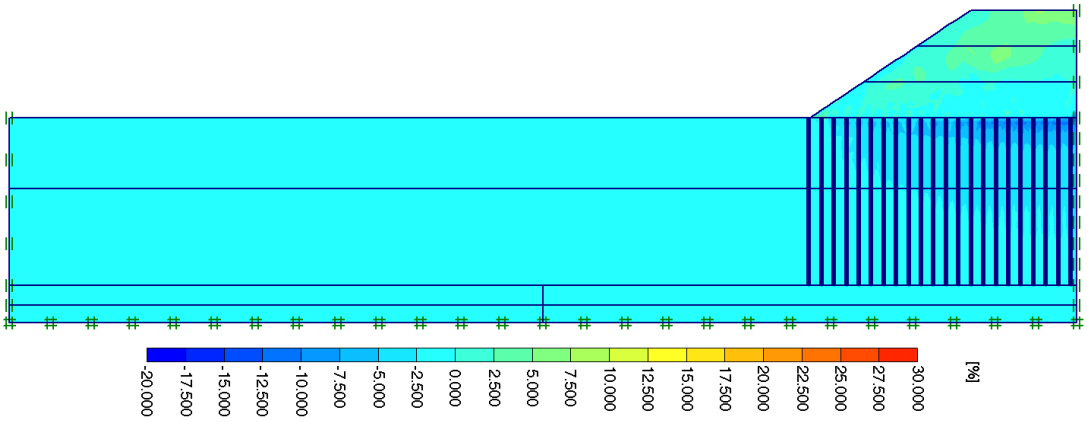

Figure E.11 Volumetric Strain Contours for Parametric Study Analysis for Smear Zone Diameter $d_s = 5.0d_w$

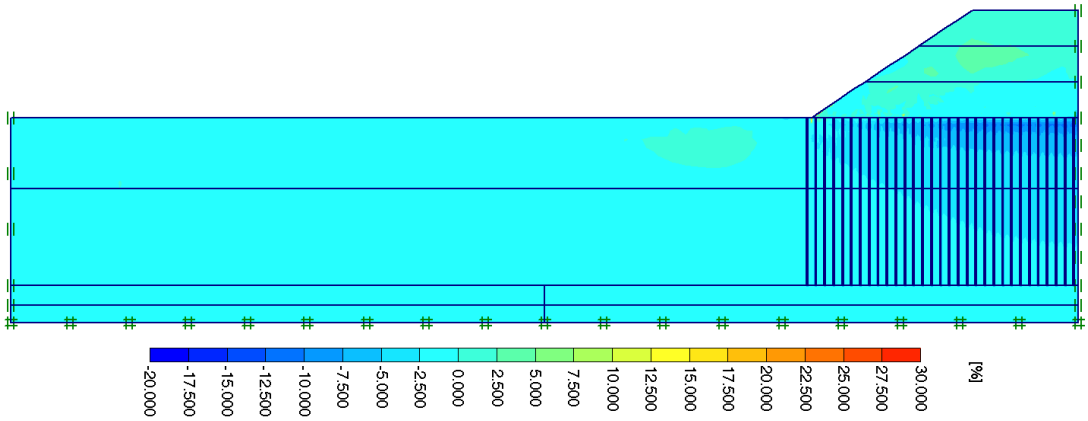

Figure E.12 Volumetric Strain Contours for Parametric Study Analysis for Drain Spacing S = 1.0 m

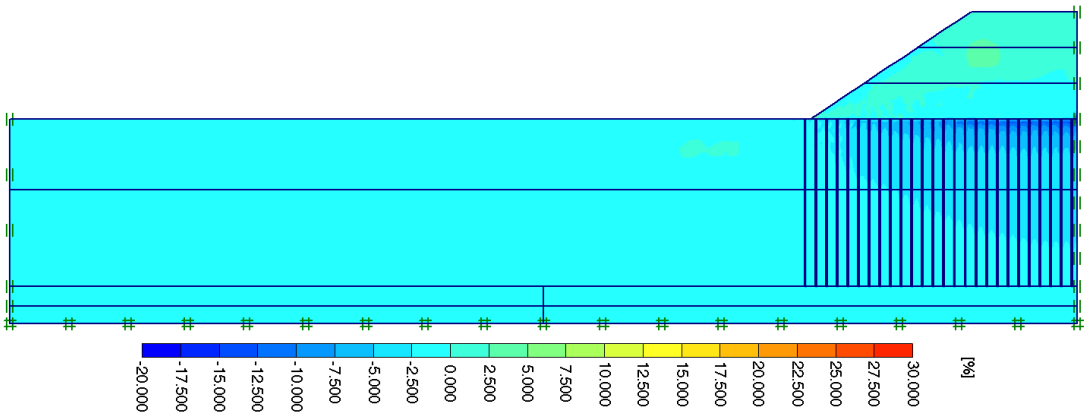

Figure E.13 Volumetric Strain Contours for Parametric Study Analysis for Drain Spacing S = 1.2 m

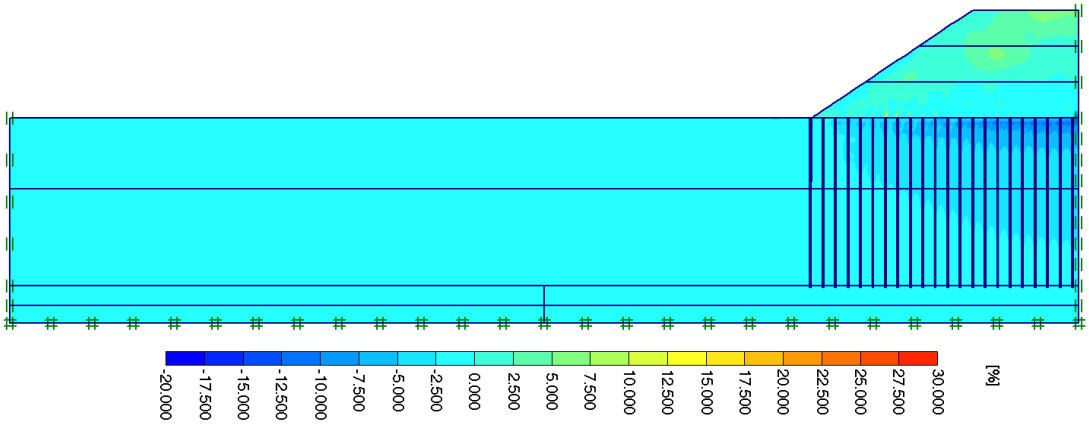

Figure E.14 Volumetric Strain Contours for Parametric Study Analysis for Drain Spacing S = 1.4 m

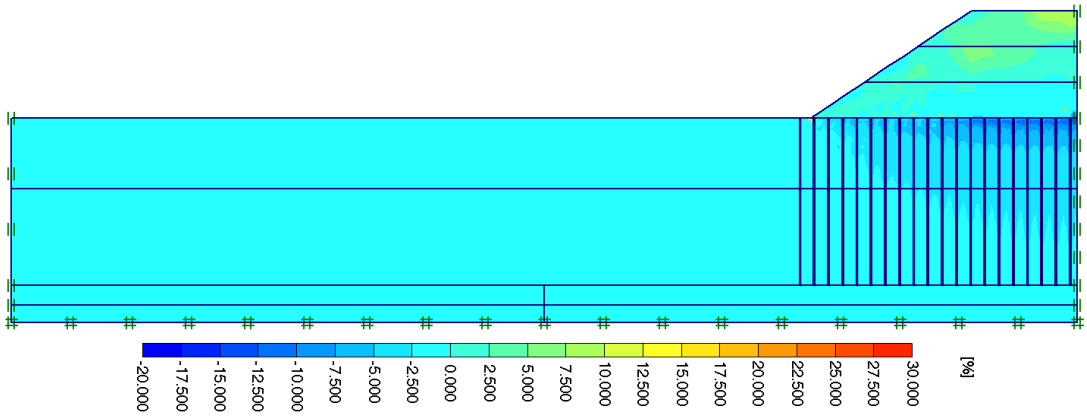

Figure E.15 Volumetric Strain Contours for Parametric Study Analysis for Drain Spacing S = 1.6 m

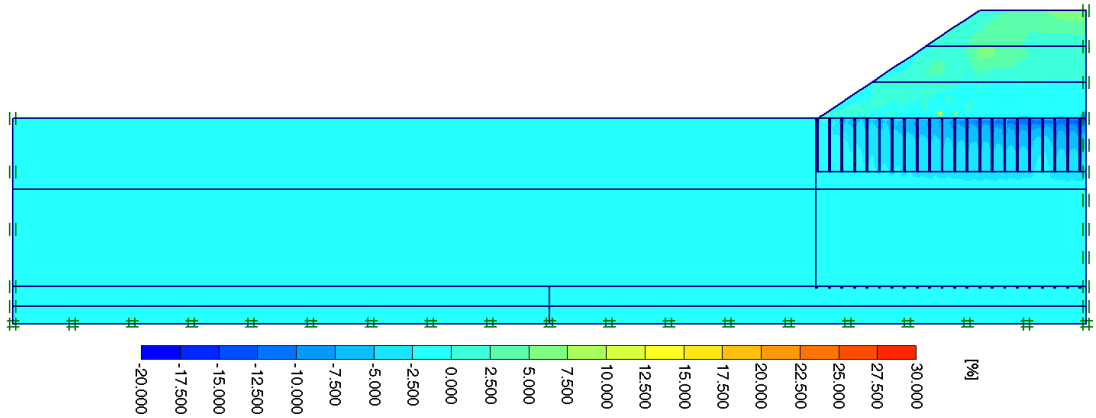

Figure E.16 Volumetric Strain Contours for Parametric Study Analysis for Drain Penetration Length L = 6.0 m

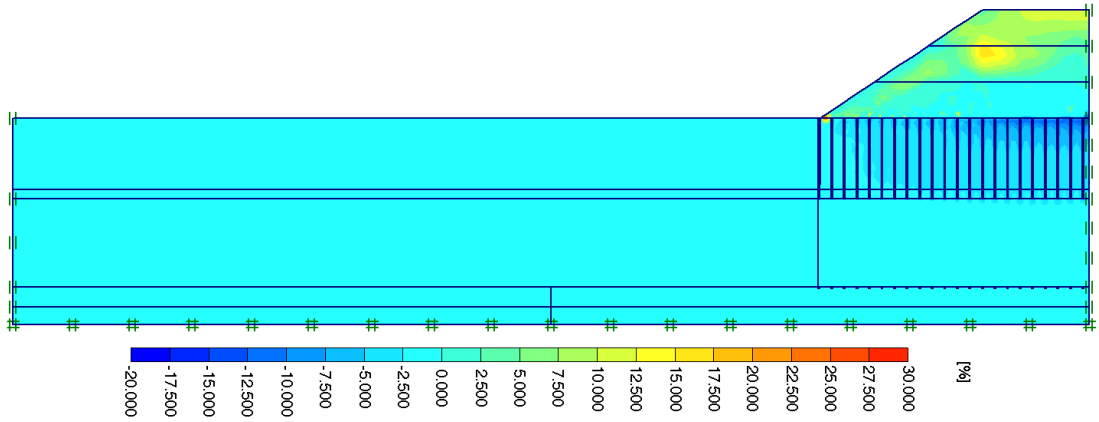

Figure E.17 Volumetric Strain Contours for Parametric Study Analysis for Drain Penetration Length L = 9.0 m

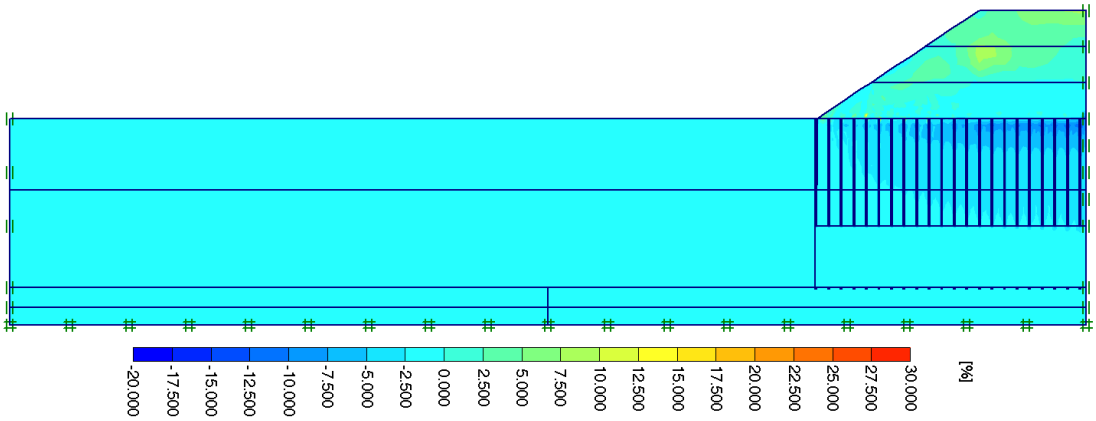

Figure E.18 Volumetric Strain Contours for Parametric Study Analysis for Drain Penetration Length L = 12.0 m

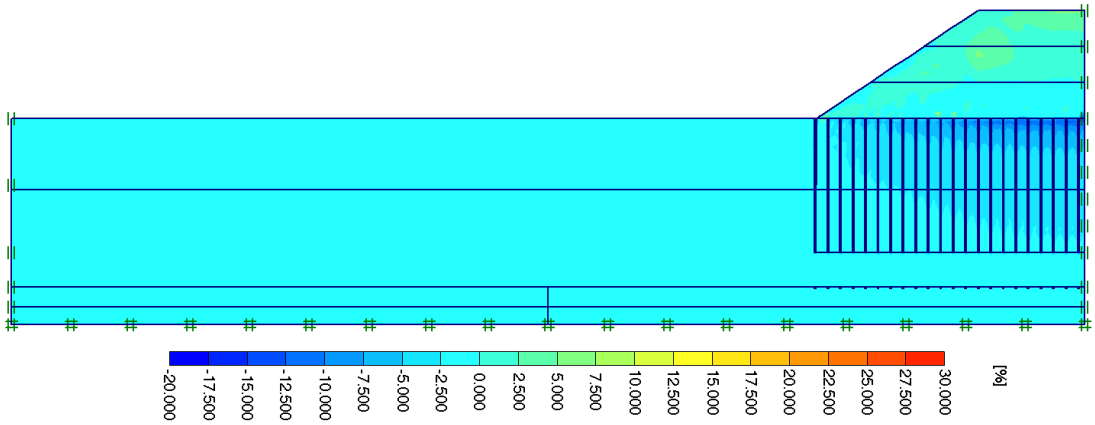

Figure E.19 Volumetric Strain Contours for Parametric Study Analysis for Drain Penetration Length L = 15.0 m

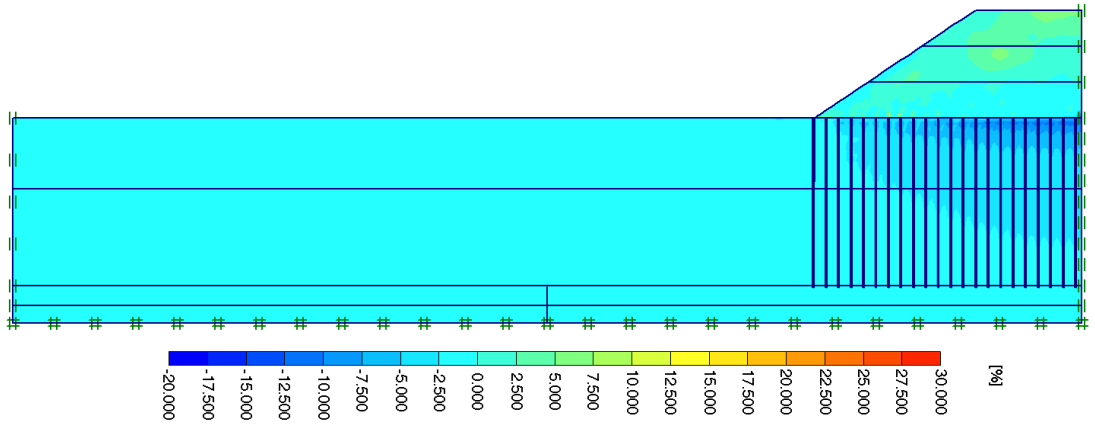

Figure E.20 Volumetric Strain Contours for Parametric Study Analysis for Drain Penetration Length L = 18.0 m